Universitat Autònoma de Barcelona

One-step electrochemical magneto assays for the development of point-of-care (POC) diagnostic devices

Gisela Ruiz Vega

Universitat Autònoma de Barcelona

Doctoral Thesis

One-step electrochemical magneto assays for the development of point-of-care (POC) diagnostic devices

Gisela Ruiz Vega

Director: Dr. Eva Baldrich Rubio
Tutor: Dr.Jordi Aguiló Llobet

PhD programme in Electronic and Telecommunication Engineering
Engineering School - Department of Microelectronics and Electronic Systems
Universitat Autònoma de Barcelona
2019

Vall d'Hebron Institut de Recerca

Vall d'Hebron Barcelona Hospital Campus

Abstract

One of the greatest challenges for monitoring and improving the health of the population at a global level is the lack of appropriate diagnostic tests for early detection of diseases, selection of appropriate treatments and patient follow-up over time. The availability of sufficiently fast, sensitive and robust diagnostic tools will be crucial to achieve patients' well-being worldwide. In this context, nanotechnology and biosensor development are rapidly evolving fields that have generated great expectations, producing tests faster and easier to carry out than most classical methods. Biosensors have been described based on the use of a wide variety of biotechnology elements and types of signal transduction. Among them, electrochemical biosensors are the most common type in use today thanks to the portability and low cost of the measuring equipment, fast, robust and quantitative measures provided, and easiness of miniaturization of the whole detection system. The recent incorporation of paper and paper-like materials for the production of paper printed electrodes and lateral flow electrochemical assays is fostering the development of extremely inexpensive devices that, thanks to the fluidic properties of paper, allow reducing assay complexity and level of manipulation for the end user. This favours the development of "Point-of-Care" diagnostic devices (POC), which can be used directly by the patient or at primary health care centres.

On the other hand, magnetic beads (MB) have been used with great success in the optimization of magneto-biosensors. MB are attractive for this purpose because, once modified with an appropriate bioreceptor, they grant simple, rapid and specific preconcentration of the targeted analyte. MB offer also relatively large 3D active surfaces, which mixed under constant agitation with the sample supply efficient and fast analyte binding as well. Nevertheless, MB display limitations too, requiring tedious and time-consuming handling that is only at reach of highly trained users.

The main objective of this PhD Thesis project was the production of rapid, easy to perform, robust and sensitive electrochemical magneto-biosensors for the detection of diagnostic biomarkers in serum, plasma and blood samples. As it will be shown, this has been achieved at two levels. First, by developing an extremely fast and simple magneto-immunoassay format. Second, by fabricating simple and inexpensive microfluidic paper electrodes, which were exploited to carry out on-chip most of the steps of the simplified magneto-immunoassay with minimal user intervention.

Acknowledgements

Ha llegado el momento de agradecer todas las contribuciones que han hecho posible la realización de este proyecto.

En primer lugar, como no podía ser de otra manera, quiero nombrar a mi directora de tesis, la Dra. Eva Baldrich. Después de conocernos de forma inesperada, hace ya cuatro años, ofreciéndome la oportunidad de realizar en su recién estrenado grupo de investigación mi proyecto final de máster, y a posteriori esta tesi doctoral, ha llegado el momento de cerrar una etapa. Gracias Eva por ver algo en mí y querer formarme como investigadora. Ha sido un largo camino lleno de obstáculos, y por supuesto también de logros. Gracias por tu apoyo y guía que han hecho posible que hoy tengamos en nuestras manos esta tesis doctoral.

También quería agradecer la ayuda del Dr. Javier del Campo, sin él a este trabajo le hubiera faltado una gran parte. Gracias por dedicarme tu tiempo, y enseñarme con tanta ilusión el mundo de los electrodos de papel, ha sido un gran y precioso descubrimiento.

No quiero olvidarme de los compañeros y amigos de laboratorio que han ayudado a este proyecto, sin su trabajo y esfuerzo esta tesis hubiera estado incompleta. Gracias a Erica, por su gran compañerismo, y por ser la reina de los ELISAs. A Elena por aprender tan rápido y obtener tan buenos resultados en el estudio de conjugación de partículas magnéticas. A Adaris, por ser esa voz amiga que le da otro punto de vista a la vida. A Ana, por su comprensión durante este camino, y por ofrecerme siempre su ayuda. Y a Kevin, el último en llegar, gracias por darle el toque masculino al laboratorio que tanta falta le hacía.

Por último gracias al pilar más grande que puede tener una persona, la familia. A mis padres y hermano, por siempre acompañarme en mis decisiones, animándome y comprendiéndome con tanto amor. A mi familia política, por estar siempre pendiente del transcurso del proyecto, valorando y apoyando el esfuerzo que supone.

Y finalmente a Javier, por haberme animado en su día a empezar esta senda. Él, que ha llevado como parte suya esta tesis, que ha compartido cada día mis penas y alegrías, que ha escuchado con paciencia mis infinitos discursos, y que me ha ayudado tanto a ver siempre el lado positivo de las cosas. Él, que siempre ha estado ahí cuando lo he necesitado. A él, un gracias enorme.

Agradecer también el apoyo económico de las entidades que han hecho posible este trabajo. Al Instituto de Salud Carlos III (ISCIII) y al Fondo Europeo de Desarrollo Regional (FEDER), con los proyectos CP13-00052, DTS14/00004, PMP15/00022 y DTS17-00145. Al VHIR, y als “amics del VHIR”, por hacer posible esta beca predoctoral con la que tantísimo he aprendido.

List of Abbreviations

A_{450}	Absorbance at 450 nm
ABTS	2,2′-azino-di-(3-ethylbenzthiazoline sulfonic acid
Ab	Antibody
ACD	Acid-citrate-dextrose
Ag	Antigen
ANOVA	Analysis of variance
AP	Alkaline phosphatase
AU	Absorbance Unit
AuNPs	Gold nanoparticles
bc-MAb	Biotinylated capture monoclonal antibody
bd-MAb	Biotinylated detection monoclonal antibody
bd-PAb	Blood collection tubes
BSA	Bovine serum albumin
CE	Counter electrode
c-Ab	Capture antibody
c-MAb	Capture monoclonal antibody
CNT	Carbon nanotubes
CS	Carotid stenosis
CV	Cyclic voltammetry
%CV	Coefficient of variation
CVDs	Cardiovascular diseases
d-Ab	Detection antibody
DPV	Differential pulse voltammetry
EDC	1-ethyl-3-(3-dimethylaminopropyl) carbodiimide hydrochloride
EDTA	Ethylenediaminetetraacetic acid
EIS	Electrochemical impedance spectroscopy

ELISA	Enzyme-Linked Immunosorbent Assay
FET	Field effect transistor
H_2O_2	Hydrogen peroxide
HRP	Horseradish peroxidase enzyme
HT	Haemorrhagic transformation
IgG	Immunoglobulin G
$K_4Fe(CN)_6$	Potassium ferrocyanide
LDH	Lactate dehydrogenase
LFIA	Lateral-flow immunoassays
LOD	Limit of detection
LOQ	Limit of quantification
MAb	Monoclonal antibody
MB	Magnetic beads
MES	2-(N-morpholino)ethanesulfonic acid
MF	Microfluidic
MMP-9	Matrix metallopeptidase 9
MNP	Metal nanoparticles
MPO	Myeloperoxidase
MP	Microfluidics paper
MP-SPCE	Microfluidic paper screen-printed carbon electrode
PAb	Polyclonal antibody
PBS	Phosphate buffered saline
PBST	Tween-containing phosphate buffered saline
PCR	Polymerase chain reaction
PfLDH	*Plasmodium falciparum* lactate dehydrogenase
PLDH	*Plasmodium* lactate dehydrogenase
PMMA	poly(methyl methacrylate)

POC	Point-of-care
POCT	Point-of-care testing
Poly-HRP	Polymers of horseradish peroxidase
PVC	Polyvinyl chloride
RBC	Red blood cells
RD	Reagent Diluent
RDT	Rapid diagnostic test
RE	Reference electrode
Rpm	Revolutions per minute
RT	Room temperature
SD	Standard deviation
SEM	Scanning electron microscopy
SPCE	Screen-printed carbon electrode
SPE	Screen-printed electrode
SPR	Surface plasmon resonance
Strep	Streptavidin
SWV	Square wave voltammetry
S/N	Signal-to-noise ratio
TIMP	Tissue inhibitor of metalloproteinase
TMB	3,3’,5,5’-tetramethylbenzidine
tPA	Tissue-type plasminogen activator
WE	Working electrode
WHO	World Health Organisation

Chapter 1

Introduction

1. Introduction

1.1. Summary

Over the last decades, the glucose meter has raised considerable interest due to the vast biomedical, social and economic success attained by this family of products, which is often taken as an example of the huge potential that electrochemical immunosensors display for point-of-care testing (POCT)[1]. POCT entails a paradigm shift from classical differed diagnostics to near-patient analysis, providing real-time results for an early diagnosis, facilitating prompt treatment selection and implementation, and reducing disease complications and fatalities. In this case, glucose POCT relies in the availability of portable low-cost sensors and measurement equipment, which are also inexpensive, robust, simple, and easy to use, and a relatively simple enzymatic assay format as well[2]. Generally speaking, the development of portable electrochemical measurement devices can be achieved with more or less success through the technological miniaturization of classical desktop equipment, the direct exploitation of commercial hand-held systems, or via the design and production of customized measurement equipment[3]. Miniaturizing the whole detection protocol, including sample acquisition and pre-treatment, analyte identification, binding and detection, and result analysis and display, entails a highly multidisciplinary work that can be considerably more complex and resource consuming.

Compared to other transduction strategies, electrochemical biosensors are often proposed as an effective answer for fast, specific and sensitive analyte detection[4,5]. Electrochemistry provides measurement equipment and transducers that are robust, inexpensive and easy to miniaturize for the production of user-friendly and portable devices. This results in low power requirement and compatibility with POCT[6]. Nevertheless, producing an electrochemical immunosensor entails the optimization of numerous steps (such as antibody (Ab) immobilization, sensor appropriate blocking to prevent nonspecific binding, serial incubations and washings, detection), which is certainly more complex to carry out and automate than glucose sensing. Moreover, electrode immuno-modification produces partial physical shielding of the electrode surface as well, and affects negatively signal transduction[7]. Besides, electrode reutilization is restricted due to the permanent immobilization of the molecules and the limited success of the regeneration protocols reported to date[8,9].

For these reasons, many efforts have been devoted to the development of single-use immunosensors using disposable and low-cost screen-printed electrodes (SPE) and attempts to separate the surfaces used for immunocapture and electrochemical detection have been reported, such as by employing magnetic beads (MB)[10,11]. MB stand as one of the most versatile tools currently used in analytical chemistry. In this context, the utilization of MB for the production of magneto-immunosensors provides a number of advantages useful in a wide variety of biomedical applications[8,12,13]. Electrochemical magneto-immunosensors take advantage of MB for enhanced analyte binding and concentration, and of electrochemistry for fast and quantitative detection[14,15]. MB can be magnetically confined onto the surface of a transducer for immunoassay detection and be then released by removing the magnet for sensor regeneration[16]. Hence, the sensor does not need to be treated extensively to incorporate Ab and to prevent nonspecific fouling, which results in improved performance compared to immuno-modified transducers in classical biosensors. In electrochemical magneto-immunosensing, the use of MB for target immunocapture guarantees that the incubation with potentially complex samples and reagents is carried out far away from the electrode where the electrochemical detection takes place[17]. In addition, MB provide sample agitation and homogenisation, and antigen (Ag) magnetic separation and concentration, decreasing the assay limit of detection (LOD) and/or the assay time[18].

However, immunomagnetic assays involve numerous incubation and washing steps, as well as the alternating application of a magnetic field for MB sequential recovery and release. This makes MB difficult to handle for unqualified users, complicates automation using low-cost point-of-care (POC) devices, and is a serious drawback for POCT. This suggests that the implementation of magneto-immunosensors in-field will require the availability of simple and inexpensive POC platforms appropriate for their operation with minimal user intervention. For this reason, most electrochemical magneto-immunosensors described to date entail a magneto-immunoassay accomplished completely out of the chip, and only electrochemical detection performed at the electrode device[19–21].

Microfluidic has been exploited for the production of fast and sensitive electrochemical magneto-immunosensors in order to solve these drawbacks[16,22]. Although classical microfluidic platforms require pumping components and valves, which increases the device final cost and hardens mass production, they are also compatible with

multiplexing and automation. Alternatively, the field has recently benefited from the increasing interest raised by paper-based devices[23–25], which are being employed as economical and versatile platforms for the simple and scalable fabrication of disposable electrochemical POCT devices[26,27].

Paper has been used in analytical applications since the 1940s, when paper chromatography was applied to protein separation by Consden and others[28]. Then the first urinary dipstick reached the market around 1956[29]. Since then, a variety of rapid lateral flow diagnostic tests has been developed and is commercially available, such as the lateral flow immunoassay (LFIA) pregnancy test[30,31]. LFIA tests are easily transported and stored, and their utilization does not depend on power sources. Hence, they represent an excellent solution for in-field diagnosis. However, LFIA often display limited sensitivity and selectivity, and a characteristic qualitative or semi-quantitative response derived from the optical, and thus subjective, interpretation of the results[32,33]. Furthermore, recent reports demonstrate that unacceptably dissimilar results are produced by commercial kits from different providers, and even by different lots and products of the same companies[34]. In order to solve the current LFIA limitations, there have been attempts to integrate electrochemical detection and hand-held optical readers, and an increasing interest has been also directed to implement analyte pre-concentration and signal enhancement strategies, in order to produce more sensitive, accurate, and quantitative devices[35–37]. Nevertheless, these have hitherto been few and relatively unsuccessful examples from a commercial standpoint.

In this context, the combination of paper-based microfluidics, which are popular because of their low cost, ease of fabrication and disposability, with SPE and MB, which potentially provide fast, sensitive and quantitative results, should allow producing portable, sensitive and robust detection platforms well-suited for POC diagnostics[38,39]. This PhD Thesis explores how these three technologies can complement each other and exploits this synergy to develop a novel type of electrochemical biosensor in which paper microfluidics (MP) is employed to carry out electrochemical magneto-immunoassays with little user intervention.

1.2. Objectives

The overall aim of this PhD Thesis was the development of fast, sensitive, robust and easy to use electrochemical magneto-immunosensors, with the purpose to facilitate protocol automation using a low-cost POCT device that could detect diagnostic biomarkers in biological fluids with minimal user intervention. In order to ensure the transferability of the developed protocols, mature and commercially available materials and technology have been used wherever possible. However, part of the accomplished work involved the development of new technological tools, including a multiplexed magnetic holder and microfluidic paper screen-printed electrodes (MP-SPE), which were carried out in collaboration with Dr.'s Javier del Campo team (Biomedical Applications Research Group, Institut de Microelectrònica de Barcelona, IMB-CNM, CSIC).

In order to accomplish the general Thesis aim, work targeted three specific objectives over time, which are detailed next:

1. Identification of critical parameters for the development of magneto-immunoassays for the fast and sensitive quantification of diagnostic biomarkers.
    a. Optimization of the critical assay parameters for magneto-immunoassay simplification.
    b. Use of enzymatic polymers as signal amplifiers for magneto-immunoassay shortening.

2. Development of single-step electrochemical magneto-immunosensors.
    a. Production of immuno-modified enzymatic polymer signal amplifiers to perform sandwich magneto-immunoassays in a single step.
    b. Implementation of electrochemical detection using commercial SPE and enzyme substrate solutions.
    c. Validation of the one-step electrochemical magneto-immunosensor format in two different diagnostic scenarios.

3. Development of MP devices for magneto-immunosensor operation with minimal user intervention.
    a. Use of a paper device to replace the manual MB washing by MB on-chip washing and detection using commercial SPE.

b. Fabrication of MP-SPE for magneto-immunoassay on-chip washing and detection performance.

In order to ensure that the protocols and devices produced were truly applicable, each development was validated before passing to the following phase. This was done by detecting the corresponding target biomarker in real sample matrices, such as serum, plasma or whole blood, depending on the analyte, the clinical interest and sample availability.

In terms of the diagnostic biomarkers examined, this Thesis work started with a detailed study of different parameters affecting magneto-immunoassay performance, for which myeloperoxidase (MPO) was used as the model analyte. MPO had been proposed as a potential biomarker for the diagnosis and prognostic study of several inflammatory pathologies. MPO was used as a target analyte in the optimization of a one-step magneto-immunoassay, which was next detected by employing the first MP screen-printed carbon electrode (MP-SPCE) produced in this project. This part of the work, which was carried out in the context of project CP13-00052, cofunded by Instituto de Salud Carlos III (ISCIII) and the European Regional Development Fund (FEDER), allowed demonstrating for the first time that MB washing and detection could be accomplished on-chip by exploiting MP.

Following this preliminary study, a polymeric signal amplifier, Poly-HRP, was exploited to produce two simplified one-step sandwich magneto-immunosensors. One was optimized to detect matrix metallopeptidase 9 (MMP-9), a biomarker of ischemic stroke complications, in the context of projects DTS14/00004 and PMP15/00022 (ISCIII-FEDER). The MMP-9 one-step magneto-immunoassay was detected electrochemically using a multiplexed magnetic-device with MP washing implementation. The other one-step sandwich magneto-immunoassay developed detected *Plasmodium falciparum* lactate dehydrogenase (PfLDH), an enzyme produced by *Plasmodium*, the parasite responsible for human malaria, a work that was funded by project DTS17-00145 (ISCIII). Most of the steps of this one-step magneto-immunoassay were integrated in the second generation of MP-SPCE produced, enabling rapid, simple and quantitative malaria diagnosis.

The whole Thesis was possible thanks to a Vall d'Hebrón Research Institute (VHIR) predoctoral fellowship, an internal program that is covered by Amics del VHIR.

1.3. Thesis overview

This Thesis describes the development of three different magneto-immunoassays, and the corresponding electrochemical magneto-immunosensors, for the fast, simple and sensitive detection of diagnostic biomarkers. Work focused in the optimization of simplified assay paths, and the subsequent integration of most assay steps on-chip, reducing as much as possible the manipulation of the MB to take the assays closer to the requirements of POCT. This was accomplished by using paper as a microfluidic platform, which allowed carrying MB washing and detection procedures in an easy form and with minimal handling.

Two strategies were explored in order to achieve this goal. On the one hand, a customized paper device was integrated in commercial SPCE. The paper device developed was a mobile piece which was assembled in a multiplexed magnetic device. It worked as an absorbent pad to retain the waste volumes generated during the magneto-immunoassay without interfering in the electrochemical detection. On the other hand, two types of MP-SPCE were designed and produced. The objective was minimizing the magneto-assay manipulation, accommodating sample injection and MB washing and electrochemical detection in a cheap and simple lateral flow electrode device. The first generation of MP-SPCE detected MPO in diluted human serum. In the second version, the design and fabrication procedure were improved to achieve higher detection efficiency and sensitivity. This device was applied to the diagnosis of malaria in lysed whole blood samples.

The Thesis contents have been organized in nine chapters plus annexes.

Chapter 1 presents a brief summary of the work antecedents and motivation, and details the Thesis objectives. Chapter 2 summarizes the state of the art and a general overview of the use of MB, SPCE and paper for the development of POC devices is presented. Chapter 3 describes the reagents, materials and procedures used during the dissertation.

The results and discussion are presented in Chapters 4-8. Chapter 4 identifies the critical parameters for magneto-immunoassay development, applied to MPO detection.

Chapter 5 analyses the development of simplified magneto-immunoassays using enzymatic polymers as signal amplifiers. The targets detected were MMP-9 and PfLDH. In Chapter 6, the simple magneto-immunoassays of Chapter 5 are formatted to produce one-step electrochemical magneto-immunosensors. Chapter 7 summarizes how the manipulation of one of the electrochemical one-step magneto-immunosensors was reduced by using SPCE with integrated paper microfluidics, which was applied to MMP-9 detection. Finally, Chapter 8 presents the production of MP-SPCE for the magneto-immunodetection of MPO and PfLDH.

The general conclusions and the future work are presented in Chapter 9.

Finally, the annexes include copies of the scientific articles published as a result of this PhD Thesis and a list of the works presented in congresses, seminars and other scientific events.

Chapter 2

State of the art

2. State of the art

2.1. Point-of-care (POC) diagnostic devices

The clinical diagnostic field is in constant evolution, with the last few years having witnessed important progresses. In industrialized countries, current diagnostic techniques are mostly performed in centralized clinical laboratories, generally employing expensive and sophisticated instrumentation and entailing laborious and time-consuming procedures carried out by trained professionals[40,41]. In contrast, in resource-limited settings and developing countries, most inhabitants have reduced access to laboratory techniques and medical centres, which entail costs that are not affordable for the National Healthcare Systems and are incompatible with the systemic lack of technicians and other trained personnel[42,43]. This enters in conflict with the general expectation that health should be democratized worldwide, and that the National Healthcare Systems should provide the tools and means for early disease diagnosis and personalized and continuous health monitoring to everyone. It is widely accepted that the availability of enhanced diagnostic tools will play an increasingly important role in controlling disease outbreaks, rising the survival rate of patients, and improving overall the quality of life of the citizens (Figure 2.1a). Similar demands apply to diagnostics at primary healthcare centres, emergency departments, mobile health units, or in isolated settlements, where the strategies currently available are unfeasible, because personalized medicine will be possible only if diagnostic devices can be used by or close to patients[44]. Nowadays, in conventional laboratory-based testing the samples must be collected, stored and transported to the centralized facilities, having to wait for long periods of time before the samples are analysed by trained personnel and the results are sent back to the clinicians and reach the patients[45]. Under these circumstances, simple, easy to use and robust diagnostic systems, able to deliver results without the need of special training or facilities, are highly demanded[46].

The use of POCT devices offers a promising solution to this situation, allowing to provide diagnostic information near the site of the patient and in real time[47]. Most POCT devices can work with small volumes of biological samples and reagents, offering unique advantages such as a low assay cost, fast turnaround time, simple-to-use operation and fully integrated devices implementable in resource-limited settings[48,49]. It has been defended that POCT should facilitate early disease diagnosis, potentially

enabling local patient stratification, prognosis determination and treatment response monitoring, and ultimately smoothing quick medical decision taking, leading to improved patient outcomes[50,51]. Furthermore, the use of POC diagnostic devices could reduce as well the medical costs, and the risk of sample mislabelling and mishandling[52]. Within this framework, issues such as the rising occurrence of lifestyle diseases, the global prevalence of infectious diseases, the risk of global infection outbreaks[53], the increasing incidence of chronic diseases[54], or an aging population worldwide, seem to have encountered an ally in the fast growing field of the technological innovations[55], becoming the driving motors for POC development and commercialization. It is worth noting that the global POCT market is expected to grow from US$ 28.4 in 2018 to US$ 40.5 billion in 2022, entailing an annual growth (CAGR) of 7.4% during the forecast period 2018–2022 (Figure 2.1b). In this field, North America accounts for most of the global POCT market, followed by Europe[56].

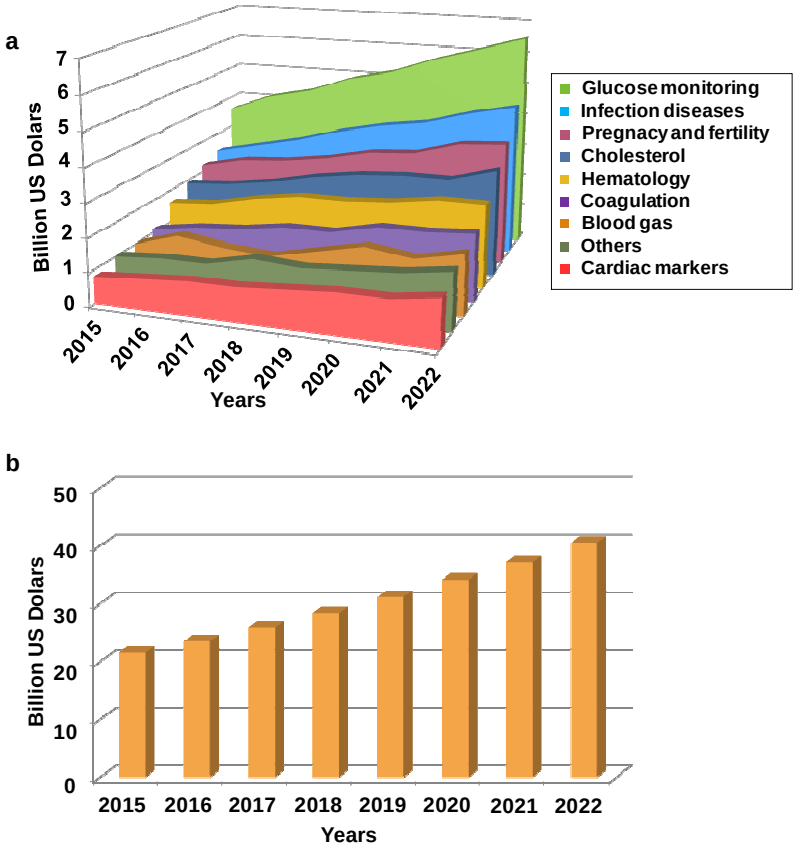

Figure 2.1. (a) Analysis of the size in US$ of the POC diagnostics market from 2015 to 2022, by product. (b) Size in US$ of the global POCT diagnostics market from 2015 to 2022. Based in [57].

2.1.1. Requirements for POCT

According to the World Health Organization (WHO), the ideal POC diagnostic device for the health care system should fit the ASSURED criteria (be Affordable, Sensitive, Specific, User-friendly, Rapid and Robust, Equipment-free and Deliverable to end-users), which has become a valuable framework in the challenging development of POCT (Table 2.1)[58]. According to these guidelines, the whole POCT system should be inexpensive, robust and either handheld or at least portable, indicating a high degree of compactness[34].

Requirements	Description
Affordable	Less than US$ 500 per machine, less than US$ 10 per test
Sensitive, Specific	Low limit of detection (depending on the target), minimal sample matrix interference
User-friendly	1-2 days of training, easy to use
Rapid	<30 minutes for diagnosis
Robust	Minimal consumables, shelf life > 1 year at room temperature, high throughput
Equipment-free	Compact, battery powered, on-site data analysis, easy disposal, easy sample handling
Deliverable	Portable, hand-held

Table 2.1. ASSURED requirements and specifications for the evaluation of POC devices[59].

Taking into account the ASSURED requirements, an important landmark in the field has been the use of smartphones for the production of portable diagnostic equipment, because it is estimated that 68% of the world population had a smartphone in 2018[60]. A smartphone is a device essentially self-powered, with small size, inexpensive and that can be network-connected. These advantages entail a tremendous opportunity for the miniaturization of current analytical instruments and the development of POCT diagnostic devices (Figure 2.2a)[61,62]. It is worth noting that the majority of the smartphone-based POC reported are based on optical sensing[63], such as by using the phone camera for microscopic[64], colorimetric[65,] and spectroscopic[66] detection of the assays. However, these optical techniques are limited by the camera resolution and the ambient lighting conditions[67].

Alternatively, electrochemical sensing has the advantage of being mostly independent of the smartphone capabilities[68]. Among the examples reported, Guo and co-workers proposed a medical dongle for β-Ketone monitoring as a miniaturized electrochemical analyser. This device was powered by and communicated with a smartphone, which

provided the electronic interface for the medical data transmission and upload[69]. Besides, economical, robust and either portable or hand-held potentiostats are commercially available, with the glucose meter as the best example in the field. Two alternatives have been proposed to the employment of hand-held low-power consumption electrochemical measurement equipment. On the one hand, the utilization of long-duration batteries and solar cells, which could power a variety of portable and bench-top devices. On the other, the exploitation of self-powered sensors using bio-fuel cells, which would be convenient in remote locations with limited or null power supply[26].

Finally, an ideal POCT device should automate the whole analytical procedure, from sampling, to sample pre-treatment, dilution and analysis. Non-invasive or minimally invasive sample acquisition is preferred, such as the procurement of capillary blood, saliva, tears or sweat. Examples of minimally invasive recovery tools have been reported, such as micro/nanoneedles for low pain and tissue damage during capillary blood recovery, or patch-shaped and wearable biosensors for low volume detection in sweat[44].

2.1.2. Limitations of current POC devices

Although attempts have been made to produce the corresponding automated low-cost POC platforms, classical techniques like microscopy, ELISA and nucleic acid amplification are still vastly limited to laboratory settings, where they are carried out with specific instruments used by professional operators[44]. In contrast, the development of POCT devices has raised increasing interest in the case of portable, wearable and implantable sensors. However, the majority of the examples having reached the market are either devices to monitor vital signs on a continual basis (such as heart rate, blood oxygen saturation level, body and/or skin temperature, respiration rate, or blood pressure) or enzymatic sensors (like the electrochemical sensor for glucose determination), which are technologies not easily applicable to the development of an affinity immunoassay. In this field, the glucose meter is often considered the gold standard when referring to portable electrochemical equipment. Marketed for home-use since the early 80s, glucose meters are economical handheld devices that offer high-speed quantitative detection in a drop of blood and extremely simple operation.

Alternatively, the most common format for the integration of immunoassays in a POCT are the LFIA, which provide a simple but qualitative diagnosis. The LFIA, also called rapid diagnostic test (RDT), is probably the most widely used commercially available POC diagnostic format worldwide[70,71]. A LFIA platform is fabricated by assembling strips of different membrane-like materials, part of which are employed as a physical substrate and reservoir for dried reagents that are activated by the addition of a fluid sample. The typical elements of LFIA include an assembly of usually 4 porous substrate components (sample pad, conjugate pad, nitro-cellulose detection membrane and absorbent pad), two different capture antibodies immobilized on the detection membrane forming the test and control lines, a signal-generating system (generally a detection antibody (d-Ab) conjugated to coloured micro- or nanoparticles) and a holder or cartridge that encloses the rest of components and facilitates handling[72] (Figure 2.2b). When the sample is added by the user at the sample pad, it flows via capillary force to the conjugate pad. While the sample pad provides sample pre-treatment (for instance by filtering and retaining blood cells), the conjugate pad acts as a dry-reagent storage unit, displaying a color-coded d-Ab specific for the target analyte. This d-Ab is resuspended as the sample flows, and binds the target analyte molecules present in the sample. When the d-Ab-analyte complexes formed pass through the test line, they are captured by the specific recognition element. The excess of d-Ab is trapped later on by a second set of capture Ab (c-Ab) placed at the control line. In both cases, when the immunoreaction occurs, a coloured signal band is generated within a few minutes. This signal takes place in spatially defined reactive zones of the detection membrane and is interpreted visually[73,74].

LFIAs are low-cost, simple, fast and portable tests, which do not need for complicated equipment and technical expertise to be performed. However, they display some drawbacks also, including limited sensitivity and selectivity, qualitative or semi-quantitative response, poor reproducibility, and lack of a communication and data collection system (for example to store the result or diagnosis for patient follow up, for subsequent result confirmation, or for epidemiology studies, to cite but a few examples). In addition, the visual interpretation of the result is subjective and differences in colour perception between individuals are a common occurrence[75,76]. In order to counteract the limitations of LFIA and satisfy the clinical requirements, strategies for analyte pre-concentration and signal enhancement, and especially the implementation of hand-held

readers, have been explored in an attempt to produce more sensitive, accurate, and quantitative devices. Nevertheless, these technological improvements often affect the final analysis cost and duration as well[32,77,78].

The technological gap between the simple-to-use LFIA tests and the high-precision laboratory bioanalytical techniques could be fulfilled by microfluidic (MF) devices. In principle, MF diagnostic systems are portable fluid-handling devices able to carry out the multiple steps of classical analytical procedures into a compact space with little intervention of the user[79] (Figure 2.2c). Their operation requires small volumes of samples and reagents and provides a rapid, accurate and sensitive analysis[80,81]. All of this, together with the possibility to incorporate features such as component miniaturization, operation automation and real-time monitoring, make MF devices powerful platforms for POCT in biomedical applications[82,83]. An example of laboratory development is a MF chip reported for the simultaneous detection of HIV and syphilis using silver enhanced immunoassays[84]. These devices were based in the employment of air bubbles to separate reagents in the microfluidic channels, and silver reduction to enhance the colorimetric signals, enabling ELISA-like sensitivity and specificity within 20 min. Furthermore, the whole system was integrated into a small cartridge that could be read by a mobile device, such as an iPod touch[85]. Another example, currently in the market, is the i-STAT System (Abbott Laboratories, Abbott Park, IL, USA). The i-STAT uses test reagent-preloaded cartridges capable of performing a wide variety of tests in a drop of blood, such as the determination of arterial and venous blood gas and electrolytes, common metabolites, cardiac troponin I, haematocrit and haemoglobin, and coagulation tests such as the international normalized ratio and activated clotting time[86]. However, MF presents challenges that will need to be addressed, especially the complex and expensive manufacturing methods, which in general demand for a large degree of hands-on experience. Furthermore, MF operation depends strongly on the employment of instrumentation, including a power supply, a flow control unit and portable detection equipment. All these drawbacks make difficult the transfer of MF devices from research to effective commercialization[87,88].

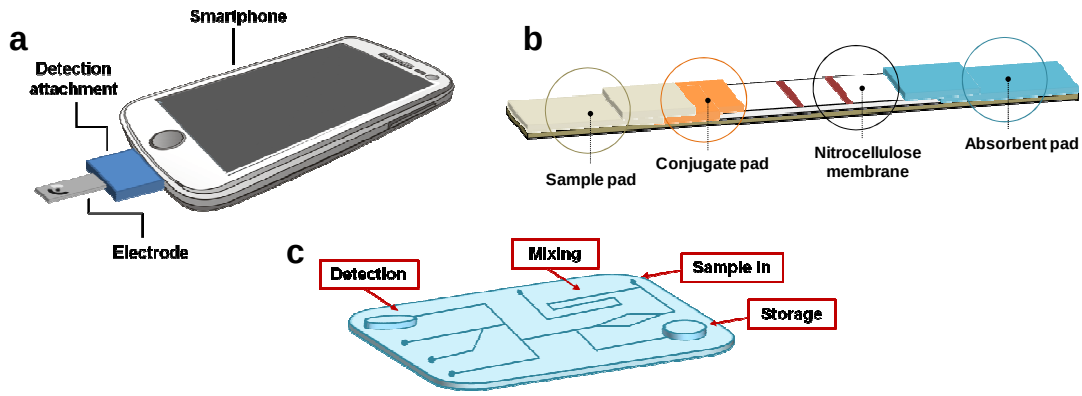

Figure 2.2. Examples of different current POCT devices. (a) POC-smartphone with electrochemical sensing unit. (b) Components of a LFIA device. (c) MF system combining several assay procedures.

In brief, there are many difficulties for the development of POC diagnostic devices that are realistically applicable[76,89]. A promising alternative for POCT is the employment of biosensor devices, which hold an increasingly potential role as technological solutions to analyze samples in a rapid way[46].

2.2. Electrochemical immunosensors

2.2.1. Definition and classification of biosensors

According to the International Union of Pure and Applied Chemistry (IUPAC), a biosensor is a bio-analytical device capable of providing analytical information using a biological recognition element combined with a signal transduction element, in order to detect the analyte of interest in a selective and quantitative form[90]. A wide variety of bioreceptors have been explored for this purpose, including Abs, nucleic acids, enzymes, phages, whole cells and biomimetic materials[91]. The bioreceptor provides the selectivity to the sensor. A special case are the biocatalytic biosensors, in which the biological elements involved in the reaction are enzymes or enzyme suppliers (such as tissues, cells, microorganisms) that also catalyse the chemical reaction and amplify the product formed in the detection[92].

The purpose of the transducer is converting the physicochemical changes, occurred at the biosensor surface because of the biorecognition event, into a measurable electrical signal. This signal should be proportional to the concentration of the analyte of interest and could be displayed by a signal processor or a reader device in a user-friendly way[93] (Figure 2.3). Biosensors are classified according to the signaling mechanism of the

transducer element into optical (e.g., surface plasmon resonance (SPR), chemiluminescence, fluorescence, colorimetry), electrochemical (e.g., volta-amperometry, potentiometry, conductimetry, impedance, field effect transistor (FET)), thermometric, magnetic and gravimetric (e.g., quartz crystal microbalances (QCM), cantilevers, surface acoustic waves (SAW)). In all cases, efforts are continuously made to produce increasingly sensitive, specific, rapid and portable biosensors, compatible with the study of complex samples, such as whole blood, and requiring minimal sample preparation prior to the analysis[94,95]. Moreover, the ability to miniaturize the different components of many biosensor types facilitates the fabrication of small, cheap and easy-to-use devices for their implementation in POCT.

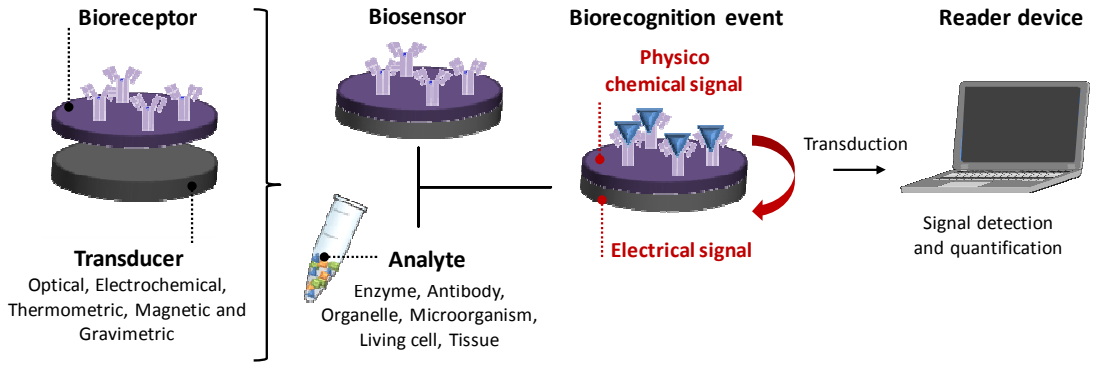

Figure 2.3. Schematic representation of a biosensor

2.2.2. Characteristics of electrochemical biosensors

Electrochemical biosensors are based on the measurement of changes in the electrochemical properties of the sensor-sample interface, and the relationship between these changes and the concentration of a given analyte in the vicinity of the sensor. Electrochemical sensors are classified according to the parameter measured into amperometric (measuring current flow), potentiometric (measuring changes in potential or charge accumulation), conductometric (measuring variations in the conductivity between two electrodes, for instance caused by changes in the conductive properties of the medium) and impedimetric (which measure impedance)[96,97] (Figure 2.4). Such changes are often produced by the confinement of electro-active species at the surface of the sensing electrode. These species are bound, produced, or consumed as a result of the reaction between the (bio)receptor and the target analyte, and their concentration is proportional to the concentration of the analyte studied[98].

Amperometric and voltammetric biosensors measure the current resulting from the electrochemical oxidation or reduction of an electroactive species in a biochemical reaction, which concentration is proportional to the concentration of the target analyte in the analyzed sample[99]. These biosensors operate by applying a controlled potential to the working electrode (WE) with respect to a reference electrode (RE). While amperometric sensors operate at a fixed potential, in voltammetry the current response is measured as a function of a potential that is adjusted either step by step or continuously. The resulting current is directly correlated to the bulk concentration of the electroactive species or its production or consumption rate within the adjacent biocatalytic layer. The best example of a commercially available amperometric biosensor is the glucose meter[100]. Amperometric sensing has numerous advantages in terms of low-cost, simplicity and maturity of the measurement technology employed[101]. Among its drawbacks, it could be cited that amperometric detection requires a certain control over the reaction solution temperature, pH and composition to obtain stable and reproducible results. Although the accurate selection of the potential applied imposes selectivity to the measurement, the presence of non-target molecules displaying electroactivity in a similar potential window will affect detection, which is of special importance for the analysis of complex samples of unknown composition. Accordingly, amperometry is frequently employed for indirect analyte detection, by employing well-characterized labels in detection solutions on controlled composition.

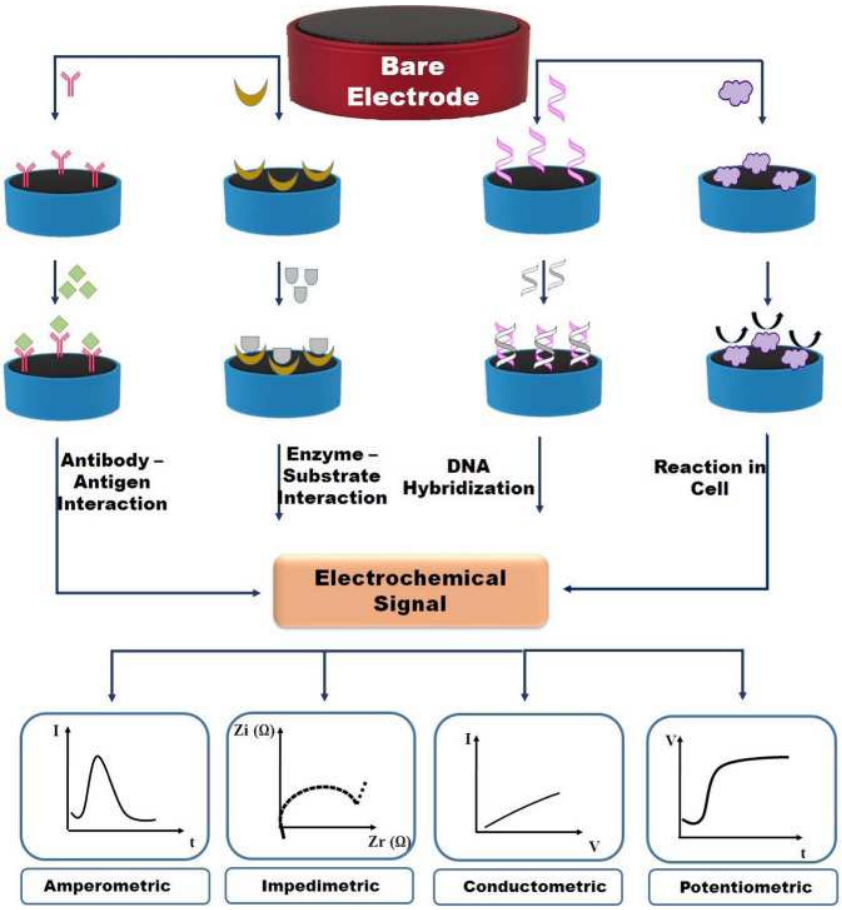

Figure 2.4. Schematic representation of different types of electrochemical biosensors, classified according to the bioreceptor and detection strategy. Reprinted from ref. [102] with permission from Elsevier, Copyright 2015**.**

On the other hand, potentiometric biosensors measure potential changes between the WE and RE when there is no significant current flowing through them. The potentiometer provides also information about the ion activity in an electrochemical reaction[103]. Common types of potentiometric electrochemical biosensors are an ion-selective electrodes (ISE) and field effect transistors (FET). ISE include an ion-selective membrane that allows passing through only the ion that is to be detected. The selective diffusion of the analyte produces a differential accumulation of ions at the two sides of the membrane, whereby a potential difference is generated. The best-known ISE is probably the pH meter. FETs consist of a selective membrane integrated over a transistor gate, which modulates the current from a source in response to analyte interaction. The electrical noses and the electrical tongues are FET sensors. Potentiometric applications are advantageous for the detection of species that are not electroactive *per se*[104].

Conductometric electrochemical biosensors measure changes in conductivity of an electrolyte solution resulting from differences in the ionic charges due to changes in their mobility or composition in response to the chemical reaction. A conductometric electrochemical biosensor consists of two metal electrodes separated by a constant distance, and do not require the use of a RE. In general, conductivity offers a fast, reliable, non-destructive and inexpensive measurement of the ionic content of a sample. Furthermore, conductometric sensors are insensitive to light and medium turbidity, suitable for miniaturization and applicable to the detection of a wide range of compounds[105]. However, conductivity does not distinguish between different types of ions, quantifying instead the combined effect of all ions present. Besides, conductivity is measured less accurately as the concentration of salts or ions increases in samples. Therefore, these sensors are regularly used to monitor solutions of known composition or to study relatively pure (single solute) preparations.

Impedimetric electrochemical biosensors allow monitoring the changes in both bulk and interfacial electrical properties of the electrode system[106]. In this way, the biorecognition event can produce changes in different parameters measurable by electrochemical impedance spectroscopy (EIS), which are electrolyte resistance, adsorption of electroactive species, charge transfer at the electrode surface, and mass transfer from the bulk solution to the electrode surface. Impedance can be measured in the presence (faradic EIS) or in the absence (non-faradic EIS) of a redox couple. In faradic biosensors, the biorecognition event that takes place at the electrode surface produces changes in the faradaic current (interfacial electron transfer resistance), either by modifying physically the access of the label to/from the electrode surface, or by inducing its electrostatic attraction or repulsion. Non-faradaic EIS, on the other hand, provides label-free detection. However, it displays also decreased sensitivity compared to label-included biosensors[106]. EIS exhibits several advantages, including that it is an extremely sensitive and non-destructive technique. Impedance sensors are easily miniaturized and integrated into multi-array diagnostic tools, are compatible with the development of remotely controlled implanted sensors, and imply the use of potentially mass-produced electrodes and cost-effective instrumentation that does not need high-energy sources. However, numerous requirements have to be accomplished in order to obtain a valid impedance spectrum, which depend not only on the technical precision of the instrumentation, but also on the operating procedures. This makes that impedimetric

biosensors often exhibit limited detection limits, low reproducibility between devices and independent measurements, and also limited performance in complex matrices such as undiluted biological samples[107].

Many advantages make electrochemical biosensors particularly attractive for their use in POC diagnostics compared with currently available methodologies. They offer high specificity, reproducibility and sensitivity, and the possibility to carry out real-time measurements. Many electrochemical biosensors can work in low operating volumes and with minimal power requirements. On the other hand, both the electrochemical transducers and measurement equipment are relatively easy to miniaturize, which facilitates the production of hand-held or portable, simple and economical instrumentation. One of the key advantages of electrochemical biosensors relies on the possibility to integrate the biosensor with electronics to carry out robust and rapid measurements using miniaturised easy-to-use portable systems[101].

2.2.3. Screen-Printed Electrodes (SPE): miniaturized electrochemical cells to produce disposable electrochemical biosensors

Many electrochemical biosensors consists of a classical three-electrode electrochemical cell comprised of a *reference* electrode (RE), a *working* electrode (WE) and a *counter* or *auxiliary* electrode (CE)[108] (Figure 2.5a). The RE should have a well-defined and stable equilibrium potential and is used as the reference against which the potential of other electrodes is measured in the electrochemical cell. Accordingly, the potential applied to the WE is typically reported "*vs*" the RE used. Some common reference electrodes used in aqueous media include the saturated calomel electrode (SCE), the standard hydrogen electrode (SHE), and the AgCl/Ag electrode. They all have an electrode potential independent of the electrolyte used in the cell and are generally separated from the solution by a porous frit. Since these classical RE use to be bulky devices, miniaturized cells, such as printed and microfabricated electrodes, often include a pseudo-reference (also called quasi-reference) made of a single material, such as a Ag, carbon, Au or Pt. Although pseudo-RE can shift their potential during long measurements, which depends on the current density applied, they can work reasonably well for short measures performed under controlled conditions and are simple to produce and use[109]. Keeping

the RE at a fixed distance from the reaction site is crucial to maintain a stable potential over the measurement.

The WE is the electrode where the pursued reactions take place. It serves as the transducer for the biochemical reaction and is prepared by using a chemically stable conductive material, such as platinum, gold and carbon, which should be redox inert in the potential range of interest. Carbon graphite has been extensively employed for this purpose due to its low fabrication costs, good electrical conductivity, high thermal stability and versatility for the implementation of a diversity of (bio)functionalization strategies.

The CE, often composed of a highly stable metal such as platinum or carbon graphite, completes the electrical circuit. In this way, while the current flows between WE and CE, the RE is used to measure accurately the potential applied relative to a stable reference reaction. The CE is constructed to display larger surface area than the WE to ensure that the reaction occurring at the CE does not interfere or affect those occurring at the WE[97,110].

Classical three-electrode cells are bulky and consume relatively large volumes of sample and/or reagents. Besides, conventional macroelectrodes use to require extensive pre-treatment before its utilization and between independent measurements (such as physical polishing, extensive washing, or electrochemical activation). In recent years, SPEs have become key tools for the development of electrochemical biosensors for POCT, transitioning away from the traditional and more sophisticated strategies based on the use of cumbersome electrochemical cells and bulky electrodes[111] (Figure 2.5b).

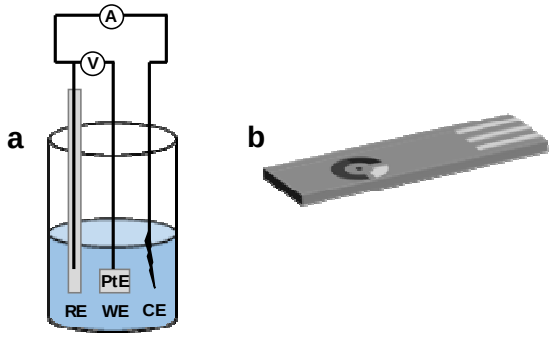

Figure 2.5. (a) A classical three-electrode electrochemical working cell. (b) Disposable SPE.

SPE have gained interest in the electrochemical biosensors' field because they can be mass produced using low-cost and relatively rapid manufacturing procedures with high reproducibility. Furthermore, screen-printing presents the capability to miniaturize the biosensor size, integrating all the electrodes of the electrochemical cell in a single device, providing advantages such as portability, simplicity of operation and reduction of the volume of sample and reagents required. Nowadays, SPEs can be developed in a variety of geometries and materials, which allows great versatility of design, facilitating the development of customized, application-tailored and multiplexed biosensors[112].

In terms of analytical behaviour, SPE present wide linear output, low power requirement, fast response and high sensitivity. Indeed, these disposable electrodes can be used with most commercially available benchtop and portable measuring equipment by employing appropriate connection cables, and have been also extensively coupled to custom-made instruments equipped with USB ports, laptops, smartphones and low-cost potentiostats[113].

Screen-printing consists of stamping the electrodes layer-by-layer by depositing conductive and non-conductive inks through mesh screens. The central steps for the screen-printing process are (1) the design of the screens which will define the geometry, size and relative location of the different components of the SPE (i.e., WE, RE and CE), and (2) the selection of the materials/inks that will be used to print each layer/component, so that their composition and properties are in accordance with the desired application[114]. During the fabrication procedure, a screen is placed onto the substrate and the appropriate paste is squeezed over, penetrating through the perforations of the screen to form the desired patterns. After screen removal, paste/ink drying and temperature-curing steps follow. The electrodes and connection paths are printed using conducting inks, which consist of a mixture of conductive materials with the ability to transfer electrons and binders and additives that provide mechanical properties. The most commonly used material for printing the WE and CE is carbon/graphite, although gold and platinum are also employed. However, pseudo-RE and tracks are mostly produced with a silver or Ag/AgCl paste. Device printing generally includes at least a layer printed with insulating ink, which is used to delimitate the surface area of the electrodes and to protect the connecting tracks from the exposure to samples and reagents. The selection of each material/ink composition may determine the selectivity and sensitivity of the SPE produced and should be decided carefully.

Figure 2.6 shows a simplified scheme of the screen-printing process employed for the fabrication of this type of devices.

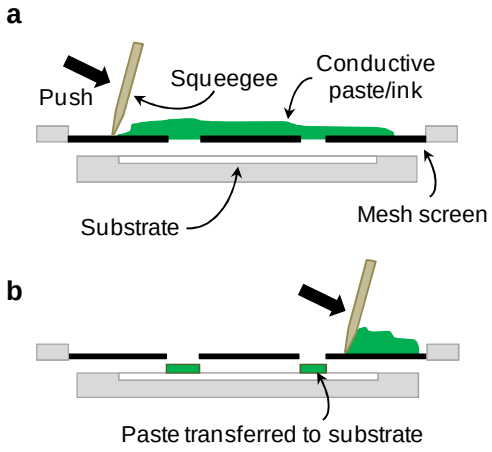

Figure 2.6. Fabrication of SPE using conductive pastes/inks and mesh screens.

The main advantages of this technology are the relatively high design flexibility afforded, potential process automation, good reproducibility, and the wide choice of materials available[115]. For instance, screen-printing can be done on various types of planar material, such as polymer, plastic, ceramic, glass and paper. There are many examples of SPEs based on paper or transparency which were effectively applied to detect a wide variety of analytes[116]. Recent technological advances on SPE include the employment of flexible and stretchable materials as a printing substrate to produce wearable sensors, including tattooed enzymatic sensors, and the optimization of nanostructured devices for enhanced detection. Contrary to classical bulk electrodes, many SPE can be used straightforward, without requiring any pre-treatment such as electrode polishing or electrochemical pre-activation. SPE are compatible with the study of small sample volumes and are easy to integrate in microfluidic systems. In addition, numerus strategies have been reported for the biofunctionalization of SPE, and the planar geometry of SPE has been also exploited for the production of magneto-immunosensors in which there was no necessity to immobilize a recognition element on the WE surface. The recognition element could be in this case immobilized on a separate support (magnetic micro or nano beads) and, at the end of the immunological procedure, beads were placed onto the unmodified WE surface for the electrochemical measurement of the enzymatic product[117].

2.2.4. The use of antibodies (Ab) as affinity binders for the production of immunoassays and electrochemical immunosensors

2.2.4.1. Description of antibodies (Ab)

Abs are glycoproteins from the immunoglobulins (Ig) family, which are naturally produced by the immune system to neutralize potential pathogens, such as bacteria or viruses. Accordingly, Abs are capable of recognizing Ag with high specificity. The most abundant Ab in serum, and the most often used for immunoassay development, is immunoglobulin G (IgG). IgG can be represented schematically as a Y-shaped molecule (Figure 2.7)[118]. The molecule is formed by the assembly of four polypeptide chains – two identical heavy chains (molecular weight ~ 50 kDa each) and two identical light chains (molecular weight ~ 25 kDa each)[119]. The upper branches located at the very ends of the two arms of the Y display the Ag-binding sites. The binding sites of different molecules differ in their amino acid sequence, which makes Ab capable of identifying specific Ag due to their unique binding sites. In this way, the recognition between Ab and Ag takes place by spatial complementarity following what is often described as a lock and key model. The subsequent establishment of the Ab-Ag interaction depends on a combination of weak and non-specific forces, including electrostatic forces, hydrogen bonds and hydrophobic interactions, with stronger van der Waals forces. Figure 2.7 shows the typical structure of and IgG Ab molecule with the Ag-binding sites.

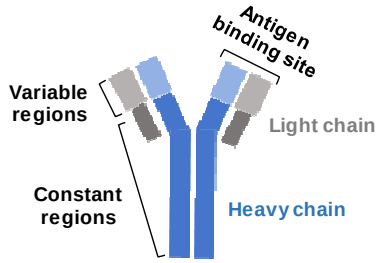

Figure 2.7. Ab structure (IgG type).

There are two the two main types of Ab that are widely used in immunoassay development and commercially available, monoclonal Ab (MAb) and polyclonal Ab (PAb). PAb are produced by immunizing animals with a target analyte, so that its immune system produces Ab in an attempt to neutralise the intruder. After a period of time, the animal is bled to recover its serum, which will contain a collection of antibodies recognising different regions (or epitopes) of the antigenic analyte. The

production of PAb is a highly variable process that displays important batch-to-batch differences. However, PAb are useful in approaches not demanding extremely high detection specificity (such as detection of fast-evolving viral Ags, or simultaneous detection of several isoforms of a protein Ag). On the other hand, MAb are produced *in vitro* by using hybridomas, which are established by fusing an immortal tumour cell line with a single blood cell precursor isolated from the immunised animal. Each hybridoma behaves as a clone and produces a single type of Ab against a single epitope, and this Ab displays high selectivity for its target Ag. This methodology allows the consistent production of high amounts of MAb, with no significant batch-to-batch differences, and reproducible specificity and sensitivity. While MAb are highly specific for a single epitope, diminishing the chance of cross-reactivity, PAb can bind multiple epitopes on an Ag, showing a heterogeneous immunological response. For this reason, the selection of Ab often depends on the analytical application desired[120,121]. The most important properties of Ab that could affect the performance of the immunoassay developed are the strength of the Ab-Ag binding and the level of selectivity and specificity for the analyte[122].

2.2.4.2. Immunoassay types and formats

An immunoassay is a quantitative biochemical method of analysis based on the specific biorecognition of a given Ab for its target Ag. The binding constants of the Ab-Ag interaction can reach up to 10^{11} M and result in extremely selective and sensitive detection, which has made immunoassays a widely accepted analytical method. A broad range of antigenic species can be detected using Ab, including biological macromolecules such as proteins (glycoproteins, nucleoproteins, lipoproteins), peptides, polysaccharides and nucleic acids, but also small molecules (e.g., drugs) and whole cells and viruses, to cite some few examples[123]. However, in most of the cases the binding of an Ab to its Ag does not induce major changes in the medium and is not detectable straightforward. For this reason, an extensive part of the immunoassays employ labels, for instance incorporated or chemically conjugated to a detecting Ab, to perform the indirect detection of the Ag. The label element could be a radioisotope, fluorescent components, metal nanoparticles, enzymes, and other reagents. The most significant label-linked immunoassays are the radioimmunoassay (RIA), the fluoroimmunoassay (FIA) and the enzyme-linked immunosorbent assay (ELISA)[124].

The RIA was the first immunoassay technique developed and it was widely used for many years because of its high sensitivity. In this type of immunoassay, a radioisotope is used as the label, often attached to a competing Ag or to a detecting Ab. Although it is a very sensitive and fast method, the safety problems associated with the use of radioactive substances caused the passage toward safer methods[124].

In FIA the Abs are labelled with fluorescent probes. After incubation with the Ag, the Ab-Ag complexes are isolated, and the fluorescent intensity is measured. An increasing variety and availability of stable fluorophores allows nowadays the simultaneously measurement of multiple molecules with good precision and sensitivity, and the advances in miniaturization of the measurement equipment have enabled fluorescence detection to become a leading method in centralized clinical diagnostic immunoassays[124].

ELISA is the type of immunoassay most widely used by many users in fields as diverse as analytical chemistry, clinical diagnostic, food safety monitoring or environmental control. ELISA consists of the binding of an enzymatic label to the Ab that is used to detect the presence of a specific target Ag. The enzyme catalyses a chemical reaction on an appropriate enzymatic substrate, producing a quantifiable coloured product. The most common enzymes utilized in ELISA are horseradish peroxidase (HRP), alkaline phosphatase (AP), and β-galactosidase.

Generally, an ELISA protocol consists of several consecutive incubations carried out using microtiter plates, which are intercalated with series of washing steps to remove non-specifically or poorly bound components. Depending on the number of steps and reagents used, ELISAs can be grouped into the three main categories, direct, competitive and sandwich assay formats, and all of them can be detected though direct and indirect detection[119,125] (Figure 2.8). In all cases, the assay starts with plate modification and blocking, which provides specificity and prevents non-specific adsorption of non-target components, and finishes with the incubation of an enzyme-labelled detecting reagent. In direct detection, this reagent is an enzyme-labelled d-Ab specific against the Ag. In indirect detection, the d-Ab is incubated first, and a new incubation follows, this time with an enzyme-labelled reagent that will bind the d-Ab. The most widely used indirect detection strategy consist of employing a biotinylated d-Ab (bd-Ab) and a (strept)avidin-enzyme conjugate for detection.

Other strategies include the use of enzyme-labelled secondary Ab (such as anti-mouse Ab for the labelling of MAb) and enzyme-labelled protein A/G. Using indirect detection extends the protocol, but usually provides a certain level of signal amplification as well. In all cases, the amount of enzyme that binds the plate will be proportional to the amount of Ag captured. After a new wash, a colour-less substrate solution is provided, that will trigger the enzymatic activity of the enzyme label, promoting the evolution of a coloured reaction product. In some cases (for instance when exploiting fast enzymatic reactions), the enzymatic reaction is stopped by adding a stopping buffer, usually acid or detergent. Finally, colour development is quantified spectrophotometrically at a specific wavelength and the readout is directly correlated to the presence and abundance of the target Ag. Nowadays, ELISA are completely automated and run by robotized platforms at centralized laboratories in a matter of minutes[126].

Direct ELISA is the most straightforward protocol among the ELISA techniques, needing fewer reagents and steps than any other. First, a volume of the sample that is analysed for the presence of Ag is incubated onto the surface of the microtiter plate to promote the immobilization of its biocomponents. Intensive washing is then performed to remove unbound or poorly bound components, which is followed by plate blocking. Next, a d-Ab that is specific to the Ag is added and incubated. The plate is washed again, a substrate solution is provided, and the enzyme label reacts and develops the colour. Although simple, direct ELISA has certain limitations when dealing with complex samples, in which the attachment of non-target components onto the solid phase introduces a high risk of non-specificity of the assay[126]. For this reason, direct ELISA is usually employed only to characterize and titrate Ab and not for sample analysis.

Competitive ELISA entails a competitive binding process between the Ag in a sample and an add-in modified Ag for a certain number of Ab binding sites. There are two main competition assay formats. In the first one, Ags in the sample compete with enzyme-labelled Ag for binding the Ab immobilized on the plate surface. In the second format, Ag (alone or conjugated to a carrier protein, depending on the size) is immobilised on surface and competes with native Ag in the sample for an enzyme-labelled d-Ab present in solution. The major advantage of a competitive ELISA is that it is useful for the detection of analytes (such as drugs) that are too small to be bound simultaneously by

two Ab in a sandwich assay format, or when only one Ab is available for the target Ag. Competition assays use to be short and still provide high sensitivity and selectivity even in crude or impure samples. However, the signal generated in the competitive ELISA is inversely proportional to the concentration of the Ag, which makes it difficult to identify false positives caused by enzyme-inhibiting interferents [124].

Sandwich ELISA is one of the most commonly used immunoassay format in commercial kits for the quantification of clinical biomarkers. The sandwich ELISA procedure involves the immobilization of a capture Ab (c-Ab) specific for the Ag in the microtiter plate surface. Then, as in the other formats, a blocking buffer covers the unoccupied surface to reduce subsequent nonspecific binding. The sample is next incubated for analyte immunocapture, and unbound components are eliminated by washing. Then, the binding of an enzyme-labelled d-Ab to the analyte forms a sandwich immuno-complex. The enzymatic substrate is incubated, reacts with the enzymatic label, generates the coloured product and the absorbance is measured. The benefit of this protocol is the high specificity and sensitivity of this type of assay. However, it is the most tedious and time-consuming immunoassay format and entails consumption of more reagents as well[124]. Optimizing a sandwich ELISA is complex and appropriate matched pairs of Ab can be very difficult to find.

ELISA is extensively used and is often employed as a “gold-standard” reference method. However, ELISA displays a number of limitations, including the complexity of the assay, the cost of the reagents, the time-consuming operation, and the relatively complex and expensive equipment needed for detection[127].

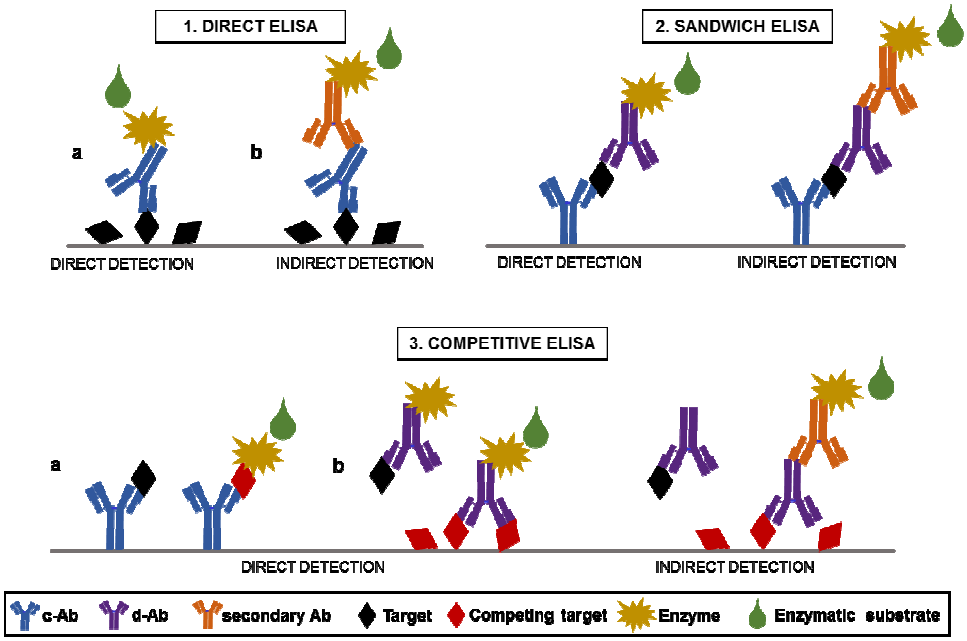

Figure 2.8. ELISA formats. (1) Direct ELISA coupled to either direct (a) or indirect detection (b). (2) Sandwich ELISA with direct or indirect detection. (3) Competitive ELISA with direct detection with (a) Ag-enzyme or (b) Ab-enzyme, and indirect detection.

2.2.4.3. Electrochemical immunosensors: characteristics and types

Electrochemical immunosensors are affinity analytical devices in which the bioreceptors employed to bind the Ag, forming a stable complex, are Ab[96]. The electrochemical transducer detects then the changes produced in the physicochemical properties when the immunocapture reaction occurs (Figure 2.9). Electrochemical immunosensors combine the high affinity, specificity, sensitivity and selectivity provided by the immunorecognition event with the advantages of electrochemical transduction, such as the rapid generation of results, and the low cost, robustness, easiness of use, high compatibility with miniaturization, easiness of integration into portable platforms, and possibility for multiplexing of both electrochemical transducers and measurement equipment. Thanks to these features, electrochemical immunosensors are currently used in clinical diagnosis, environmental monitoring and food safety monitoring, among others[128].

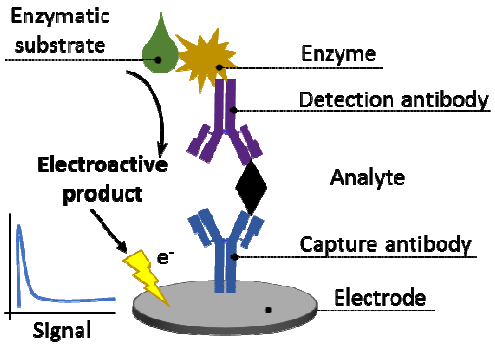

Figure 2.9. Schematic representation of an electrochemical immunosensor based in a sandwich assay format with detection of an enzymatic label.

Compared to current immunoassay methods, electrochemical immunosensors are characterized by their versatility, reliability and fast analysis time, with the possibility to employ handheld devices, which can be used for POCT[128,129]. Electrochemical immunosensors measure the signals resulting from the biorecognition event, in most of the cases using the c-Ab coupled to the transducer surface (WE). The immobilization procedure constitutes a crucial step in the preparation of electrochemical immunosensors. The way the WE is modified conditions the immunoassay strategy applied later on: direct, competitive and sandwich format (with either direct or indirect detection)[130] (Section 2.2.1.1.2). Furthermore, the immobilization strategy affects the sensitivity and stability of the resulting device. Numerous immobilization procedures, both based in non-covalent and covalent interactions, have been employed to achieve a suitable modification of the electrode surface, including biomolecule random physisorption, cross-linking, affinity binding, polymeric entrapment and electrodeposition[131]. Additionally, the increasing interest in nanoscience and nanotechnology have impacted electrode modification, and the use of nanomaterials as electrode modifiers, Ab/tag nanocarriers, nanotags and signal amplifiers has became common in the development of advanced immunosensors. Ideally, a biofunctionalized electrode should display enough amounts of active bioreceptor on surface, the immobilized molecules should be stable during the measurement process, and the immobilization procedure should not have any deleterious effect in signal transduction[132].

On the other hand, according to the detection mode, electrochemical immunosensors can be divided in label-less and label-based (Table 2.2). In label-less electrochemical immunosensors, Ag immuno-binding is directly translated into a measurable signal, and

the incubation with labelled bioreceptor is not required. FET and non-faradaic EIS immunosensors are good examples. In some other cases, the sensor measures in fact the activity of an electrochemical mediator, which evolves proportionally to the physicochemical changes induced by Ag immunobinding on the sensor surface. This is the case of faradaic impedance and some voltametric immunosensors. Label-less electrochemical techniques present short analysis time, simplicity of operation, cost-efficiency and direct acquisition of results[133,134].

Label-based electrochemical immunosensors require first the capture of the Ag by the c-Ab immobilized on the electrode surface and then the addition of a second labelled d-Ab to produce the electrochemical signal. The label is usually an enzyme (AP, HRP) or nanomaterials (metallic or semiconductor particles)[135]. Although entailing longer assay paths, composed of numerous incubation and washing steps, this type of electrochemical immunosensor is more sensitive, specific and versatile than the label-less alternatives.

	Detection	Sensitivity	Specificity	Assay steps	Reusability
Label-based	Electroactive signal generated by the label	High by signal amplification	High (often sandwich assay format)	Several (serial incubation and washing steps; enzyme substrate addition)	Not reusable
Label-less	Physical change in the surface by the biorecognition event	Low for small molecules	Low (often single immunocapture)	Few (ideally, sample incubation and washing)	Regenerated using potential modulation

Table 2.2. Characteristics of label-based and label-less electrochemical immunosensors[136].

Although numerous examples of electrochemical immunosensors have been described in the literature for POCT, most of the examples reported still entail complex protocols, with multiple steps and high level of manipulation by the user, which would difficult to implement for POCT and carry out by poorly trained users[46].

2.3. Magnetic Beads (MB) and the development of electrochemical magneto-immunosensors

2.3.1. MB: types, properties, advantages and drawbacks

MB are one of the most powerful and versatile tools currently used in bioanalytical applications[137–140]. The utilization of MB for the magnetic separation, pre-concentration and/or removal of selected target molecules offers several advantages compared to other

separation strategies, such as filtration, centrifugation or dielectrophoresis, offering the possibility to scale-up relatively easily and compatibility with process automation[18,141,142].

MB display superparamagnetic behaviour, which implies that they are attracted by external magnetic fields, exhibiting zero remanence (non-magnetic state) when the magnetic field stops acting[143,144]. The possibility to confine them magnetically provides relatively fast, efficient, simple and gentle separation and concentration in different types of matrices, allowing washing between solutions[145]. Other advantages of MB are their large surface area and the diverse possibilities of biofunctionalization, because MB are commercially available that display an assortment of reactive groups on surface. MB can be produced locally, or be acquired commercially from a wide range of suppliers, sizes, materials, surface coatings and magnetic properties[146] (Figure 2.10).

Generally, MBs contain a uniform paramagnetic core made of an iron oxide, such as magnetite (Fe_3O_4) or maghemite (γ-Fe_2O_3), widely used because of their facile synthesis, strong magnetic property and biocompatibility. The magnetic behaviour depends on many factors of these core characteristics, as composition, crystallinity and magnetic moment. Besides, MB are coated or encapsulated by a polymeric, proteinic, or silica thin layer that provides stability, reduces metal leakage, facilitates bioengineering, and prevents the nonspecific binding of undesired components[147].

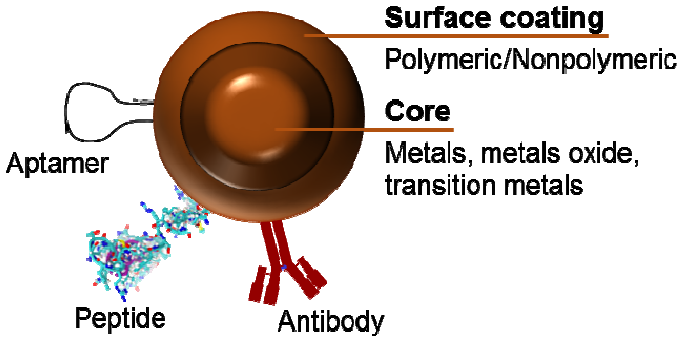

Figure 2.10. Schematic representation of a MB, including the magnetic core, surface coating and conjugated bioreceptors.

MB dimensions may range from the nanometre to the micrometre scale, often 1 - 10 μm in diameter. However, magnetic nanobeads under 200 nm in diameter require special magnetic devices to be manipulated. Such equipment is not available in every laboratory and is less compatible with magneto-immunosensor development and high-

throughput analysis[144]. It is for this reason that micrometric MB are the majoritarian choice when magneto-assays and magneto-sensors are developed.

2.3.2. **MB biofunctionalization**

Nowadays, MB immuno-modification is a relatively easy task because of the significant number of MB commercially available with different functionalities on surface[8,148]. During or after their production, MB can be modified to display on surface different reactive functional groups (amine, carboxyl, hydroxyl, epoxy, tosyl) and (bio)molecules (protein A/G, secondary Ab, (strep)avidin)), which enables the coupling of many biological macromolecules (cells, enzymes, proteins, Ab and nucleic acids) through diverse chemical paths and affinity-binding strategies, and specifically producing immuno-modified MB (Ab-MB).

Covalent linkages are strong and stable bonds, which can be formed between functional groups found on the MB surface and those available in the molecules that should be incorporated. Commercial cross-linking reagents are available for this purpose. The most common chemical strategy is the carbodiimide coupling reaction. In this case, carboxylic acids are covalently linked to primary amines, often using 1-ethyl-3-dimethylaminopropyl carbodiimide (EDC). EDC reacts with carboxylic acid groups to form an active O-acylisourea intermediate. This intermediate is then displaced by nucleophilic attack of primary amino groups, creating an amide bond between the original carboxyl and amino groups, and releasing a soluble urea derivative. Because the O-acylisourea intermediate is unstable in aqueous solutions, the coupling efficiency can be enhanced by the addition of stabilizing agents such as n-hydroxysuccinimide (NHS) or its water soluble counterpart sulfo-NHS. In this case, EDC couples NHS to the carboxyl groups, forming a succinimide ester that is considerably more stable than the O-acylisourea intermediate[149,150]. Other widely used crosslinkers are Sulfo-SMCC (sulfosuccinimidyl 4-(N-maleimidomethyl) cyclohexane-1-carboxylate), which contains an NHS-ester and a maleimide reactive group at opposite ends of a spacer arm and that promoted the reaction between amino and sulfhydryl groups; and glutaraldehyde, a carbonyl (–CHO) reagent that crosslinks two amine groups via Mannich reaction and/or reductive amination.

When these strategies are not possible, MB modified with protein A/G or secondary Ab (e.g. anti-mouse Ab, anti-rabbit Ab) can be used to couple Ab[145]. This functionalization allows a certain degree of Ab orientation on surface, which might improve performance, and require lower amounts of Ab than chemical conjugation[151]. However, A/G proteins may produce cross-reaction binding with any IgG molecules present in the sample, potentially interfering in sandwich assay formats and the study of clinical samples[152]. Finally, biotinylated Ab (or other biotinylated molecules) can be incorporated by affinity binding using MB coated with streptavidin, neutravidin or avidin.

Independently of the procedure chosen for MB modification, the surface of the MB should be physically and/or chemically blocked to inactivate the remaining reactive groups and prevent later non-specific interactions. The most widely used reagents for MB physical blocking are proteins (such as BSA, non-fat dry milk and casein) and polymers (such as dextran and ethylene glycol). On the other hand, chemical blocking after EDC and glutaraldehyde crosslinking can be accomplished using amine-containing small molecules, such as Tris, lysine, glycine, or ethanolamine. In the case of (strept)avidin-biotin binding, the incubation of the modified MB with free biotin is recommended for blocking unreacted biotin-binding sites and prevent subsequent reagent cross-binding[153].

Once MB are immuno-modified, they may display low toxicity, high biocompatibility, and chemical and physical stability for weeks if stored at 4ºC[148].

2.3.3. **Magneto-immunoassay optimization**

Considering the advantages of MB commented above, three features determine magneto-immunoassay performance. First, the large MB surface-to-volume ratio, which facilitates coupling many bioreceptor molecules. Second, the constant rotation/shaking during incubations needed to prevent MB sedimentation, which grant active sample mixing and efficient Ag binding as well. Third, the superparamagnetic properties of the MBs, which allow magnetic concentration, supernatant removal after incubation or washing, and the performance of serial incubations in different solutions. The combination of these factors provides enhanced assay sensitivity, reduced reaction times, requirement of small volumes of samples and reagents, and efficient performance even in complex sample matrices (Figure 2.11) [154].

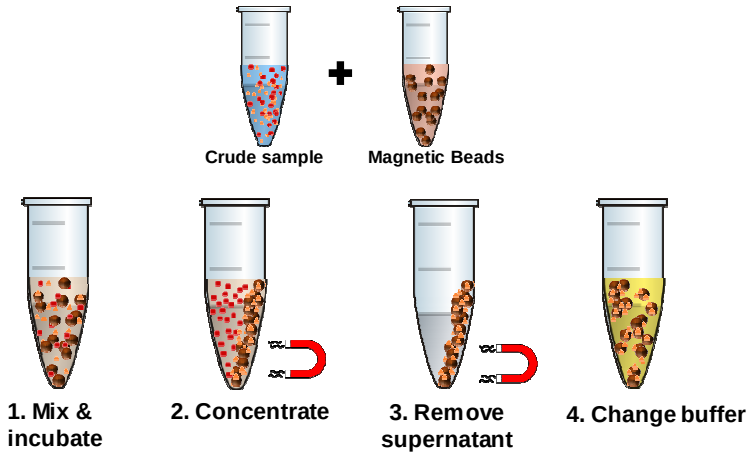

Figure 2.11. Basic steps of a magneto-immunoassay. The magnetic properties of MBs allow that, after incubation in agitation with a sample, MB are concentrated using a magnet. The sample and non-bound sample components can then be removed for MB washing and resuspension in the buffer of choice.

Nevertheless, magneto-immunoassay optimization has to be carried out step-by-step to achieve optimal results. One of the parameters that should be studied is the amount of MB used per sample, which is decisive for magneto-immunoassay performance. In general, increasing amounts of Ab-MB provide higher signals and faster assays, which reflect the higher availability of Ab and better mixing with the sample. The assay reproducibility is also improved, which is often attributed to enhanced MB magnetic recovery after incubation and washing[148].

Other parameters that can have an important effect on assay performance and should be optimized for each immunoassay are sample volume, immunocapture time and conditions, number of washings and washing buffer, or procedure for real sample dilution, with a wide variety of magneto-immunoassay conditions having been employed.

For instance, sample volumes between 50-100 μL are common when studying biological samples such as blood or urine, while detection of bacteria and environmental pollutants often entails the study of 0.5-1.0 mL sample volumes. Although increasing sample volumes display a higher total amount of target molecules, they may also augment the volume of reagents needed, the time required for efficient MB concentration on the magnet, and consequently the final assay cost and time.
On the other hand, while incubations at room temperature produce lower levels of non-specific adsorption, some few works reported enhanced immunobinding at 35-37ºC[147,155].

Because MB sediment over time, Ab-MB incubation is commonly carried out under agitation to maintain MB suspended in the solution, for which mixing wheels, tilt rotation or vortex-like shaking (such as using a thermomixer) can be employed[156]. Finally, series of washing steps with a detergent-supplemented buffer (e.g., 0.01–0.1% Tween-20) are usually implemented. For studies of complex samples or hydrophobic analytes, 5-minute washings performed under agitation may be needed to remove non-specifically adsorbed molecules.

Many authors have shown the advantages of using MB for immunoassay development compared to classical assay formats. Table 2.3 displays a selection of magneto-immunoassays reported previously, priorizing those having been tested in real samples or real sample matrices.

Assay format	MB	Time of functionalization	Target	Label	Assay steps	Assay time	Substrate	Detection time	Assay range	LOD	Samples	Ref.
Sandwich	MB-COOH	2 h 30min	DNMT1	HRP	3	4 h 30 min	Luminol-H_2O_2-BIP	-	0.5 - 128 ng mL^{-1}	0.01 ng mL^{-1}	36 lung cancer serum samples	157
Sandwich	MB-COOH	30 min	CEA	TiO_2/SnOx–Au	2	1 h 20 min	TMB	6 min	5 pg mL^{-1} - 2.5 ng mL^{-1}	5 pg mL^{-1}	5 human serum samples	158
Sandwich	MB-COOH	8 h	IL-6	CeO_2 spheres	2	1 h	OPD	30 min	0.0001 - 10 ng mL^{-1}	0.04 pg mL^{-1}	5 serum samples	159
Sandwich	MB-COOH	1 h	HBsAg	AP	2	1 h	AMPPD	20 min	1 - 200 ng mL^{-1}	0.1 ng mL^{-1}	35 human serum samples	160
Sandwich	MB-COOH	23 h	PA	HRP	2	35 min	Luminol-PIP-H_2O_2	5 min	0.05 - 1000 ng mL^{-1}	0.01 ng mL^{-1}	6 human serum samples	161
Sandwich	MB-COOH	21 h 30 min	NGAL	EU^{3+}	1	1 h	-	-	10 - 1500 ng mL^{-1}	0.32 ng mL^{-1}	115 urine samples	162
Sandwich	MB-COOH	6 h 30 min	CEA	EU^{3+}	3	1 h	-	5 min	1 - 1000 ng mL^{-1}	0.5 ng mL^{-1}	239 human serum samples	163
Sandwich	MB-COOH	28 h 30 min	PSA	GO	2	2 h	HQ	10 min	0.1 - 10 ng mL^{-1}	4 ng mL^{-1}	Human serum samples	164
Sandwich	MB-COOH	1 h 15 min	CEA	AuNP-HRP	2	45 min	TMB	15 min	6 - 781 ng L^{-1}	12 ng L^{-1}	8 human serum samples	165
Sandwich	MB-COOH	15 h 30 min	HE4	AP	1	30 min	Lumigen APS-5	-	0 - 1000 pmol L^{-1}	1.35 pmol L^{-1}	60 human serum samples	166
Sandwich	MB-strept	30 min	TBA15, TBA29	AuNP	2	1 h 30 min	-	-	27 pM to 27 nM	0.27 pM	Foetal bovine serum	167
Sandwich	MB-strept	1.5 h	HER-2, HE4, CA15-3	Eu^{3+}, Tm^{3+} and Lu^{3+}	2	2 h	HNO_3	15 min	12 - 1000 ng mL^{-1}, 8 - 2000 $pmol^{-1}$, 5 - 200 U mL^{-1}	3.94 ng mL^{-1}, 2.59 pmol L^{-1}, and 1.62 U mL^{-1}	Human serum samples	168
Sandwich	MB-NH_2	1h 15 min	HP	DyLight 488	2	3 h 16 min	-	-	0.2 - 3.0 mg mL^{-1}	AD patients 3.03 ± 0.85 mg mL^{-1}, controls 1.23 ± 0.26 mg mL^{-1}	40 human plasma samples	169
Sandwich	MB-NH_2	20 h	PSA	GOx-AuNP	2	1 h	SQA	30 min	1.0 pg mL^{-1} - 30 ng mL^{-1}	0.5 pg mL^{-1}	12 human serum samples	170
Sandwich	MB-NH_2	29 h	PSA	CAT-AuNP	3	1 h 30 min	TMB	30 min	0.05 - 20 ng mL^{-1}	0.03 ng mL^{-1}	12 human serum samples	171

Sandwich	MB-NH_2	4 h 30 min	CEA	nSe-QDs	2	2 h	Formic acid	10 min	0.02 - 100 ng mL^{-1}	0.006 ng mL^{-1}	3 human serum sample	172
Sandwich	MB-tosyl	36 h	HRPII	HRP	2	2 h	TMB	30 min	1.31 - 62.5 ng mL^{-1}	1.31 ng mL^{-1}	12 human serum samples	173
Sandwich	MB-tosyl	6 h	Survivin	HRP	1	1 h	Luminol-H_2O_2	-	0 - 200 ng ml^{-1}	0.949 ng ml^{-1}	Urine samples: 200 BC, 81 RCC and 114 healthy	174
Sandwich	MB-boronic acid	-	AFP, CEA	AuNP and AgNP	3	4.5 h	Formic acid	10 min	0.2 - 50 ug mL^{-1}	0.086 µg L^{-1} and 0.054 µg L^{-1}	3 human serum samples	175
Sandwich	MB-antiFITC	-	CEA	HRP	2	1 h 40 min	Luminol-H_2O_2	5 min	5 - 250 ng mL^{-1}	0.61 ng mL^{-1}	2 human serum samples	176
Sandwich	MB-protein G	-	HCMV	HRP	3	3 h	TMB	10 min	90 - 700 pgmL^{-1}	90 ± 2 pg mL^{-1}	3 human urine samples	177
Sandwich	MB	5 h	PSA	GQDs@Ag	2	4 h	H_2O_2	10 min	1 pg mL^{-1} - 20 ng mL^{-1}	0.3 pg mL^{-1}	5 human serum samples	178
Competitive	MB-protein G	10 min	COC	HRP	2	50 min	TMB	20 min	0.01 - 50 ng mL^{-1}	0.09 ng mL^{-1} (urine), 0.15 ng mL^{-1} (saliva), 0.06 ng mL^{-1} (serum)	Urine, saliva and serum samples	179
Competitive	MB-COOH	26 h 30 min	IgG	HRP	2	1 h	Luminol and H_2O_2	-	0.2 - 4.0 nM	2.9 × 10−11 M	5 human serum samples	180
Competitive	MB-antiCD3	-	CD4	HRP	2	1 h	TMB	30 min	3 - 979 CD4 cells μL^{-1}	50 CD4 + cells μL^{-1}	Whole blood sample	181
Direct	MB-COOH	10 h	HBV, HCV, HIV	SA-AP	2	1 h	AMPPD	5 min	-	10 HBV copies, 10 HCV copies, 100 HIV copies	12 Human serum samples	182

Table 2.3 Examples of magneto-immunoassays reported in the bibliography that have been validated by studying clinical samples or real sample matrices.*****AD, Alzheimer's disease; AFP, alpha-fetoprotein; AgNP, silver nanoparticles; AP, alkaline phosphatase; AMPPD, 3-(2′-spiroadamantane)-4-methoxy-4-(3′-phosphoryloxy)phenyl-1,2-dioxetane; AuNP, gold nanoparticles; BD, bladder cancer; BCIP, 5-bromo-4-chloro-3-indolyl phosphate; CA, cancer antigen; CAT, catalase; CEA, carcinoembryonic antigen; COC, cocaine; DNMT1, DNA methyl transferase 1; EU3, europium (III); GO, glucose oxidase; GQD, graphene oxide quantum dots; HBV, hepatitis B virus; HBsAg, hepatitis B surface antigen; HCMV, human cytomegalovirus; HCV, hepatitis C virus; HE4, human epididymis protein 4; HER2, human epidermal growth factor receptor 2; HIV, human immunodeficiency virus; HP, Haptoglobin; HQ, hydroquinone; HRP, horseradish peroxidase; IgG, human immunoglobulin G; ICP-MS, Inductively coupled plasma mass spectrometry; IL-6, interleukin-6; NGAL, neutrophil gelatinase-associated lipocalin; OPD, o-phenylenediamine; PA, human prealbumin; PIP, p-iodophenol; PSA, prostate specific antigen; QDs, quantum dots; RCC, renal cell carcinoma; SA-AP, streptavidin-modified alkaline phosphatase; SERS, surface-enhanced Raman scattering; SQA, squaric acid; Strept, streptavidine; TA, thrombin aptamers; TMB, 3,3′,5,5′-tetramethylbenzidine; UCNPs, upconversion nanoparticles

2.3.4. **Electrochemical magneto-immunosensor development**

An attractive approach for the use of MB is the combination with SPE to develop inexpensive and portable electrochemical biosensors with (bio)analytical application[14,183,184]. Electrochemical magneto-immunosensors exploit MB as the solid phase to separate and concentrate the Ag/Ab complex and enhance analyte binding, and electrochemistry to provide a fast and quantitative detection (Figure 2.12)[185]. In this way, electrochemical magneto-immunosensors circumvent some of the main drawbacks of conventional immunosensors.

Generally, classical electrochemical immunosensors are based on the direct immobilization of the cAb at the sensor surface (WE), which is followed by blocking to prevent subsequent non-specific adsorption[186]. This procedure provides specificity to the sensor, but entails also some drawbacks, such as passivation of the sensing surface, resulting in poor electron transfer, reduced electrochemical signal and limited or null sensor reusability.

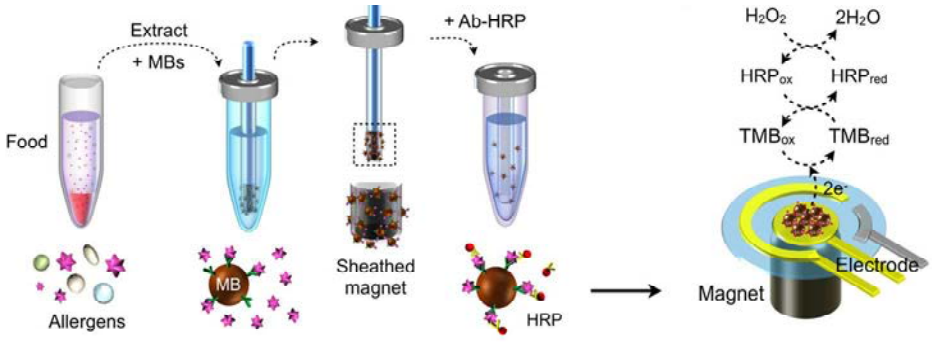

Figure 2.12. Magneto-immunosensor performance. Adapted with permission from ref. [187] with permission from the American Chemical Society, Copyright 2017.

In this context, the production of magneto-immunosensors provides several advantages[13,188,189]. Chiefly, the majority of the electrochemical magneto-immunosensors entail a magneto-immunoassay performed off-chip. Then, the MB are magnetically confined onto the electrode surface for the detection with the assistance of an external magnetic field. After detection, MB can be easily re-suspended in solution by re-positioning or removing the magnet. This makes it easy sensor regeneration and reutilization, and guarantees that a bare (non-passivated) electrode is used for detection, which improves the performance of the electrochemical biosensor. In addition, using MB facilitates immunoassay optimization, standardization of the electrochemical detection protocol, and successful target detection in real sample matrices compared to

classical biosensing[190,191]. Accordingly, magneto-immunosensors allow a relatively easy, fast and cost-effective detection, with a high sensitivity and specificity[192]. Table 2.4 shows examples of magneto-immunosensors reported for the detection of several analytes in different types of real samples.

The clue parameters when optimizing an electrochemical magneto-immunosensor are the magneto-immunoassay itself, the type of electrode used for detection, the strategy for MB magnetic confinement onto the WE and the amount of MB used per sample, which might be different from the optimal quantity for colorimetric monitoring. In this respect, the confinement of too many MB onto the electrode surface might contribute to its partial sheltering and affect negatively the electrochemical transduction. Several authors have reported that better detection of low analyte concentrations and lower LOD are attained with intermediate MB loads, which suggests that using as many beads as possible is not necessarily the best solution[151,193].

Detection	Assay format	MB	Time of funcionalization	Target	Label	Assay steps	Assay time	Substrate	Assay range	LOD	Electrode	Samples	Ref.
Amp.	Sandwich	MB-COOH	2 h 45 min	IL-13Rα2	HRP	3	1 h 15 min	HQ	3.9 - 100 ng mL^{-1}	1.2 ng mL^{-1}	C	Raw cell lysates	194
Amp.	Sandwich	MB-COOH	12 h 30 min	CA15-3	HRP	1	14h 40 min	HQ	10 - 1000 µU mL^{-1}	6 µU mL^{-1}	MFS - C	6 human serum samples	195
Amp.	Sandwich	MB-COOH	3 h 10 min	TGF-β1	Poly-HRP	3	1 h 20 min	HQ	15 - 3000 pg mL^{-1}	10 pg mL^{-1}	C	2 serum samples	196
Amp.	Sandwich	MB-COOH	2 h 35 min	PR, Era	HRP	3	2 h 10 min	HQ	313 ng mL^{-1} - 2.0 mg mL^{-1}	22 pg mL^{-1}	C	Spiked human serum samples	197
Amp.	Sandwich	MB-COOH	2 h	CD105	HRP	1	30 min	HQ	0.8 - 10.0 ng mL^{-1}	0.2 ng L^{-1}	C	4 human serum samples	198
Amp.	Sandwich	MB-COOH	2 h 15 min	β-LG	HRP	2	1 h	HQ	2.8 - 100 ng mL^{-1}	0.8 ng mL^{-1}	C	Spiked milk samples	199
Amp.	Sandwich	MB-COOH	2 h 15 min	IL-6	Poly-HRP	3	1 h 30 min	HQ	1.75 - 500 pg mL^{-1}	0.39 pg mL^{-1}	C	Spiked urine samples and 3 human saliva samples	200
Amp.	Sandwich	MB-COOH	2 h 35 min	TNFa	HRP	3	2 h 10 min	HQ	5 pg mL^{-1} - 5 mg mL^{-1}	2.0 pg mL^{-1}	C	Spiked human serum samples	201
Amp.	Sandwich	MB-tosyl	36 h	HRP2	HRP	2	2 h	HQ	0 - 250 ng mL^{-1}	0.36 ng mL^{-1}	C	Spiked human serum samples	173
Amp.	Sandwich	MB-tosyl	1 h 45 min	HBsAg	AuNPs	2	1 h	HCl	0 - 1000 mIU mL^{-1}	3 mIU mL^{-1}	C	5 human serum samples	202
Amp.	Competitive	MB-COOH	2 h 50 min	Fib	HRP	2	1 h 30 min	HQ	-	0.044 µg mL^{-1}	C	Spiked human plasma samples	203
Amp.	Competitive	MB-protein G	30 min	TC	-	1	30 min	HQ	12.5 - 676.2 ng mL^{-1}	44 ng mL^{-1}	C	Spiked milk samples	204
Amp.	Competitive	MB-protein A	10 min	T	HRP	1	45 min	HQ	5.0 pg mL-1 - 50 ng mL^{-1}	1.7 pg mL^{-1}	C	Spiked human serum samples	205
SWV	Competitive	MB-COOH	3 h 30 min	OP-BChE	QDs	2	1 h	-	40 - 70 nM	0.5 nM	C	6 plasma samples	206

SWASV	Sandwich	MB-tosyl	14 h	ApoE	CdSe@ ZnS@ QDs	5	1 h 25 min	NaOAc	0 - 200 ng mL^{-1}	12.5 ng mL^{-1}	PDMS MFS - C	Human plasma samples	[207]
DPV	Sandwich	MB-protein A	1 h 10 min	HER2	AP	3	1 h 30 min	1-naphthyl phosphate	0 - 30 ngmL^{-1}	6 ng mL^{-1}	C	9 human serum samples	[208]

Table 2.4 Examples of magneto-immunoassays reported in the bibliography that have been validated by studying clinical samples or real sample matrices. *α-LA, alpha-lactalbumin; AP, alkaline phosphatase; Amp., amperometry; ApoE, apolipoprotein E; AuNP, Gold Nanoparticles; β-hCG, human chorionic gonadotropin; β-LG, β-lactoglobulin; C, Carbon; CA15-3, carbohydrate antigen 15-3; CdSe@ZnSQDs, cadmium-selenide/zinc-sulfide@quantum dots; CD105, endoglin; CEA, carcinoembryonic antigen; CNT, Carbon nanotubes; CV, cyclic voltammetry; DPV, differential pulse voltammetry; Era, estrogen receptor a; FBS, Fetal bovine serum; Fib, fibrinogen; Fe(C5H5)2, Ferrocene; FMDV, foot-and-mouth disease virus; HBsAg, Hepatitis B surface antigen; HCl, hydrochloric acid; HER2, human epidermal growth factor receptor 2; HE4, human epididymis protein 4; HQ, hydroquinone; HRP, horseradish peroxidase; HRP2, histidine-rich protein 2; HuSA, human serum albumin; IL-13Rα2, IL-13 receptor Rα2; IL-6, Interleukin-6; MB, Magnetic Beads; MFS, microfluidic system; NaOAc, Acetate solution; OP-BChE, Organophosphates- butyrylcholinesterase; PDMS, Polydimethylsiloxane; PR, progesterone receptor; PSA, prostate-specific antigen; p.f. HRP2, Plasmodium falciparum histidine-rich protein 2; Py/Py-COOH, poly(pyrrole-co-pyrrole-2-carboxylic acid; Strept, Streptavidine; SWASV, Square wave anodic stripping voltammetry; SWV, Square wave voltammetry; S.typhi, Salmonella typhimurium; T, testosterone; TC, tetracycline; TMB, 3,3′,5,5′-Tetramethylbenzidine; TNFα, tumor necrosis factor-alpha; TTEG, tetraethylene glicol.

2.3.5. Signal amplification strategies for magneto-immunoassays and magneto-immunosensors

Attempts have been made to improve magneto-immunoassay / magneto-immunosensor sensitivity by employing nanomaterial-, enzyme- and DNA-based signal amplifiers[68]. Since most analytes do not generate signals *per se*, their magneto-immunodetection is often accomplished indirectly by using a dAb modified with a signal-producing tag. Most magneto-immunoassays reported to date depend on the utilization of enzyme labels. In this context, the oldest and simplest signal amplification strategy has been for long the utilization of a biotinylated Ab for detection (bdAb), followed by incubation with a (strept)avidin-bound enzyme[209]. Over the last years, a battery on new reagents and nanomaterials have been increasingly used in the field as signal amplifiers. Although their use is still limited, the results claimed suggest that some of these components will provide in future enhanced magneto-immunoassays, in some cases faster and more sensitive than those achieved using classical tags.

2.3.5.1 Nanomaterials used as electroactive tags

In recent years, there has been increasing interest in using nanomaterials as enzyme mimetics and nonenzymatic labels[210–212]. Some examples involve noble metal nanoparticles (MNP), carbon nanomaterials, semiconductor nanocrystals (or QD), metal oxide nanostructures, and hybrid nanostructures, which in some instances have provided LODs 10 times lower than those registered using classical Ab-enzyme conjugates[210,213]. Compared to classical Ab-enzyme conjugates, nanomaterials display high surface-to-volume ratios and higher storage stability in a wider range of conditions. Besides, the production and modification of nanomaterials can be tailored to control their final properties and characteristics. Consequently, highly efficient nanotags can be produced that exhibit on surface elevated numbers of Ab, increasing the possibility of Ab-Ag binding, as well as numerous label units able to provide signal amplification. In this respect, either electroactive molecules such as thionine, ferrocene derivatives, and methylene blue, and the nanomaterial itself have been employed for signal generation.

In spite of the many advantages described, the utilization of nanotags in magneto-immunoassays faces also a number of drawbacks[211]. For instance, the employment of nanomaterials, such as MNP and QD, as electroactive tags are usually accomplished by stripping voltammetry after metal (electro)dissolution in acidic solution, a procedure

that can damage the MB and release the iron content. Accordingly, the magneto-immunocomplexes are often disrupted with acid, allowing MB removal previous to the electrochemical detection[214]. Although some teams have demonstrated that non-acidic detection is possible as well[215,216], this strategy involves in any case the addition of a reagent and is not necessarily shorter or simpler that using an enzyme label. The employment of QD as fluorescent labels faces also the potential interference and auto-fluorescence produced by MB. Therefore, as before, most examples reported release the QDs before detection by treating the complexes with acidic or basic buffers supplemented with urea, which enhances the resolution of the assay but extends the detection protocol[217,218]. In addition, most nanomaterials have a strong tendency to aggregate in saline solutions, which makes difficult their direct utilization in biological sample matrices. On the other hand, many QD are made of potentially toxic heavy metal ions (e.g. Cd^{2+}), which may hamper their practical application. Another factor that should be considered is the effect of nanotag nonspecific binding. Because nanomaterials provide important levels of signal amplification, their nonspecific interaction with either MB or target molecules might produce significant signals and ultimately result in biosensor lack of reliability[210].

2.3.5.2 Detection based on enzyme labels

Magneto-immunoassays are often done by using a dAb modified with enzymatic signal-producing tags. Among them, HRP is a relatively inexpensive and small molecule (around 45 kDa), for which numerous spectrophotometric, fluorescent and electrochemical substrates have been described. A classical substrate for HRP is a mixture of hydroquinone (HQ) and hydrogen peroxide (H_2O_2), in which HRP catalyses the reduction of H_2O_2 coupled to the oxidation of HQ into benzoquinone (BQ), and BQ is then reduced back to HQ at the WE surface. However, HQ and BQ are highly toxic. Safer 3,3',5,5'-tetramethylbenzidine (TMB) and 2,2'-azino-bis(3-ethylbenzothiazoline-6-sulphonic acid (ABTS) are extensively used for immunoassay spectrophotometric detection and are commercially available as ready-to-use solutions. Some of these have been exploited for HRP electrochemical detection, with some TMB ready-to-used substrate solutions having produced results comparable to HQ, and ABTS preparations generating signals 10-15 times lower but wider assay linear ranges[219].

Another widely employed enzyme tag is AP, generally using α-napthyl phosphate (α-NPP), 4-nitrophenol phosphate, or phenyl phosphate as the substrate, coupled to the oxidation of the corresponding product (α-naphthol, 4-nitrophenol and phenol, respectively) at the electrode surface. AP is bigger (80-150 kDa), more expensive and more sensitive to chemical modification than HRP, and most of its enzymatic products produce electrode passivation. Nevertheless, many authors claimed slightly more sensitive detection using AP (LODs between 5 pg mL^{-1} and 3.74 ng mL^{-1}) than HRP (LODs from 21 pg mL^{-1} to 6 ng mL^{-1}).

Ab modification allows for the incorporation of a limited number of enzyme molecules. Signal amplification strategies have been reported, such as the use of (strept)avidin-enzyme conjugates, Ab-enzyme coated nanomaterials, and polymeric streptavidin-enzyme complexes such as Poly-HRP[220,221].

The (strept)avidin-biotin technology relies on the extremely high and specific affinity of (strept)avidin for biotin ($Kd \approx 10^{-14}$ - 10^{-16} M). Some of the drawbacks classically related to these systems, such as the high levels of nonspecific adsorption typically reported for avidin, a glycosylated protein that displays an isoelectric point (Ip) of approximately 10, have been solved over the last years as new engineered (strept)avidin molecular derivatives have been produced and commercialized (such as extravidin and neutravidin, both with neutral Ip, commercialized by Sigma-Aldrich and Invitrogen - Thermo Scientific, respectively). (Strept)avidins are also exceptionally stable proteins. In addition, using indirect (strept)avidin-biotin detection strategies, the experimentalist uses a bdAb that has suffered a less severe modification than an enzyme-conjugated counterpart. Hence, lower amounts of biocomponents are usually needed, which also provide improved performance. Besides, each bdAb can be bound by more than one (strept)avidin molecule, which may display on surface more than one enzyme unit. Accordingly, this indirect detection strategy typically results in signal amplification compared to direct detection using an Ab-enzyme. On the contrary, indirect detection implies extending the assay with additional incubation and washing steps compared to direct detection using an enzyme-labelled Ab, without forgetting that signal amplification works for both specific and nonspecific signals.

Recently, a number of nanomaterials have been also explored in the field as enzyme-loaded signal amplifiers. Enzyme coated nanomaterials display enhanced catalytic

reaction activity by orders of magnitude. Several nanomaterials have been used with this purpose, including various MNP, semiconductors, carbon nanomaterials, softer dendrimers, or even biologically derived materials. Among them, quantum dots (QDs) and gold nanoparticles (AuNPs) are the most extensive used. QDs provide access to a plethora of unique quantum-confined properties including narrow, size-tunable photoluminescence (PL) coupled to broad absorption spectra and the capacity to induce resonance energy transfer. AuNPs can be produced in a wide range of sizes with particular SPR behavior, and even PL for the smallest cluster materials. In all cases, nanomaterial modification with an enzyme requires the previous study of its surface chemistry in order to select the best fitting functionalization approaches. QDs and AuNPs can be very uniform in structure and size due to their crystalline nature, which contributes to their low polydispersity and their spectral properties[184].

Amid the examples reported in which enzyme-loaded nanomaterials were employed for electrochemical detection, the team of Cheng Fang developed an electrochemical immunosensor for detection of human alpha-fetoprotein (AFP). The system used colloidal AuNPs co-modified with MAb against AFP and HRP (Ab-Au-HRP) as the trace label and immuno-modified paper SPCEs as signal transducers. While the Ab-Au-HRP nanoprobe was dispensed on the polyester membrane used as conjugate pad, the cAb was immobilized onto a nitrocellulose membrane strip that was mounted on the SPCE. An absorbent paper was placed downstream to draw the sample to successively flow through the conjugate, capture and absorbent pads. Under optimum conditions the immunosensor could detect AFP with an LOD of 0.25 ng/mL[222].

Recently, some research groups have also employed Ab-enzyme coated nanomaterials in magneto-immunoassays, for the easy physical separation of target and non-target sample components while simultaneously leading to an increase in enzymatic activity. Wenqiang Lai et al. described a colorimetric competitive enzyme magneto-immunoassay in which ascorbate oxidase and AuNPs-labeled Ab were used for the determination of aflatoxin B1 (AFB1). The combined use of MB with anti-AFB1 Ab-labeled AuNPs resulted in sensitivity improvement, with an LOD of 0.1 ng mL^{-1} [223].

Nevertheless, it is worth noting that indirect detection implies increasing the number of incubation and washing steps of the assay and its final length and cost, and that signal amplification may enhance both specific and non-specific signals.

2.3.5.3. Enzymatic polymers: Poly-HRP

Several forms of streptavidin-HRP conjugates are commercially available for biotin-based detection assays. However, biotin-binding conjugates are normally limited to carrying 1 to 3 HRP molecules per protein to maintain enzymatic activity. This molar ratio of conjugation is effective in routine experiments, but may lack the sensitivity required for detecting targets present in low picogram to femtogram amounts without the use of additional steps to amplify the signal.

Poly-HRP is an alternative to solve this limitation using polymers with between dozens and hundreds of HRP molecules that are conjugated to streptavidin[224]. This results in increase of the molar ratio of HRP-streptavidin conjugate available to react with the substrate. The used of many signal-generating enzyme molecules per bound analyte molecule produces an increase of sensitivity to detect proteins present in very low amounts, in contrast to other methods, such as bridge, complex, multilayer and catalyzed reporter deposition techniques. This innovation has been used to produce sensitive immunoassays and immunosensors achieving high enzymatic activity, eliminating the need for additional steps, saving time and reducing costs. Poly-HRP is stable in aqueous solutions and has a loose linear-branched structure (Figure 2.13) which maintains 100% activity of the composite enzyme. Some of the commercial Poly-HRP complexes can be covalently coupled to virtually any anti-analyte, and streptavidin-containing Poly-HRP can be modified as well with biotinylated bioreceptors.

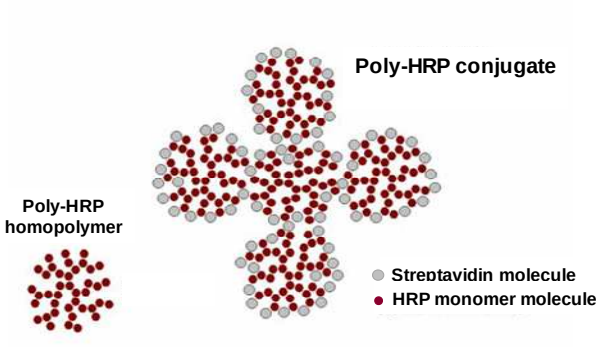

Figure 2.13. Simplified (2D) schematic representation showing the molecular design of SA-PolyHRP conjugate. Reprinted from: https://www.sdt-reagents.de/?action=polyhrp_application_note, with permission of SDT Reagents, German Copyright law.

Furthermore, there are no technical limitations associated with Poly-HRP. The detection is very simple and no changes of principle must be done that would affect an assay

scheme. It is compatible with chromogenic, fluorogenic and chemiluminescent HRP substrates used in ELISA and other techniques (such as Western blotting, immunohistochemistry and nucleic acid hybridization). This also means that Poly-HRP is compatible with existent and emergent ELISA instrumentation, which is advantageous over competing technologies, such as AP based enzymatic cascade amplification using cyclic cofactor regeneration (NADH/NAD+).

Poly-HRP was synthesized for the first time in 1987 by D. Ju. Plaksin and E. T. Gromakovskaya[225]. Following this synthesis methodology, Vasilov RG and Tsitsikov developed in 1990 an ultrasensitive immunoassay for human IgE measurement in cell-culture supernatant with a detection limit of 10 pg ml^{-1} [226]. Poly-HRP was commercialized by SDT in 1991[227] and it was used as an enhanced method for immunoassays and nucleic acid hybridization detection during the 90s[228–230]. Currently, Poly-HRP products are available worldwide through Fitzgerald Industries International[231], except in Japan where Funakoshi Co. Ltd is the exclusive distributor.

The beginning of the twenty first century witnessed a growth in the use of Poly-HRP as a tool to improve detection sensitivity. Christophe A. Marquette et al. used Poly-HRP for the first time to enhance a chemiluminescent immunoassay for anti-HIV-1 Ab detection, achieving an increment of 20 times for the maximum signal and a 10-times improvement for the LOD[232]. In 2009 Poly-HRP was employed in an ELISA for trastuzumab quantification, achieving an assay linear range from 1.6 to 1600 ng ml^{-1} in undiluted serum and demonstrating the compatibility of Poly-HRP with the study of serum and plasma samples[233].

Bernard S. Munge et al. produced their own Poly-HRP conjugate and it was applied for the first time in an electrochemical immunosensor for matrix metalloproteinase-3 detection (MMP-3). Multiple HRP labels were attached to polymeric beads and secondary Ab to produce a giant molecular tag, loaded with ~4200 enzyme labels. The electrochemical immunosensor also presented single-wall carbon nanotubes (SWCNT) and detected a concentration of MMP-3 of 4 pg mL^{-1} in calf serum samples[234].

In another example, dual SPCE, custom-modified with 4-carboxyphenyl-functionalized CNT, were used for the simultaneous determination of interleukin-1b (IL-1b) and tumour necrosis factor α (TNF- α) using a commercial Poly-HRP complex as the signal amplifier[235]. This sensor achieved LODs of 0.38 pg mL^{-1} (IL-1b) and 0.85 pg mL^{-1}

(TNF-a), based on a sandwich immunoassay that included 3 consecutive incubation steps with the corresponding series of washes, and took 150 min. Otherwise, the combination of ultrasensitive customized nanostructured SPCE and immunomodified Poly-HRP provided detection of alpha-fetoprotein and HIV p24 Ag in about 30–35 min, with LODs of 1–2 pg mL^{-1}, in both cases entailing production paths that took days and a 2-step immunoassay format[236,237].

Among the examples reported, the use of Poly-HRP improved the sensitivity of two electrochemical magneto-immunosensors produced for detection of interleukin-6 (IL-6) and transforming growth factor-1 (TFG) (LODs of 0.39 pg mL-1 and 10 pg mL-1, respectively), but involved long multi-step assay procedures[200,238].

Table 2.5 shows a comparison of these examples using Poly-HRP for signal enhancement.

Assay format	Detection type	Analyte	Time of functionalization	Assay steps	Assay time	Detection time	LOD	Samples	Ref.
ELISA	Chemiluminescent	anti-HIV IgG	3 h (ELISA plates & protein biochip)	4	4 h	10 min	Ab titter 1:25000	-	[232]
ELISA	Colorimetric	trastuzumab	1 h - 4 days	3	3 h 45 min	15 min	-	46 plasma samples	[233]
Competitive ELISA	Colorimetric	aflatoxin B1	ON+ 1 h (ELISA plates)	3	1 h 45 min	15 min	0.077 ± 0.070 µg Kg^{-1}	--	[239]
Electrochemical immunosensor	Amperometric (SWCNT)	MMP-3	18 h (SWCNT); 4 h (Ab & blocking)	3	3 h 45 min	1 h 25 min	4 pg mL^{-1}	2 serum samples	[234]
Electrochemical immunosensor	DPV (Au electrode with AuNP)	AFP	ON + 2 h 30 min (electrode-Ab1); ON (polyHRP-Ab2)	2	35 min	NS	2 pg mL^{-1}	6 serum samples	[237]
Electrochemical immunosensor	Amperometric (SPCE with Fe_3O_4@SiO_2-Ab1)	p24 antigen	>2 days (Fe_3O_4@SiO_2-Ab1 & AuNP-PolyHRP-Ab2)	2	30 min	NS	1 pg mL^{-1}	6 serum samples	[236]
Electrochemical immunosensor	Amperometric (SPCE with MWCNT-Ab1)	TGF-β1	ON + 1 h 30 min (SPE)	3	1 h 20 min	> 5 min	1.3 pg mL^{-1}	2 serum samples	[240]
Electrochemical DNA sensor	Voltammetric (CV) and amperometric (Au electrode)	uidA	2 h 30 min	3	3 h	2 min	0.2 pg $µL^{-1}$	-	[241]
Electrochemical immunosensor	Amperometric (SPCE with Phe-DWCNT)	IL-1β and TNF- α	2 h 30 min (Phe-DWCNT-SPE)	3	2 h	> 5 min	0.38 pg mL^{-1} (IL-1β) and 0.85 pg mL^{-1} (TNF-α)	Spiked serum samples and 2 saliva samples	[235]
Electrochemical immunosensor	Amperometric (inkjet printed gold 8x array)	HER-2	24 h + ON (Ab) + 1 h	3	15 min	3 min	12 pg mL^{-1}	Spiked serum samples	[242]
Electrochemical immunosensor	Amperometric (pPPA electrode)	endoglin (CD105)	2 h	3	1 h 45 min	3 min	140 pg mL^{-1}	16 serum samples	[243]
Microchip based magneto-ELISA	Colorimetric	TDM IgG	25 h (MB)	3	15 min	5 min	AUC = 0.77	146 plasma samples	[244]
Electrochemical magneto-immunosensor	Amperometric (SPCE)	IL-6	2 h 15 min (MB)	3	1 h 30 min	NS	0.39 pg mL^{-1}	1 spiked urine sample and 3 saliva samples	[200]

Electrochemical magneto-immunosensor	Amperometric (SPCE)	TGF–β1	3 h 4 min (MB)	3	2 h 20 min	> 5 min	10 pg mL^{-1}	3 spiked urine samples	[196]

Table 2.5 Different immunoassays and electrochemical immunosensors reported using Poly-HRP for signal enhancement. *AFP, alpha fetoprotein; AUC, Area Under Curve; AuNP, Gold nanoparticle; DPV, differential pulse voltammetry; DWCNT, double-walled CNT; $Fe_3O_4@SiO_2$, Silica coated magnetite; HER-2, Human Epidermal Growth Factor Receptor 2; HIV, human immunodeficiency virus; IL, interleukin; MMP-3, matrix metalloproteinase-3; pPPA, poly(-pyrrolepropionic) acid; ON, Overnight; SWCNT, single-walled CNT; TDM, trehalose 6,6′-dimycolate, TGF-β1, Transforming growth factor beta 1; TNF α, Tumor necrosis factor.

2.4. Microfluidic Paper (MP) sensors

2.4.1. Paper properties and benefits of application

Paper is considered an attractive material for fabricating analytical devices, such as sensors and biosensors[245], and paper-like materials have been used for decades for the production of colorimetric LFIA pregnancy tests[246]. Due to its mechanical properties, porous structure and natural origin, paper presents several advantages compared to conventional materials, such as silicon, glass and rigid polymers[247]. Paper is an economical substrate that can be printed, cut and chemically modified with biomolecules and nanomaterials readily and rapidly[38,248]. In addition, paper is light, globally accessible, biocompatible and biodegradable. Furthermore, paper is flexible, foldable and rollable[249], making it an ideal platform to develop locally low-cost and portable diagnostic devices[78,250].

Typically, the main component of paper is cellulose fibre, a highly attractive fabric thanks to its porous structure[247]. However, a wide range of different types of paper-like materials are currently employed to produce MP-sensors depending on their properties, such as grade, flow rate, thickness, rugosity and pore size. The choice of the paper material often varies depending on the assay requirements, the target analyte and the specific analytical application[250,251]. For instance, the porosity of the paper matrix conditions the diffusion rate resulting for the wicking of liquids throughout the platform[252]. Moreover, paper grades are characterized by the pore size[253], and the capillary flow shows the absorption capability of the paper matrix when fluid comes in its contact.

Nowadays, two main kinds of paper are widely utilized to fabricate POC diagnostic devices, which are cellulose- and nitrocellulose-based materials[78,254]. On the one hand, cellulose fiber is a linear chain macromolecule composed of hundreds of glucose units[255]. Cellulose paper is fibrous, hydrophilic, biodegradable and presents superior wicking ability that grants reproducibility and uniformity. Cellulose allows liquids to penetrate into its hydrophilic fibre matrix, and be transported through capillary forces without the need of an active pump or external power source, greatly simplifying the device design and construction[256–258]. Moreover, cellulose fibres can be functionalized physico-chemically, in order to tune traits such as its hydrophilicity, permeability and

reactivity[254,259,260]. Cellulose paper is extensively used as filter paper, absorbent pad, and chromatography paper.

On the other hand, nitrocellulose membrane is produced by nitration addition. Nitration contributes to strengthen the chemical functional groups, allowing the covalent immobilization of biomolecules, and modulates cellulose hydrophilicity to produce a more hydrophobic material. It is the key material for LFIA, in which capture Ab are bound and the test and control lines are formed[246]. Finally, paper-like membranes made of alternative materials, such as glass fibber, polyester, polysulfone, or nylon, to cite some few, are commercially available and can provide additional properties to a device. For instance, glass fibre paper may display faster wicking than some cellulose materials, lower retention of sample components and reagents, and exceptional resistance to most organic and inorganic solvents.

In brief, the properties of paper provide (1) high surface to volume ratio, with an elevated number of possible reagents immobilised; (2) absorbency, allowing reagent storage inside the matrix; (3) capillary action, to transport volumes without any external force; and (4) compatibility with biological samples[261,262]. Finally, MP-devices can be easily fabricated using several practical fabrication techniques. Considering the remarkable properties of paper and paper-like materials, MP-sensors represent a promising technology for fluid handling and analysis[39].

2.4.2. Dipsticks, lateral-flow assays and paper-based analytical devices

The area of POC testing has benefited from the increasing interest in the use of paper and paper-like materials for the production of analytical devices. Depending on the complexity of fluid handling, detection precision needed and components' materials, paper-based biosensors could be classified into dipsticks, LFIA, and microfluidic paper-based analytical devices (μPADs) [24,263,264].

Dipstick biosensors are a simplistic diagnostic device which contains pre-deposited reagents and provide qualitative detection. The first dipsticks were initially utilized to quantify glucose in urine in 1956[265]. Nowadays, dipstick biosensors are applied as pH, uric acid and pathogen detection strips. However, studies using dipstick immunosensors have rarely been published in the last decade.

Dipsticks are simple to design, easy to manufacture, easy to use, fast to provide results, and facile to interpret. However, their main drawbacks are the inaccuracy and qualitative results they usually produce[266]. The dipstick assays are based on blotting the sample onto a piece of paper pre-loaded with reagents. The sample is dispensed on the paper, the pre-loaded regents react with the analyte in the sample and results are developed as colour bands, which are referred to a standard indicator card for visual intrepretation[267]. Figure 2.14a-b shows a typical colorimetric dipstick assay.

Paper-based LFA are an advanced version of dipsticks, which offers controlled fluid flow. This allows increasing the total number of captured and detected analyte molecules in a given time, improving the device LOD. The best known LFA device is the pregnancy test. This technology evolved considerably over the 1980s, and LFAs have become standard platforms for other applications in many areas, including food safety, environmental monitoring, and veterinary diagnostics[251].

LFA are usually devices consisting of four overlapping pads (the sample pad, conjugation pad, detection pad and absorbent pad), which contain preloaded dried reagents and integrate on-chip sample flow[268] (Figure 2.14c). The combination of porous materials provides a flow driving force based on the capillary effect, and a nitrocellulose membrane or similar provides a physical platform for both reaction and detection during the assay[269]. When the assay is performed, a small volume of sample is applied onto the sample pad. The sample flows along the sample and conjugate pads. While the first provides sample pre-treatment (such as filtration), the conjugate pad houses pre-loaded d-Ab conjugated to a signal indicator (for example, AuNPs). As the sample flows, the Ag binds the labelled d-Ab. The sample continues migrating along the detection pad, which displays c-Ab immobilized forming two lines in the middle of the device, one as the control line and the other as the test line. While the test line captures the complexes formed by Ag and labelled d-Ab, the control line binds the excess of unreacted dAb. Both events result in the formation of coloured bands that are visually interpreted[270]. By this means, various assay designs, such as sandwich, competitive, and multi-detection formats, can be employed.

LFAs are an easy-to-use and portable platform for the detection of specific biomolecules. Most of these strip assays are ideal POCT tools because LFAs require small sample volumes on the order of 10–100 µL, and results can be easily interpreted

by the naked eye in few minutes. They are also simple and cheap to manufacture providing an affordable medical test that can be used either at home or in the clinic. However, LFAs show poor detection limits and qualitative or semi-quantitative response. For that reason, the existing assay formats do not meet the current market diagnostic demands. Upgraded paper-based LFAs have been developed to overcome these drawbacks, introducing complex designs for multistep assay quantitative analysis[256].

The original paper strip tests (dipsticks and LFAs) have lower specificity and sensitivity than conventional laboratory-based diagnostic instruments. With the arising of μPADs in 2007[271], paper replaced conventional microfluidic substrates (silicon, glass, and polymer) to develop microfluidic devices used for rapid diagnostic tests[261] (Figure 2.14d-f). μPADs have garnered significant interest in recent years for the potential multianalyte detection and quantification capabilities they offer for complex sample analysis. Their simple design allows the facile operation without training for the user. In addition, they are inexpensive and simple to produce. Nonetheless, there are still many challenges to overcome in the design of paper-based diagnostics, for instance to make them more user-friendly or guarantee accurate and direct answer generation.

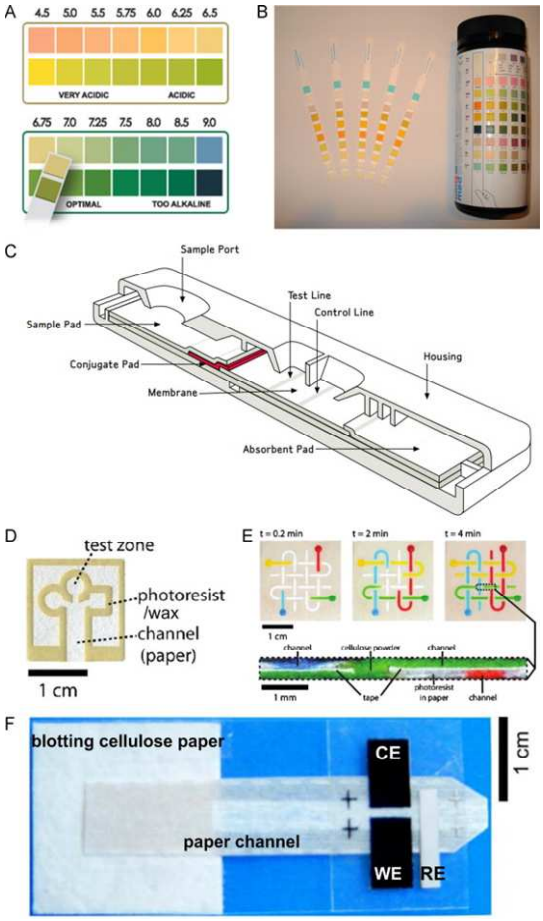

Figure 2.14. Types of MP-sensors. Reprinted from ref. [78] with permission of Elsevier, Copyright 2014. Dipstick strips (a-b), lateral flow strip (c), and µPAD (d-f): (d) 2D µPAD[272] (e) 3D µPAD[273] (f) electrochemical µPAD[274].

µPADs are generally based on the creation of hydrophilic/hydrophobic microchannels to define a reaction zone for the measurement of analytes[275]. The dimensions of the resulting channels and the ambient conditions (temperature and humidity) can affect the wicking rate of fluids. These devices function via capillary action because of the wicking properties of paper. They produce results faster than the current laboratory techniques and only need small volumes to work, without requiring external equipment. These devices are also suitable for measuring single or multiple target analytes in parallel and in a short period of time. Finally, several parameters, such as the type of paper, the geometry of the device, and the membrane pre-treatment, can be finely tuned to produce µPADs for different applications and biological targets[276]. Hence, µPADs have great potential for POCT and on-site diagnostics.

All these devices are characterized by their simple design, low cost, easy fabrication, user-friendly handing, and fast sample analysis. Furthermore, MP-sensors are capable of working with small sample and reagent volumes, may provide multiplexed analysis and

are highly compatible with miniaturization (Figure 2.15). Due to these many advantages, MP-sensors are giving shape to an emerging and promising diagnostic format especially well fitted for developing countries[25]. Carefully selecting the type of membrane used, the geometry of the different device components, or the coating of the paper of the MP-sensors, allows the production of customized gadgets for different applications[248,262]. Nowadays, the development of MP-sensors is a discipline in continuous evolution that is providing functional and versatile devices in a variety of fields, such as medical diagnostics[277,278], food safety monitoring, environmental analysis[279] and cell culture[280].

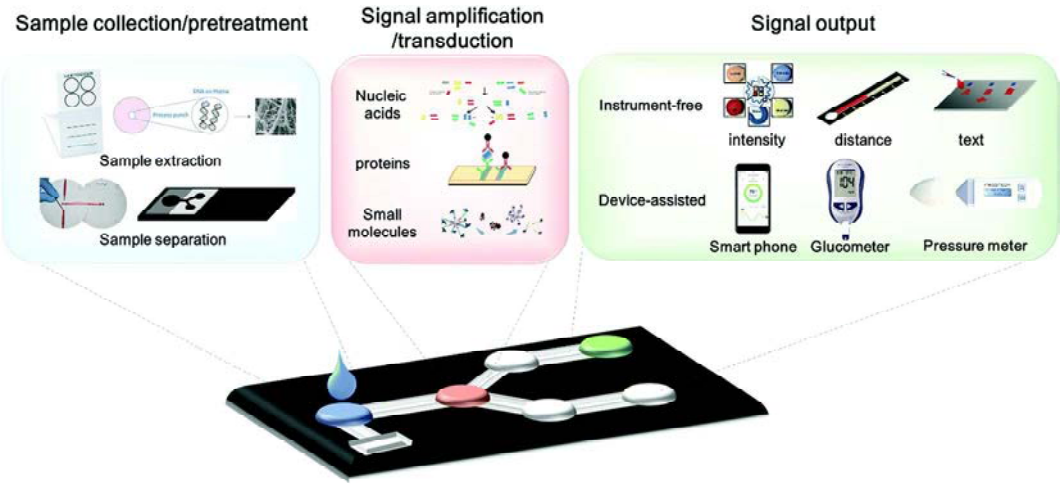

Figure 2.15. Schematic representation on an ideal MP device integrating the different steps of a bioassay. Reprinted from ref. [263] with permission from Royal Society of Chemistry, Copyright 2017.

2.4.3. MP-electrochemical sensors

A large majority of the MP-sensor devices reported entail a colorimetric detection method, which measures colour intensity proportional to the concentration of the analyte. They are specifically designed to provide visual or optical qualitative interpretation, and often semi-quantitative information relies on the use of traditional techniques and measurement equipment[39,264,281]. For that reason, these types of sensor present limited sensitivity and accuracy, and high variability, affecting the results with a large number of false-positive and false-negative outcomes[282,283].

Most popular transduction methods have been applied to MP-sensor detection in order to counteract their limitations and obtain more objective, accurate and quantitative results, including electrochemical sensing, fluorescence, chemiluminescence and electrochemiluminescence. Although the various sensing mechanisms have their

respective advantages and disadvantages, electrochemical detection remains among the most common, versatile and effective methods for MP-devices due to its accuracy, reliability and quantitative fast results, which provide improved sensitivity and selectivity compared to the colorimetric methods[284]. However, there are still some crucial challenges (e.g., miniaturization, integration and cost) that hinder the wide application of MP-electrochemical sensors[285].

The first demonstration of a MP-electrochemical sensor was published by Henry's group in 2009 (Figure 2.16a). This filter paper device included a star-like arrangement of three microfluidic channels produced by photolithography, each one with the corresponding SPCE. The sensor was used to measure simultaneously the concentrations of glucose, lactate, and uric acid in biological samples[286]. Since then, electrochemistry has become the second most used transduction system after colorimetry for MP-sensors, with examples reported using different transduction modes, including cyclic voltammetry (CV), chronoamperometry, square wave voltammetry (SWV) and potentiometry[287,288].

MP-electrochemical sensors are cost-effective detection devices that combine the merits of paper as a solid support, to the high sensitivity and selectivity of electrochemical detection. The resulting devices are usually characterized by their low cost, portability, simplicity of use, low electrical power consumption, and minimal instrumentation requirement[281,286]. On the other hand, MP-electrochemical sensors are well suited for miniaturization into useful, robust, portable, accurate and disposable sensing platforms, with digital reading that provides flexibility and quantification to the biochemical detection[289].

MP-electrochemical sensors are based on the fabrication or deposition of electrodes on a paper substrate for the detection of electrochemical reactions happening within the paper matrix, which might be accompanied by microfluidic structures to direct solution flow. The most widely used technologies for the fabrication of MP-electrochemical sensors are wax printing, inkjet printing, laser printing, plasma treatment, flexographic printing, photolithography and screen-printing[290,291] (Figure 2.16b). In all cases, some parameters of interest that should be considered and optimized for optimal fabrication are the materials used, deposition thickness and uniformity, device dimensions and tolerances, and space limitations.

The materials used for electrode fabrication are important because they contribute conductive or semi-conductive properties to the paper for the electrochemical detection, as it is the case for carbon, silver, gold, graphite, nickel, and conductive epoxy-based inks. Materials of selected hydrophobicity/hydrophilicity can be used to delimit hydrophobic/hydrophilic areas onto the paper surface. This allows constructing hydrophilic channels and hydrophobic barriers in order to define the working zones and the solution flow paths[250,252]. The arrangement of the different device elements can give shape to two-dimensional (2D) and three-dimensional (3D) structures. In 2D structures, the microchannels and the defined electrodes are patterned on a single flat strip. In contrast, 3D structures are generally fabricated by printing the electrodes and channels in different segments of the paper, which are stacked or folded during the detection procedure[78,292–295].

MP-electrochemical sensors can be easily produced in various configurations thanks to the inherent properties of this material, including adjustable thickness, flexibility and hydrophilicity. Moreover, the high roughness and porosity of paper substrates result useful to collect, store, separate, extract and concentrate the sample, facilitate the integrated operation of different assay steps, and improve the response of the electrochemical sensor. The paper matrix reduces the effect of convection of liquids caused by random motion, vibration, and heating[73]. Furthermore, a stagnant assay can be easily transformed into a flow measurement by making the reagents run across a paper electrode device. At the same time, MP-electrochemical sensors may provide a very convenient combination of sample pre-treatment, capillary passive pumping for fluid transport, and self-powered hand-held electrochemistry commercial readers[296] or customized smartphone technology[281].

The current areas of interest for MP-electrochemical sensor development include the improvement of the technologies available for paper and electrode fabrication and modification; the development of simple and low-cost mass fabrication methods that could lead to successful commercialization of these devices; and the design and fabrication of inexpensive miniaturized platforms of enhanced detection sensitivity[297].

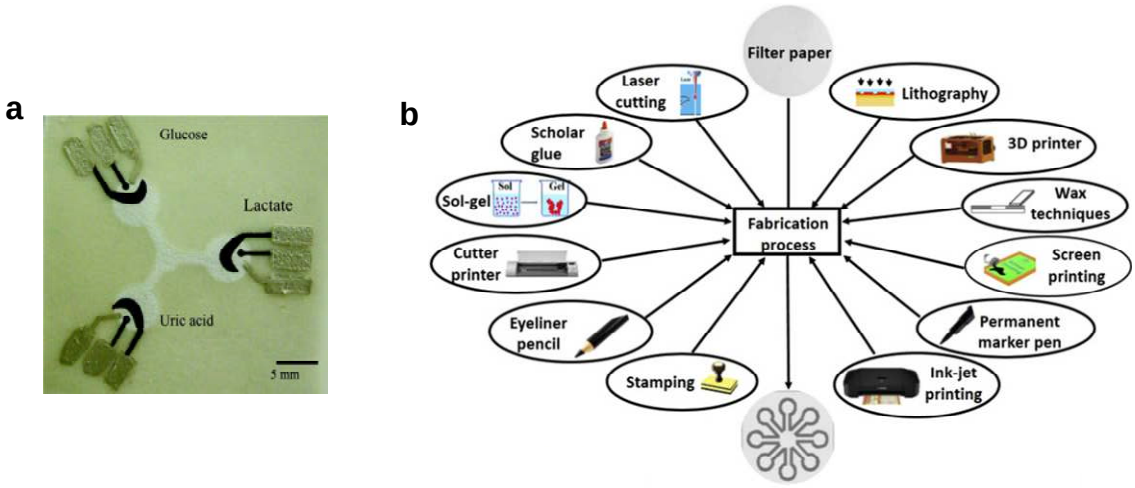

Figure 2.16.(a) Image of the first MP-electrochemical sensor reported in the literature. Reprinted from ref. [286] with permission from American Chemical Society, Copyright 2009. (b) Techniques available for MP-sensor fabrication. Adapted from ref. [298] from Elsevier, Copyright 2017.

2.4.4. Microfluidic Paper Screen-Printed Electrodes (MP-SPE): application to magneto-immunoassay detection

Screen-printing is the first and most frequently used method for the fabrication of MP-electrochemical sensors due to the ease of fabrication, which allows the large-scale production of reproducible and cost-effective electrodes[296,299,300]. As explained in Section 2.2.3, screen-printing is a relatively simple process that utilizes masks, conductive and insulating inks, and a squeegee. Dungchai et al.[301] were among the first to exploit this methodology for the production of paper-based electroanalytical devices, demonstrating the integration of SPE in a Whatman 1 filter paper. Solid wax was melted using a hot plate to incorporate to the paper hydrophobic barriers, delimited by a designed mask. The utility of the µPAD fabricated was demonstrated by electrochemical and colorimetric detection of glucose and total iron in human serum samples.

As in the case described above, most of the works published to date combine screen-printing for the production of the electrodes and conducting parts, and wax printing[302] to define the fluidic structures and electrode passivation areas, which results in a batch manufacturing process. Works describing fully screen-printed devices are scarce.

In this field, paper-like materials have been used as a support substrate for the scree-printing of the electrochemical cell (working, reference and counter electrodes)[299,303]. However, examples exist describing alternatively the combination or attachment of the paper to a commercial SPE. This strategy is practical and simple as the cellulose matrix

can be used as an immobilization layer in direct contact with the electrode surface[304]. For instance, a SPCE was modified with graphene/polyaniline/AuNPs/glucose oxidase (Gr/PANI/AuNPs/GOD) biocomposite and then covered by a paper disk impregnated with the sample[305] (Figure 2.17a). After introducing PBS on the paper disk, the electrochemical measurement was carried out. The assay was based on measuring the current decrease of flavin adenine dinucleotide (FAD) in GOD provoked by the enzyme–substrate reaction using differential pulse voltammetry (DPV). In a similar way, an origami paper device was used to reduce the interference by non-target sample components in a glucose electrochemical enzymatic sensor (Figure 2.17b). The origami paper device was formed by a base tab and a cover tab. The base tab was pasted onto a commercial SPCE and the enzymes were loaded on the cover tab. This allowed controlling the electrochemical reactions of interferents and substrates by folding the tabs as needed[306]. In another example, a combination of membranes was exploited as a reagent reservoir and to promote sample and reagents flow above a screen-printed gold electrode (SPGE) electrochemical immunosensor for detection of dengue virus Ag NS1 (Figure 2.17c). In this case, the conjugate pad was modified with immunomodified AuNPs electroactive tags, which reacted with the NS1 protein present in the sample added through the device window. The immunocomplexes formed flowed to the biofunctionalized SPGE, where they were captured and immobilized for the electrochemical detection[307].

The use of paper for the development of electrochemical magneto-immunosensors has been scarce. For example, magnetic titanium particles (Fe_3O_4@TiO_2NPs) were used for the design of a disposable electrochemical immunosensor test-strip for determining organophosphorous pesticides-phosphorylated butyrylcholinesterase (OP–BChE) in human plasma (Figure 2.17d). Magnetic Fe_3O_4@TiO_2NPs were confined onto the test strip using a small magnet and were employed to capture target OP-BChE from the flowing sample. Further recognition was completed by HRP and anti-BChE Ab co-immobilized AuNPs. Once the sample solution containing OP-BChE had migrated through the whole strip by capillary action, the test zone containing the immunocomplexes was cut, was placed on the SPCE cell, and detection was performed by SWV after the addition of thionine and H_2O_2[308].

In another case, Ge et al. used magnetic silica nanoparticles (Fe_3O_4@SiO_2NPs) as signal labels in the preparation of a simple origami electrochemical immunosensor for

microcystin-LR detection. An AuNPs-modified porous paper (Au-PW) was prepared, resulting in interconnected AuNPs layers on the surface of the cellulose fibres. Then, they were azide-functionalized to be used as solid support to immobilize an alkyne-end-terminated Ab (Ab1) by a click reaction. In parallel, Fe_3O_4@SiO_2NPs were modified with both alkyne Ab (Ab2) and alkyne-HRP on the surface. A sandwich-type immunoassay was employed and the electrochemical detection was carried out by placing the reaction zone of the Au-PW support above the active surface of a SPCE[309].

More recently, M. Crooks team developed two MP-based electrochemical sensors using commercial MB and Whatman grade 1 chromatography paper. In a first example, a paper-based sensor was used to detect a 30-base DNA sequence characteristic of the hepatitis B virus (HBV) with a detection limit of 85 pM. The design combined an origami (paper folding) assembly and the open structure of a hollow-channel paper analytical device, and wax was used to print the three-electrode cell (Figure 2.17e). The device used silver nanoparticles (AgNPs) and MB, both modified with oligonucleotides, as label and capture probes, respectively. The target DNA formed a sandwich with the label and capture probes and it was retained on the WE with a magnet. After chemical oxidation of the AgNPs, the Ag^+ ions were determined by anodic stripping voltammetry[310].

In the second one, a paper-based assay was developed for detection of ricin. The electrochemical MP-sensor was assembled by origami paper folding using four wax-patterned paper layers (Figure 2.17f). The device used AgNPs as labels and MBs as the capture support to form a ricin immunosandwich. The sample was introduced in a hollow channel and flowed by capillary action across the different paper layers. With this system, ricin was detected at concentrations as low as 34 pM in less than 10 min[311].
In a different approach, at least two examples reported the use of nanoporous alumina membrane as a platform for magneto-immunosensor development. The team of Yang M. detected electrochemically *E. coli* O157:H7 employing a nanoporous alumina membrane and Ab-MB for bacteria concentration from samples.[312]. Ab-MB were confined on the nanoporous membrane using an external magnet, and produced an enhancement in sensitivity, allowing bacteria detection down to 10 CFU mL^{-1} by measuring the changes in impedance across the membrane. In collaboration with them, the research group of Sun P. developed a biofunctionalized nanoporous alumina membrane for electrochemical histamine determination, exploiting this time magnetic

nanobeads for Ag concentration and signal amplification[313]. The sensing platform measured by EIS the blocking effect produced by the histamine-bound magnetic nanobeads in the nanopores, achieving an LOD as low as 3 nM.

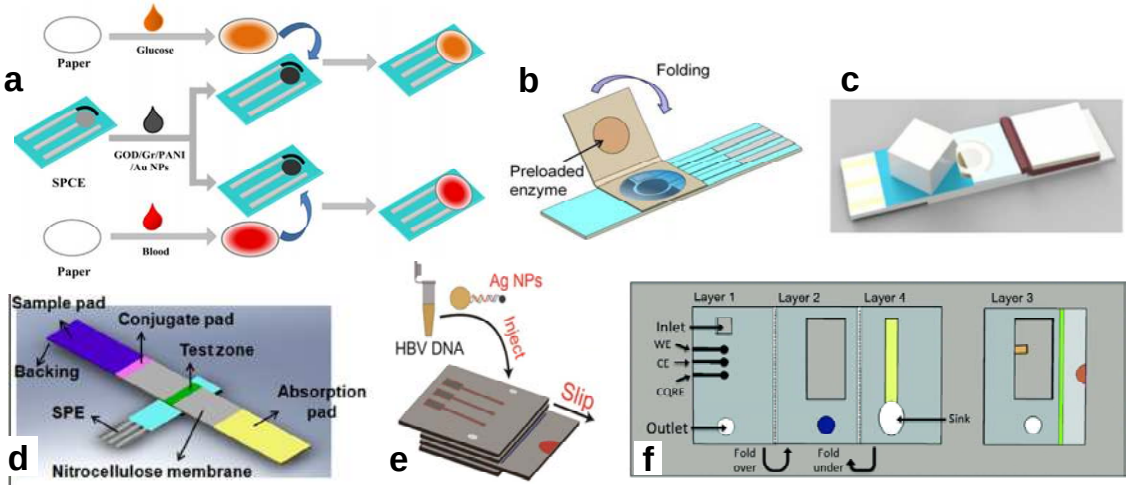

Figure 2.17. (a-c) Examples of devices formed by assembling paper components and a commercial SPE. (a) Paper disk-SPE, in which paper was usd for sample pre-treatment. Adapted from ref. [304] with permission from Elsevier, Copyright 2014. (b) Origami-SPE, in which paper was pre-loaded with the assay reagents. Adapted from ref. [306] with permission from Elsevier, Copyright 2017. (c) Lateral flow assay integrated in a SPE. Adapted from [307] with permission from Elsevier, Copyright 2018. (d-f) Assays using magnetic beads as label or support: (d) LFIA onto SPE. Adapted from ref. [308] with permission from Elsevier, Copyright 2013. (e) 3D paper folding electrode. Adapted from ref. [310] with permission from American Chemical Society, Copyright 2015. (f) Four-layer paper origami electrode. Adapted from ref. [311] with permission from Royal Society of Chemistry, Copyright 2015.

One of the contributions of this Thesis has been the demonstration that MP-SPE can be exploited to carry out on-chip part of the steps of an electrochemical magneto-immunosensor, simplifying the level of handling for the user. Three examples will be described in Chapters 7 and 8. In the first case, paper was exploited to carry out directly on a commercial SPCE all the washing and detection steps of a one-step electrochemical magneto-immunosensor for detection of MMP-9 (manuscript submitted). In this system, immuno-modified MB were incubated with the sample and a Poly-HRP immuno-conjugate for 5 min, and this mixture was transferred to a SPCE, where a magnet retained the MB-bound analyte. Meanwhile, a movable paper device adsorbed the reagents for waste storage and promoted washing under flow conditions. Finally, the paper device was relocated, and electrochemical detection took place under static conditions. The sensor produced in this way achieved detection of MMP-9 in patient plasma samples in about 10 min, with little intervention of the user.

As an alternative, a single-piece MB-SPCE was produced to detect MPO using a one-step magneto-immunoassay[314]. After a single 5-min incubation of the sample with all

the assay reagents, the mixture was directly pipetted on the MB-SPCE. While a magnet retained the MB onto the WE, the rest of reagents and components flowed downstream. Washing was carried out on-chip by just pipetting and allowing to flow the wash solution, which was followed by addition of an enzymatic substrate and amperometric measurement. MPO was detected at clinically relevant concentrations in 1:100 diluted human serum in about 13 min. However, the currents registered were 30-times lower than those obtained at commercial SPCE after classical off-chip washing. To improve this drawback, an upgraded MB-SPCE was produced by double-sided screen-printing, which included double-sided graphite WE and CE and registered current more efficiently. This device was used to detect PfLDH in lysed whole blood, again exploiting a one-step magneto-immunoassay format. As it will be shown, the sensor afforded quantitative detection of PfLDH in synthetic samples down to 2.47 ng mL^{-1}, provided quantitation of PfLDH in *Plasmodium*-infected cultured red blood cells (RBC) proportional to parasitemia in a range between 0.006% and 1.5%, and distinguished between whole blood samples from healthy individuals and malaria patients presenting parasitemias >0.3%. Furthermore, the signals registered were 20 times higher than those provided by the MB-SPCE used previously for MPO detection and close to those generated by commercial SPCE.

2.5. Protein diagnostic biomarkers in POCT: three case examples

The International Programme on Chemical Safety (formed by the WHO, the International Labour Organization (ILO) and the United Nations Environment Programme (UNEP)) defined biomarker as any substance, structure, or process that can be measured in the body and influences or predicts the incidence or outcome of a disease, and/or the effect of treatments, interventions, and even unintended environmental exposure, such as to chemicals or nutrients[315]. Biomarkers are generally studied in the patient's blood, although they might be traced as well in other body fluids and tissue biopies, and can be specific cells, molecules, genes, gene products, enzymes, or hormones[316].

The use of biomarkers in clinical research is currently in development and lots of resources and efforts are being devoted to improve and refine the understanding and

significance of the biomarker candidates reported to date. The key for the detection of biomarkers is determining the relationship between any given measurable biological element and a relevant clinical endpoint, in an accurate and reproducible manner, improving our understanding of a disease and providing new knowledge of biological mechanisms or processes[317].

The measured biomarkers are evaluated as an indicator of normal biological states, pathological processes, or a response to a therapeutic intervention[318]. In this context, biomarkers can be classified in diagnostic, predictive or prognostic. A diagnostic biomarker is a parameter that aids the diagnosis of diseases. A predictive biomarker includes those characteristics that are objectively measured and evaluated to predict response to a therapeutic intervention, allowing defining subpopulations of patients that are likely going to benefit from a specific therapy. The prognostic biomarkers provide information useful to predict the course of a disease among patients with the same characteristics, helping to anticipate the outcome of the patient[319].

2.5.1. Cardiovascular diseases: Myeloperoxidase

The WHO points at cardiovascular diseases (CVDs) as one of the leading causes of death worldwide[320]. In 2016, there were 56.9 million deaths in the world, and 9.43 million were caused by ischemic heart disease, the biggest killer[321]. In order to improve this situation, prophylaxis and treatment of these conditions have been studied substantially over the last few years. In rich countries, the combination of physical activity and healthy diet with pharmacological and surgical strategies has proven to be very effective. However, CVDs will become especially important in developing countries, where globalization of sanitation and access to drugs and medical care will presumably result in increased longevity, while changes in dietary consumption and lifestyle will have a negative effect in the health of the global population[320,321].

Nowadays, CVDs are usually diagnosed via classical methods, which must be conducted in central laboratories by specialized staff and may take several hours or even days. For instance, cardiac characterization by electrocardiogram, chest X-ray, electrophysiology, biopsy, and imaging are the most common methods of diagnostic. Furthermore, a biochemical analysis of the patient’s blood for the quantification of

cardiovascular biomarkers such as troponin, creatine kinase, myoglobin, and MPO is needed[322,323].

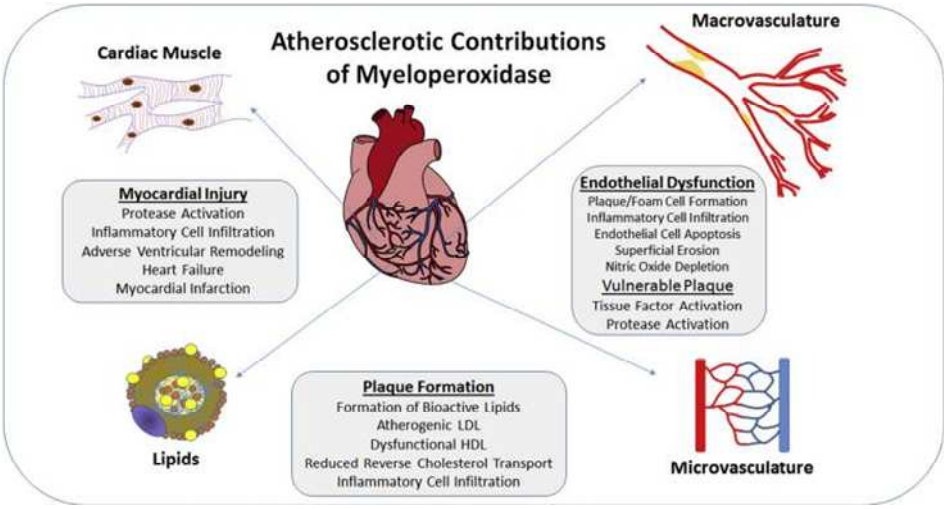

Figure 2.18. MPO role in CVD. Reprinted from ref. [324] with permission from Elsevier, Copyrigth 2016.

MPO is an iron-containing enzyme of the superfamily of the heme peroxidases, which is expressed in neutrophils and monocytes that play a central role in microbial killing and regulation of oxidative stress during inflammation[323,325]. MPO constitutes an endogenous mechanism for the production of hypochlorous acid, a potent antimicrobial agent for host defence against invading microorganisms[326,327]. Furthermore, MPO catalyses reactions that consume hydrogen peroxide and generate reactive oxygen species responsible for oxidative stress. Emerging evidence suggests that MPO may be involved in the regulation of numerous physiological processes, such as vascular tone, angiogenesis, synthesis of collagen and extracellular matrix, protease activity, gene expression, posttranslational protein modifications, signal transduction, intracellular protein transport, neurotransmitter modulation, and modulation of innate and adaptive immunity[326].

In addition, MPO has been proposed to be implicated in the pathogenesis of multiple inflammatory pathologies, including infection, a number of neurodegenerative diseases (such as, Alzheimer's disease, Parkinson's disease, amyotrophic lateral sclerosis, multiple sclerosis, stroke, and epilepsy), atherosclerosis, and related CVDs (Figure 2.18)[328]. Several studies suggest the association of an elevated MPO level in plasma (i.e., concentrations above 400 ng mL^{-1}) with the risk of suffering CVDs or adverse

vascular events, such as arterial hypertension, pulmonary arterial hypertension, ischemia/reperfusion injury, stroke, cardiac arrhythmia and venous thrombosis[329,330].

Some groups have worked in the development of magneto-biosensors for the rapid and sensitive detection of MPO[331,332]. For example, Moral-Vico et al.[17] produced a low-cost microfluidic device for the multiplexed electrochemical detection of magneto-bioassays. As a proof of concept, the device was used to quantitate MPO and monitor in parallel its activity. The authors claimed that screening both activity and mass of an enzyme biomarker could be useful to study how the two parameters are affected by the patient's pathological state or treatment. In this example, while MPO concentration was detected by registering steady state currents (Iss) under substrate flow, MPO activity, which generated lower currents, was measured through the peak currents (Ip) produced in a stopped flow approach, with LODs of 0.2 ng mL^{-1} and 0.004 ng mL^{-1}, respectively. Finally, the dual chronoamperometric magneto-immunoassay was applied to the study of 10 real plasma samples, allowing patient stratification according to the risk of suffering a cardiovascular event. In another case, Herrasti et al.[333] detected MPO chronoamperometrically using immuno-functionalized MBs to capture and concentrate the protein, and enhancing the signal registered by exploiting CNT wiring on a disposable SPE. The optimized assay could be performed in 30 min and yielded LODs of 6 and 55 ng mL^{-1} in PBS and undiluted human serum, respectively, making it useful for the identification of patients at risk of CVD. A few more examples accomplished also the detection of MPO using other detection formats[334–339].

2.5.2. Neurological disease: MMP-9

Stroke is among the leading causes of death and the main reason for permanent disability in adults in developed countries[340]. Atherosclerotic disease of the internal carotid artery results in carotid stenosis (CS), an established cause of ischemic stroke. The prevalence of hemodynamically relevant CS (≥50%) in subjects >65 years of age is quite high (5–10%)[341]. This data indicates that there is no optimal strategy to predict ischemic stroke in patients with asymptomatic CS.

Lots of effort has been devoted over the last decades to the identification of biomarkers that could help to prevent or early diagnose an ischemic stroke. It is nowadays clear that finding a single biomarker specific and sensitive enough for its use as a diagnostic

and/or prognostic tool in clinical settings will not be an easy task[342]. For that, combining different biomarkers into a panel has been suggested as a better option in order to increase diagnostic and/or prognostic performance[343,344]. One of the biomarkers proposed to take place in these panels has been matrix MMP-9.

MMPs are a group of enzymes involved in the breakdown of extracellular matrix in various physiological processes, including embryonic development, morphogenesis, reproduction, and tissue resorption and remodelling[345,346]. They are grouped into collagenases, gelatinases, stromelysins, matrilysins, membrane type MMPs and others based on domain organization and substrate preference[347]. MMPs use to be minimally expressed in normal physiological conditions. In contrast, overexpression of MMPs results in an imbalance between the activity of MMPs and tissue inhibitor of metalloproteinase (TIMP) that can lead to a variety of pathological disorders[348,349]. MMP-2 and MMP-9 belong to the gelatinases group, which are the major components of the basal lamina around cerebral blood vessels[350]. For that, an increment of MMP-9 levels accelerates matrix degradation, associated with neuronal damage, apoptosis and blood-brain barrier opening, which may cause a cerebral edema, haemorrhagic transformation (HT) and reperfusion injury[347,351].

Some studies have demonstrated that MMPs may play a role in vascular remodelling and destabilization of atherosclerotic plaques in the internal carotid arteries[352]. Furthermore, it has already been shown that patients at increased risk of ischemic stroke can be identified based on the elevated plasma level of MMP-9 and reduced activity of TIMP[348]. In addition, many studies have also shown the correlation between high level of MMP-9 during the ischemic stroke and a higher probability to suffer HT[353], with MMP-9 concentrations ranging from <40 ng mL^{-1} to >200 ng mL^{-1} having been measured (Figure 2.19)[354,355]. HT is a secondary bleeding occurring in the infarcted brain area due to the disruption of the blood-brain barrier.

The treatment with tissue plasminogen activator (tPA) has been for long the only one approved to treat a patient after an ischemic stroke. tPA has a narrow therapeutic window and the National Institute of Neurological Disorders and Stroke (NINDS) and European Cooperative Acute Stroke Study (ECASS) trials recommend that tPA must be administrated within 3-4 hours after stroke onset to be effective[353,356–358]. However, the tPA given to disrupt the thrombus can also contribute to induce HT and even produce

the dead of the stroke patient. This suggests that early MMP-9 quantification may help to identify stroke patients at risk of suffering HT and who should be treated by mechanical thrombolysis instead[359]. Since the therapeutic window of tPA is very narrow and patient level of recovery after a stroke depends on thrombus removal celerity, a rapid and accurate prediction would be essential to guarantee that patients who can benefit of tPA are treated as soon as possible[360] (Figure 2.19).

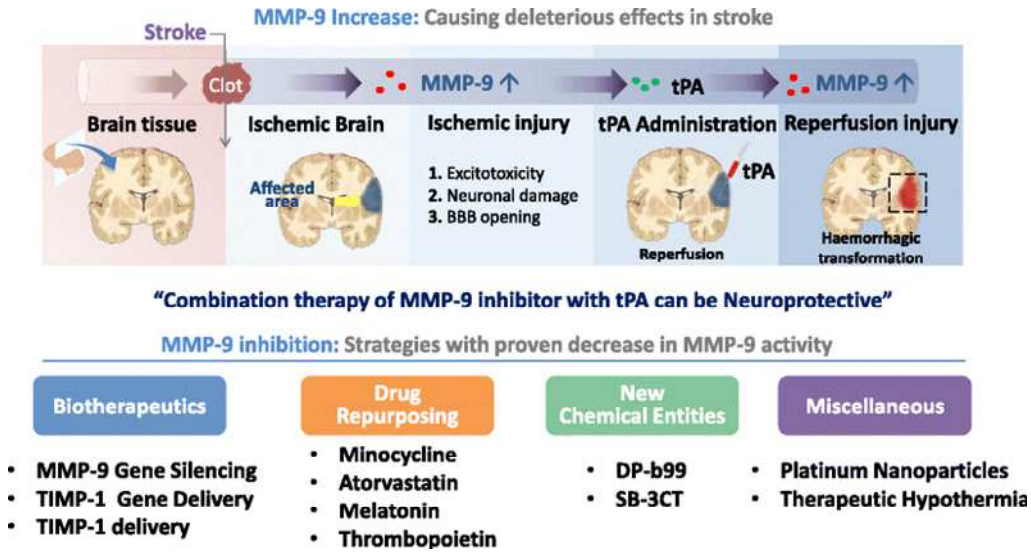

Figure 2.19. tPA treatment and correlation with MMP-9 level in ischemic stroke. Reprinted from ref. [345] with permission of Springer Nature, Copyright 2013.

Over the last decade, the growing interest for MMPs has pushed the development of a variety of devices based on different recognition and signal transduction methods. Although the use of classical assays such as ELISA is still more extended, the development of MMP-9 POC biosensors with high sensitivity, specificity, and selectivity, which could be used at mobile and emergency health units, is highly demanded.

The Table 2.6 summarizes some recent studies describing the development of MMP-9 biosensors. For example, MMP-9 presence has been detected by monitoring its hydrolytic activity on a transducer coated with a hydrogel film[361]. In this biosensor design, electrodes were first coated with oxidized dextran. A peptide substrate containing a specific MMP-9 cleavage site was then cross-linked to the dextran to form the hydrogel layer. Therefore, MMP-9 caused cleavage of the peptide substrate at the cleavage site and the hydrogel layer degraded, which generated changes in the signal registered by the biosensor. In another case, an SPR immunosensor was employed for

the real-time and label-free detection of MMP-9[362]. In this research, an anti-MMP-9 MAb was immobilized via its primary amine groups onto the carboxymethyldextran-coated transducer surface. The interaction between MMP-9 and the MAb impelled changes in the refractive index, which allowed measuring MMP-9 with an LOD of 8 pg mL^{-1}.

Assay format	Detection type	Time of functionalization	Assay steps	Assay time	Detection time	LOD	Samples	Ref.
ELISA	Colorimetric	ON + 1 h (ELISA plates)	4	27 h	NS	10 pg ml^{-1}	50 human cerebrospinal fluid samples	363
Magneto-immunoassay	LC–MS/MS (Immunoaffinity)	1 h 45 min (MB)	2	2 h 45 min	35 min	2-500 ng mL^{-1}	30 mouse serum samples	364
Electrochemical sensor	CV ($[Fe(CN)_6]^{3-/4-}$)	ON + 13 h (GCE/AuNP-PDA-silica/Ab)	1	20 min	-	60 pg mL^{-1}	6 serum samples	365
Electrochemical sensor	EIS (SPGE-competition assay)	15 h 45 min (SAM of thiolated Ab)	2	40 min	5 min	1.1 nM	Serum samples	366
Electrochemical sensor	DPV (electrically heated carbon electrode)	>13 h (MWNTs-PPy-GCE-Ab1; QD-Ab2)	2	40 min	-	0.033 pg mL^{-1}	4 serum samples	367
Electrochemical sensor	SWV (electrically heated C-SPE, HSPCE)	>13 h (GNR-HSPCE-Ab1 & PS@PDA-metal-Ab2)	2	50 min	-	5 fg mL^{-1}	4 serum samples	368
Electrochemical sensor	CV (surface-confined Mblue)	3 h (peptide-MBlue-TFGE)	1	60 min	-	7 pM	-	369
Vertical lateral flow	Fluorescence (sandwich)	ON + 1 h (BSA + Ab)	2	1 h 30 min	15 min	100 ng mL^{-1}	Saliva samples	370
Fluorescence	Fluorescence (AuNC/GO)	22h 50 min (pMAG)	4	14 h 45 min	5 min	0.15nM	-	371
SPR enzymatic sensor	SPR (response units; label-free)	1 h (peptide-coated CM5 SPR sensor)	1	30 min	Real time	70 pg ml^{-1}	-	372
SPR	SPR (Ag-Ab)	3 h	4	40 min	10 min	8 pg mL^{-1}	Saliva samples	362
SERS	SERS (MSB)	13 h (MB)	1	30 min	-	1 pg mL^{-1}	10 serum samples	373
Piezoelectric aptasensor	QCM (sandwich)	50 min (Au-QCS)	2	60 min	Real time	100-560 pg mL^{-1}	Spiked serum samples	374

Table 2.6. Examples of assays reported in the literature for MMP-9 detection. * Ag, antigen; AuNC, Gold Nanoclusters; GCE, glassy carbon electrode; GNR; graphene nanoribbon; GO, graphene oxide; HSPCE, heated SPCE; EIS, electrochemical impedance spectroscopy; LC-MS/MS, liquid chromatography–tandem mass spectrometry; MBlue, Methylene Blue; MSB, Magnetic Separation Biosensor; MUA, mercaptoundecanoic acid; MWCNTs, multi-walled CNT; ON, Over night; PD, polystyrene; PDA, Polydopamine; pMAG, peptide-MUA/AuNC/GO; PPy, polypyrrole; QCM, quartz crystal microbalance; QCS, quartz crystal sensor; SAM, Self-Assembled Monolayer; SERS, Surface-enhanced Raman spectroscopy; SPGE, Screen-printed Gold Electrode; SWV, Square wave voltammetry; TFGE, Thin film gold electrode.

2.5.3. Infectious diseases: PLDH

Malaria is one of the infectious diseases with the highest impact and incidence in the world. According to the WHO, more than three billion people are at risk of acquiring malaria, and only in 2017 malaria produced 219 million cases of infection (92% in Africa) and about 500000 casualties[375]. Owing to the noticeable increase in international traveling and migration, the number of malaria cases imported via tourists and immigrants is rising dramatically, with as much as a 400% increase in reported cases over the last 20 years[376,377].

Malaria is caused by protozoan parasites of the genus *Plasmodium* that are transmitted through the bite of infected female *Anopheles* mosquitoes. There are five *Plasmodium* species that infect humans, *P. falciparum, P. vivax, P. malariae, P. ovale and P. Knowlesi,* of which *P. falciparum* is the most prevalent and the most dangerous, responsible for over 90% of deaths due to malaria[375,378]. *Plasmodium* displays a complex life cycle with different phases (Figure 2.20). The infectious pathway entails the asexually-proliferative parasites, which reproduce in the RBCs of host patients. Parasite-caused RBC lysis results in anemia, microcirculatory obstruction and end-organ dysfunction. Malaria symptoms include fever, fatigue, headaches, and, in severe cases, seizures and coma, eventually leading to death[378].

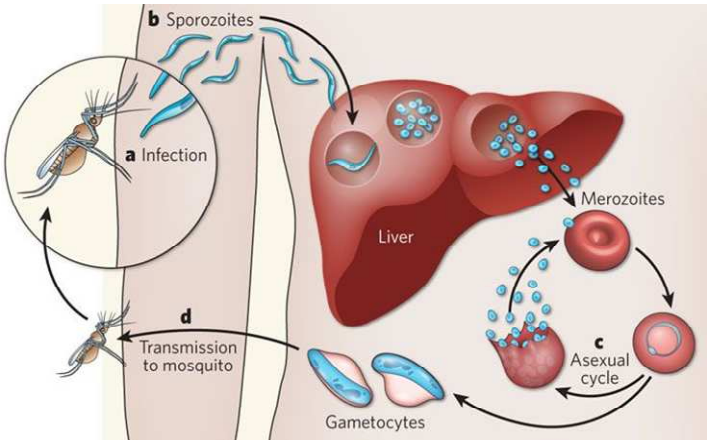

Figure 2.20. Scheme of the different phases of malaria infection. Reprinted from ref. [379] with permission of Springer Nature, Copyright 2009.

Diagnosing malaria in its early stages is vital to prevent the spread of the disease and reduce patient mortality through prompt treatment. Accordingly, expanding population access to rapid diagnosis is the most effective way to guarantee early detection of

malaria and reduce worsening into severe and fatal cases, and has become a priority for the WHO[380,381]. Besides, appropriate treatment selection and treatment response monitoring over time should permit re-adjusting drug dose as needed or identifying treatment failure caused by drug-resistant plasmodia, which is essential to minimize side effects, patient life risk, and pathogen spreading[382]. However, these requirements are not easy to accomplish in resource-poor settings, such as the developing countries in which most malaria cases occur, with the methods currently available for malaria diagnosis[383,384]. It is worth noting that, although a range of devices and methods have been reported in the literature in an attempt to provide upgraded malaria diagnostic tools, including biosensors and microfluidic platforms[385,386], malaria is still diagnosed predominantly by light microscopy, molecular techniques based on the polymerase chain reaction (PCR) and Ag RDTs. Table 2.7 shows some of the current and novel techniques for malaria detection[173,218,387–399].

Microscopy is the gold standard method for the identification of *Plasmodium* infected RBC[381]. The study of thick blood smears allows parasitaemia determination, parasite species identification and disease staging. However, microscopic analysis is not standardized and requires trained staff. The counting of infected RBC generally takes 1 h per sample, with a cut-off of between <10-50 parasites per μL of blood (p μL^{-1}; approximately 0.001% parasitemia) to 100-500 p μL^{-1}, depending on the microscopist skills and experience[400].

On the other hand, molecular techniques based on PCR started to be also used by end of the 1980s thanks to their high sensitivity. This methodology grants detection limits below 5 p μL^{-1} (equivalent to a 0.0001% parasitemia[401]), but is time consuming, expensive and needs sophisticated installations and well-trained personnel. In addition, molecular methods cannot distinguish between viable and non-viable parasites, which make them useless for treatment response monitoring.

Nowadays, several Ag RDTs are available for malaria detection, which are mostly lateral flow immuno-chromatographic devices that are extremely economical, fast and simple to use[383]. In RDTs, while the sample and reagents flow along the device, plasmodia Ags are sandwiched between a flowing immunoconjugate and the immobilized c-Ab, forming coloured bands in 15-30 min that are interpreted visually. The WHO recommends the employment of RDTs for malaria diagnosis in developing

countries due to their portability, simplicity, quick visual result and low cost. Nevertheless, RDTs have several drawbacks as well, such as lack of sensitivity (cut-offs >100-200 p μL^{-1}, equivalent to 0.002% parasitemia, when detecting *Plasmodium falciparum* histidine-rich protein II, PfHRP-II[401]), variability, and qualitative or semi-quantitative response[384].

The detection of certain biomarkers of *Plasmodium* infection in the early stages of malaria can be crucial for devising disease management strategies and choosing correct prophylaxis. The host immune response can express a unique pattern against the pathogen, which may be directly correlated with disease progression[402,403]. Currently, several malaria-associated biomarkers have been identified, including PfHRP-II, which is only produced by *Plasmodium falciparum*, *Plasmodium* aldolase (PALD), lactate dehydrogenase (PLDH), and *g*lutamate dehydrogenase (PGDH), which are produced by the different species, and products such as hemozoin[403]. However, the most widely used biomarker, especially in RDTs, is PfHRP-II, with an increasing presence of PLDH[402].
PfHRP-II is a water-soluble protein, rich in histidine and alanine amino acids, which is mostly confined in the cytoplasm of the parasite. However, substantial amounts of the protein are secreted by the parasite into the host's bloodstream and can be detected in RBC, serum, plasma and urine of the infected individuals[404]. HRP-II is a *P. falciparum*-specific Ag. Therefore, assays based in HRP-II detection are unable to detect other human-infecting *Plasmodium* species. In some patients, HRP-II will persist for several weeks in peripheral blood after the resolution of clinical symptoms and parasitemia. Consequently, this biomarker cannot be used reliably to monitor patient response to therapy[403].

On the other hand, PLDH is a water-soluble enzyme secreted by all the human-infecting *Plasmodium* species during infection, but with specific isomers in each of them[405]. PLDH is required for anaerobic ATP generation in the parasite, a glycolytic pathway during which the enzyme converts pyruvate into lactate. PLDH expression level increases gradually and reaches its peak within the first 24 to 30 hours of infection. However, some reports indicate that the PLDH enzyme disappears within 24 hours of effective malaria treatment[406]. For this reason, PLDH has been proposed by some authors as a good target to monitor parasite response to treatment and predict treatment failure[407,408]. Interestingly, PLDH can be easily distinguished from mammalian LHD due to presence of a long substrate specificity loop[409].

Assay format	Detection type	Target	Assay steps	Assay time	Detection time	LOD	Samples	Ref.
Electrochemical Magneto-immunosensor	Amperometric (GEC electrode)	PfHRP-II	2	2 h	2 min	0.36 ng mL^{-1}	Human serum samples	173
Electrochemical sensor	CV, EIS and SWV (CNTs electrode)	Ag Pv (CSP and TRAP)	3	30-60 min	2 min	50 fg mL^{-1}	Mouse serum sample	388
Electrochemical sensor	Amperometric (sandwich AuNPs)	pLDH	3	ON (cAb) + 2 h	2 min	23 pg mL^{-1}	Serum samples	390
Electrochemical sensor	Impedimetric (CZnONF GCE electrode)	PfHRP-II	4	15 h + ON (Electrode)	-	6.8 ag mL^{-1}	-	398
Chemiresistive sensor	Chemiresistive (MWCNT-ZnO nanofiber electrode)	PfHRP-II	5	9 h (Electrode)	30 min	0.97 fg mL^{-1}	-	387
Microfluidic chip	Electrochemical (SWV)	PfHRP-II	2	15 min	1 min	16 ng mL^{-1}	Spiked human serum samples	394
Microfluidic chip	Fluorescence (IGSS assay)	PfHRP-II	2	20 min	-	6 ng mL^{-1}	Spiked serum samples	391
Droplet microfluidic chip	Fluorescence (REEAD)	PTopI	3	45 min	1 h 45 min	< 1 parasite mL^{-1} blood 60 parasite mL^{-1} saliva	20 blood and 5 saliva samples	393
Magneto-Droplet based microfluidic device	Fluorescence (QD-MB)	PfHRP-II	3	1 h 30 min	-	0.1 ng mL^{-1}	Spiked serum samples	218
Fluorescence Immunoassay	Fluorescence (AuNP-MUA)	PfHsp70	2	30 min	3 h	2.4 µg mL^{-1}	Pf RBC culture	392
Fluorescence Magneto-immunoassay	Photoluminescence (QD-MB)	PfHRP-II	3	4 h	-	0.5 ngmL	Urine and serum samples	399
3D LFIA	Test line (AuNPs-ATPS)	pLDH	1	5 min	20 min	1.0 ng mL^{-1}	Fetal bovine serum	395
2D µPAD	Colorimetric flatbed scanner (sandwich-HRP)	PfHRP-II	4	3 h	60 - 90 min	0.1 ng mL^{-1}	Fetal bovine Serum	396
2D µPAD	Colorimetric (sandwich)	PfHRP-II	3	20 min	5 min	5.0 ng mL^{-1}	-	389
3D µPAD	Multiplexed Colorimetric (AuNPs)	PfHRP-II and PLDH	3	20 min	20 min	HRP2: 46.1 ng mL^{-1} LDH: 100.7 ng mL^{-1}	Lysed whole blood samples	397

Table 2.7. Examples of current tools for malaria diagnosis. *Ag, antigen; ATPS, micellar aqueous two-phase system; CSP, Circumsporozoite protein; CZnONF/GCE, Cu-doped ZnO nanofiber; EIS, electrochemical impedance spectroscopy; GCE, Glassy carbon electrode; GEC, graphite epoxy composite; HRP-II, histidine-rich protein 2; IGSS, immuno-gold silver staining; MUA, mercaptoundecanoic acid; MWCNT, multi walled CNT; Pf, Plasmodium falciparum; PfHsp70, Plasmodium falciparum heat shock protein 70; PTopI, Plasmodium topoisomerase I; Pv, Plasmodium Vivax; REEAD, rolling-circle enhanced enzyme activity detection; SWV, Square Wave voltammetry; TRAP, Thrombospondin related anonymous protein; uPAD, microfluidic paper-based analytical device.

Chapter 3

Materials and Methods

3. Materials and methods

3.1. Chemicals, Biocomponents and Reagents

3.1.1. Magnetic Beads (MB)

The MB used in this work were superparamagnetic spheres composed of highly cross-linked polystyrene with evenly distributed magnetic material, coated with a hydrophilic layer of glycidyl ether to confine the iron oxide inside them and prevent leakage. In this work, we used streptavidin-coated MB (MyOne Streptavidin (Strep) T1, Ø=1 μm, Ref. 65601) and carboxylic acid-coated MB (Dynabeads MyOne Carboxylic Acid, Ø=1 μm, Ref 65011), both provided by Fisher Scientific (Alcobendas, Spain) (Figure 3.1).

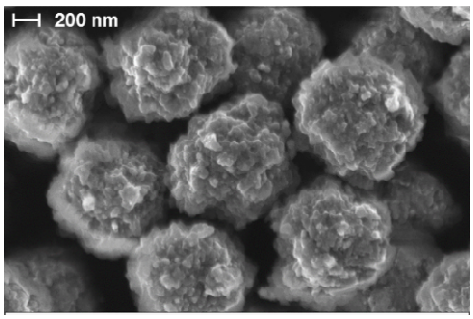

Figure 3.1. Scanning electron microscopy (SEM) images of MyOne carboxylic acid Dynabeads[410].

3.1.2. Biocomponents

Proteins and antibodies (Ab) employed for each study were obtained from different sources depending of the target biomarker as detained next:

- For Myloperoxidase (MPO) detection, full length native human MPO protein (MPO; Ref. ab98926) was from Abcam (Cambridge,UK) and biotinylated mouse anti-MPO monoclonal capture Ab (MPO-bc-MAb; Ref. 4M43B, 16E3) and HRP-conjugated detection Ab (HRP-d-Ab; Ref. 4 M43C, 16B7), were from HyTest (Turku, Finland).

- Matrix metallopeptidase 9 (MMP-9) detection was carried out using the Human MMP-9 DuoSet ELISA Development kit (DY911) from R&D (R&D Systems Europe, Ltd, UK), which was composed by human MMP-9 protein, mouse anti-MMP-9 monoclonal capture Ab (MMP-9-c-MAb) and biotinylated goat anti-MMP-9 polyclonal detection Ab (MMP-9-bd-PAb).

- For *Plasmodium* lactate deshydrogenase (LDH) detection, recombinant LDH from *Plasmodium falciparum* (PfLDH, Ref. A3005) was provided by CTK biotech (San Diego, USA), and PAN *Plasmodium* LDH monoclonal capture Ab (PLDH-c-MAb, Ref. C01834M) and detection Ab (PLDH-d-MAb, Ref.C01835M) were purchased from Biospacific (California, USA).

Unless otherwise recommended by the provider, proteins and Ab were aliquoted immediately after being received, and were stored at -20ºC in isofreeze colour-changing racks. For the ELISA performance, generally, each aliquot was thawed just once and kept at 4ºC until used.

3.1.3. Buffers

All buffer solutions were prepared with milli-Q water and all reagents were of the highest available grade. The composition of these solutions is described in Table 3.1:

Name	Composition	pH
PBS_{1X}	10 mM phosphate, 138 mM NaCl, 2.7 mM KCl	7.4
$PBS\text{-}BSA_{1}$	PBS, BSA 1%	7.4
$PBS\text{-}BSA_{0.1}$	PBS, BSA 0.1%	7.4
$PBST_{0.025}$	PBS, tween 0.025%	7.4
$PBST_{0.05}$	PBS, tween 0.05%	7.4
$PBST_{0.1}$	PBS, tween 0.1%	7.4
MES	150 mM 2-(N-morpholino)ethanesulfonic acid	5.4
RBC lysis buffer	50 mM KH_2PO_4, 300 mM NaCl, 0.25 M imidazole, 1% triton	8.0
Carbonate buffer	0.1 M sodium carbonate ($NaHCO_3/Na_2CO_3$)	9.5

Table 3.1. Composition of the buffered solutions used in this work.

3.1.4. Enzymatic signal amplifiers

Immunoassay spectrophotometric and electrochemical detection was achieved indirectly by monitoring the activity of horseradish peroxidase (HRP) enzymatic labels. Four HRP conjugates were tested:

- Streptavidin-HRP (Strep-HRP; Ref. DY998, R&D).
- Pierce®High Sensitivity Streptavidin-HRP (HS-Strep-HRP; Ref. 21130). According to the supplier's description, this is a peroxidase-streptavidin

conjugate that provides signal amplification like Poly-HRP. It is supplied at 1.1 mg mL^{-1} in an undisclosed stabilizer solution and should be diluted 1:8000 – 1:40000 in PBS-BSA_1 for its utilization.

- Pierce® Streptavidin Poly-HRP (Poly-HRP; Ref. 21140) consists in polymerized HRP conjugated to streptavidin. It is received at 0.5 mg mL^{-1} in an undisclosed stabilizer solution and should be diluted 1:2500 – 1:10000 in PBS-BSA_1.

- Streptavidin-Peroxidase Polymer, Ultrasensitive (Strep-HRP-polym; Ref. S2438; Sigma Aldrich) entails streptavidin and HRP covalently conjugated to a hydrophilic polymer backbone. Received at 1 mg mL^{-1} in PBS-$glycerol_{50\%}$, the provider suggests a dilution 1:200 – 1:1000 in PBS or PBST.

3.1.5. Enzymatic substrates

Six ready-to-use enzyme substrate solutions were compared for the spectrophotometric detection of the Enzyme-Linked Immunosorbent Assays (ELISA) and magneto-immunoassays, or for the electrochemical detection of HRP and MPO. They contain hydrogen peroxide (H2O2) and either 3,3',5,5'-tetramethylbenzidine (TMB; ES-1 – ES-5) or 2,2′-azino-di-(3-ethylbenzthiazoline sulfonic acid) (ABTS; ES-6) at unrevealed concentrations in an acidic buffer (pH 3.50-3.90) of undisclosed composition. Their main characteristics are shown in the Table 3.2. These substrate solutions were stored at 4°C and protected from light, as recommended by the providers. Before their utilization, they were temperate at room temperature and were used straightforward, without requiring any modifycation, addition or dilution.

	Substrate complete name	Provider	Ref.
ES-1	TMB Liquid Substrate System for ELISA	Sigma	T0440
ES-2	TMB Liquid Substrate System	Sigma	T8665
ES-3	TMB Liquid Substrate, Supersensitive	Sigma	T4444
ES-4	Enhanced K-Blue TMB Substrate	Neogen	308175
ES-5	K-Blue Aqueous Substrate	Neogen	331175
ES-6	ABTS	Sigma	A3219

Table 3.2. Ready-to-use enzyme substrate solutions tested for HRP and MPO detection.

3.1.6. Filter paper

Nine different GE Healthcare membranes designed for lateral flow test fabrication were studied in this work to produce microfluidic devices and electrodes. Table 3.3 shows the characteristics of these commercial membranes[411].

Description (Ref.)	Material	Properties	Lateral flow application	Thickness (µm)	Capillary flow rate (s/4cm)	Water absorption (mg/cm^2)
LF1 (8121-1750)	Bound glass fibre	Compatible whole blood and serum samples. Can act as a blood separator	Blood separation	247	35.6	25.3
MF1 (8122-2250)			Blood separation	367	29.7	39.4
VF2 (8124-1750)			Blood separation	785	23.8	86.2
Standard 17 (8134-2250)		Faster flow sample retention than cotton	Conjugate release	370	34.5	44.9
GF/DVA (8145-2250)		Compatible with saliva samples. Can act as a blood separator	Blood separation	785	28.2	93
CF5 (29008181)	100% cotton linter	Medium weight	Absorption pad	954	63.3	99.2
CF4 (8114-2250)			Sample application-Absorption pad	482	67.3	49.9
Fusion 5 (8151-9915)	Glass fibre–based material that contains a plastic binder	Can be used as a lateral flow blood separator	Blood separation – Conjugate release	370	38	40
Prima 40 (13549500)	Nitrocellulose		Backed reservoir pad	192	44	-

Table 3.3. Characteristics of the different commercial GE Healthcare membranes tested in this work.

3.1.7. Other reagents

Several chemical reagents used during this work were purchased from Sigma Aldrich (Spain), including bovine serum albumin (BSA), Tween x20, potassium ferrocyanide ($K_4Fe(CN)_6$), biotin, imidazole 1 M (Ref. 68268), and PAP pens for immunostaining (Ref. Z672548-1EA). 1-Ethyl-3-(3-dimethylaminopropyl) carbodiimide hydrochloride (EDC), sulfuric acid 1M, StartingBlock (Ref. 37538) and biotin XX-SSE (B6352) were acquired from Fisher Scientific (Spain). Reagent Diluent Concentrate 2 (RD; RYD-DY995) was provided by R&D. Aquablock liquid (Rubson SX9000) was from Henkel (Germany). Methylene blue (Ref. J60823) and Triton 100X (A16046) were obtained from Alfa Aesar (Germany).

3.2. Instrumentation

3.2.1. Agitation equipment

Several rotation and agitation equipment were used during this work to study the effect of agitation in MB immunocapture, which are described in this section.

• Stuart SB2 rotator (Bibby Scientific Limited, Stafford-shire, UK). This equipment included a wheel 22 cm in diameter that rotated at a fixed speed of 20 rpm and whose angle of inclination could be adjusted (Figure 3.2a).

• Mini Lab Roller rotator (Labnet International, New Jersey, USA). This compact equipment displayed a 15-cm wheel that could be placed either in vertical or horizontal position, and that rotated at a fixed speed of 24 rpm (Figure 3.2b,c).

• Licuos Vortex (Nirco S.L., Madrid, Spain). This economical vortex agitator accommodated a platform that hold up to 15 Eppendorf tubes and that could vibrate between speeds ranging approximately between 100 rpm and 2500 rpm (Figure 3.2d).

• Vortex Genie 2 (Scientific Industries; Bohemia, USA). This robust vortex agitator accommodated a wide platform that hold up to 30 Eppendorf tubes. Vibration speed could be regulated between approximately 600 rpm and 3200 (Figure 3.2e).

• Grant-bioPTR-30 agitator (Grant Instruments, Cambridge, UK). This was a compact equipment containing a helical wheel placed horizontally, which could be subjected to orbital rotation, reciprocal motion (equivalent to tilting), and vortexing, all at variable speed, as well as a combination of them (Figure 3.2f).

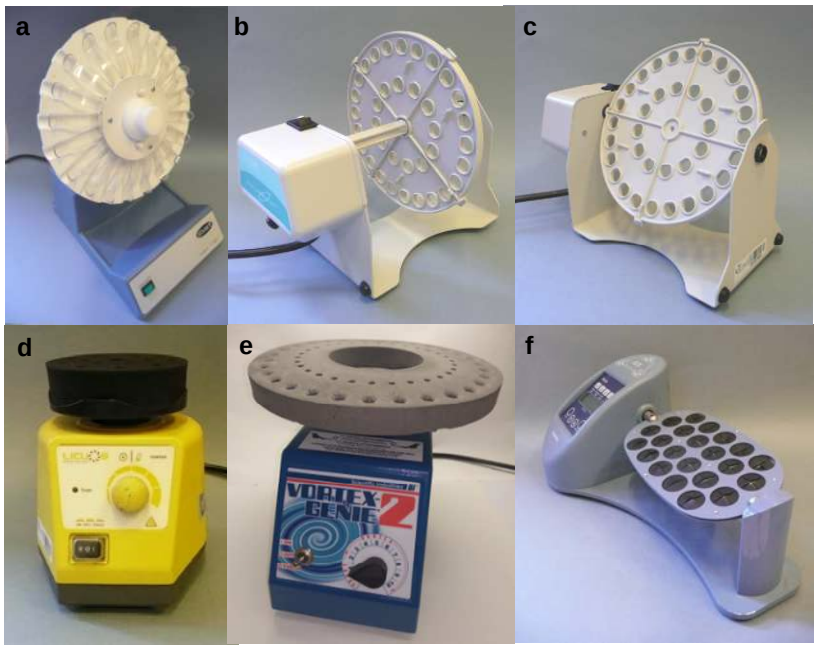

Figure 3.2. Images of the different equipment used for MB incubation under agitation conditions. (a) Stuart Rotator SB2; (b) Mini Lab Roller under vertical rotational position; (c) Mini Lab Roller under horizontal rotational position; (d) Licuos Vortex; (e) Vortex Genie 2; (f) Grant-bio PTR-30 mixer.

3.2.2. Electrochemical measurement equipment

Most electrochemical measurements were performed with a µStat 8000 multipotentiostat (Figure 3.3a), using either a µStat 8000/P Cable Connector (Figure 3.3b**)** or eight µStat Cable Connectors arranged in a parallel position (Figure 3.3c) to connect eight individual electrodes (Dropsens, Llanera, Spain). A portable bipotentiostat µStat 400 with a boxed connector, from the same company, was used alternatively for POC testing (Figure 3.3d). The two potentiostats worked with the Dropview 8400 Software (Dropsens).

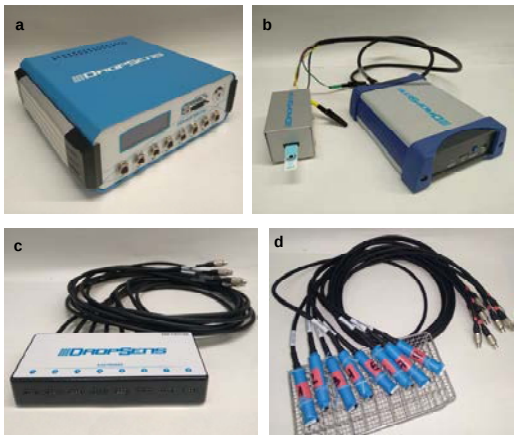

Figure 3.3. Images of the different potentiostats and connectors used for electrochemical measurements. (a) µStat 8000 multipotentiostat. (b) µStat 400 Portable bipotentiostat and a boxed connector for a single electrode. (c) Multiplexed connector for eight individual electrodes. (d) Eight individual cables arranged in parallel for connection of eight electrodes.

3.3. Electrochemical sensors

The electrochemical detection of the magneto-immunoassays was performed using screen-printed carbon electrodes (SPCE).

Three types of electrodes were used along this thesis project, commercial SPCE, custom-made microfluidic paper single-sided SPCE (MP-ssSPCE) and custom-made microfluidic paper double-sided SPCE (MP-dsSPCE). The latter two were produced in collaboration with Dr. Javier del Campo at *Institut de Microelectrònica de Barcelona* (IMB-CNM, CSIC). This section describes the characteristics of each one.

3.3.1. Commercial Screen-Printed Electrodes

A commercial SPCE has been used, which is shown in Figure 3.4 (DRP-110; DropSens, Oviedo). It included 3-electrode electrochemical cell printed on a ceramic substrate (L33 x W10 x H0.5 mm). The electrochemical cell consisted on a carbon working electrode (WE) (4 mm diameter), a carbon counter electrode (CE) and a silver pseudoreference electrode (RE), all connected by silver electric contacts.

Figure 3.4. Images of the commercial carbon SPCE used in this work DRP-110.

3.3.2. Production of Microfluidic Paper Single-Sided SPCE

Two types of custom-made paper SPCE were produced along this thesis project, in both cases using Fusion 5 membrane as the physical substrate for printing. MP-ssSPCE were formed by three electrodes, printed in one of the sides of the microfluidic device (i.e., 6 x 80 mm Fusion 5 strips), which were used as the carbon WE (1 mm x 2 mm), the CE (3 mm x 2 mm) and the Ag pseudo-RE (1 mm x 2 mm) (Figure 3.5a). Each fabrication process involved 6 steps to produce 5 MP-ssSPCE per run.

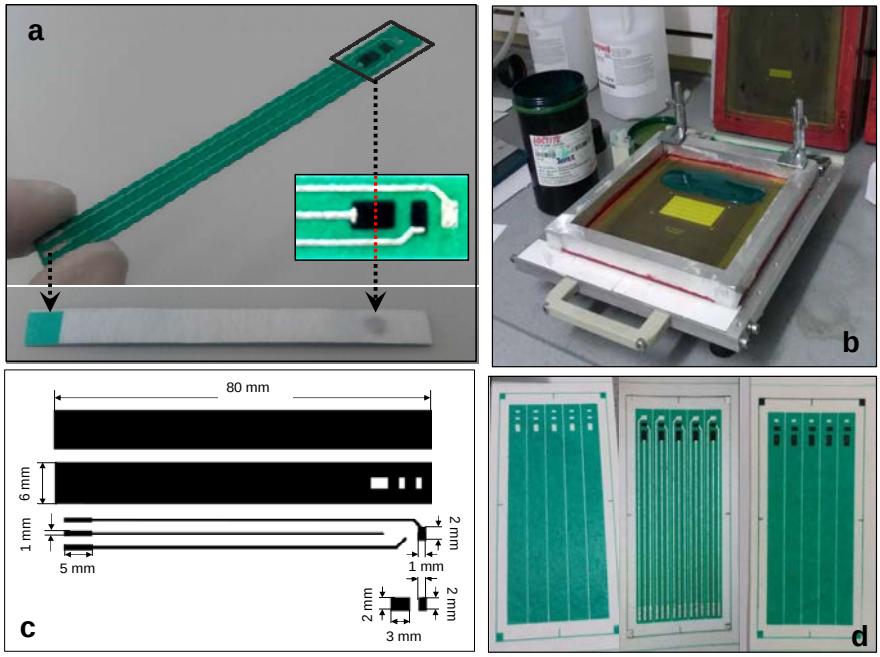

Figure 3.5. MP-ssSPCE fabricated in the IMB-CNM-CSIC. (a) Photography of the devices, with 3 electrodes screen-printed on one of the sides. (b) Photography of the home-made manual press used. (c) Dimensions of the different electrodes. (d) Images of different printing stages.

The masks for screen-printing were designed using Vectorworks 2016 (Techlimits, ES). Production of the screens (25x25cm/21x21cm, outer dimensions/inner dimensions, with different mesh and mesh angles as it will be detailed next) was subcontracted to Paymser (Spain). Mesh count is given in threads per cm unless otherwise stated.

The fabrication procedure consisted of the following steps:

I. Fusion 5 substrates (60 x 120 mm) were cut by laser to facilitate their alignment along the consecutive printing steps.

II. A layer of dielectric UV curable dielectric paste (Electrodag™ PF-455B; Henkel, Spain) was printed in two consecutive steps, and accomplished four purposes: (1) it insulated the conducting tracks between the contact pads and the electrodes, (2) it defined the electrode areas, (3) it provided control over the free volume inside the lateral flow membrane (see results and discussion in Section 8.1), and (4) it provided mechanical stability to the strip and prevented the need for a backing tape. It was found that using a 120–34 mesh screen (120 threads per cm, with fibres 34 mm in diameter) for the first step was enough to provide an effective barrier whilst leaving most of the membrane volume free at a high fabrication yield. Next, the same pattern was printed through a 90–48 mesh screen. The purpose of this second layer was to smooth the surface of the Fusion

5 strip, characterized by high roughness (2.9±0.4 μm rms), and provide mechanical stability to the device. Indeed, roughness was reduced from 2.9±0.4 μm to 1.6±0.2 μm after the second layer printing of the dielectric coating.

III. Next, the WE and CE were printed using a carbon paste (C2030519P4; Gwent Electronics materials Ltd, UK) and were cured at 90ºC for 20 min.

IV. The silver paste Electrodag™ 725A (Henkel, ES) was used to print the pseudo-RE, tracks and contact pads through a 77–48 mesh screen, followed by curing at 120ºC for 15 min. A mesh count of 77 was chosen due to the roughness of the Fusion 5 material, to ensure continuous tracks of low resistance.

V. The tracks were then protected with a new dielectric coating, this time printed through a 90–48 mesh screen.

VI. Last, to prevent that the solutions soaked the connectors, a 1 cm-wide band was printed on the back of the contacts through a 43–90 mesh screen. The aim was to dispense enough paste to saturate the membrane.

VII. After printing, the Fusion 5 substrates were laser-cut into individual strips that were ready to use with a standard 2.54 mm pitch connector.

All the prints were made on a home-made manual press using shore 75 square polyurethane squeegees (15 x 1 cm). The press was built using a set of 2 hinge clamps (Paymser, ES) and mounted on a 1 cm-thick aluminium flat board. Snap-off distances could be controlled using custom-made stackable 0.5 mm-thick gauges (Figure 3.5b).

3.3.3. Production of Microfluidic Paper Double-Sided SPCE

MP-dsSPCE were produced by a double-sided screen-printing process (Figure 3.6a), using in this case masks designed using CorelDRAW 2017 (Corel Corporation, Canada). The resulting devices included an Ag pseudo-RE printed in the bottom side and double-sided graphite WE and CE. The dimensions of the different device components have been summarized in Figure 3.6c. 16 chips (10x20 mm) were printed per production batch through a process involving 8 printing steps that are detailed next.

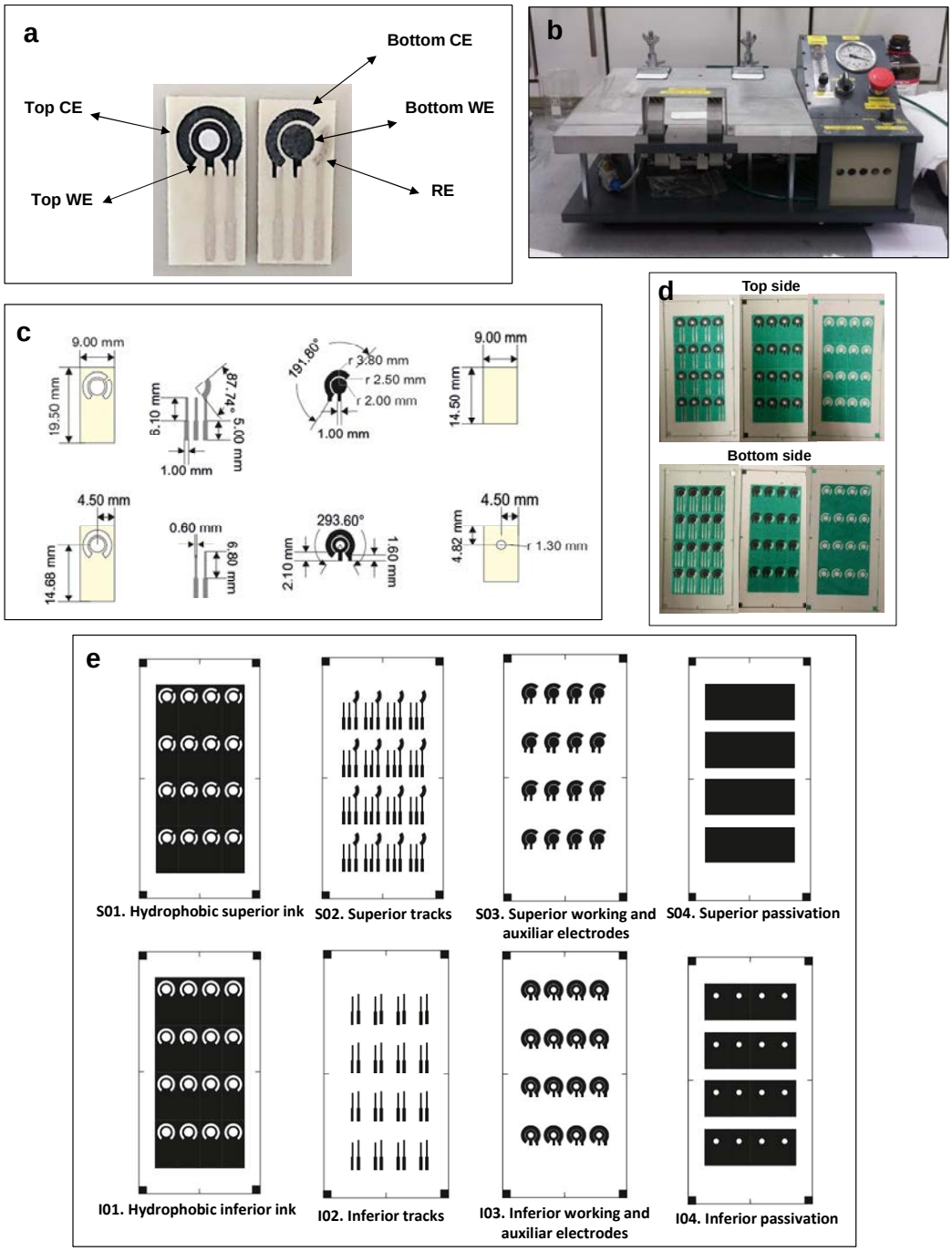

Figure 3.6. MP-dsSPCE fabricated in the IMB-CNM-CSIC. (a) Photography of the devices, with 2 electrodes printed on the top side and 3 electrodes screen-printed on the bottom side. (b) Photography of the commercial manual equipment used for printing. (c) Dimensions of the different electrodes. (d) Images of different printing stages. (e) Images of the masks used for printing.

The fabrication procedure consisted in printing the electrodes on the two sides of the Fusion 5 substrate. First, the top side was printed, the inks were cured in an oven, the Fusion substrate was flipped upside-down, and the process was repeated on the other side. For the steps I-III, the conditions followed for the screen-printing of the top side were the same than in the Section 3.4.3 I-II.

III. The silver paste Electrodag™ 725A (Henkel, ES) was used to print the tracks and contact pads through a 77 mesh screen, followed by curing at 120ºC for 15 min.

IV. The tracks were then protected with a new dielectric coating, this time printed through a 90 mesh screen.

V. The Fusion 5 substrate, with a side already printed and cured, was turned upside-down and the screen-printing process proceeded in the bottom side.

VI. A layer of dielectric UV curable dielectric paste was printed following the same method than in the top side.

VII. Next, the WE and CE were printed as already described in Section 3.4.3 III.

VIII. A silver paste was used to print the pseudo-RE, tracks and contact pads through a 77 mesh screen, followed by curing at 120ºC for 15 min.

IX. The tracks were then protected with a new dielectric coating through a 90 mesh screen.

X. After printing, the Fusion 5 substrates were laser-cut into individual strips that were ready to use with a standard 2.54 mm pitch connector.

3.3.4. Electrochemical characterisation of the electrodes

Before their utilization, commercial SPCE were rinsed with ethanol 70% and water, and were dried under an air flow. It was observed that this treatment improved the performance and reproducibility of these devices, which could be re-used 4-5 times. On the contrary, the MP-SPCE could not be washed or reused.

The electrochemical method used for electrode characterization was cyclic voltammetry (CV), which was employed to assess the status and functionality of the electrodes and discard those performing worse than the average. CV consists of scanning linearly the potential of a stationary working electrode (in a non-stirred solution) using a triangular potential waveform. Here, electrodes were characterized by CV in 0.1M KCl, 1mM $K_4Fe(CN)_6$. Outliers displaying peaks above/below 10% of the average values were discarded (Figure 3.7).

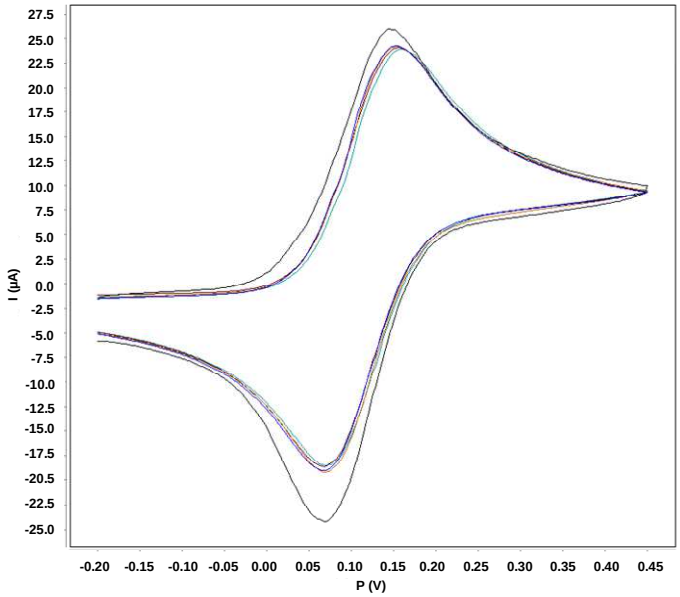

Figure 3.7. SPCE electrode characterization by CV in $K_4Fe(CN)_6$. The image displays the CV registered for eight independent SPCE, including an outlayer that produced peaks wider and higher than the average and had to be discarded.

CV was also used to estimate the electron transfer coefficient (k0) of electroactive species at the different electrodes tested using the method Nicholson's treatment[412,413] using the following equation,

$$\Psi = k0[\pi Dn\nu F/\,(RT)]^{-1/2}$$

where Ψ is a kinetic parameter, D is the diffusion coefficient ($cm^2\ s^{-1}$), n is the number of electrons involved in the process, v is the scan rate ($V\ s^{-1}$), F is the Faraday constant (96485 $C\ mol^{-1}$), R the gas constant ($J\ mol^{-1}\ K^{-1}$), and T the temperature (K). The kinetic parameter, Ψ, is tabulated from the experimental peak separation, ΔEp, at a set temperature (298 K) for a one-electron process whatever the scan rate employed.

The function of Ψ (ΔEp), which fits Nicholson's data, for practical usage is given by

$$\Psi = (-0.6288 + 0.0021X)/(1 - 0.017)$$

where X = ΔEp is used to determine Ψ as a function of ΔEp of the recorded voltammetry. Following these premises, k0 ($cm\ s^{-1}$) corresponds to the slope of the plot of Ψ versus $[\pi DnF/\,(RT)]^{-1/2}\nu^{-1/2}$.

On the other hand, diffusion coefficients were calculated chronoamperometrically employing the Cottrell equation:

$$i = (nFAC_o\sqrt{D})/\sqrt{\pi t},$$

where i is current (A), n the number of electrons (to reduce/oxidize one molecule of analyte, F the Faraday constant (96485 C mol^{-1}), A the area of the (planar) electrode in cm^2, Co the initial concentration of the reducible analyte (mol cm^{-3}), D the diffusion coefficient for the species (cm^2 s^{-1}) and t the time (s).

3.4. Magnetic bead modification with capture antibody

Capture antibody (c-Ab) incorporation onto MB surface can be accomplished by different means[8]. Because a significant number of MB with different functionalities on surface are commercially available, numerous protocols and reagents exist for MB immuno-modification[16,414]. Here, the c-Ab was alternatively coupled to MB displaying a reactive group on surface (-COOH) employing chemical cross-linkers, or biotinylated and coated onto streptavidin-coated MB trough affinity binding, an efficient and stable interaction.

3.4.1 Streptavidin MB immunomodification

MPO detection was performed using streptavidin-coated MB modified with MPO-bc-MAb. Briefly, 400 µL of streptavidin-coated MB (10 mg mL^{-1}, equivalent to ~7–10 × 10^9 beads mL^{-1}) were washed twice with PBS using a magnetic separator and were incubated with 60 µg of MPO-bc-MAb for 45 min under rotation (24 rpm). MPO-bc-MAb-MB were then washed twice with 800 µL of PBS, were incubated with biotin 2.5 mM for 15 min in order to block any biotin-binding sites remaining free, were washed again three times with $PBST_{0.05}$-$BSA_{0.1}$ and were resuspended in 800 µL of PBS-$BSA_{0.1}$ for storage at 4°C at a final concentration of 3.5–5 × 10^9 MB mL^{-1} (equivalent to 5 mg mL^{-1}).

3.4.2 Carboxylic acid MB two-step immunomodification

Formation of amide bonds between primary amino groups in the c-Ab and the carboxylic acid groups on the surface of the MB was mediated by carbodiimide activation. A two-step protocol, consisting of carboxylic acid activation with EDC and subsequent immobilization of c-Ab on the MB surface, was used for the MMP-9

detection (Figure 3.8). For that, 200 µL of carboxylic acid coated MB were washed twice with PBS using a magnetic separator and were incubated with EDC (4 mg mL^{-1} in MES) for 30 min in darkness, under shaking at 600 rpm using a Vortex Genie 2. MB were next washed once with MES and once with PBS (200 µL each) and were incubated with 50 µg of MMP-9-c-MAb for 2 h under the same conditions. MMP-9-c-MAb-MB were then washed twice for 5 min with 100 µL of $PBST_{0.1}$ and were re-suspended in 1 mL of $PBST_{0.1}$-$BSA_{0.2}$ for storage at 4°C (final concentration of 1.4 – 2.4×10^9 MB mL^{-1}, equivalent to 2 mg mL^{-1}).

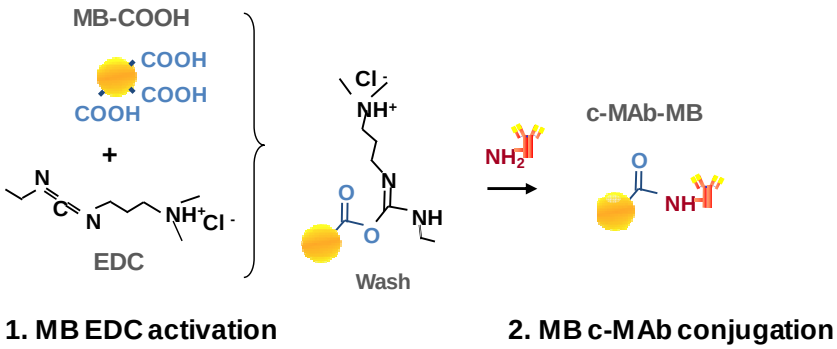

Figure 3.8. Scheme of carboxylic acid MB 2-step immunomodification.

3.4.3 Carboxylic acid MB one-step immunomodification

In order to improve MB immunomodification and increase the sensibility of the magneto-immunoassay, MB immunomodification was re-optimized. The best performing protocol was a one-step procedure that was initially optimized for MMP-9 detection and later transferred for PfLDH detection (Figure 3.9). In this case, 200 µL of MB were washed twice with 15 mM MES, pH 6, using a magnetic separator. MB were next incubated for 2 h in the dark with 50 µg of c-MAb in 100 µL of EDC (4 mg mL^{-1} in MES), under shaking at 600 rpm using a Vortex Genie 2. After that, MB were serially washed with 200 µL of MES and PBS and were blocked with PBS-BSA_1 for 1 h. The c-MAb-MB were then washed twice for 5 min with 100 µL of PBS-$Tween_{0.1}$ and were resuspended in 1 mL of $PBST_{0.1}$-$BSA_{0.2}$ for storage at 4°C (final concentration of 1.4-2.4×10^9 MB mL^{-1}, equivalent to 2 mg mL^{-1}).

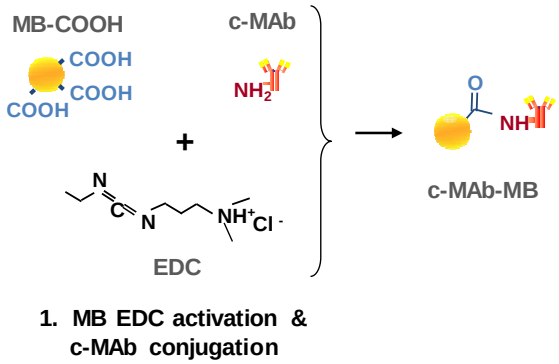

Figure 3.9. Scheme of carboxylic acid MB one-step immunomodification.

3.5. Detection antibody biofunctionalization procedures

In the following section, we provide detailed descriptions of the procedures used in this dissertation for the modification of detection antibodies (d-Ab).

3.5.1 Antibody biotinylation

Biotinylated d-Ab (bd-Ab) were necessary for binding Strep-HRP or Strep-Poly-HRP enzymatic labels in the immunoassays. When bd-Ab were not commercially available, they were modified in the laboratory using Biotin-XX, SSE (6-((6-((Biotinoyl)Amino)Hexanoyl)amino)Hexanoic Acid, Sulfosuccinimidyl Ester, Sodium Salt; Ref. B6352; Thermo Fisher) (Figure 3.10). Biotin-XX, SSE exhibits a succinimidyl ester group that reacts with amines, a sulfonate group that provides water solubility, and a 14-atom spacer that enhances the accessibility of biotin to the relatively deep biotin-binding sites of streptavidin.

A concentrated solution of Biotin-XX, SSE, 2.5 mg/mL, was prepared in MiliQ water immediately before its utilization. Appropriate volumes of this stock solution were added to the d-Ab to reach a molar excess of 18:1 (which had been previously optimized by other members of the team), and the mixture was incubated in rotation for two hours in a room temperature. To calculate the volume of biotin necessary for each d-Ab preparation, it was used the next equation:

$$\mathrm{V(biotin)} = \frac{\left[\left(\frac{\mu g\ Ab}{\text{molecular mass Ab}}\right) * 1000\right] * (\text{Ab: biotin ratio})}{\text{biotin molarity}}$$

After this time, the bioconjugate was purified through a desalting column PD MiniTrap G-25 (GE Healthcare, Ref. 28-9180-07) and eluted with PBS 1X (1.5 mL), recovering 200 µL fractions of the elute. The concentration of bd-Ab in each fraction was analysed with a Nanodrop Spectrophotometer 2000 (Thermo Scientific, USA) at 280 nm. Lastly all the fractions containing bd-Ab were combined and concentrated using a centrifugal filter 100 K Amicon Ultra-0.5 100K (Merck, Ref. UFC510024), the final concentration was measured at 280 nm, and the conjugate was diluted in PBS-BSA_1 at the desired concentration to aliquot and store at -20ºC.

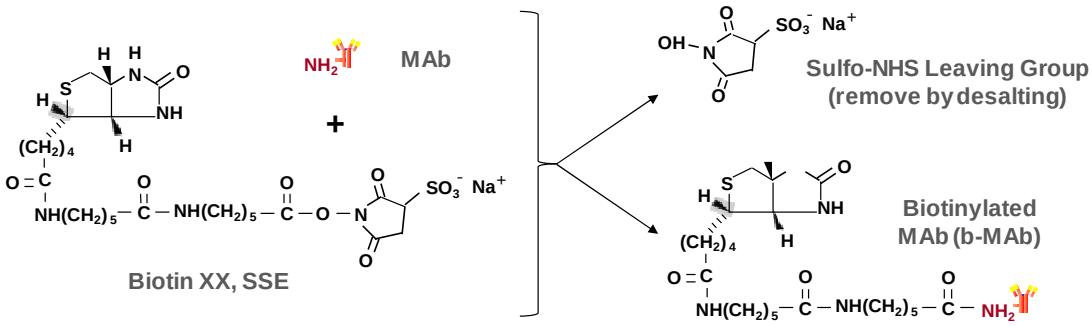

Figure 3.10. Biotin-XX, SSE reaction with NH_2 groups in the d-Ab (the illustrations are not drawn to scale).

3.5.2 Production of bd-Ab/Poly-HRP conjugate

One of the objectives of this work was the development of an extremely fast and simple electrochemical magneto-immunosensor that could be carried out by minimally trained personnel. In order to accomplish this goal, a protocol for the production a bd-Ab/Poly-HRP conjugate was optimized.

For MMP-9 detection, the MMP-9-bd-PAb/Poly-HRP conjugate was produced by incubating under rotation Poly-HRP (10 µg mL^{-1}) with MMP-9-bd-PAb (20 µg mL^{-1}) for 30 min at room temperature in PBS-$BSA_{0.1}$ (24 rpm; Mini LabRoller rotator; Labnet International, New Jersey, USA). Biotin was added (4.88 mg mL^{-1} in PBS), the conjugate was rotated for 30 min more and it was stored at 4°C for up to 1 month.

On the other hand, for PfLDH detection, the immuno-modified PLDH-bd-PAb/Poly-HRP conjugate was produced by incubating Poly-HRP (10 µg mL^{-1}) with PLDH-bd-MAb (45 µg mL^{-1}, previously biotinylated as described in Section 3.5.1), in StartingBlock, for 60 min at room temperature, under rotation (24 rpm). This PLDH-bd-

MAb/Poly-HRP conjugate was then rotated for 30 min with free biotin (4.88 mg mL^{-1} in PBS) and was stored at 4°C for up to 3 weeks.

3.6. Spectrophotometric ELISA protocols

ELISA was used for the first optimization of each assay developed for the different clinical targets studied, including selection of best performing c-Ab and d-Ab pairs, confirmation of target binding efficiency and specificity and determination of starting assay conditions. Using ELISA allowed the simultaneous detection of several samples in 96-well plates, achieving a faster development of the final protocol.

In general, ELISA was performed in 96-well high-binding microtitter plates, which were modified with the appropriate c-Ab and were then blocked with BSA to prevent non-specific binding. It followed incubation with the samples and/or analyte of interest and either direct analyte detection (such as in the case of MPO, which displays peroxidase activity), or indirect detection by serial incubation with a bd-Ab and a streptavidin-HRP/Poly-HRP conjugate. Unless otherwise stated, microtiter plates were covered with an adhesive seal to prevent evaporation during the incubations, which were protected from light, and each incubation was followed by a series of 3 washes with $PBST_{0.05}$.

ELISA spectrophotometric detection was accomplished by monitoring the peroxidase enzymatic activity of either MPO or streptavidin-HRP/Poly-HRP enzymatic labels. In all cases, a commercial ready-to-use chromogen substrate containing H_2O_2 and TMB was used (Ref. T4444, Sigma Aldrich), which had been selected among 6 commercial solutions tested[415](Table 3.2). The TMB in this solution was in its reduced state and was colour-less. In the presence of peroxidase, the enzyme catalysed the oxidation of TMB coupled to the reduction of H_2O_2, yielding a half-oxidised blue complex with an absorbance at 370 nm and 652 nm (Figure 3.11a). In this dissertation, all the spectrophotometric assays were performed by stopping the enzymatic reaction before detection by adding 50 µL of sulphuric acid 1 M, turning the TMB into a yellow fully oxidised product and reading the absorbance at 450 nm using a Sunrise plate reader (Tecan, Switzerland).

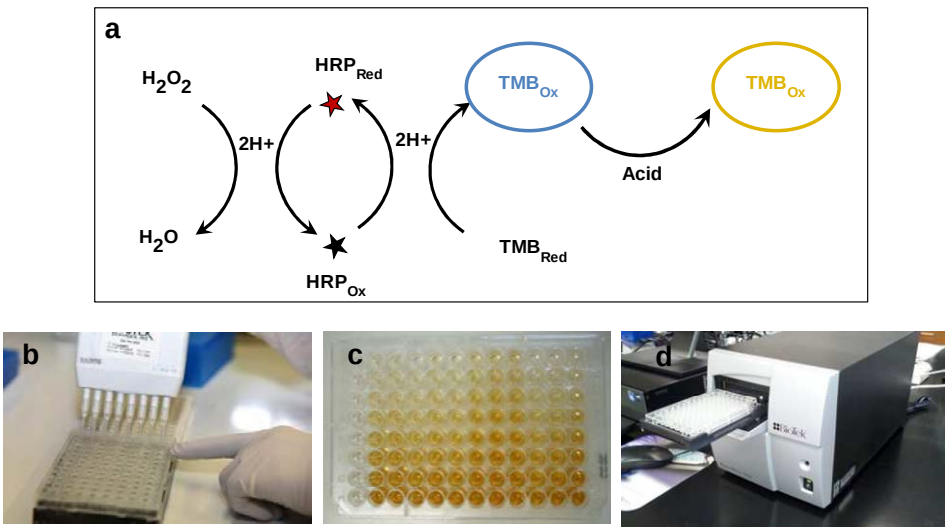

Figure 3.11. (a) Scheme of the detection of HRP using H_2O_2 and TMB for colorimetric detection. (b) Example of multichannel pipette used for the simultaneous addition of solution to rows/files of wells in a microtiter plate. (b) Example of ELISA after incubation with TMB substrate and addition of acid to stop the reaction. (d) Microplate reader.

3.6.1 Direct ELISA

A direct ELISA was optimized for MPO detection. Unless otherwise stated, this assay included incubations at 37ºC under gentle agitation and protected from light, and washes with $PBST_{0.05}$ after each incubation. Briefly, ELISA plates were incubated for 45 min with MPO-bc-MAb at concentrations ranging between 3.9 ng mL^{-1} and 4 µg mL^{-1} in PBS (50 µL per well), were washed twice with $PBST_{0.05}$ (150 µL per well), and were blocked with $PBS\text{-}BSA_2$ (150 µL per well) for 45 min. The plates were next incubated for 30 min with increasing concentrations of MPO (50 µL per well, in $PBST_{0.05}\text{-}BSA_{0.1}$) and were washed four times with $PBST_{0.05}$. Finally, TMB substrate solution was added (100 µL per well), the endogenous MPO peroxidase reaction proceed for 30 min at room temperature and the detection was performed as explained above (Figure 3.12).

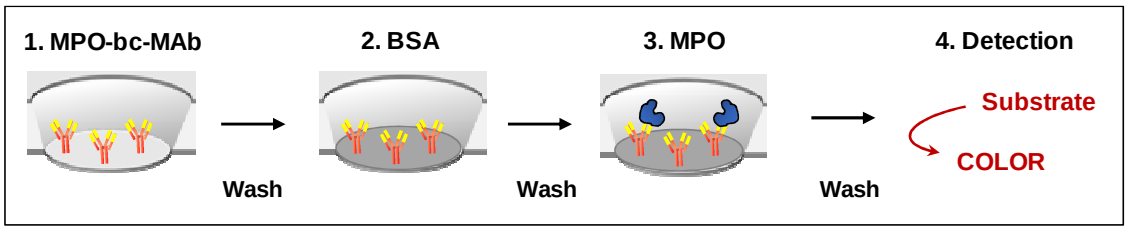

Figure 3.12. Steps to perform a direct ELISA for MPO detection.

3.6.2 Sandwich ELISA

A classical multistep sandwich ELISA was performed for MMP-9 detection using the Human MMP-9 DuoSet ELISA development kit from R&D Systems and following the provider's protocol. A similar assay was used for PfLDH detection, which had been optimized by other team members (unpublished results).

In both cases, the incubations were performed with 100 µL of solution per well, inside an incubator thermostatized at 24°C, and were followed by three washes with $PBST_{0.05}$ (200 µL/well). Briefly, microtitter plates were modified overnight with the corresponding c-Ab (1 µg mL^{-1} MMP-9-c-MAb or 2.5 µg mL^{-1} of PLDH-c-MAb, in PBS) and were blocked with $PBS\text{-}BSA_1$ for 1 h. After washing, the plates were incubated for 2 h with the analyte (30–2000 ng mL^{-1} of MMP-9 in $PBS\text{-}BSA_1$, or 0.0016–100 ng mL^{-1} of PfLDH in $PBST_{0.05}\text{-}BSA_1$). Plates were next incubated with bd-Ab (for 2 h with MMP-9-bd-PAb 100 ng mL^{-1} in $PBS\text{-}BSA_2$, or for 1 h with PLDH-bd-MAb 37.5 - 100 ng mL^{-1} in $PBST_{0.05}\text{-}BSA_1$). The last steps were performed similarly for the two ELISAs, which were incubated with strep-HRP (1:200 in $PBS\text{-}BSA_1$) during 20 min. After four more washes, the plates were incubated for 20 min with TMB and detected (Figure 3.13).

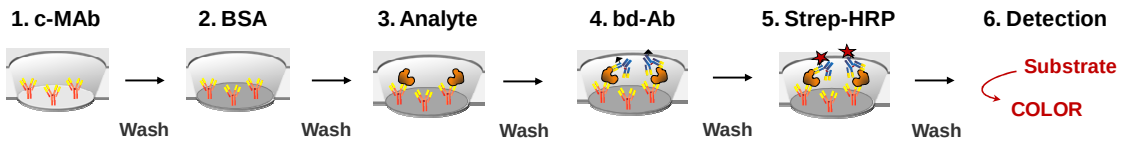

Figure 3.13. Steps to perform a classical sandwich ELISA.

3.6.3 Shortened sandwich ELISA

A shortened ELISA protocol had been developed by other team members and was used here in parallel to the classical protocol as a reference assay[416]. Upon optimization, the "shortened" ELISA consisted of modification of the microtitter plate with c-Ab and BSA as detailed above, followed by a 30 min simultaneous incubation with the protein and the d-Ab. For MMP-9 detection, 15–2000 ng mL^{-1} of MMP-9 and 100 ng mL^{-1} of MMP-9-bd-PAb were incubated in $PBS\text{-}BSA_2$. On the other hand, *Plasmodium* Ag detection was achieved by incubating 0.1–100 ng mL^{-1} PfLDH and 37.5 ng mL^{-1} PLDH-bd-MAb in $PBST_{0.05}\text{-}BSA_1$. In both cases, the plate was washed and incubated

for 10 min with Poly-HRP (1:10000 in PBS-BSA_1), washed four times and detected (Figure 3.14).

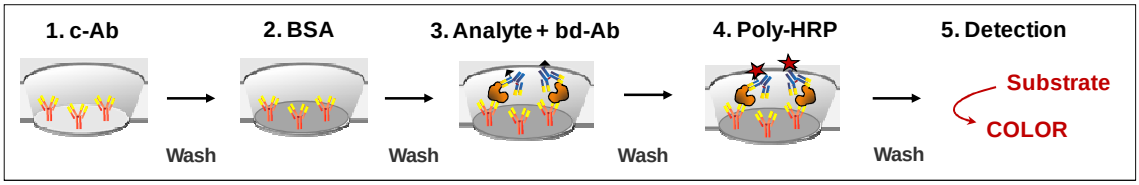

Figure 3.14. Steps to perform a shortened ELISA.

3.7. Spectrophotometric magneto-immunoassay protocols

MB concentration and washing during the magneto-immunoassays was carried out in Eppendorf tubes using a magnetic separator (BILATEST, Sigma Aldrich) (Figure 3.15). Before their utilization, the c-MAb-MB stock was re-suspended under gentle agitation and the amount of c-MAb-MB needed for the assay was transferred to an Eppendorf tube. It followed washing with two volumes of PBS and re-suspension in PBS to a final concentration of 2.5 mg mL^{-1}. MB incubations were carried out in independent Eppendorf tubes, one per each concentration analysed. Unless otherwise stated, incubations were performed at room temperature, protected from light and under agitation or rotation to prevent MB sedimentation. After the incubations, the tubes were placed in a magnetic rack for 2-3 min until MB were confined in the tube wall. The supernatant was removed using a pipette, avoiding touching or disturbing the MB sediment, and washing buffer or the reagent necessary for the next step incubation was added. Finally, MB were re-suspended in 100 µL of TMB and the mixtures were incubated for 20-30 min. For detection, MB were concentrated in the magnetic separator, the supernatant was transferred to the wells of a Non-Binding 96-well microtitter plate (Corning) and the spectrophotometric detection was carried out as before.

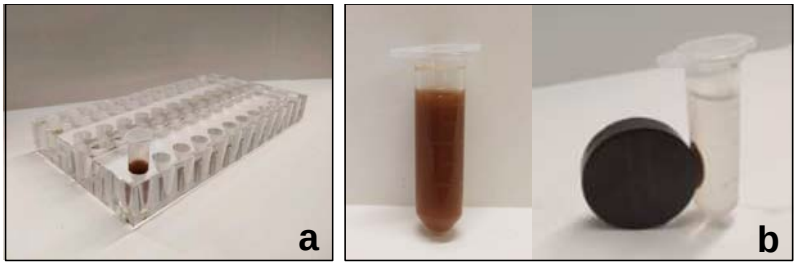

Figure 3.15. (a) Magnetic rack used to concentrate the MB during the magneto-immunoassay. (b) MB in suspension (left) and in contact with a magnet (right).

3.7.1 Three-step magneto-immunoassay

The three-step magneto-immunoassay consisted of directly transferring the conventional ELISA to the surface of the MB. It was developed for MMP-9 and for PfLDH detection also, and it was considered the starting point for magneto-immunoassay optimization (Figure 3.16).

First, 2 µg of c-Ab-MB (either MMP-9-c-MAb-MB or PLDH-c-MAb-MB) were incubated for 30-120 min in 100 µL of increasing concentrations of target analyte (MMP-9 in PBS-BSA_1 or PfLDH in $PBST_{0.05}$-BSA_1). Following washing, MB were resuspended in 100 µL of bd-Ab (10 ng of MMP-9-bd-PAb in PBS-BSA_2 or 37.5 ng of PLDH-bd-MAb in $PBST_{0.05}$-BSA_1). MB were rotated for 30-120 min, were washed twice with $PBST_{0.05}$ and were incubated for 20 min with 100 µL of strep-HRP (1:200 in PBS-BSA_1). Finally, 100 µL of TMB were added and the enzymatic reaction was allowed to proceed under continuous stirring for 20 min. The tubes were then placed in the magnet for 2 min and 100 µL of the supernatants were transferred to a 96-well Non-Binding microtiter-plate for detection.

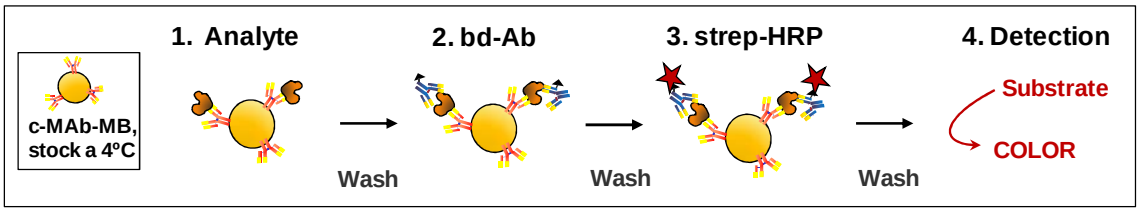

Figure 3.16. Steps to perform a three-step magneto-immunoassay.

3.7.2 Two-step magneto-immunoassay

The magneto-immunoassay described above was next optimized to produce a shorter assay. For this, the two incubations, one with the protein and the other with the bd-Ab, were combined in a single step. Strep-HRP was next substituted by the enzymatic signal amplifier Poly-HRP. The various assay parameters were then re-optimized step-by-step, including duration of the combined one-step incubation, duration of the incubation with the different enzyme conjugates, bd-Ab concentration, Poly-HRP concentration and amount of MB per sample (Figure 3.17).

For *MMP-9 detection*, the shortened 2-step magneto-immunoassay developed consisted of a single 5-min incubation of MMP-9 samples in 100 µL of PBS-BSA_1 with 20 µg of MMP-9-c-MAb-MB and 10 ng of MMP-9-bd-PAb.

In the case of the *PfLDH detection*, a 5-min incubation was performed in 100 µL of $PBST_{0.05}$-BSA_1 with PfLDH, 20 µg of PLDH-c-MAb-MB and 75 ng of PLDH-bd-MAb. Then, it the two cases, 100 µL of Poly-HRP (diluted 1:10000 in PBS-BSA_1) were incorporated and MB were incubated for 5 min more under continuous stirring. MB were washed twice with $PBST_{0.1}$, and colorimetric detection proceeded.

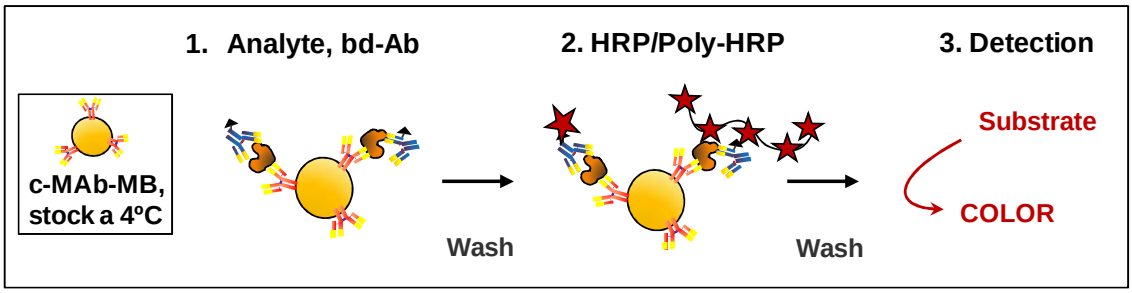

Figure 3.17. Steps to perform a two-step magneto-immunoassay.

3.7.3 One-step magneto-immunoassay

The magneto-immunoassay performed for MPO detection took advantage of the endogenous peroxidase MPO activity, which allowed performing in parallel a one-step magneto-immunoassay (direct MPO detection) and sandwich immunoassay (indirect MPO detection using a HRP-d-Ab). First, the MPO-c-MAb-MB were washed with two volumes of PBS and were re-suspended in PBS to a final concentration of 2.5 mg mL^{-1}. In parallel, MPO was serially diluted in 100 µL of $PBST_{0.05}$-$BSA_{0.1}$. For the direct detection, MPO-containing samples were incubated with MPO-c-MAb-MB for 15 min (Figure 3.18a). Instead, for the sandwich magneto-immunoassay, the MPO-c-MAb-MB were incubated in MPO samples and amount HRP-d-Ab for 5–15 min (Figure 3.18b). In both cases, MB were next washed twice with 500 µL of $PBST_{0.05}$ and once with 100 mL of PBS. Finally, MB were re-suspended in 100 µL of TMB and were incubated for 30 min at room temperature in the dark. At the end, the MB were concentrated in the magnetic separator, the supernatant was transferred to the wells of a microtitter plate and the spectrophotometric detection was carried out.

In the case of MMP-9 and PfLDH detection, the one-step sandwich magneto-immunoassays were optimized using customized immunomodified Poly-HRP conjugates (Section 3.5.2; Figure 3.18c). For that, samples were submitted to a single 5-min incubation with 20 µg of c-MAb-MB and the bd-Ab/Poly- HRP (1:200). MB were then washed twice with 150 µL of $PBST_{0.1}$, were resuspended in 100 µL of TMB and

were incubated for 20 min at room temperature in the dark under shaking. Finally, detection was performed as described above.

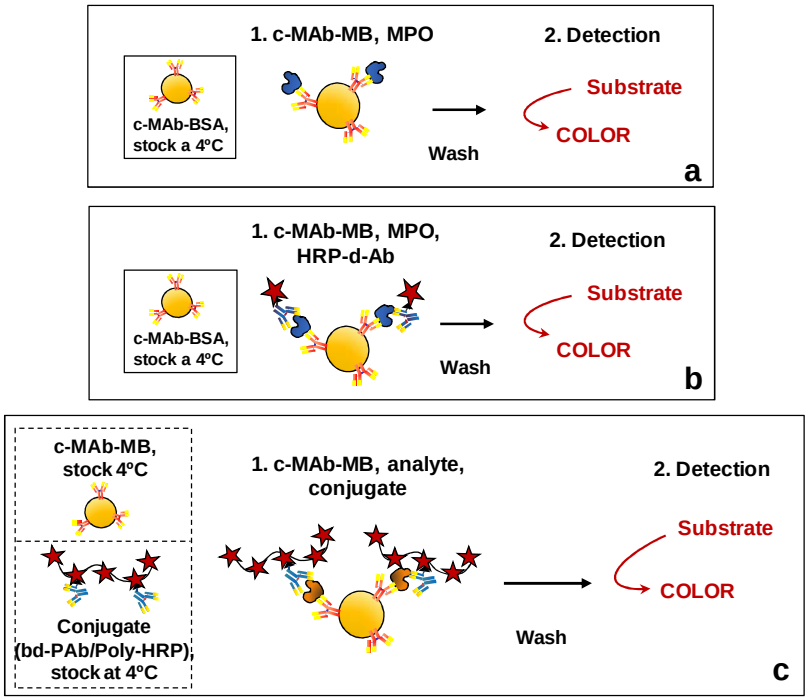

Figure 3.18. Steps to perform a one-step magneto-immunoassay. (a) Direct MPO magneto-immunoassay. (b) Indirect MPO magneto-immunoassay. (c) One-step sandwich magneto-immunoassay.

3.8. One-step electrochemical magneto-immunosensors

The electrochemical detection of the magneto-immunosensors was performed by measuring chronoamperometrically the enzymatic activity of the HRP/Poly-HRP labels. For this, a commercial ready-to-use mixture of TMB/H_2O_2 was used as a substrate/mediator system, which was selected among 6 commercial products tested[415] (Ref. T0440 Sigma Aldrich; Table 3.2). In this system, HRP catalyses the reduction of H_2O_2 coupled to the oxidation of TMB_{red} into $TMB_{ox.}$ The TMB_{ox} mediator was then reduced at the electrode surface back into TMB_{red} by applying a reduction potential on the surface of the electrode. The current measured over time was directly proportional to the concentration of HRP/Poly-HRP on the MB and was thus correlated to the amount of analyte in the sample (Figure 3.19).

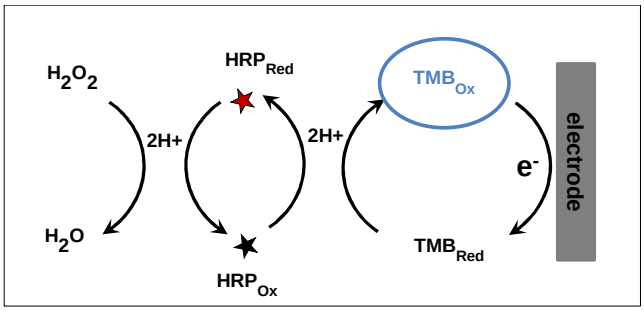

Figure 3.19. Scheme of the electrochemical detection of HRP using H_2O_2 and TMB.

3.8.1 Electrochemical detection using SPCE and a customized magnetic holder after MB manual washes

For the electrochemical detection of the one-step magneto-immunoassays, commercial SPCE were placed in a multiplexed customized 8×magnetic holder[415] (Section 5.2.3; Figure 3.20**)**.

The device contained a base that housed up to 8 SPCE and a sliding component that accommodated 8 neodymium magnets. This movable piece could reach two different positions. In the "on" position, the magnets were placed immediately below the SPCE, which promoted the magnetic confinement of the MB onto the WE. In the "off" position, the magnets were moved away from the WE and MB could be released for SPCE washing and reutilization. The holder was completed with a cover that contained 8 wells, sealed onto the 8 SPCE through o-rings to guarantee tight sealing and prevent liquid spreading. O-rings of two different materials were tested, Viton (7.6 mm internal diameter, 1.78 mm wall thickness; Sigma Aldrich Ref. Z542504) and Fluoroelastomer with Tetrafluorolethylene Additives (FETFE; 7.6 mm internal diameter, 1.78 mm wall thickness; Sigma Aldrich Ref. Z504696).

The procedure using the magnetic holder was always the same regardless of the analyte detected. After the one-step incubation for the immunocapture, MB washes were performed manually. Then, MB were re-suspended in 50 µL of PBS, were transferred to the wells of the magnetic holder, could settle on the SPCE WE for 1 min, and current was allowed to stabilize at 0.00 to −0.05 V *vs*. the Ag pseudo-RE. The measurement was then paused, PBS was substituted by 50 µL of TMB, and the measurement was resumed to register current over the following 150 s (Figure 3.21a).

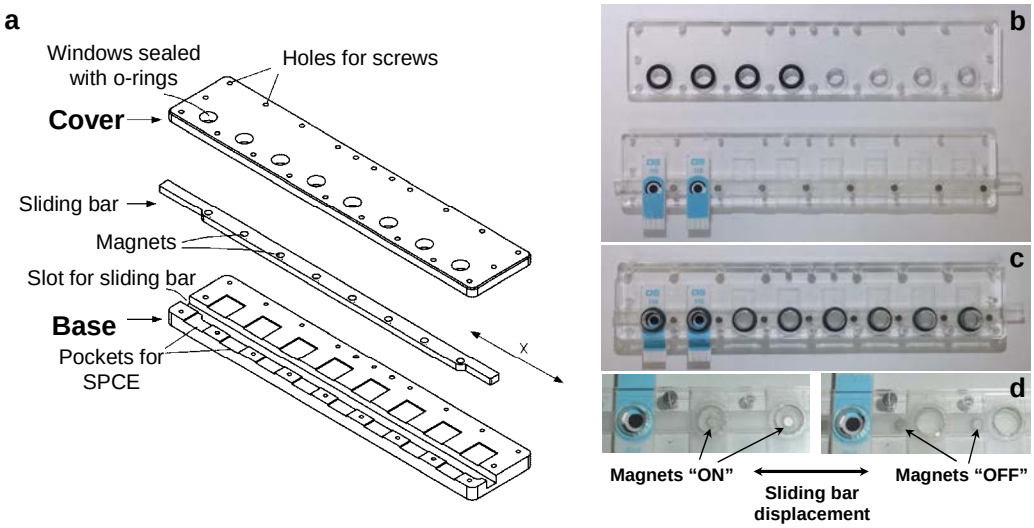

Figure 3.20. Customized magnetic holder for magneto-immunoassay electrochemical detection. (a) Holder components. (b–c) Holder prototype either (b) disassembled or (c) assembled. (d) Performance of the sliding magnetic bar.

3.8.2 Performing paper-driven washes on-chip using commercial SPCE

MB manual washing in tubes was time-consuming, required user training and was an important source of result variability. To replace the manual washes performed to the MB, an absorbent paper device was produced, which was placed above the SPCE to carry out the washes directly on the chips (see Chapter 7). This device included 8 spike-like protrusions, which were approached to or separated from the SPCE electrodes through lateral displacement. This allowed washing the magnetically-confined MB under flow conditions, while the electrochemical detection was carried out under static conditions. In order to facilitate handling of multiple SPCE, the microfluidic device was inserted in the magnetic holder described in Section 3.8.1.

After the immunocapture incubation, the mixture obtained in the one-step magneto-immunoassay was transferred to the SPCE for integrated washing and amperometric detection (Figure 3.21b). First, the sample/MB/reagents mixture was pipetted onto the SPCE though the wells of the magnetic holder and MB were magnetically confined onto the WE surface. Then the microfluidic paper component was used to absorb the mixture of sample and reagents whereas the MB remained on the electrode. The washing step was next performed by two consecutive additions of 50 µL of $PBS_{0.1}T_{0.025}$ through the cover windows. Finally, the paper device was moved away from the electrodes, 50 µL of TMB were added, and the measurement took place for 150 s at 0.00 to −0.05 V *vs.* the Ag pseudo-RE.

3.8.3 Magneto-immunoassay integrated washing and electrochemical detection using MP-SPCE

The first version of the MP-ssSPCE developed (Section 3.3.2) was used for MPO electrochemical detection. For that, 25-µL samples containing MPO, MPO-c-Ab-MB and MPO-d-MAb were pipetted onto the paper surface immediately after the 5-min incubation. MB were retained within the paper membrane and above the WE with the aid of a neodymium magnet. Two consecutive washes were then carried out by adding 50 µL of $PBST_{0.05}$ each time, while current was stabilized at 0 V *vs*. the Ag pseudo-RE for 150 s. TMB enzyme substrate (30 µL) was finally added and current was monitored for 400 s more.

The second improved version of the MP-dsSPCE (Section 3.3.3) was applied to PfLDH detection (Figure 3.21c). After the 5-min incubation, the mixture was pipetted immediately onto the paper surface. MB were retained within the paper membrane and above the WE with the aid of a neodymium magnet. Four consecutive washes were then carried out by adding 100 µL of $PBST_{0.1}$ each time, while current was allowed to stabilize at -0.05 V *vs*. the Ag pseudo-RE for 300 s. TMB enzyme substrate (100 µL) was finally added and current was monitored for 150 s more.

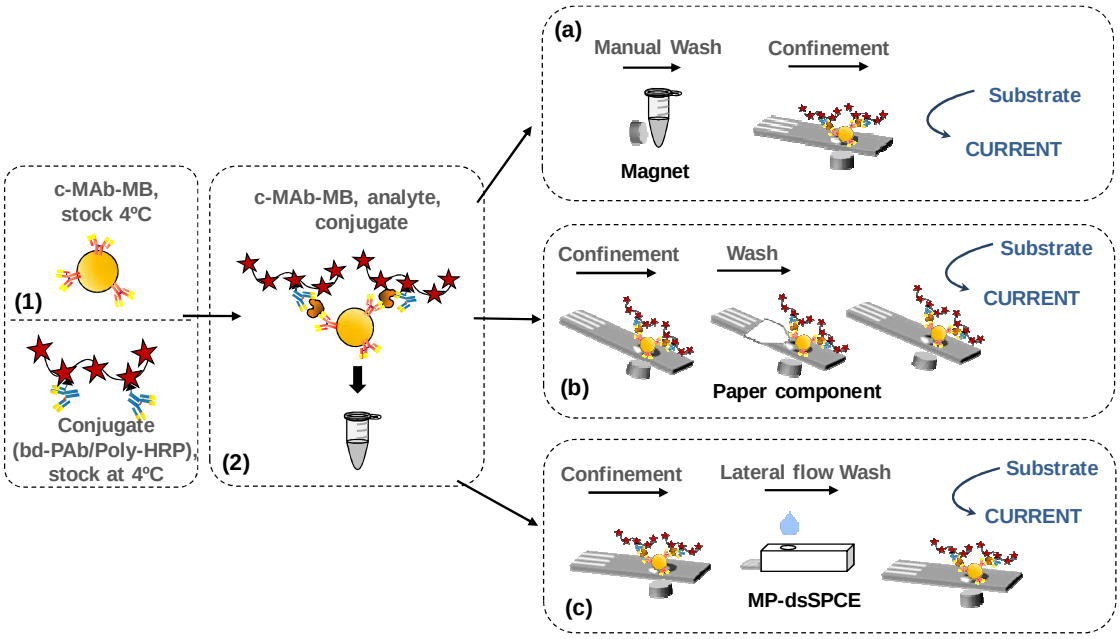

Figure 3.21. Procedure to perform the one-step magneto-immunoassays/sensors. (1) Production of the cAb-MB and the Poly-HRP immunoconjugate. (2) On-step incubation of the c-Ab-MB, the sample and the reagents. (a) Colorimetric and electrochemical detection with manual washes. (b) Electrochemical detection using a microfluidic paper component to perform on-chip washes. (c) Electrochemical detection and washes integrated on-chip using a MP-SPCE.

3.9. Magneto-immunoassay testing in spiked and clinical samples

All the magneto-immunoassays developed were validated by studying real sample matrices of growing complexity. They were first assayed by spiking increasing concentrations of the target analyte in pooled serum, plasma and/or blood obtained from healthy individuals. The objective was to evaluate the accuracy of the methods in these matrices compared to performance in saline solution, and the existence of any matrix effect. Table 3.3 summarizes the characteristics of the different commercial pooled samples acquired for this purpose.

Sample	Anticoagulant	Provider	Reference
Human serum	EDTA	Sigma Aldrich	H6914
Human plasma	Citrate-phosphate-dextrose	H2B	20000 P
Human plasma	Sodium heparin	Zenbio	PLP030916LR

Table 3.3. Commercial real samples used in the spiking experiments.

The validation process of the magneto-immunoassays was completed by studying next plasma and/or blood samples from patients having suffered the disease investigated, comparing the results with those obtained with the corresponding reference ELISA.

Detection of MMP-9 in patient plasma samples

Samples from stroke patients were obtained in the context of the projects DTS14/00004 and PMP15/00022, headed by Dr. Joan Montaner (Neurovascular Diseases Group, VHIR).

Peripheral blood samples were drawn in Ethylenediaminetetraacetic acid (EDTA) collection tubes before the administration of any treatment, from patients recruited at the emergency department of the Vall d′Hebron Hospital (Barcelona, Spain) from 2003 to 2005. All presented an acute ischemic stroke within the first 4.5 h after symptoms onset and were diagnosed by computed tomography. The local Ethical Committee approved the study (PR(HG)89/2003) and informed consent was signed by all patients or relatives. All recruited patients were treated with tPA (Actylise®, Boehringer Ingelheim International GmbH, Germany) in a standard dose (0.9 mg Kg-1, 10% bolus,

90% continuous infusion for 1 hour). Plasma was immediately separated by centrifugation at 1500 rcf for 15 min at 4 °C and was stored at −80 °C until use.

For detection, plasma samples were diluted 1:250 with the commercial reagent diluent recommended in the MMP-9 Duoset kit (1xRD, equivalent to PBS-BSA_1 with undisclosed additives) and were assayed in parallel using the magneto-immunoassay (Sections 5.1, 6.1 and 7.2) and the DuoSet ELISA as the reference method.

Detection of PfLDH in Plasmodium-infected erythrocytes cultured in vitro

Plasmodium falciparum was cultivated *in vitro* in red blood cells (RBC) to produce synthetic samples with a wide range of known parasitaemias. These cultures were produced in the context of a collaboration with the Nanomalaria Research Group of the Institute for Bioengineering of Catalonia (IBEC), Esther Koplowitz Center, with the contribution of Dr. Xavier Fernandez Busquets and Dr. Livia Neves Borgheti Cardoso. Parasites (thawed from glycerol stocks) were cultured at 37°C with RBC in Roswell Park Memorial Institute (RPMI) complete medium (supplemented with 5 g L^{-1} Albumax II and 2 mM glutamine) under a gas mixture of 92% N_2, 5% CO_2, and 3% O_2. Synchronized cultures were obtained by 5% sorbitol lysis[417], and the medium was changed every 2 days maintaining 3% haematocrit. For standard assays, *Plasmodium*-infected RBC were centrifuged, were resuspended in fresh RBC to reach 45% haematocrit and 3% parasitaemia, and were diluted serially in RBC to obtain samples with parasitaemia spanning 3-0.00001% in 45% haematocrit. Parasitaemia was assessed in parallel by flow cytometry counting and PCR.

For detection using the magneto-immunoassay/sensor, samples were diluted 1:1 with erythrocyte lysis buffer, were incubated for 5 min, were next diluted 1:25 and 1:50 with 1 x RD and were processed as described in Section 5.2, 6.2 and 8.2. The samples were analysed 3 times independently and were assayed in parallel using the ELISA reference method.

Detection of PLDH in patient plasma and whole blood samples

Samples from malaria patients were obtained in the context of project DTS17/00145 (funded by *Instituto de Salud Carlos III*), with the contribution of Drs. Israel Molina

and Adrián Sánchez Montalvá, of VHIR's Infectious Diseases Group, and Dr. Elena Sulleiro, of Vall d'Hebron University Hospital (HUVH) Microbiology Department.

Peripheral blood samples had been drawn in EDTA and heparin collection tubes before the administration of any treatment from 15 patients recruited by the professionals of the International Health Program (PROSICS-Barcelona, *Institut Català de la Salut*, ICS, Spain). All the patients presented a malaria acute infection and were diagnosed by PCR and light microscope blood analysis. The local Ethical Committee approved the study (PR(AG)30/2018) and informed consent was signed by all patients.

Plasma was immediately separated by centrifugation at 1500 rcf for 15 min at 4°C. Whole blood was lysed for 5 min after diluting 1:1 with erythrocyte lysis buffer (Table 3.1) to release intracellular parasite Ag. Plasma and lysed whole blood samples were aliquoted and stored at -80ºC, and each aliquot was thawed only once. Untreated whole blood was used fresh, immediately after its acquisition.

For detection, plasma, untreated whole blood and lysed whole blood samples were diluted with 1xRD and were assayed in parallel using the magneto-immunoassay/sensor (Sections 5.2, 6.2 and 8.2) and the ELISA reference method.

3.10. Data analysis

All the experiments included negative controls (1xRD without the analyte) to assess the level of Ab cross-binding and biocomponent nonspecific binding, and to determine the ratio between specific and nonspecific responses.

The lower limits of detection (LOD) and quantification (LOQ) were calculated as the average of the blanks plus 3 and 10 times their standard deviation (SD), respectively. The sensitivity corresponded to the slope of the assay linear range. The variability was calculated in terms of variation coefficient (%CV=(SD/mean) X 100). The signal-to-noise ratio (S/N) was the signal registered for each protein concentration divided by the averaged signal of the blanks.

Performance of the magneto-immunoassays/sensors developed was compared to that of reference ELISA in terms of analyte recovery (%Recov). This was calculated for each sample concentration tested as the percentage amount of protein detected by the

magneto-immunoassay compared to that registered by ELISA (%Recov=([analyte]MBassay/[analyte]ELISA)x100).

Over protocol optimization, a single parameter was optimized per experiment series, each experiment was repeated at least twice and best performing conditions were selected as those displaying lowest LOD/LOQ, highest S/N, and lowest %CV.

A matched-pairs t-test was used to determine whether the quantitation provided by each method for each Ag concentration was significantly different from that obtained by classical ELISA. The null hypothesis was that the results provided by the methods compared were similar, and it was accepted if the t-statistic calculated for each pair of data (t_{cal}) was lower that the tabulated t-statistic (t_{tab}) for a two-tailed test and n-1 degrees of freedom, where n was the number of replicates considered.

Chapter 4

Identification of critical parameters for magneto-immunoassay development. Application to myeloperoxidase (MPO) detection

4. Identification of critical parameters for magneto-immunoassay development. Application to myeloperoxidase (MPO) detection.

The development of magneto-bioassays usually involves the optimization of several parameters, such as MB bio-functionalization strategy, amount of MB per sample, incubation time, or detection path. On the contrary, issues such as sample volume and type of agitation of the MB with the sample are less often considered. For example, most works report on sample volumes ranging 50–100 µL, with the exception of detection of bacteria and environmental pollutants which are frequently studied in 0.5–1 mL sample volumes[418,419]. This is presumably related to the fact that, while larger sample volumes display higher total amounts of target molecules, they consume more reagents and increase the final assay cost. Finally, since MB sediment over time, incubation must be carried out under agitation conditions to keep the beads suspended in the solution. This active agitation of MB with the sample lowers also the dependence on analyte diffusion across the sample, because molecules only migrate through the narrow fluid paths between neighbouring beads. As a result, the combination of MB agitation and MB large active area grants faster assay kinetics, higher maximal signals, and lower LOD than the affinity capture on two-dimensional sensing surfaces[418,420]. The different teams working in the field use for this purpose equipment such as a rotating wheel, tilt rotation, or vortex-like shaking (usually a thermomixer), but the literature lacks studies comparing the efficiency of the different strategies. For this reason, this thesis work started with a detailed study of different parameters affecting magneto-immunoassay performance, for which MPO was used as the model analyte.

This chapter describes the optimization of a reference ELISA and an extremely simple magneto-immunoassay for MPO detection, and the subsequent study of the effect of different types of agitation and sample volumes in magneto-immunoassay performance.

4.1. Optimization of a direct ELISA for MPO detection

ELISA is founded on the exceptional specificity of Ab for their target Ags and has been extensively employed in clinical diagnostics and analytical chemistry since it was described[421,422]. Along this thesis, ELISA was used to characterize the different sets of biocomponents, to determine their optimal working conditions, and as the starting point for the subsequent development of magneto-immunoassays.

For the optimization of an ELISA for MPO detection, microtitter plates were modified with increasing concentration of bc-MAb, were blocked with BSA, and were incubated with serial dilutions of MPO. For detection, a ready-to-use TMB substrate solution was added and the endogenous peroxidase activity of MPO was monitored over time, Figure 4.1 (Section 3.6.1).

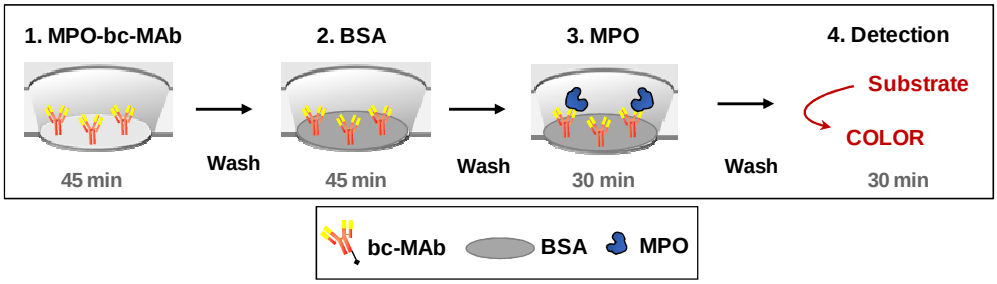

Figure 4.1. Scheme of the immunoassay developed for direct MPO ELISA detection.

As it can be observed in Figure 4.2a, MPO immuno-capture efficiency was proportional to the amount of bc-MAb for MPO concentrations above 500 ng mL^{-1}. However, detection of lower MPO concentrations did not improve for bc-MAb loads higher than 5 µg mL^{-1}, which were also more expensive to implement (Figure 4.2b). Besides, MPO non-specific binding was nearly undetectable in the control wells modified with only BSA.

Figure 4.2c shows the results obtained for 5 µg mL^{-1} of bc-MAb after MPO immunocapture for 15, 30 or 45 min. The signals measured increased by 35% when the incubation was extended from 15 to 30 min, to decrease by 2% after 45 min of immunocapture. While both the LOD and LOQ improved proportionally to the incubation time (15.84 ng mL^{-1} and 35.52 ng mL^{-1} for 15 min, 4.87 ng mL^{-1} and 13.66 ng mL^{-1} for 30 min, 4.56 ng mL^{-1} and 6.78 ng mL^{-1} for 45 min), the assay sensitivity was 66% and 20% higher after 30 min than for 15 and 45 min, respectively. Figure 4.2d demonstrates that although all the incubation times studied allowed detecting MPO in

similar concentration ranges, the signals registered for a 15-min immunocapture were nearly half of those obtained with 30 or 45 min. According to this, a 30-min immunocapture was selected as the optimal condition, since it provided the best ratio between efficient immunocapture and short assay time. Under these conditions, the whole ELISA took more than 3 h.

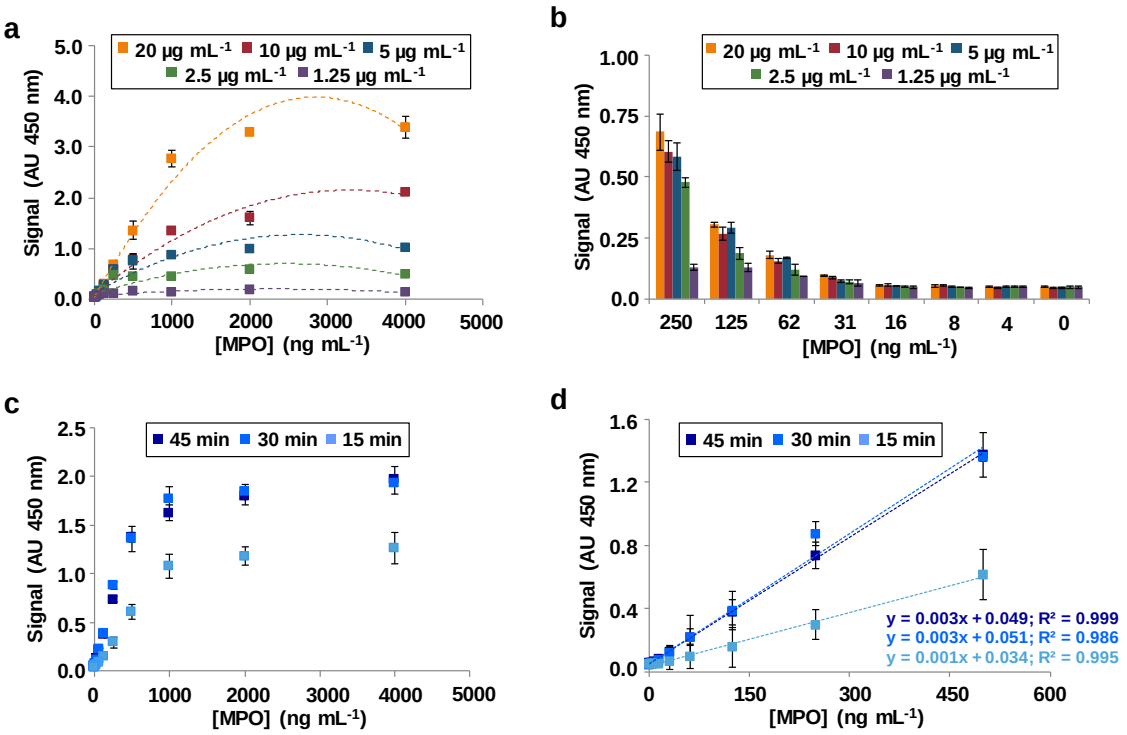

Figure 4.2. Optimization of a classical ELISA for detection of MPO. (a) Graph illustrating the signals registered for detection of increasing concentrations of MPO using different concentrations of capture bc-MAb immobilized on the microtiter plate. (b) Signals obtained in the low-concentration range of MPO for different concentrations of bc-MAb (c) Results obtained for 5 µg mL^{-1} of bc-MAb, which was considered as the optimal concentration for plate immunomodification, after MPO immunocapture for 15, 30 or 45 min. (d) Amplification of (c) illustrating the linear range for each assay condition (15, 30 and 45 min of immunocapture with 5 µg mL^{-1} of bc-MAb).

4.2. Optimization of a magneto-immunoassay for MPO detection

MPO was next detected following a similar approach but using bc-MAb-MB instead of ELISA plates (Figure 4.3). Previous reports had showed that MPO detection using MB resulted in shorter assay times than in classical ELISA[333]. In addition, MPO-bc-MAb-MB could be stored at 4ºC for more than 1 month without any decrease in performance[333].

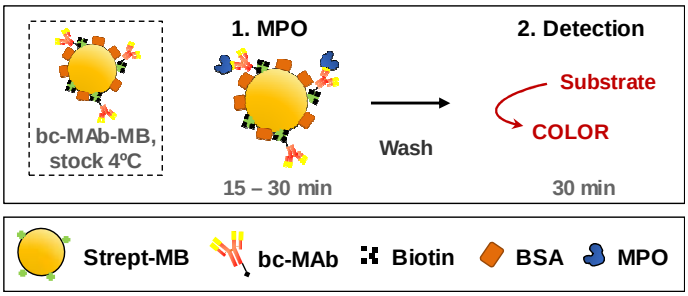

Figure 4.3. Scheme of the magneto-immunoassay developed for direct MPO detection.

Here, MB were modified with a fixed amount of MPO-bc-MAb following the protocol in Section 3.4.1, and different amounts of MPO-bc-MAb-MB (i.e.: 3, 6, 9 and 12 µL, equivalent to 7.5; 15; 22.5 and 30 µg) were incubated in parallel with MPO. In accordance with previous works, the assay consisted initially of a 15-min immuno-capture, followed by washing and detection as described in the experimental Section 3.7.3. As is can be observed in Figure 4.4a, the signals registered were proportional to the concentration of MPO for all the amounts of MPO-bc-MAb-MB tested. Noteworthy, all signals were higher than those produced by similar concentrations of MPO in the ELISA, which suggested that immunobinding was more efficient when using MB as the active surface. It had been previously discussed that employing MB provided a large active surface for both Ab immobilization and target immunocapture, as well as efficient mixing with the sample, which produced enhanced target binding and signal generation[12].

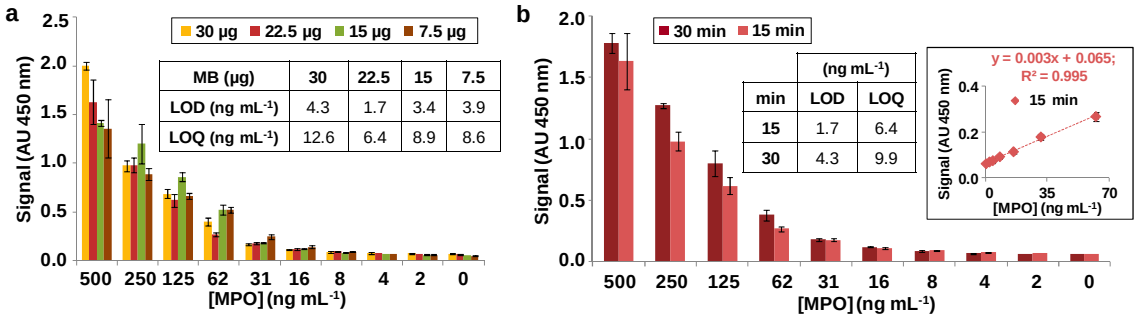

Figure 4.4. Optimization of a magneto-immunoassay for detection of MPO. (a) Results obtained for the MPO magneto-immunoassay using different amounts of MB per sample. The signals registered were proportional to the concentration of MPO for all the amounts of MPO-bc-MAb-MB tested. (Insert) Summary of the LOD and LOQ displayed by the assay for the different amounts of MPO-bc-MAb-MB tested. (b) Signals registered for the magneto-immunoassay after either 15 min or 30 min of incubation with MPO. (Insert) LOD and LOQ displayed by the magneto-immunoassay after 15-min and 30-min immunocapture times and linear range for of MPO concentrations obtained for the optimized magneto-immunoassay (15-min immunocapture with 22.5 µg of MPO-bc-MAb-MB).

We also noticed that the background noise increased with the amount of MB used, even in the negative controls incubated with no MPO. For instance, 504, 565, 625, and 690

mAU were registered for negative controls carried out with 7.5; 15; 22.5 and 30 µg of MB, which implies an increase in the background noise of about 10% for every 7.5 µg of MB added (not statistically significant difference between groups as determined by one-way ANOVA ($F(3.32) = 2.9$ $p > 0.05$)). Since the assay consisted of a direct immunocapture and no additional reagents were added, this presumably denoted that the metallic component of the MB contributed to the spontaneous oxidation of TMB in the substrate solution. Consequently, the background noise was proportional to the amount of MB present. Besides, the signal trend registered was very similar for all the amounts of MPO-bc-MAb-MB studied, which generated LODs and LOQs of the same order of magnitude (1.7–4.3 and 6.4–12.6 ng mL^{-1}, respectively).

On the other hand, the lowest amounts of beads tested (7.5 µg and 15 µg) produced signal variability 20% and 10% higher in average than using 22.5–30 µg of MB. This was attributed to better magnetic recovery of higher MB loads after the incubation and washing steps, which was in agreement with previous reports[148]. Because of this combination of variability and background noise, the assay LOD/LOQ seemed to improve when the MB load increased from 7.5–15 µg to 22.5µg, to decrease again for 30 µg (LOD/LOQ of 3.97/8.65 for 7.5 µg of MB; 3.42/8.93 for 15µg; 1.71/6.43 for 22.5µg; 4.30/12.61 for 30 µg). Accordingly, 22.5 µg of MPO-bc-MAb-MB were selected for subsequent experiments. Figure 4.4b shows that compared to the ELISA, in which a 30-min immunocapture produced the best results, the magneto-immunoassay detected MPO in the whole concentration range studied in just 15 min of incubation. Although the 30-min experiment generated signals 10–40% higher for MPO concentrations above 62 ng mL^{-1}, the signals produced for lower concentrations of MPO were not statistically different in both cases ($p < 0.05$).

4.3. Effect of sample volume and agitation type in magneto-immunoassay performance

The magneto-immunoassay developed in Section 4.2 was used to compare the effect of sample volume and type of agitation in immunocapture efficiency, which was evaluated in terms of low LOD, high analytical sensitivity and low level of non-specific absorption (i.e., high specificity). The optimized magneto-immunoassay consisted of a 15-min immunocapture of MPO present in solution using 9 µL (22.5 µg) of MPO-bc-

Ab-MB per sample. Here, the immunocaptures were performed alternatively with three different sample volumes (100 µL, 500 µL and 1 mL) and submitting the tubes to either fast shaking or slower rotation motion. Four different equipment were used in parallel for this purpose, which imposed to the tubes 5 types of mixing conditions.

4.3.1 Magnetic Bead incubation under rotation conditions

Incubation of MB is often performed under rotation conditions, which prevents MB sedimentation and guarantees the correct homogenization of the MB with the sample. The rotator agitators used for this purpose are equipment that include one or various wheels that rotate and impose a rotating movement to the tubes. Three different rotating conditions were compared in this work.

The first equipment tested was a Stuart SB2 rotator, which displayed a wheel 22 cm in diameter that rotated at a fixed speed of 20 rpm. The angle of inclination of this wheel could be adjusted, but it was used here in a vertical position (Figure 4.5a, insert). As a result, the Eppendorf tubes were submitted to relatively slow rotation that successively placed then in vertical, horizontal and vertical upside-down positions. Figure 4.5a illustrates the results obtained when samples 100 µL and 500 µL in volume were assayed alternatively (larger sample volumes were too heavy and produced tube falling from the wheel, generating unacceptably variable results). Sample volumes of 500 µL produced higher signals than the 100 µL ones over the whole MPO concentration range tested. Although the assay linear range was wider for 100 µL samples, the study of 500 µL samples produced lower LOD and LOQ (1.36 ng mL^{-1} and 3.70 ng mL^{-1} for 500 µL; 3.22 ng mL^{-1} and 8.42 ng mL^{-1} for 100 µL) and higher sensitivity (measured as the slope of the linear range). It was noticed that under these slow rotating conditions, both 100 µL and 500 µL volumes spread inside the tubes, moistening relatively wide areas of the tube wall. This caused partial drying of both MB and sample solution and caused variability between replicates equal or above 10% in half of the concentrations.

The second rotating conditions entailed the employment of a Mini Lab Roller rotator that included a 15-cm wheel placed in horizontal position and that rotated at a fixed speed of 24 rpm (Figure 4.5b, insert). As before, the Eppendorf tubes were submitted to continuous dextro rotation, but in this case the movement was comparatively faster due to the smaller diameter of the wheel. Under these experimental conditions,

immunocapture efficiency improved with sample volume and higher signals were registered for most MPO concentrations incubated in 1 mL (Figure 4.5b). Even if the assay linear range was shorter for 1 mL samples, the LOD, LOQ and assay sensitivity improved by 30%, 50% and 60%, respectively, compared to 500 µL volumes. The exception were the two highest concentrations tested, for which saturation was reached with 500 µL.

To achieve a third rotating condition, the wheel of the MiniLab Roller rotator was flipped 90º to reach a vertical position (Figure 4.5c, insert). In this case, the Eppendorf tubes were maintained horizontally, and rotation made the MB roll over the lateral walls of the tubes. The signals recorded in this experiment were lower than those observed for the other rotating conditions and signal saturation was not observed in the MPO concentration range studied (Figure 4.5c). This indicated that immunocapture was less efficient under these experimental conditions, which produced worse mixing of the MB with the samples. Independently of this, the assay improved when performed in 500-µL instead of 100-µL volumes (LOD, LOQ and sensitivity of 1.64 ng mL^{-1}, 3.82 ng mL^{-1}, and 183 AU mL ng^{1} in 500 µL, compared to 4.17 ng mL^{-1}, 12.35 ng mL^{-1}, and 33.76 AU mL ng^{-1} in 100 µL).

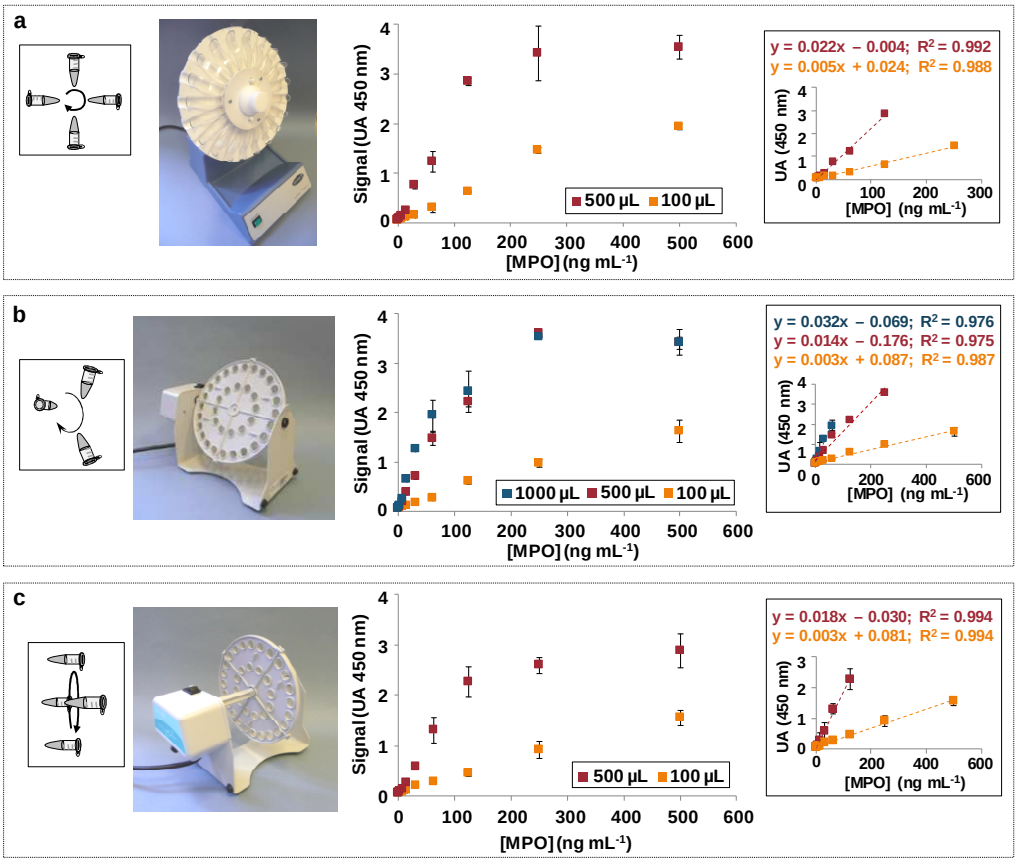

Figure 4.5. Comparative performance of the magneto-immunoassay when MPO magneto-immunocapture was carried out under different rotation conditions. (a) Results produced in 100 µL and 500 µL samples with the Stuart Rotator SB2. (b) Results obtained for 100 µL, 500 µL and 1000 µL samples with the Mini Lab Roller rotator with the wheel placed in horizontal position. (c) Signals generated for 100 µL and 500 µL samples with the Mini Lab Roller rotator with the wheel placed in vertical position. The inserts show the images of the different equipment used for MB incubation, the type of movement that is impelled to the tubes in each case, the assay linear range and the corresponding fitting equations for the tested conditions.

As it can be observed, the rotating conditions that provided more efficient mixing of the MB with the sample were the ones that produced also the highest magneto-immunobinding efficiency. For instance, horizontal rotation of the tubes, which made MB rolled over the surface of the tube, displayed poorer results than vertical mixing, in which upside-down agitation kept the MB suspended and produced more efficient solution homogenization. Independently of this, immunocapture under the mild rotation conditions tested benefitted in all cases from an increase in sample volume. However, the increase in signal was not proportional to the growth in sample volume. For instance, signals registered for 500 µL samples were approximately twice higher than those generated for 100 µL volumes and showed only a slight improvement when 1 mL volumes were assayed. This was attributed to MB surface saturation, but higher rotation speeds should be tested to discard that high sample volumes needed more efficient mixing. In relation to this, it is worth noting that rotation of big sample volumes

produced also more spreading of the samples inside the tubes and formation of small droplets that were difficult to recover in the magnetic rack. As a result, signal variability increased also. Barallat and coworkers also observed that larger sample volumes produced higher spreading during tube rotation, which made them work with 100 µL sample volumes[332].

4.3.2 Magnetic Bead incubation under shaking conditions

MB are alternatively incubated under fast shaking conditions by some few teams, often using a thermomixer[205,419,423,424]. In contrast, Barallat et al. observed that MB incubation in a microtiter plate using an orbital shaker did not prevent MB settling and provided an assay linear range shifted toward higher analyte concentrations and poorer result reproducibility than incubation in Eppendorf tubes under rotation conditions[332]. This moved us to investigate magneto-immunocapture efficiency under shaking conditions.

In this case, two different equipment and agitation conditions were evaluated. The first one was a Licuos Vortex equipped with a platform that could accommodate up to 15 Eppendorf tubes (Figure 4.6a, insert). This equipment was used at the minimal speed (equivalent to approximately 100 rpm), which induced MB vibration inside the tubes at a speed significantly faster than in any of the agitation conditions assayed. Under these experimental conditions, the MB did not sediment over the incubation time and the signals registered for 100 µL samples were higher than for any other equipment tested (Figure 4.6a). In this case, assaying larger volumes only resulted in a minor improvement and the three sample volumes analysed (100 µL, 500 µL and 1000 µL) displayed similar LODs (around 2 ng mL^{-1}). On the other hand, signal saturation was not reached for the MPO concentration range studied. These results suggested that immunocapture was extremely efficient for small sample volumes and low analyte concentrations, but that MB mixing and analyte immunocapture did not improve when the total sample volume had been scaled up.

In contrast, the variability between replicates was relatively high (6–24% in most of the cases). This was attributed to the large sample spreading and formation of droplets over the surface of the tubes produced by vortexing. Consequently, samples were difficult to recover completely, which favoured the loss of MB during the incubation and washing

steps. A report by Wang and co-workers had modelled the performance of a magnetic stirrer that produced MB vibration inside a microchannel to mix two co-flowing solutions[425]. This study showed that at small actuation forces, the MB oscillated laterally within a small distance. Accordingly, micromixing was better at narrow microchannels and did not improve if volume was scaled-up. This was attributed to the fact that, for a fixed amount of MB, there were fewer MB per volume unit that agitated the fluid in a large microchannel. Applying a similar reasoning to MB vortexing, it was inferred that a fixed amount of MB failed to mix efficiently volumes of solution higher than 100 µL. However, assaying higher amounts of MB would increase the assay cost and background signal, and higher vortexing speeds would produce more sample spreading in the tubes.

The second equipment tested was a Grant-bioPTR-30 agitator (Figure 4.6b, insert). This was a compact equipment containing a helical wheel placed horizontally, which could be subjected to variable-speed orbital rotation, reciprocal motion (equivalent to tilting), and vortexing, as well as a combination of them. The equipment was used here to tilt the tubes at 15 rpm and 90º, combined with vortexing for 1 s at each extreme position. These agitation conditions were proposed as intermediate agitation conditions between rotation and vortexing. In agreement with this, the signals registered were between those obtained for the rotators and the ones registered for the vortex (Figure 4.6b). For example, 100 µL samples produced relatively high signals (i.e.: smaller than in the vortex, but higher than with the rotators), they improved with sample volume, and displayed variability between independent replicates below 8% for most MPO concentrations. Higher sample volumes generated also a narrower linear range, higher assay sensitivity, but LODs of the same order of magnitude (e.g.: LODs of 1.79 ng mL^{-1}, 1.5 ng mL^{-1} and 1.34 ng mL^{-1} for 100 µL, 500 µL and 1 mL, respectively; not statistically different in a one-way ANOVA test, $p > 0.05$). This trend was presumably caused by the combination of rotary and vibrating motion, which guaranteed more efficient agitation than rotation, but lower sample spreading in the tubes than vortexing. Accordingly, it was concluded that, depending on the type of sample and target analyte, combinations of different types of agitation could provide better magneto-immunocapture efficiency than a single type.

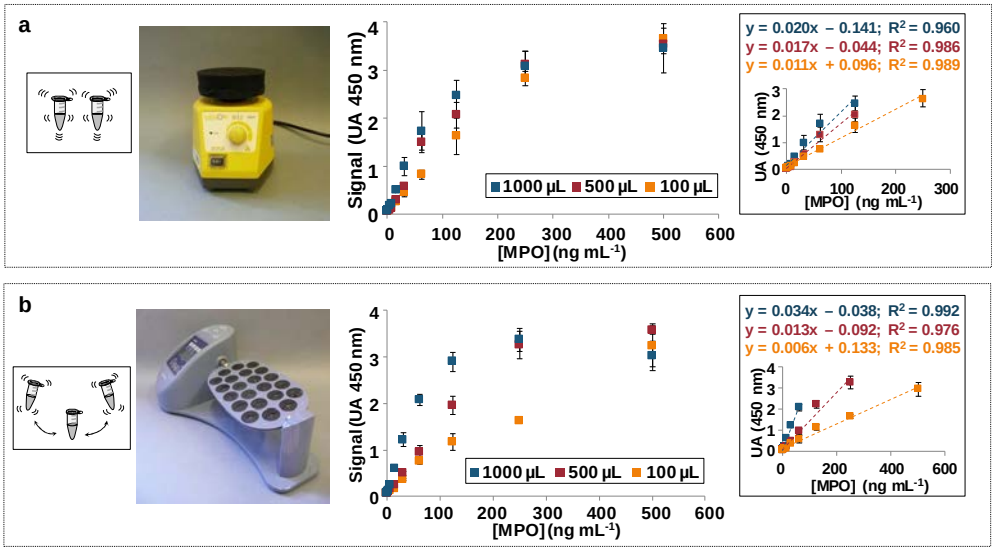

Figure 4.6. Comparative performance of the magneto-immunoassay when MPO magneto-immunocapture was carried out under different shaking conditions. (a) Results obtained for 100 µL, 500 µL and 1000 µL samples with the Licuos Vortex. (b) Results obtained for 100 µL, 500 µL and 1000 µL samples using the Grant-bio PTR 30 rotator. The inserts show the images of the different equipment used for MB incubation, the type of movement that is impelled to the tubes in each case, the assay linear range and the corresponding fitting equations for the conditions tested.

4.3.3 Comparative performance of the different agitation conditions

The performance of the different agitation conditions was finally compared (Figure 4.7). In general, larger sample volumes produced higher MPO recovery rates. This was attributed to the availability of more analyte molecules that could be bound by the migrating MB. Nevertheless, bigger volumes often correlated also with higher sample spreading into the tubes and MB loss over the incubation and washing steps. Depending on the agitation conditions, this produced unacceptable variability between replicates. For incubations performed under rotation conditions, the signals registered improved significantly when sample volume increased from 100 µL to 500 – 1000 µL, for which different levels of signal saturation were observed. However, rotation of the wheel in the vertical plane, in which the tubes laid down and the MB rolled over the tube wall, produced considerably lower signals than when rotation made the tubs flip over their longitudinal axis (upside-down). This indicated that complete homogenization of the MB with the sample was essential to guarantee optimal magneto-immunobinding. On the contrary, sample vortexing provided the best sensitivity for small sample volumes, although it also produced important variability between replicates due to sample spreading (Figure 4.7). As a result, while the signals obtained for 100 µL sample volumes incubated under vortexing nearly doubled those registered in the rotators

(Figure 4.7a), the results obtained for 500 µL sample volumes were not significantly different for the different agitation types (Figure 4.7b-c).

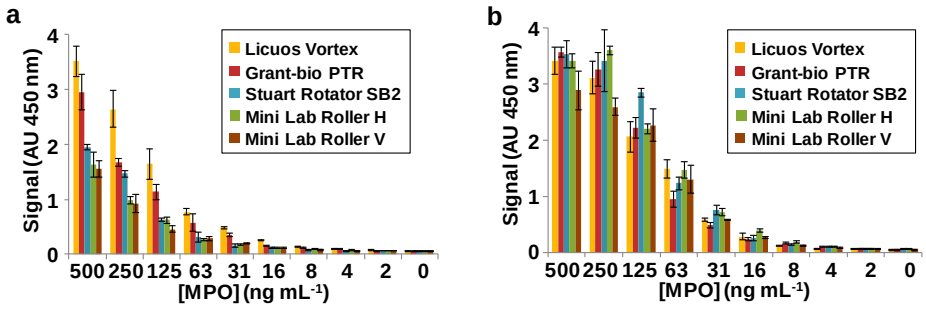

c

(ng mL^{-1})	100 µL		500 µL	
	LOD	LOQ	LOD	LOQ
Licuos Vortex	2.10	4.17	2.05	4.02
Grant-bio PTR	1.79	3.34	1.5	3.87
Stuart Rotator SB2	3.22	8.42	1.36	3.70
Mini Lab Roller V	4.17	12.35	1.64	3.82
Mini Lab Roller H	1.71	6.43	1.70	3.29

Figure 4.7. Effect of agitation in immunoassay performance for a fixed sample volume. Comparison of the results obtained for (a) 100 µL or (b) 500 µL samples when MB were incubated under different agitation conditions. (c) Summary of the LOD, LOQ and linear range for each agitation condition in 100 µL (a) or (b) 500 µL samples.

These results suggest that sample volume has different effects in magneto-immunobinding efficiency under different agitation conditions. This might be of extreme importance if a magneto-assay had to be automated and operated in minute samples volumes. In this context, agitation strategies such as rotation, apart from being difficult to integrate in a POC platform, would provide limited magneto-immunobinding efficiency. On the other hand, integration of vortexing-like agitation would have to deal with the problem of sample spreading, bubbles formation and the difficulty to recover efficiently the whole MB volume. Besides, fast continuous agitation may not be suitable for the magneto-immunocapture of relatively fragile targets, such as whole cells, which could be severely damaged along the incubation. Accordingly, effective automation of magneto-assays may have to entail a combination of agitation types to generate optimal results depending on analyte type and sample volume. As an illustrative example, incubation under a combination of tilt and short vibration produced here efficient MPO immunocapture with low variability, could be easier to integrate in a POC device than rotation, and would be less aggressive for fragile targets than vortexing.

4.4. Improving the sensitivity of a magneto-immunoassay: a sandwich immunocapture format to MPO detection

The one-step magneto-immunoassay for MPO detection optimized previously (section 4.2; procedure detailed in the Section 3.7.3) was re-optimized for the improvement of sensitivity. In order to do so, a MPO sandwich magneto-immunoassay was developed readjusting the reagents concentrations (**Figure 4.8a**)[426]. The protocol consisted of MPO immunocapture in 25-100 µL sample volumes, to which 10 µL of MPO-bc-MAb-MB and 0.6 µg mL^{-1} of bd-MAb-HRP had been added, in a single 5-min incubation. MB were then washed with PBST, TMB substrate solution was added to the tubes, the enzymatic reaction could proceed for 30 min, and the supernatant was finally measured spectrophotometrically. Previous works showed that this assay was highly specific for MPO, even in clinical serum and plasma samples[332,426].

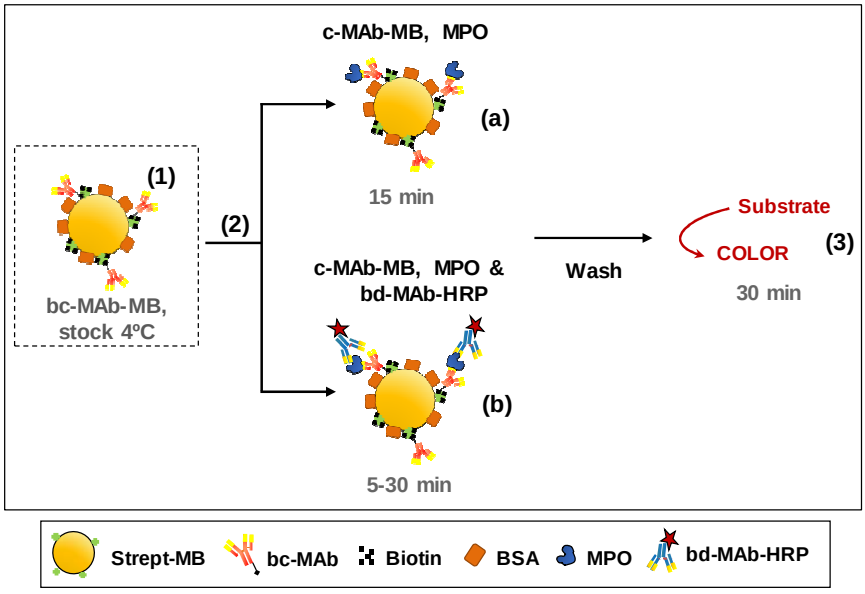

Figure 4.8. Comparison of the schematic representation of the MPO magneto-immunoassay protocol: (1) MBs are modified with biotinylated Ab, blocked with biotin and stored in a PBS-BSA solution at 4ºC. (2a) The immunoassay consists of single 15-min incubation of MPO and c-MAb-MB. (2b) The immunoassay consists in a sandwich immunocapture of 15-30 min of MPO, c-MAb-MB and bd-MAb-HRP. This is followed by a series of washes with PBS-T, which take about 7 min for a single sample and up to 20 min for a series of 8-12 samples handled in parallel. (3) Addition of the substrate solution to the tubes for spectrophotometric detection of the assay, the enzyme reaction is allowed to proceed for 30 min and is stopped with acid. MBs are then concentrated using a magnet, the supernatant is transferred to the wells of a microtiter plate and absorbance is read.

4.4.1 Optimization of the 1-step sandwich magneto-immunoassay for MPO detection

The objective of the current work was to perform a sensitive MPO detection with the magneto-immunoassay in the minimum time and with the lowest number of reagents possible. Accordingly, several parameters of the spectrophotometric assay, including incubation time (5–15 min) and bd-MAb-HRP concentration (100–700 ng mL^{-1}) were re-optimized. As it can be observed in Figure 4.9, with 15- and 10-min incubation times the signals registered for 700 ng mL^{-1} and 350 ng mL^{-1} of bd-MAb-HRP were comparable and higher than those obtained for 100 ng mL^{-1}. In the case of the 5-min incubation, only 700 ng mL^{-1} of bd-MAb-HRP produced higher signals than the other concentrations tested. The main drawbacks associated to these high signals were that the higher background noise interfered in detection of the lowest concentrations of MPO tested, and on the other hand, that signal saturation was reached at lower MPO concentrations shortening the assay linear range. On the contrary, 100 ng $mL^{-1}$of bd-MAb-HRP produced signals at the same order of magnitude for the three incubation times tested (5, 10 and 15 min).

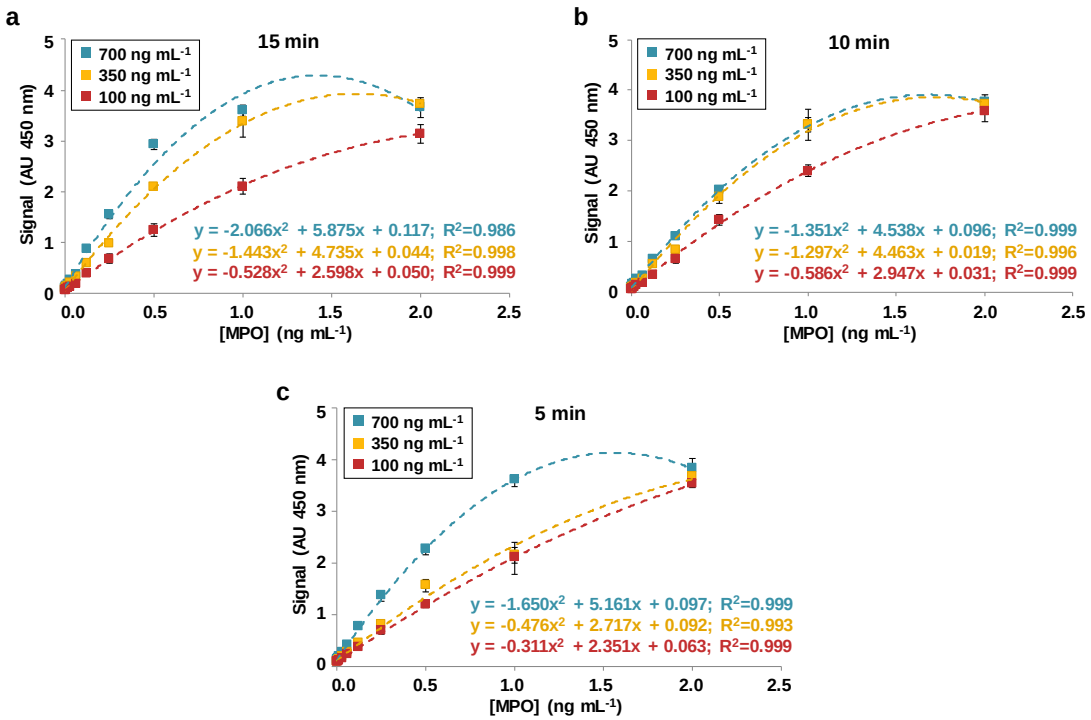

Figure 4.9. Optimization of the MPO immuno-magnetic binding efficiency with 100-700 ng mL^{-1} MAb-HRP, in different incubations times. (a) 15 min.(b) 10 min.(c) 5 min.

If the results obtained for 5 min were studied, the LOD and LOQ obtained were of 44 and 200 pg mL^{-1} for 350 ng mL^{-1}, and of 12 and 30 pg mL^{-1} for 100 ng mL^{-1} of bd-MAb-HRP, respectively. It was concluded that the 5-min magneto-immunoassay using 100 ng mL^{-1} of bd-MAb-HRP was faster, with LOD and LOQ low enough to discriminate MPO concentrations with diagnostic interest and using the lowest concentration of reagents. Accordingly, these conditions were selected for subsequent experiments.

Finally, magneto-immunocapture efficiency was evaluated in different sample volumes. With this aim, the spectrophotometric magneto-immunoassay was performed in parallel in 100, 50 and 25-µL sample volumes (Figure 4.10). The table in Figure 4.10b summarizes the different figures of merit of the assays performed. As it can be observed, the assay with 50 µL of sample volume produced the best results in terms of LOD, LOQ and sensitivity. The immunocapture in 25 µL of sample, on the other hand, produced in average signals 50% lower than the incubations in 50-100 µL (Figure 4.10a). However, this assay still detected the same concentrations of MPO, with LOD/LOQ of the same order. In the insert in Figure 4.10, it can be observed that although the assay in 25 µL had lower sensitivity in terms of the graph slope, it displayed the widest linear range.

a

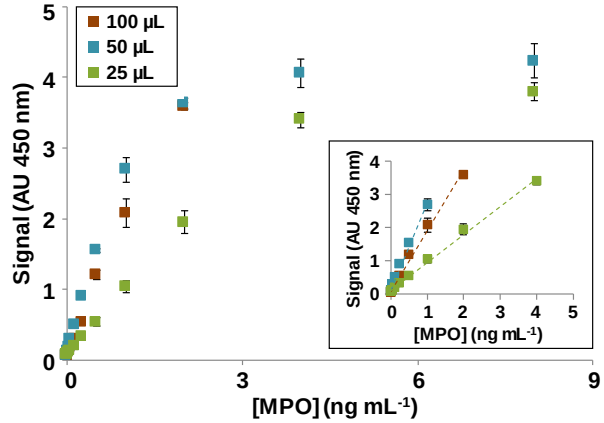

b

	25 µL	50 µL	100 µL
LOD (ng mL^{-1})	0.009	0.004	0.011
LOQ (ng mL^{-1})	0.029	0.014	0.033
Linear range (ng mL^{-1})	0.0039 - 4	0.0039 - 1	0.0039 - 2
Linear equation	0.85x + 0.10	2.66x + 0.12	1.81x + 0.09
R^2	0.996	0.994	0.992
Sensitivity*	0.85	2.66	1.81

*Measured as the linear approximation slope (UA·mL·ng^{-1})

Figure 4.10. Effect of sample volume in the performance of the spectrophotometric magneto-immunoassay**.** (a) Effect of sample volume in MPO immunomagnetic binding efficiency. Insert, linear range of the different assays (b) Table summarizing the characteristics of the assay performed with different sample volumes.

4.4.2 Evaluation of the one-step sandwich magneto-immunoassay detecting MPO in spiked serum samples

To evaluate the matrix interference produced by a real sample matrix in MPO magneto-immunobinding (25-µL sample volumes). With this purpose, the re-optimized spectrophotometric magneto-immunoassay was carried out using commercial human serum, which was diluted 1:100 with PBS-$BSA_{0.1}$ and spiked with known concentrations of MPO or no MPO at all as the negative control. Figure 4.11a shows that the signals obtained in diluted human serum were not significantly different from those registered in PBS-$BSA_{0.1}$ with MPO recovery efficiencies ranging 95%-108%.

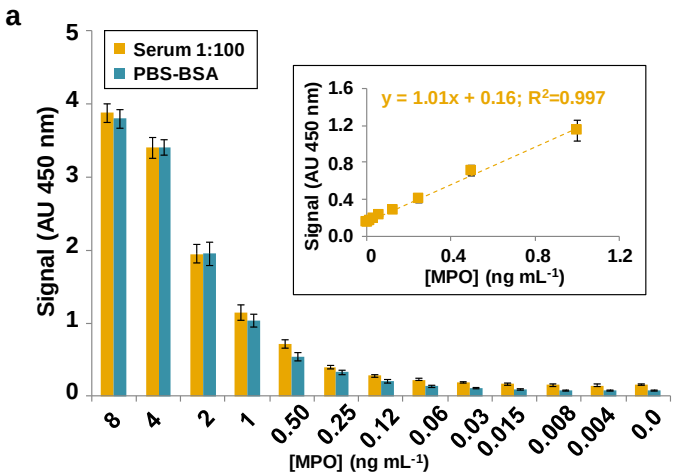

Figure 4.11. Comparison of detection in PBSB$SA_{0.1}$ and in human serum diluted 1:100 with spectrophotometric detection. Insert, linear range obtained in human serum diluted 1:100 with PBS-$BSA_{0.1}$ and spiked with increasing concentrations of MPO.

The magneto-immunoassay using 100 ng mL^{-1} of bd-MAb-HRP in a 5-min incubation, which enabled detection of MPO between 4 and 8000 pg mL^{-1}, with LOD and LOQ of 27 and 88 pg mL^{-1}, respectively in 1:100 diluted human serum. Considering that the cut-off value to distinguish between physiological and pathological concentrations of MPO is 95 ng mL^{-1} and that patients at high risk of suffering a cardiovascular event may display MPO concentrations above 400 ng mL^{-1}, it was concluded that this shortened assay would be efficient enough to discriminate between both groups[426].

4.5. Conclusions

This chapter has described the optimization of a direct ELISA for MPO detection that took 3 h and generated an LOD of 4.87 ng mL^{-1}. This assay was then formatted into a 15-min magneto-immunoassay that had an LOD of 1.65 ng mL^{-1}. This magneto-immunoassay was finally employed to study different parameters that could affect assay performance. The results confirmed that the amount of capture Ab in an assay had to be carefully optimized, because an excess of this reagent contributed to analyte detection worsening, presumably by steric hindrance. The amount of MB per sample was also determinant for optimal assay performance. While low MB concentrations resulted in high assay variability, which was attributed to MB lost during the incubation and washing steps, high MB concentrations correlated with high background noise. The best results were obtained when 22.5 µg of MPO-bc-MAb-MB were used per sample.

Concerning agitation conditions, maximal MPO detection was obtained for fast sample mixing, such as vortexing, of small sample volumes (i.e. 100 µL). However, combinations of different types of agitation could be an efficient alternative depending on analyte type and sample volume.

On the other hand, it has been demonstrated that assay sensitivity can be improved with a sandwich magneto-immunoassay compared to a classical ELISA, achieving shorter assay times without necessarily sacrificing assay sensitivity. The direct 15-min magneto-immunoassay for MPO detection performed in 100 µL of sample (under the best agitation conditions for this volume) displayed a linear range of 2 – 500 ng mL^{-1}, with LOD and LOQ of 1.79 ng mL^{-1} and 3.34 ng mL^{-1}, respectively. The addition of a bd-Ab-HRP during the immunocapture to perform 1-step sandwich immunoassay and the reduction of sample volume to 25 µL, allowed a decrease of the range of MPO concentrations studied to 0.004 ng mL^{-1} - 8 ng mL^{-1}. Furthermore, the LOD and LOQ achieved with this magneto-immunoassay were reduced nearly 200 times, reaching values of 9 pg mL^{-1} and 30 pg mL^{-1}, respectively.

Chapter 5

Development of simplified sandwich magneto-immunoassays using Poly-HRP as a signal amplifier

5. Development of simplified sandwich magneto-immunoassays using Poly-HRP as a signal amplifier

The utilization of MB provides a versatile strategy for the development of enhanced immunoassays[148,427,428]. However, most of the magneto-immunoassays reported entail relatively complex multi-step procedures. These assays require that the user performs several consecutive incubations under agitation conditions and washing steps using magnets, which usually generate higher result variability than work on two-dimensional capture surfaces, requires a certain level of training, and is certainly tedious and time-consuming. The main objective of this thesis project was reducing the level of manual handling of classical magneto-immunoassays, developing methodological alternatives that could be easier to carry out by poorly trained personnel and with minimal technical requirements. One of the means to accomplish this goal was producing extremely short and simple magneto-immunoassays. However, and as it will be discussed in this chapter, the simplified magneto-immunoassays developed in this way produced extremely low signals, which made it necessary to explore the incorporation of signal amplifiers.

Multi-label signal amplifiers, such as engineered polymeric complexes, metal nanoparticles or carbon nanotubes (CNT), to cite some examples, had been previously employed to produce enhanced immunoassays[213,429–431]. Among them, polymeric streptavidin-enzyme complexes, such as Poly-HRP, appear as a promising alternative that, contrary to customized nanocomposite-based amplifiers, have already reached the marker and are commercially available. Poly-HRP complexes are composed by from dozens to hundreds of HRP enzyme molecules chemically coupled to each other or to a polymer backbone, to which streptavidin is cross-linked[432]. Some few examples have been reported using Poly-HRP to produce highly sensitive immunoassays and immunosensors. For instance, a custom-made Poly-HRP dextran complex was exploited to develop an ELISA that detected anti-HIV Ab at concentrations 10 times lower and with signals 5–20 times higher than streptavidin-HRP[232]. The authors used the same complex later on to detect tissue plasminogen activator (tPA), obtaining signals 7 times higher than when employing streptavidin-HRP[433]. Li et al. used a commercial Poly-HRP in a competitive ELISA for the detection of aflatoxin B1, achieving 19-fold higher

signals, a wider linear range, a 3.8-fold better signal-to-noise ratio, and a 2.4-fold steeper slope than when employing an Ab-HRP[434]. In a work published by Miao and co-workers, aptamer-modified MB and a commercial Poly-HRP, additionally modified with HRP-loaded gold nanoparticles, served to detect chloramphenicol in a competitive assay format[435]. Pingarron's team has also employed Poly-HRP for the development of magneto-immunosensors. For instance, the electrochemical magneto-immunodetection of interleukin-6 (IL-6) and transforming growth factor-β1 (TGF) using Poly-HRP provided larger signal-to-blank ratios, wider linear range, and lower LOD than streptavidin-HRP in the study of spiked saliva and/or urine[200,436]. Interestingly, these examples exploited Poly-HRP to improve the sensitivity of assays that were in general time-consuming multi-step procedures[236,437].

This chapter shows how Poly-HRP can be alternative exploited to shorten the incubation times of an immunoassay, facilitating the optimization of extremely fast, simple and efficient magneto-immunoassays. Two simplified magneto-immunoassays will be described. The first one was optimized to detect MMP-9, a biomarker of ischemic stroke complications, and accomplished quantitative detection in plasma samples in approximately 40 min. The second one targeted detection of PfLDH in whole blood from malaria patients and confirmed that the protocol developed was applicable to a variety of diagnostic applications.

5.1. Development of a simplified magneto-immunoassay for MMP-9 detection in blood plasma

The development of a magneto-immunoassay for MMP-9 detection was carried out using the reagents of a Duoset kit (Ref. RYD-DY995, R&D). This kit contained all the biocomponents needed to perform a classical multistep ELISA, including a capture monoclonal MMP-9-c-MAb, the MMP-9 calibrator, a detection polyclonal MMP-9-bd-PAb, and streptavidin-HRP for indirect detection, as well as a general protocol that took >6 h (see Section 3.6.2). This ELISA protocol was taken as the starting point to develop a multi-step magneto-immunoassay, which was successively shortened by decreasing the different incubation times, was simplified by combining different steps in single incubation steps and was shortened additionally by employing a Poly-HRP signal

amplifier to substitute streptavidin-HRP. Finally, the applicability of the protocol was assessed by studying spiked and clinical samples from patients.

5.1.1. Optimization of a 3-step magneto immunoassay for MMP-9 detection

In order to produce the magneto-immunoassay, MB were chemically modified with MMP-9-c-MAb following a protocol optimized previously by other members of the team[438]. These immuno-modified MB were stable for several weeks at 4ºC, which was an advantage compared to the ELISA that was prepared daily.

MB were then used to carry out a multi-step magneto-immunoassay that was like the classical ELISA (Figure 5.1.a). Two µg of MB were used per sample following the protocol described in Section 3.7.1. This amount of MB entailed an active surface area 12-20 times smaller than that used in a microplate well (approximately 4.4-7.5 mm^2 for MB *vs*. 95 mm^2 for ELISA). However, and considering the corresponding surface modification protocols (Section 3.4.2), equivalent amounts of c-MAb were used in both cases (i.e., 100 ng of c-MAb per sample). Under these experimental conditions, the magneto-assay produced signals 40-60% lower than the ELISA for all the concentrations of MMP-9 tested. Background noise decreased also, which provided lower LOD/LOQ (4 and 16 pg mL^{-1} in average for MB, compared to 5-15 and 13-40 in the ELISA) and better discrimination of MMP-9 at low concentrations (e.g., S/N=1.5 for 31 ng mL^{-1} by ELISA; S/N=2.6 for 31 ng mL^{-1} and detection of 16 ng mL^{-1} at MB).

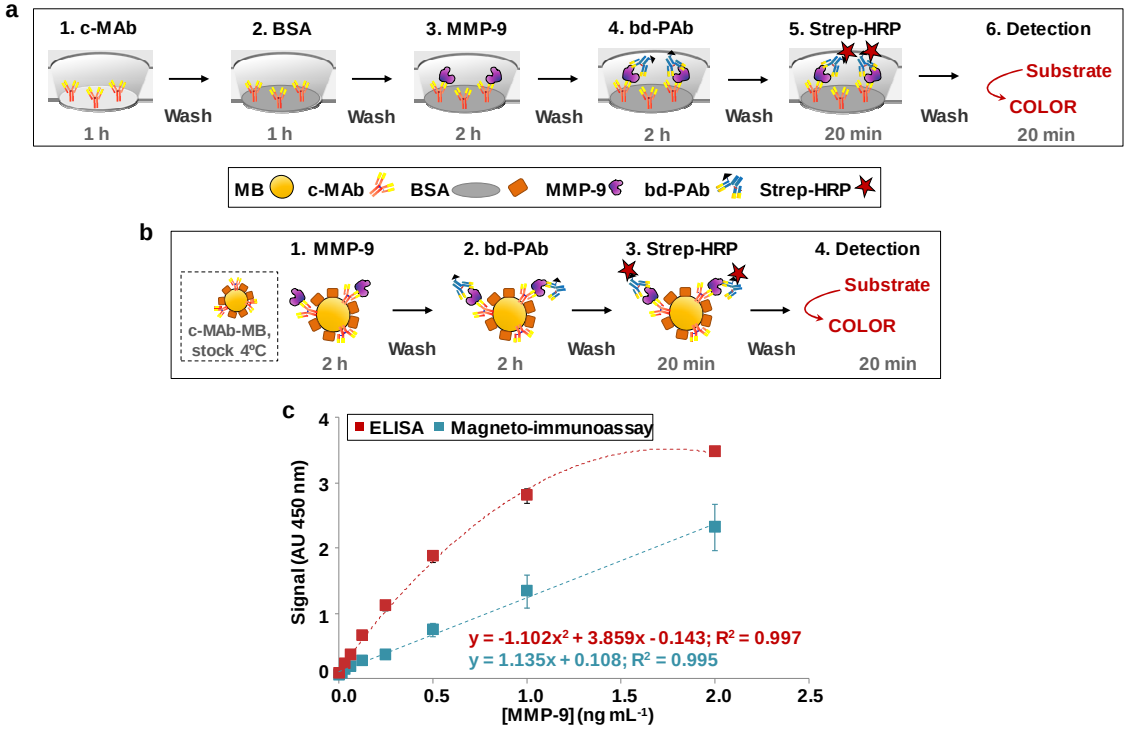

Figure 5.1. (a) Scheme of the reference multi-step ELISA. (b) Scheme of the 3-step magneto-immunoassay developed in this work for MMP-9 detection. (c) Comparison of the signals registered when detecting a dilution series of MMP-9 using alternatively the reference ELISA and the 3-step magneto-immunoassay.

5.1.2. Optimization of a 2-step magneto immunoassay for MMP-9 detection

The 3-step magneto-immunoassay was tentatively shortened by combining the two consecutive immunocaptures of MMP-9 and MMP-9-bd-PAb in a single incubation step (Figure 5.2a). In this way, the assay consisted of a single incubation of the MB with the MMP-9 containing sample and MMP-9-bd-PAb, followed by incubation for 20 min with streptavidin-HRP and colorimetric detection of the enzymatic label. Figure 5.2b summarizes the signals registered for decreasing immunocapture times for this 2-step magneto-immunoassay compared to the 3-step magneto-immunoassay. As expected, signals decreased for shorter incubations, including background noise, but the whole MMP-9 concentration range could be detected in all the experiments.

Noteworthy, LOD and LOQ were of the same order for 1-h and 2-h incubations (2.4-4.5 and 14-38 ng mL^{-1}, respectively), but worsened for longer and shorter incubation times (LOD/LOQ of 13/45 pg mL^{-1} for 3 h; LOD/LOQ of 35/112 pg mL^{-1} for 30 min). Accordingly, a 1-h incubation was selected as the starting point for further optimization.

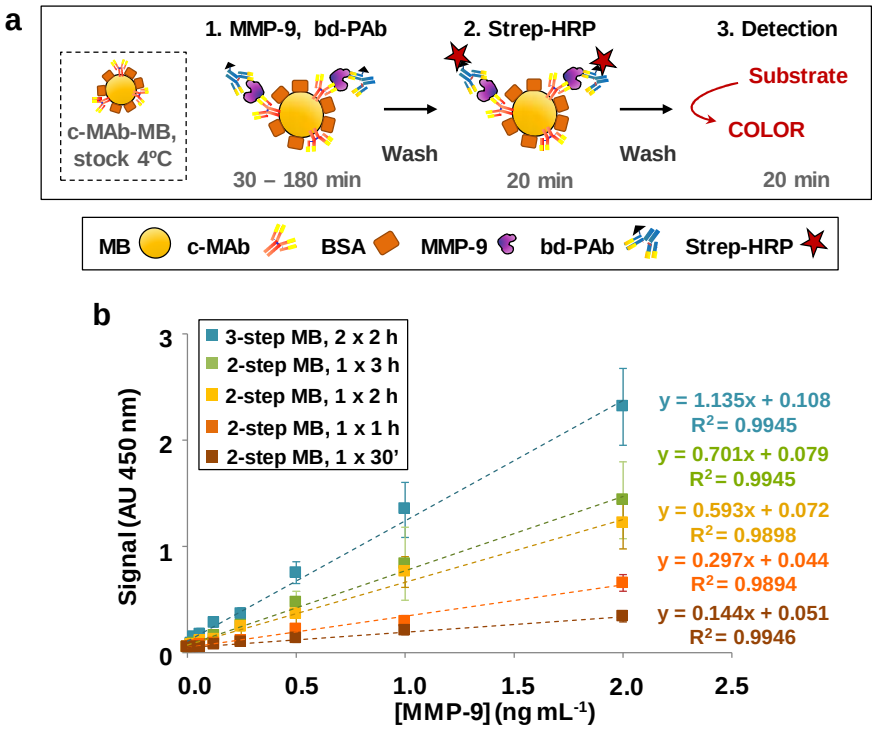

Figure 5.2. Detection of increasing concentrations of MMP-9 using different multi-step magneto-immunoassay formats. (a) Scheme of the 2-step magneto-immunoassay. (b) Signals registered with either the 3-step magneto-ELISA, or the 2-step magneto-assay versions in which MMP-9 and MMP-9-bd-PAb were incubated simultaneously for 30-180 min.

5.1.3. Using Poly-HRP to optimise a shortened 2-step magneto immunoassay for MMP-9 detection

A battery of signal amplifiers was tested by other members of the research group in an attempt to increase the signals obtained in the 2-step magneto-immunoassay. The amplifiers tested included several streptavidin-HRP conjugates and polymeric HRP complexes from different providers, as well and gold nanoparticle streptavidin-HRP custom-made assemblies. The best results were obtained when using Poly-HRP, a conjugate provided by Fisher Scientific (Ref. 21140)[438].

Poly-HRP performed optimally diluted 1:10000 and incubated for 5 min (compared to the 20-min incubations required for streptavidin-HRP) (Figure 5.3). Under these experimental conditions, Poly-HRP produced signals 40-100% higher than those produced by strep-HRP for all the concentrations of MMP-9 tested. This polymer produced also 50% higher background. However, the S/N ratios were equal or higher to those provided by strep-HRP in the whole assay range, which made this molecule an excellent choice for signal amplification.

Additional optimization of this 2-step magneto-immunoassay (Section 3.7.2, Figure 5.3a) included the study of MB concentration per sample, immunocapture time, number of washes, and MB immuno-modification procedure, as it will be detailed next.

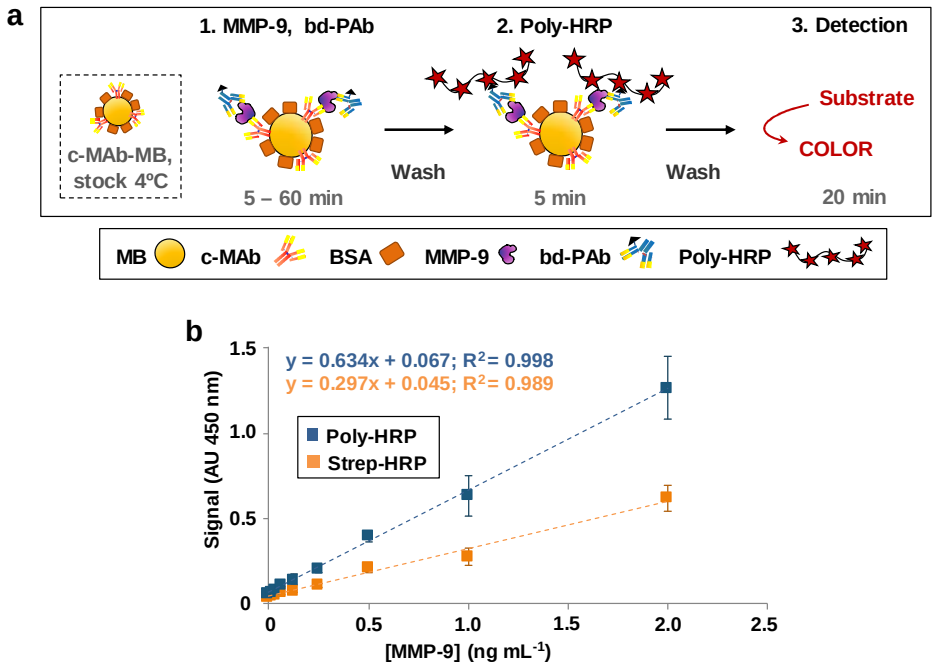

Figure 5.3. (a) Scheme of the shortened 2-step magneto-immunoassay developed for MMP-9 detection. (b) Comparison of the signals registered for the 2-step magneto-immunoassay when using alternatively streptavidin-HRP or Poly-HRP for detection.

5.1.3.1. Effect of the amount of MB used per sample in assay performance

For magneto-immunoassay optimization, a relatively small amount of MB was used per sample (2 µg of MB) (Section5.1.1). Nonetheless, several authors have observed that both target immunobinding and the signals generated improve proportionally to the amount of MB used, with optimal numbers around 30 µg when assaying 100-µL samples[151,438]. Accordingly, the effect of MB load in the 2-step immunoassay performance was investigated in a range extending 2-30 µg of MB per sample.

As summarized in Figure 5.4, the signals increased proportionally to the amount of MB up to 20 µg, to remain constant for higher MB loads (Figure 5.4a). The amount of MB had a profound effect on the assay linear range as well. For instance, for the lowest amount of MB tested, signal was linearly proportional to MMP-9 concentration up to 1 ng mL^{-1}. However, the linear range shrank to 16-500 pg mL^{-1} and 16-250 pg mL^{-1} of MMP-9 when 10 and 20-30 µg of MB were used per sample, with signal saturation above 1 and 0.5 ng mL^{-1}, respectively. The background signal was also proportional to the amount of MB, which was attributed to a combination of cross-binding between c-MAb and bd-PAb and non-specific adsorption of Poly-HRP (Figure 5.4b). Despite this, LOD and LOQ were of the same order in all cases (LOD 2.5-10 pg mL^{-1}; LOQ 14-35 pg mL^{-1}) and the highest S/N ratios for low MMP-9 concentrations were produced by 20 µg of MB (Figure 5.4c). Accordingly, this condition was selected for subsequent experiments.

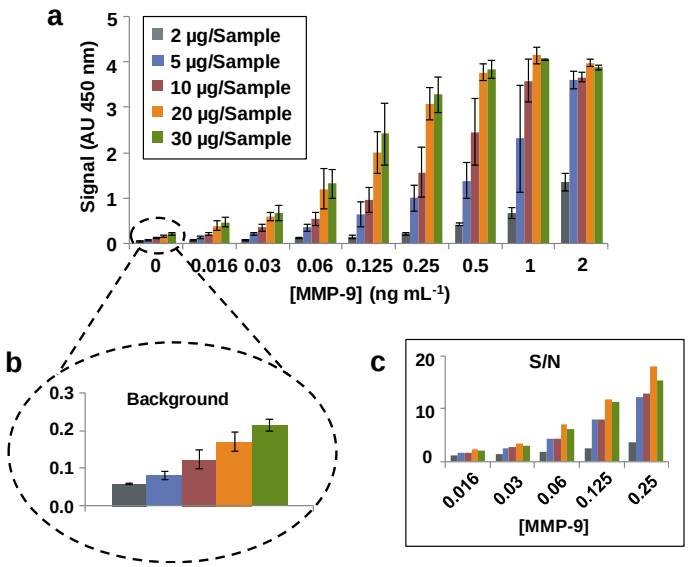

Figure 5.4. (a) Signals registered for increasing concentrations of MMP-9 using different amounts of MB per sample in the shortened 2-step magneto-immunoassay. (b) Zoom illustrating the background signals registered in the negative control experiments (without MMP-9). (c) S/N ratios obtained at low MMP-9 concentrations for the different experimental conditions detailed in (a).

5.1.3.2. Effect of the immunobinding time in assay performance

The 2-step magneto-immunoassay was additionally shortened by reducing the duration of the single incubation step of MMP-9-c-MAb-MB with MMP-9 and MMP-9-bd-PAb (Figures 5.3a and 5.5a). In this case, background noise decreased in the negative controls with the immunocapture time (Figure 5.5b). In contrast, the incubation of Poly-HRP (5 min with Poly-HRP diluted 1:10000) with a series of negative controls without MMP-9-bd-PAb did not evidence Poly-HRP non-specific binding. Therefore, background noise was attributed to Ab cross-binding, which was presumably amplified by Poly-HRP. Besides, immunobinding for 15-60 min produced comparable signal trends, with linear response for MMP-9 ranging 16-125 pg mL^{-1}, signal saturation above 0.5 ng mL^{-1}, LODs below 0.5 pg mL^{-1} and LOQs of 5-12 pg mL^{-1}. Shorter incubations, on the other hand, produced worse results, with LOD/LOQ of 9/22 pg mL^{-1} (10-min) and 11/27 pg mL^{-1} (5-min), as well as lower sensitivity in terms of graph slope. Nevertheless, 5-min incubations were the only ones in which the linear range expanded over the whole concentration range (16-1000 ng mL^{-1}). Since the main interest on the current work was to develop a short assay, 5-min incubation was selected as a compromise between reduced length and good performance.

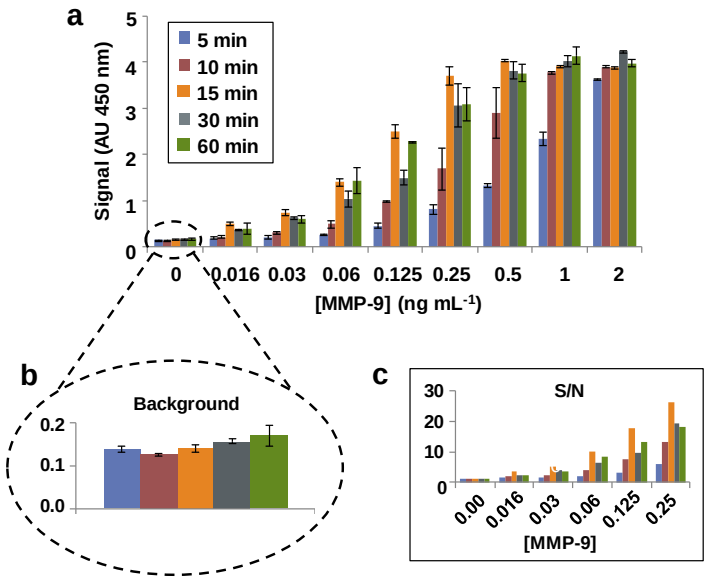

Figure 5.5. Signals registered for increasing concentrations of MMP-9 using different immunocapture times. (b) Insert illustrating the background signals registered in the negative control experiments (without MMP-9). (c) S/N ratios achieved at low MMP-9 concentrations for the different experimental conditions tested in (a).

5.1.3.3. Optimization of the washing strategy

MB manual washing using magnets is a tedious and time-consuming procedure and an important source of variability. Accordingly, it was decided that for the development of an extremely assay path, MB washing had to be optimized to be performed in the minimum time possible without losing efficiency.

Figure 5.6 displays the schematic representation of the 2-step magneto-immunoassay developed for MMP-9 detection, including the different washing conditions tested. As already exposed, the magneto-immunoassay consisted of a single 5-min incubation of the MMP-9-c-MAb-MB with MMP-9 and MMP-9-bd-PAb. Next, the supernatant was removed using a magnetic rack to retain the MB, the MB were washed and the magneto-immunocomplex was incubated for 5 min with a polymeric signal amplifier, Poly-HRP. MB were washed again, substrate solution was added to the tubes, the enzymatic reaction proceeded for 20 min, it was stopped with acid and the colorimetric detection took place.

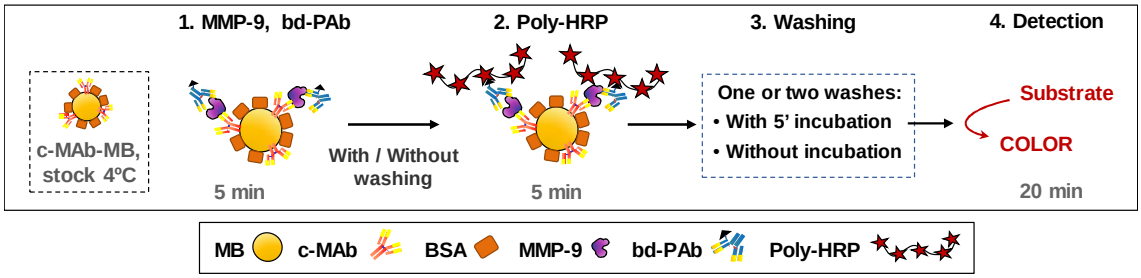

Figure 5.6. Schematic representation of the optimized 2-step magneto-immunoassay and the four different washing strategies that were evaluated in parallel.

The results in Figure 5.7a show that MMP-9 detection improved if no wash was conducted between the first two steps (1-2). At least for these specific reagents, washing with $PBST_{0.1}$ before the incubation with Poly-HRP contributed to produce lower signals and higher background noise than avoiding this washing step. This was attributed to a higher level of Poly-HRP non-specific binding on tween-coated MB but was not studied additionally.

On the other hand, after incubating with Poly-HRP, MB were washed twice with $PBST_{0.1}$ under rotation (for 5 min each time). Four different alternative washing strategies were evaluated in parallel (step 3):

- performing two 5-min washes under rotation,

- performing one 5-min wash under rotation,
- performing two fast washes without incubation, and
- performing one fast wash without incubation.

In all cases, incubation with Poly-HRP was followed by MB concentration in the magnetic rack and supernatant removal by pipetting. For washing under rotation, MB were then re-suspended in $PBST_{0.1}$, were rotated for 5 min, and supernatant was removed as before for MB resuspension in the solution of choice. For fast washing, MB were only re-suspended with $PBST_{0.1}$ (without incubating).

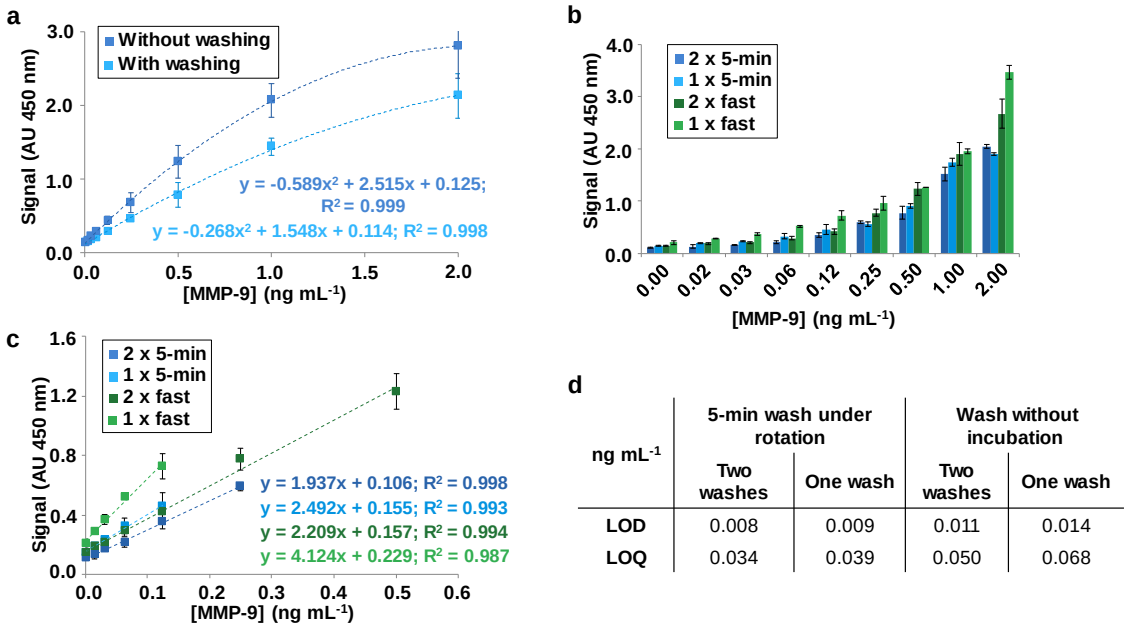

d

ng mL^{-1}	5-min wash under rotation		Wash without incubation	
	Two washes	One wash	Two washes	One wash
LOD	0.008	0.009	0.011	0.014
LOQ	0.034	0.039	0.050	0.068

Figure 5.7. (a-b) Signals registered in the 2-step magneto-immunoassay for increasing MMP-9 concentrations with/without washing between the two incubation steps (a) and under different washing conditions carried after the incubation with Poly-HRP (b). (c) Corresponding assay linear ranges and fitting equations for the experimental conditions in (b). (d) Summary of the LOD and LOQ displayed by the assay for the different washings strategies.

Figure 5.7b displays the signals obtained for increasing MMP-9 concentrations under the different washing conditions. The Figure 5.7c illustrates the corresponding assay linear ranges and fitting equations for these experimental conditions. Figure 5.7d shows a summary of the LOD and LOQ displayed by the assay for the different wash strategies. Washing under rotation was more efficient and produced lower background noise and faintly better LOD/LOQ (Figure 5.7b-d). However, this also produced lower signals for all the concentrations of MMP-9 tested. This was attributed to the partial loss of MB, because rotation produced wider spreading of the solution over the tube walls

and made MB recovery more difficult[213]. Accordingly, the experiments in which MB were submitted to fast washes produced slightly higher signal-to-noise ratios (S/N). Otherwise, the calibration obtained after carrying out just a single fast wash, without incubation, displayed the highest sensitivity in terms of slope, but also one of the narrowest linear ranges (Figure 5.7c).

It was concluded that the best results were obtained for the 2-step magneto-immunoassay performed with two fast washes without incubation, which displayed the widest linear range, as well as sensitivity, LOD and LOQ comparable to those produced when two 5-min washes were carried out.

5.1.3.4. Optimization of the conjugation procedure to prepare c-MAb-MB

Finally, the 2-step magneto-immunoassay was performed using alternatively c-MAb-MB produced by either a two-step (Section 3.4.2, Figure 5.8a) or a one-step conjugation protocol (Section 3.4.3, Figure 5.8b). In the first case, the carboxyl groups displayed on the surface of the MB were first activated with EDC. The activated MB were then washed and incubated with the c-MAb for conjugation. In contrast, in the one-step protocol, MB, EDC and c-MAb were incubated simultaneously.

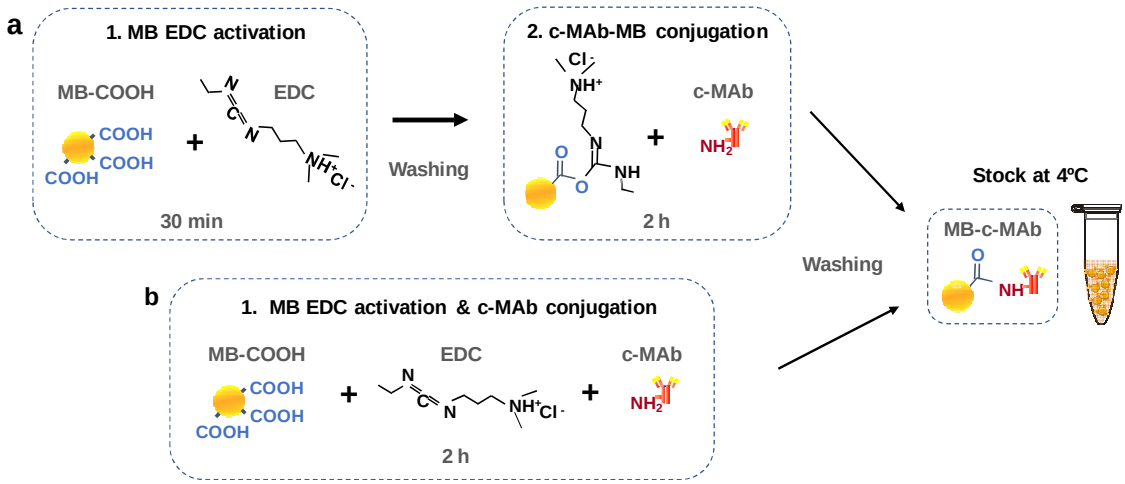

Figure 5.8. Scheme of carboxylic acid MB two-step immunomodification (a) and MB one-step immunomodification (b).

Figure 5.9 shows the signals registered in the 2-step magneto-immunoassay when testing the MMP-9-c-MAb-MB produced by the two methods. In our experiments, the one-step conjugation protocol consistently produced more efficient MMP-9-c-MAb-

MB. As it can be observed in Figure 5.9a, the signals registered were in average 30% higher than those displayed by MB produced with the two-step conjugation method for all the concentrations of MMP-9 tested. This suggested that more c-MAb and/or more active c-MAb was incorporated to the MB in the one-step protocol. This was presumably related to the fact that the reactive group incorporated by EDC chemistry is very labile and hydrolyzes very fast in aqueous media. Consequently, carrying out the conjugation of c-MAb in the presence of EDC provides fresh active groups along the conjugation (compared to using EDC-activated MB that loose active groups over time).

Using a one-step conjugation protocol may also induce a certain level of c-MAb crossbinding, which might translate into conjugation of more c-MAb on the MB as well. On the other hand, the background noise registered at c-MAb-MB produced with the one-step protocol was 5% lower, which was attributed to better protein coverage of the MB. This resulted in better LOD and LOQ (Figure 5.9a, insert). Accordingly, assay sensitivity (slope), linear range and S/N improved when exploiting the one-step protocol for c-MAb-MB preparation (Figure 5.9b).

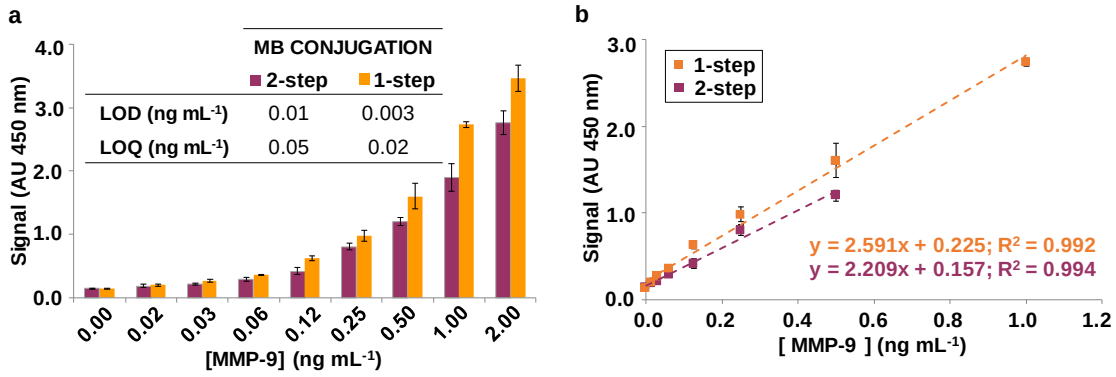

Figure 5.9. 2-step magneto-immunoassay using alternatively MB immuno-modified through two different conjugation procedures. (a) Signals registered for increasing concentrations of MMP-9 when using the two types of MMP-9-c-MAb-MB. (Insert) Summary of the LOD and LOQ displayed by the assay in both cases. (b) Linear range for the results obtained in (a).

5.1.4. Evaluation of the shortened 2-step magneto-immunoassay by detecting MMP-9 in spiked and clinical samples

Upon optimization, the shortened 2-step magneto-immunoassay included a 5-min incubation of the MMP-9-c-MAb-MB (produced though a one-step EDC conjugation) with MMP-9 and MMP-9-bd-PAb. After supernatant removal, MB were incubated with Poly-HRP for 5 min. Two fast washes followed, enzyme substrate was added, and

colorimetric detection took place. The whole assay took approximately 35 min but produced results comparable to the original commercial ELISA when operated in PBS. Lastly, it was studied if the optimized 2-step magneto-immunoassay for MMP-9 detection would be applicable to the analysis of real samples. To do so, the work started by the analysis of sample matrix effect using commercial pooled plasma from healthy individuals inoculated with known concentrations of MMP-9.

The pooled plasma was submitted to increasing dilutions, 1:125, 1:250 and 1:500, with PBS-BSA_1 and was spiked with three different concentrations of MMP-9. As it is shown in Figure 5.10a, the matrix effect increased proportionally to the complexity of the matrix, producing higher background signals. However, if the signals registered for the corresponding blanks (diluted plasma without spiked MMP-9) were subtracted from the signals obtained for MMP-9, all plasma dilutions produced comparable signals for MMP-9 concentrations up to 2 ng mL^{-1} and comparable assay sensitivities (Figure 5.10b).

On the other hand, the MMP-9 recoveries obtained for the different plasma dilutions ranged 60-110 %, 74-104%, and 90-102%, for dilutions 1:125, 1:250 and 1:500 respectively. As it can be observed, the more complex was the matrix, lower recovery of MMP-9 existed. For that reason, the plasma dilution 1:250 offered an equilibrium between matrix complexity and good protein recovery for all the MMP-9 concentrations evaluated.

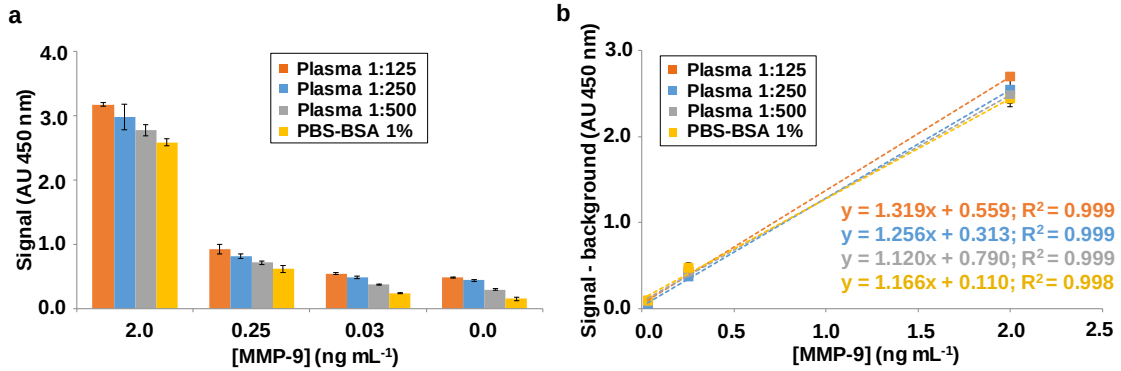

Figure 5.10. Performance of the 2-step magneto-immunoassay in spiked samples. (a) Signals registered for increasing concentrations of MMP-9 spiked in the different matrix samples tested. (b) Signals registered for increasing MMP-9 concentrations after subtracting the corresponding blanks.

Since MMP-9-spiked plasma was not complex enough to mimic clinical samples, we next tested the 2-step magneto-immunoassay in plasma samples from patients having suffered an ischemic stroke. Several teams have reported increased levels of MMP-9 in

stroke patients, with concentrations ranging from <40 ng mL^{-1} to >200 ng mL^{-1} having been measured[430,431].

The 2-step magneto-immunoassay detected MMP-9 in the 10 samples, with concentrations extending between 38 ng mL^{-1} and 300 ng mL^{-1}, which is in accordance with the ranges reported previously (Figure 5.11). The clinical plasma samples diluted 1:250, were detected also using the Duoset ELISA as a reference method. Figure 5.11 displays the concentrations of MMP-9 measured in the 10 plasma samples using alternatively the two methods. As it can be observed, the concentrations of MMP-9 estimated by the magneto-immunoassay correlated linearly with those provided by the ELISA, with a positive lineal Pearson correlation coefficient of 0.9 and recoveries ranging 97–140% in most of the cases.

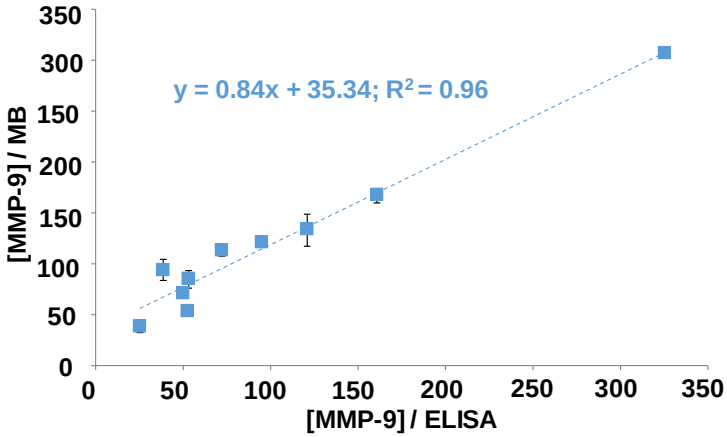

Figure 5.11. Correlation between the concentrations of MMP-9 (ng mL^{-1}) estimated by the 2-step magneto-assay in 10 clinical plasma samples and the concentrations of MMP-9 according to the reference ELISA method (n=3). While the 2-step magneto-immunoassay took approximately 35 min, the ELISA required >6 h.

In conclusion, the 2-step MMP-9 magneto-immunoassay developed could be used for detection in real samples, with a good recovery of MMP-9 in the range of concentrations of clinical interest, but significantly faster than when using a classical ELISA.

5.2. Development of a simplified magneto-immunoassay for PfLDH detection in whole blood

Once the 2-step magneto-immunoassay described in Section 5.1 had been produced, one of the main concerns was to determine if the simplified assay format developed would

be universal or only applicable to MMP-9 detection. For this reason, a similar assay format was developed for a different biomarker, this time for detection of PfLDH (Section 3.6.2). In this case, a pair of MAb provided by Meridian (PLDH-c-MAb and PLDH-bd-MAb) and recombinant LDH from *Pasmodium falciparum* (PfLDH) obtained from CKBiotech were used. Two different ELISA assays had been optimized by another member of the team and were used here as the reference methods (unpublished results). The classical multistep ELISA was capable to detect 0.85 ng mL^{-1} and quantify 2.05 ng mL^{-1} of PfLDH in <5 hours, with a linear response spanning 0.8 - 50 ng mL^{-1} (Figure 5.12a). The shortened ELISA alternative took 3.4 hours (see the protocol in Section 3.6.3), displayed an LOD of 0.08 ng mL^{-1}, an LOQ of 0.52 ng mL^{-1}, and a linear range of 0.1 - 12.5 ng mL^{-1} (Figure 5.12b). Figure 5.12c shows the improvement in assay performance observed for the shortened ELISA, which was attributed to the fact that the PLDH-c-MAb and PLDH-bd-MAb used in this work had been selected for the development of lateral flow tests, which could explain that they performed better in a one-step immunocapture.

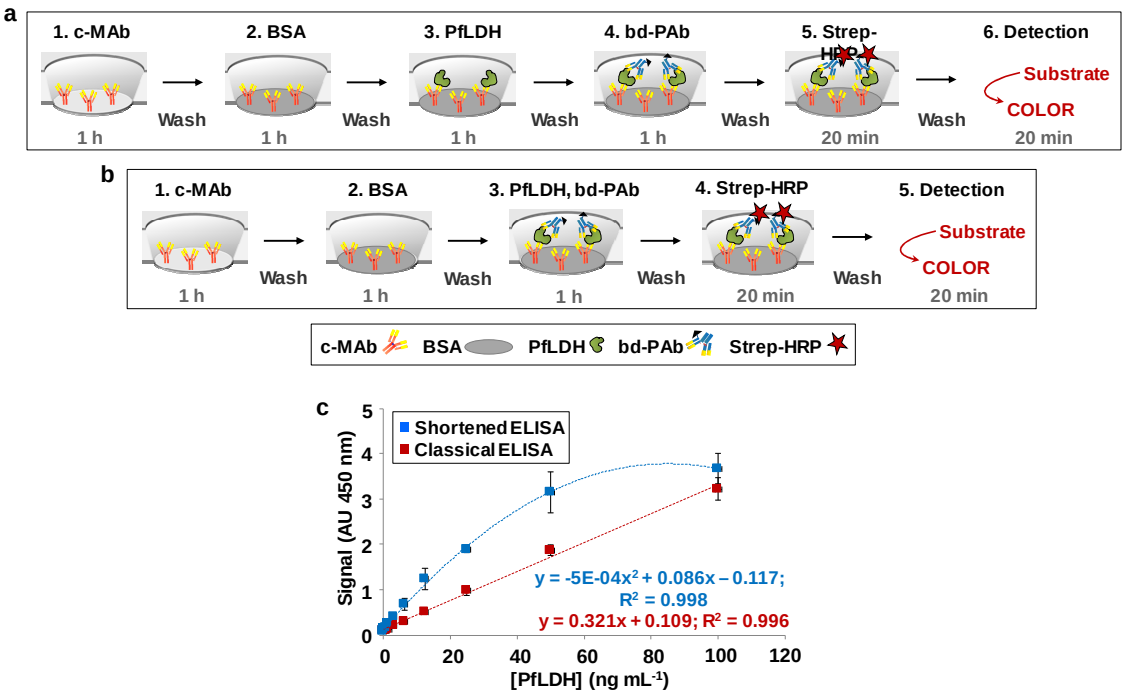

Figure 5.12. (a) Scheme of the classical multistep ELISA for PfLDH detection. (b) Scheme of the shortened ELISA for PfLDH detection. (c) Calibration plot obtained using the classical ELISA or a shorter ELISA version in which PfLDH and bd-MAb were incubated simultaneously.

5.2.1. Optimization of a 2-step magneto immunoassay for PfLDH detection

As before, the optimization of the immunoassay using MB was started pursuing the classical ELISA protocol (Figure 5.13a). For that, MB were modified with the PLDH-c-

MAb using the optimized one-step conjugation protocol and were stored at 4ºC (Section 3.4.3). For the magneto-immunoassay, MB (20 µg per sample) where incubated in three consecutive phases, with the corresponding washes in-between, with the sample, the PLDH-bd-MAb (37.5 ng mL^{-1} per sample) and streptavidin-HRP (Section 3.7.1). Each incubation was extended for 30 min, what made the whole assay last 100 min, which was 3 times shorter than the classical ELISA. This 3-step magneto-immunoassay achieved an LOD of 0.23 ng mL^{-1}, LOQ of 1 ng mL^{-1}, and a linear range of 0.8 - 12.5 ng mL^{-1}. When the classical ELISA and the 3-step magneto-immunoassay for PfLDH detection were compared, it was clearly observed that the immunocapture performed with MB was more efficient than the classical ELISA (Figure 5.14a). The signals registered were enhanced using MB for all the concentrations of PfLDH assayed. However, the assay linear range was reduced when employing MB and signal saturation was attained at lower PfLDH concentrations than when using c-Ab modified microtiter plates (Figure 5.14d). This indicates that, as it has been observed in previous works, MB helps to reduce the duration of the incubations achieving the same results than a reference ELISA in a fraction of time.

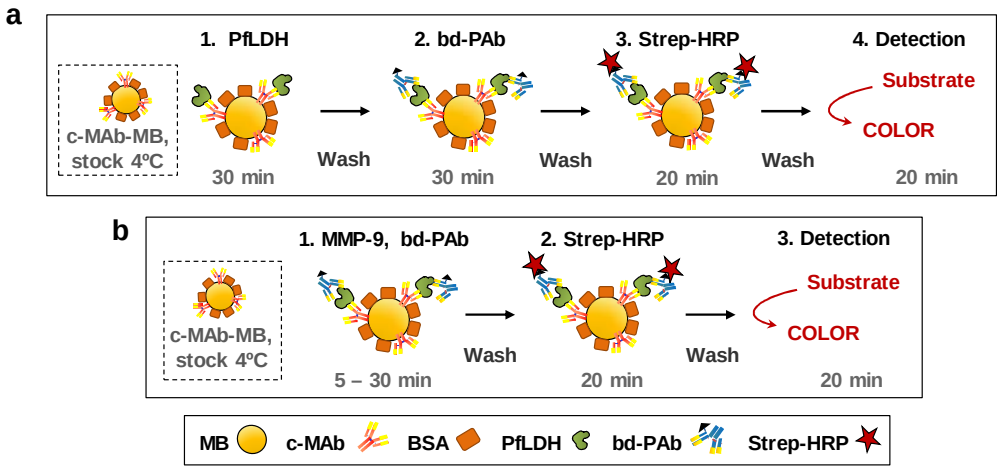

Figure 5.13. (a) Scheme of the 3-step magneto-immunoassay for PfLDH detection. (b) Scheme of the 2-step magneto-immunoassay for PfLDH detection.

A 2-step magneto-immunoassay path was next implemented by combining the two consecutive incubations of the MB with PfLDH and PLDH-bd-MAb in a single immunocapture of 30 min (Figure 5.13b) (Section 3.7.2). This shortened magneto-assay provided LOD of 0.3 ng mL^{-1}, LOQ of 0.95 ng mL^{-1} and linear range of 0.8-12.5 ng mL^{-1}. Contrary to what happens with the PfLDH ELISA, the signals registered and the sensitivity of the 3-step and 2-step magneto-immunoassays were similar to each other (not statistically different in a one-way ANOVA test, $p > 0.05$) (Figure 5.14d).

But when comparing the shortened ELISA with the 2-step magneto-immunoassay in Figure 5.14b, although both provided signals of the same order, the background noise caused for the MB (see Section 5.1.3.1) was higher, masked the lowest concentrations of PfLDH tested and provided worse assay sensitivity. As it had been observed before for the 3-step magneto-immunoassay, the 2-step counterpart displayed also signal saturation for PfLDH concentrations above 50 ng mL^{-1}. This suggested that the incubation time of the PfLDH two-step magneto-immunoassay could be reduced.

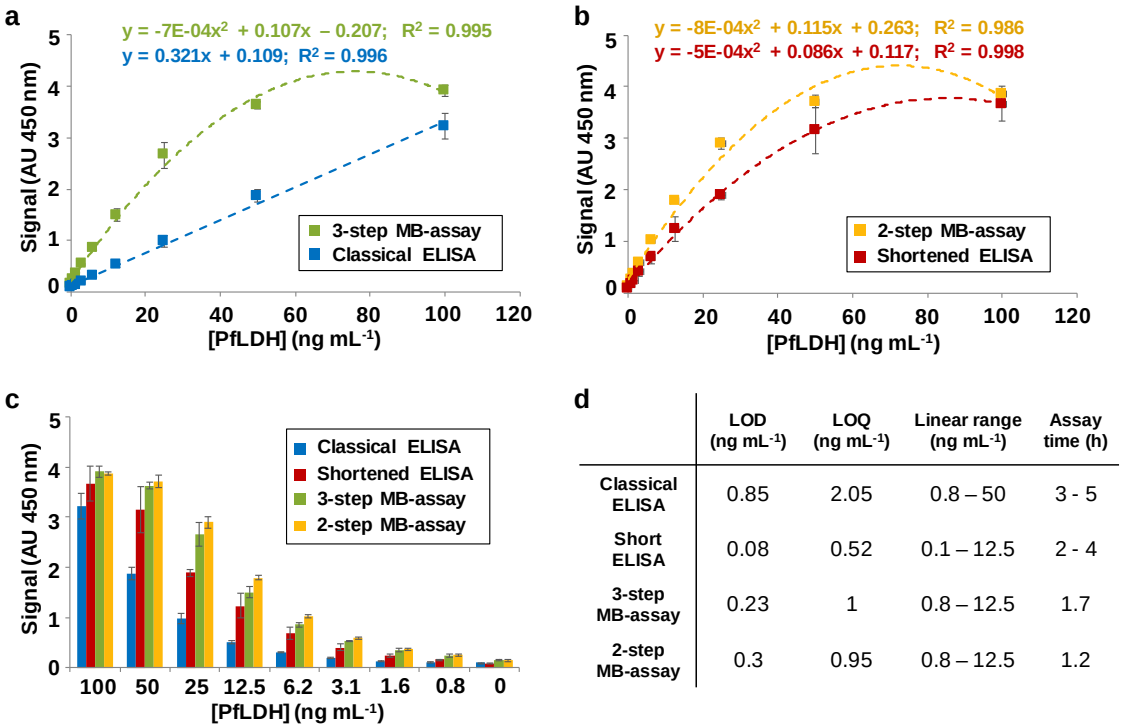

	LOD (ng mL^{-1})	LOQ (ng mL^{-1})	Linear range (ng mL^{-1})	Assay time (h)
Classical ELISA	0.85	2.05	0.8 – 50	3 - 5
Short ELISA	0.08	0.52	0.1 – 12.5	2 - 4
3-step MB-assay	0.23	1	0.8 – 12.5	1.7
2-step MB-assay	0.3	0.95	0.8 – 12.5	1.2

Figure 5.14. Detection of increasing concentrations of PfLDH. (a) Signals registered with the 3-step magneto-immunoassay and the classical ELISA. (b) Calibration curves for the shortened immunoassay versions for PfLDH detection, the ELISA and the 2-step magneto-immunoassay. (c) Comparison of the signals registered for the different ELISA and magneto-immunoassay in (a-b). (d) Summary of the LOD, LOQ and linear range for each experimental condition in (a-c). ELISA assay time includes alternatively just the assay or assay plus plate immunomodification, which was performed immediately before the assay. In contrast, ready-to-use c-MAb-MB stocks were stored at 4ºC.

The range of incubation times studied for the single immunocapture of the 2-step PfLDH magneto-immunoassay included 30 min, 15 min and 5 min (Figure 5.13b). Figure 5.15a summarizes the signals registered for the PfLDH concentrations studied (0.8 – 100 ng mL^{-1}), comparing the performance of a single immunocapture with the PLDH-c-MAb, the sample and the PLDH-bd-MAb together, with the 3-step magneto-immunoassay. It was plainly showed that the signals registered decreased proportionally to the incubation time. In contrast, the linear range was wider for shorter immunocaptures (Figure 5.15b). In terms of sensitivity, the improvement was evident for the 15 min of incubation, which provided LOD of 0.12 ng mL^{-1} and LOQ 0.55 ng

mL^{-1}, and performance equivalent to the PfLDH shortened ELISA (Figure 5.15c). On the other hand, the 5-min immunocapture produced signals 50% lower in average for all the concentrations of PfLDH tested, as well as worse LOD/LOQ. However, it was faster, which made it a good candidate for the development of a rapid diagnostic tool. Accordingly, this was the assay format selected for the subsequent optimization steps.

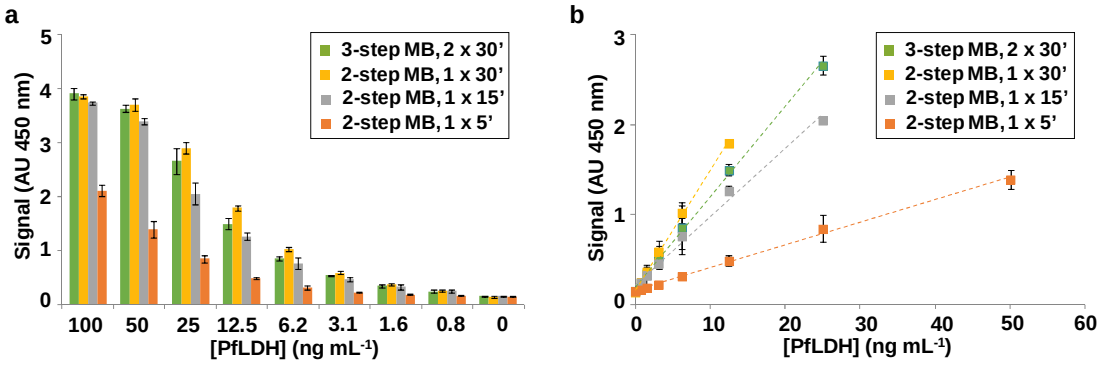

c

	3-step, 2 x 30'	2-step, 1 x 30'	2-step, 1 x 15'	2-step, 1 x 5'
LOD (ng mL^{-1})	0.23	0.30	0.12	0.49
LOQ (ng mL^{-1})	1.00	0.95	0.55	1.39
Linear range (ng mL^{-1})	0.78 – 25	0.78 – 12.5	0.78 – 25	0.78 – 50
Linear Equation	0.099x + 0.197	0.132x + 0.160	0.076x + 0.219	0.025x + 0.160
R^2	0.998	0.998	0.991	0.997
Assay time (min)	100	70	55	45

Figure 5.15. Detection of increasing concentrations of PfLDH using different magneto-immunoassay formats. (a) Signals registered with either the 3-step or the 2-step magneto-immunoassay versions in which PfLDH and PLDH-bd-MAb were incubated simultaneously for 5-30 min. (b) Linear range for each magneto-immunoassay showed in (a). (c) Summary of the LOD, LOQ and linear range for each experimental condition in (a-b).

5.2.2. Implementation of Poly-HRP in the 2-step PfLDH magneto-immunoassay

The PfLDH 2-step magneto-immunoassay with 5 min of immunocapture generated in Section 5.2.1 was additionally improved by implementing Poly-HRP.

The Figure 5.16a shows the improvement in the signals registered when HRP was substituted by Poly-HRP (both incubated for 20 min). Poly-HRP signal amplification caused an increment of the signals registered between 30-50% on average for all the PfLDH concentrations studied. The sensitivity of the 2-step magneto-immunoassay improved considerably also, achieving an LOD of 0.012 ng mL^{-1} and an LOQ of 0.24 ng mL^{-1}, which were 5 times lower than those obtained using HRP for assay detection.

Finally, the incubation time with Poly-HRP was optimized (20 min, 10 min and 5 min tested) trying to reduce even more the total magneto-immunoassay time and reach a balance between sensitivity and linear range (Figure 5.16b). Figure 5.16c summarizes the LOD, LOQ and linear range obtained for the 2-step magneto-immunoassay (carrying in all cases a single 5-min immunocapture) under the different experimental conditions tested. Although reducing Poly-HRP incubation time below 20 min had a negative effect in assay LOD/LOQ, carrying only 5 min of incubation produced better results than the 20 min of incubation with HRP.

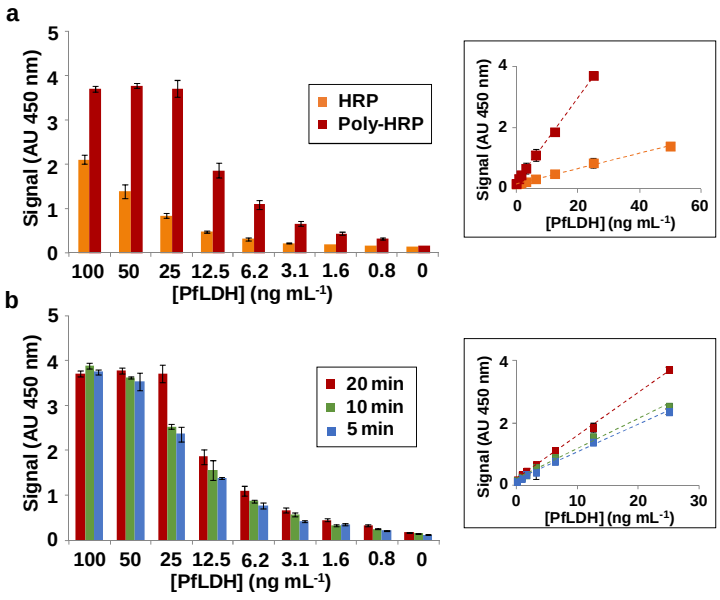

c

	HRP	Poly-HRP		
	20'	20'	10'	5'
LOD (ng mL^{-1})	0.49	0.01	0.25	0.15
LOQ (ng mL^{-1})	1.39	0.24	0.95	0.94
Linear range (ng mL^{-1})	0.78 – 50	0.78 – 25	0.78 – 25	0.78 – 25
Linear equation	0.025x + 0.160	0.139x + 0.207	0.096x + 0.224	0.089x + 0.172
R^2	0.997	0.999	0.991	0.995
Assay time (min)	45	45	35	30

Figure 5.16. Detection of increasing concentrations of PfLDH using the 2-step magneto-immunoassay (single 5-min immunocapture) using alternatively HRP or Poly-HRP. (a) Signals registered with HRP and Poly-HRP incubated for 20 min. Insert: Linear range registered in each case. (b) The 2-step magneto-assay incubating the Poly-HRP for 5-20 min. Insert: Linear range for each magneto-immunoassay showed in (b). (c) Summary of the LOD, LOQ and linear range for each experimental condition (20 min of incubation for HRP and 5, 10 and 20 min for Poly-HRP).

This work carried to develop the PLDH 2-step magneto-immunoassay corroborated the effect of Poly-HRP, demonstrated previously in Section 5.1.3, confirming that Poly-HRP amplifies the signal of the magneto-immunoassay and allows reducing the incubation times without losing sensibility, providing fast and simple magneto-immunoassays.

5.2.3. Optimization of the shortened 2-step magneto-immunoassay for PfLDH detection

The shortened 2-step magneto-immunoassay developed for malaria diagnosis took approximately 40 min and displayed LOD of 0.15 ng mL^{-1} and LOQ of 0.94 ng mL^{-1} (Section 5.2.2, Figure 5.17). The detailed protocol for the 2-step PLDH magneto-immunoassay can be found in Section 3.7.2.

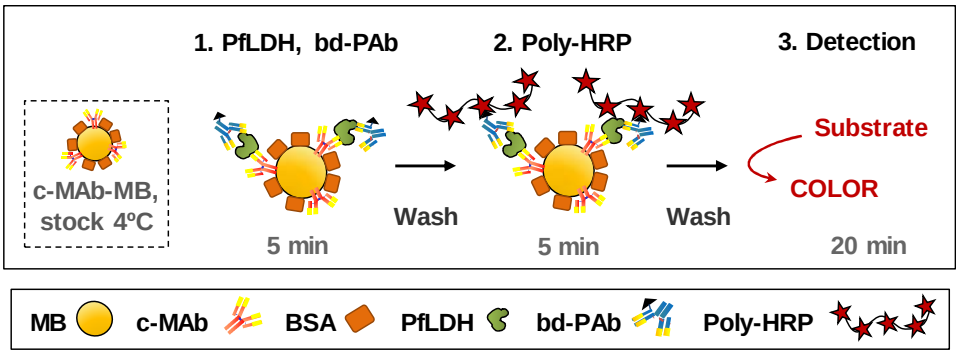

Figure 5.17. Scheme of the shortened 2-step magneto-immunoassay for PfLDH detection.

The additional optimization of this assay started by the study of the amount of MB needed per sample for optimal PLDH immnunocapture and assay performance. Increasing MB concentrations were evaluated, ranging 5-30 µg per 100 µL of sample. From the plot of the Figure 5.18a, it was observed that the signals registered in the presence of PfLDH increased with the amount of MB up to 20 µg and decreased for higher MB loads. Other assay parameters, such as LOD, LOQ and sensitivity (slope) followed a similar trend. Consistently with the results obtained previously for MMP-9, here the best results were produced by 20 µg of MB (0.15 ng mL^{-1} of LOD and 0.94 ng mL^{-1} of LOQ), the condition that was selected for subsequent experiments (Figure 5.18a, insert).

Next, the concentration of bd-MAb was escalated up to 100 ng mL^{-1} (Figure 5.18b). Although the linear detection range was wider for 37.5 ng mL^{-1} of bd-MAb, ranging from 0.4 ng mL^{-1} to 25 ng mL^{-1} of PfLDH, the sensitivity (determined by the slope of the linear calibration plot) increased proportionally to the bd-MAb concentration used (Figure 5.18b, insert graph). The 2-step magneto-immunoassay with 75 ng mL^{-1} of bd-MAb exhibited ~62% of sensitivity improvement compared to using 37.5 ng mL^{-1} of bd-MAb, achieving an LOQ of 0.58 ng mL^{-1} of PfLDH, and was selected for the next optimizations (Figure 5.18b).

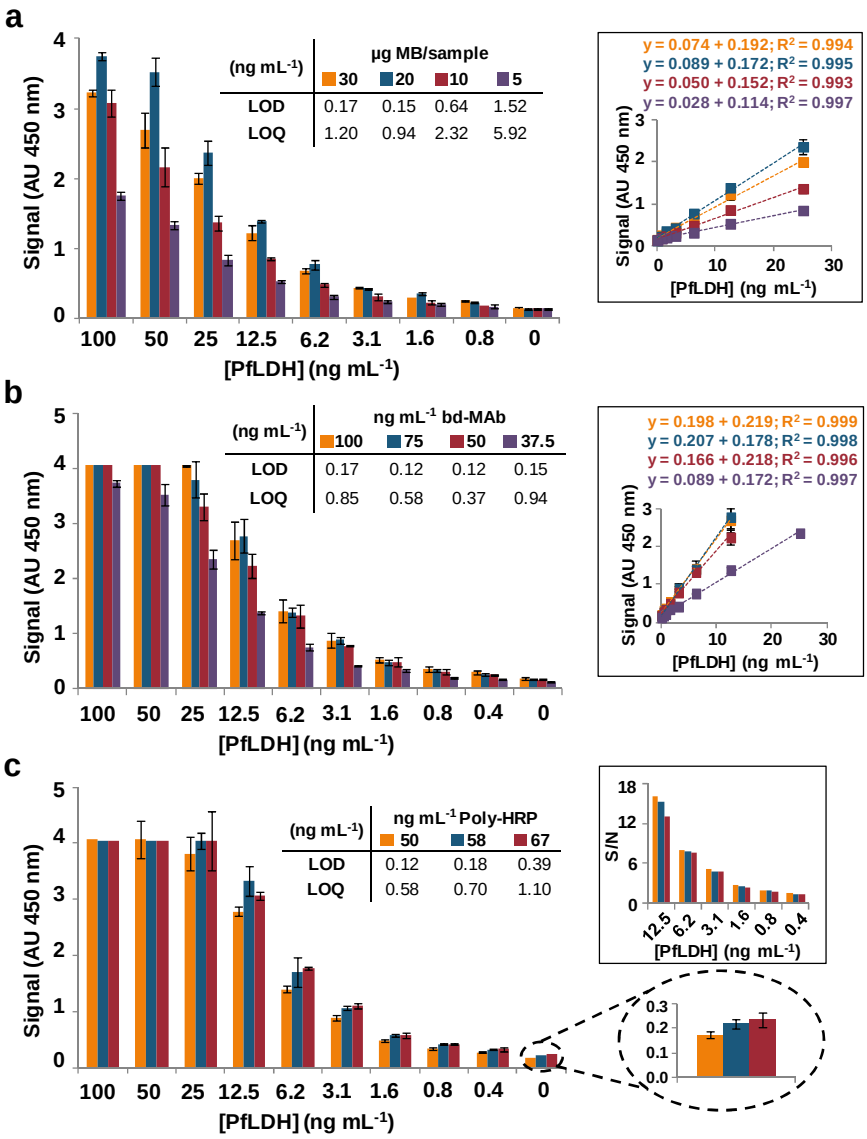

Figure 5.18. Optimization of the shortened 2-step magneto-immunoassay for PfLDH detection. (a) Signals registered for increasing concentrations of PfLDH using different amounts of MB per sample. The inserts illustrate the linear ranges of the signals registered for each MB concentration and the LOD/LOQ for these experiments. (b) Signals registered for increasing concentrations of PfLDH using different concentration of bd-MAb per sample. The inserts illustrate the linear ranges of the signals registered for each bd-MAb concentration and the LOD/LOQ for these experiments. (c) Signals registered for increasing concentrations of PfLDH using different Poly-HRP concentrations. The zoomed insert illustrates the background signals registered in the negative control experiments (without PfLDH). The inserts represent the S/N ratios at low PfLDH concentrations and the LOD/LOQ for each concentration of Poly-HRP evaluated.

Finally, different Poly-HRP dilutions were tested (1:7500, 1:8750 and 1:10000, equivalent to 67 ng mL^{-1}, 58 ng mL^{-1} and 50 ng mL^{-1}, respectively) (Figure 5.18c). Higher Poly-HRP concentrations displayed signal saturation at lower PfLDH concentrations and higher background noise in the negative controls without PfLDH. Accordingly, better S/N ratios, LOD and LOQ were obtained for lower Poly-HRP

concentrations. Nevertheless, diluting Poly-HRP further did not improve the assay additionally.

The final 2-step magneto-immunoassay optimized included the employment of 20 µg of MB per sample, incubated for 5 min with sample and 75 ng mL^{-1} of bd-MAb and for other 5 min with a 1:10000 Poly-HRP dilution in a final volume of 100 µL, before MB washing and colorimetric detection. This assay achieved PLDH detection with a linear range of 0.4-12.5 ng mL^{-1}, LOD of 0.12 ng mL^{-1} and LOQ of 0.58 ng mL^{-1}, in less than 40 min.

5.2.4. Detection of PLDH in real sample matrices using the shortened 2-step magneto-immunoassay

The optimized 2-step magneto-immunoassay for PLDH detection was next tested in real blood samples. In order to do so, the sample matrix effect was evaluated with whole blood from healthy individuals inoculated with known concentrations of PfLDH.

For these experiments, the whole blood was submitted to increasing dilutions, 1:10, 1:25, 1:50 and 1:100, with PBS-BSA_1, and was spiked with the range of PfLDH concentrations studied before (0.4 – 100 ng mL^{-1}). Figure 5.19 shows the effect of the complexity of the sample matrix, which increases proportionally the signals and the background noise. However, if the signals registered for the corresponding blanks (diluted blood without spiked PfLDH) were subtracted from the signals obtained for spiked PfLDH, all blood dilutions produced comparable assay sensitivities and signals for all the PfLDH concentrations studied (Figure 5.19, insert).

On the other hand, the PfLDH recoveries obtained for the different blood dilutions ranged 70-119%, 80-120%, 88-114 %, 92-124% for dilutions 1:10, 1:25, 1:50 and 1:100 respectively. The blood dilution 1:25 offered an equilibrium between matrix complexity and good protein recovery for all the PfLDH concentrations evaluated.

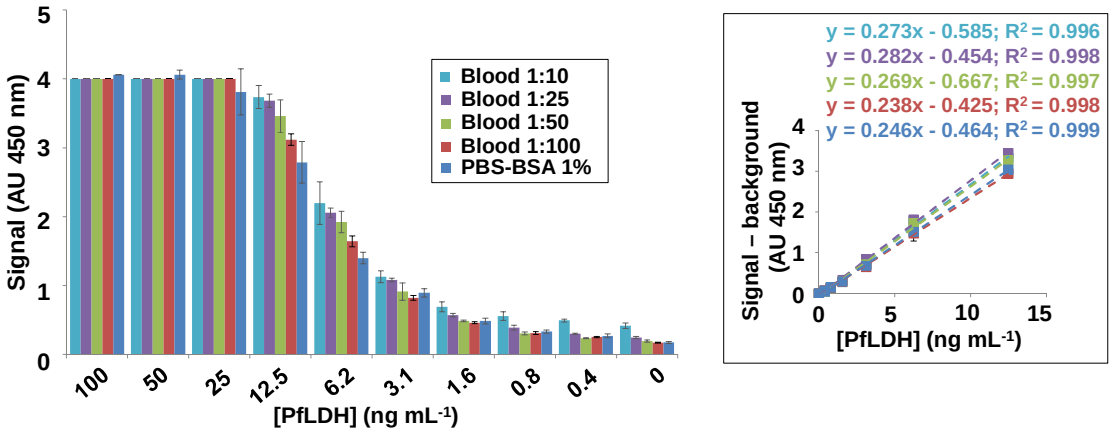

Figure 5.19. Signals registered for the 2-step magneto-immunoassay with increasing concentrations of PfLDH spiked in the different sample matrices tested. Insert, signals registered for increasing PfLDH concentrations after subtracting the corresponding blanks.

The 2-step magneto-immunoassay was finally tested in 6 lysed whole blood samples from malaria patients. The sensor detected PfLDH concentrations between 66 ng mL^{-1} and 877 ng mL^{-1}, corresponding to parasitaemia ranging 0.03 - 0.6 %. The clinical blood samples diluted 1:25, were detected also using the shortened-ELISA as a reference method. Figure 5.20 displays the concentrations of PfLDH measured in the 6 whole blood samples using alternatively the two methods. As it can be observed, the concentrations of PfLDH estimated by the magneto-immunoassay correlated linearly with those provided by the ELISA, with a positive lineal Pearson correlation coefficient of 0.9 and recoveries ranging 97–125%.

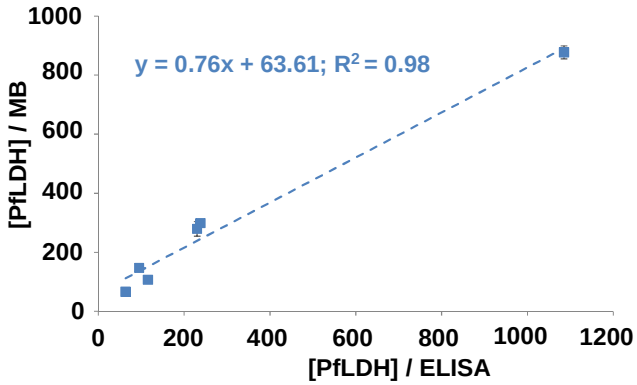

Figure 5.11. Correlation between the concentrations of PfLDH (ng mL^{-1}) estimated by the 2-step magneto-assay in 6 clinical blood samples and the concentrations of PfLDH according to the reference shortened-ELISA method (n=3). While the 2-step magneto-immunoassay took approximately 35 min, the shortened-ELISA required >3 h.

In conclusion, the 2-step PfLDH magneto-immunoassay developed could be used for detection in real samples, with a good recovery of PfLDH, but providing results significantly faster than when using a shortened-ELISA.

5.3. Conclusions

Many authors have shown that MB are useful to produce enhanced bioassays, often more sensitive and/or shorter than classical counterparts such as ELISA. Nevertheless, an important number of the magneto-assays reported rely in multi-step procedures that take hours. Both manual handling and automation of such assays is not trivial, which limits the exploitation of MB and magneto-assays outside a laboratory. For this reason, this chapter has focussed in the development of simplified magneto-immunoassays that could be easier to carry out by not specially trained personnel and easier to automate employing low-cost detection devices than current multi-step alternatives.

As it has been shown, the careful selection of the Ab pair allows optimizing simplified 2-step magneto-immunoassays. The subsequent implementation of Poly-HRP provides signal amplification, facilitating that the assay steps are additionally shortened without decreasing assay performance. As a proof of concept, two different simplified magneto-immunoassays have been developed.

The 2-step magneto-immunoassay for MMP-9 detection included a 5-min incubation of the MMP-9-c-MAb-MB with MMP-9 and MMP-9-bd-PAb. After supernatant removal, MB were incubated with Poly-HRP for 5 min. Two fast washes followed, enzyme substrate was added, and colorimetric detection took place. The whole assay took approximately 40 min but produced results comparable to the original commercial ELISA when operated in PBS, including LOD of 3 pg mL^{-1}, LOQ of 20 pg mL^{-1}, and linear range spanning 0.015-1 ng mL^{-1}. This assay was successfully applied to the study of plasma samples from patients having suffered an ischemic stroke, providing MMP-9 quantitation that correlated linearly with that obtained using a reference ELISA that took > 5h.

The 2-step magneto-immunoassay optimized for PLDH detection included also a single 5-min incubation of the MB with sample and bd-MAb, 5 more min of incubation with Poly-HRP, MB washing and colorimetric detection. This assay achieved PfLDH

detection with a linear range of 0.4-12.5 ng mL^{-1}, LOD of 0.12 ng mL^{-1} and LOQ of 0.58 ng mL^{-1}, in less than 40 min.

These results demonstrate that the simplified magneto-immunoassay format developed here is applicable to different combinations of Ab pair and target analyte, providing extremely fast, simple and efficient diagnostic tools.

Chapter 6

Development of one-step magneto-immunosensors for protein biomarker detection

6. Development of one-step magneto-immunosensors for protein biomarker detection

The use of MB for immunoassay development has been demonstrated in Chapter 5, showing that MB can provide improved analyte immunobinding efficiency, and relatively fast and simple analyte preconcentration and separation from non-target sample components. Several authors have exploited additionally MB for the production of fast and sensitive electrochemical magneto-immunosensors[148,414]. However, these electrochemical magneto-immunosensors often consist of numerous incubations and washing steps, with serial buffer replacements using external magnets in-between. For this reason, magneto-immunosensor automation tends to require devices containing different chambers, microchannels, magnetic field generators, moving parts, and/or fluid flow features[439–442]. Accordingly, the attempts to produce inexpensive analytical tools for this purpose have only achieved detection of assays performed off-line, the study of discrete samples, or operation of simplified immunoassay paths of limited sensitivity[443–446]. This hampers the implementation of electrochemical magneto-immunosensors in POC settings, were extremely simple protocols and inexpensive devices are needed.

Attempts have been made to improve electrochemical immunosensor sensitivity by employing nanomaterial-, enzyme- and DNA-based signal amplifiers[68,220,447]. Among them, Poly-HRP stand out as affordable commercial products. For instance, dual carbon screen printed electrodes (SPCE), custom-modified with 4-carboxyphenyl-functionalized carbon nanotubes, were used for the simultaneous determination of interleukin-1b (IL-1b) and tumour necrosis factor α (TNF- α)[235]. This sensor achieved LODs of 0.38 pg mL^{-1} (IL-1b) and 0.85 pg mL^{-1} (TNF-a), based on a sandwich immunoassay that included 3 consecutive incubation steps with the corresponding series of washes, and took 150 min. Otherwise, the combination of ultrasensitive customized nanostructured SPCE and immunomodified Poly-HRP provided detection of alpha-fetoprotein and HIV p24 antigen in about 30–35 min, with LODs of 1–2 $pgmL^{-1}$, in both cases entailing productions paths that took days and a 2- step immunoassay format[236,437]. Poly-HRP-based electrochemical magneto-immunosensors have been also produced, in which immunomodified-MB were serially incubated with sample, biotinylated detection Ab and Poly-HRP, washed after each incubation, and finally

confined onto SPCE for substrate addition and electrochemical detection. In these examples, detection of interleukin 6 (IL-6) and transforming growth factor beta 1 (TGF-β1) took 90 and 140 min, respectively, providing LODs of 0.39 pg mL^{-1} and 10 pg mL^{-1}[196,200].Interestingly, although most examples targeted LOD improvement, in Sections 5.1.3 and 5.2.2 it was confirmed that Poly-HRP could also serve to produce shorter and simpler immunoassays if sensitivity could be slightly compromised.

The objective of the work summarized in this chapter was to produce two electrochemical magneto-immunosensors, for the quantitative detection of MMP-9 and PfLDH, respectively, whose speed and handling simplicity approached to a certain extent the requirements of POC testing. The starting point were the 2-step colorimetric magneto-immunoassays described in Chapter 5, which although performed in 45 min with efficiency comparable to the 5-h reference ELISA, were still too long and complex for POC implementation. Here, it was pursued the development of a faster and simpler assay path that could be accomplished with minimal technical requirements by lay persons. To do so, immuno-modified Poly-HRP signal amplifiers were produced, which allowed optimizing fast and simple one-step magneto-immunoassays. Next, electrochemical detection was implemented using a ready-to-use commercial substrate solution and a customized multiplexed magnetic holder, which allowed reducing the detection time from 20 to just 5 min. Finally, the methods developed were calibrated by studying clinical samples (blood plasma for MMP-9 detection and whole blood for PLDH detection). As it will be shown, the electrochemical magneto-immunosensors developed quantified the diagnostic biomarker in <15 min, without requiring sophisticated equipment or complex production paths.

6.1. Development of a one-step electrochemical magneto-immunosensor for MMP-9 detection in plasma samples

The final objective of this part of the work was to produce a short and simple electrochemical MMP-9 magneto-immunosensor compatible with POC testing. For this, the 2-step colorimetric magneto-immunoassay that had been produced previously[438] was simplified additionally (see Section 5.1.3). With this purpose, an immuno-modified Poly-HRP signal amplifier was produced, which allowed optimizing a one-step 5-min magneto-immunoassay, and electrochemical detection was implemented, which reduced

the detection time from 20 to less than 5 min. The resulting electrochemical magneto-immunosensor could be carried out in <15 min.

6.1.1. Production of a Poly-HRP immunoconjugate and optimization of a one-step magneto-immunoassay for MMP-9 detection

The 2-step magneto-immunoassay produced previously entailed two consecutive 5-min incubations with sample/bd-PAb and Poly-HRP, respectively. This required that MB were concentrated magnetically and washed twice between both incubations. Incorporating the bd-PAb directly onto Poly-HRP to produce an immuno-modified signal amplifier pursued optimizing a simpler magneto-immunoassay that consisted of a single incubation step (Figure 6.1**).** Although not significantly shorter, the new assay format was anticipated to entail less handling for the user.

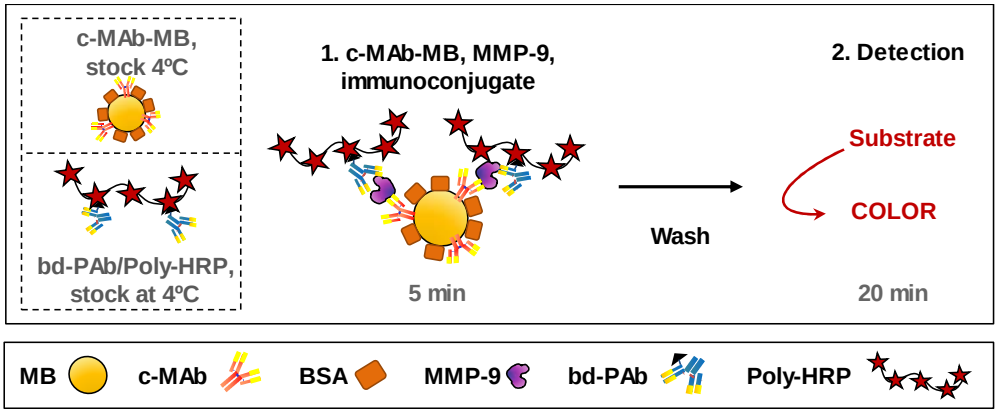

Figure 6.1. Scheme of the one-step magneto-immunoassay for MMP-9 detection.

According to the provider's description, Poly-HRP contained biotin-binding protein conjugated with polymers of HRP. The conjugate was devoid of unconjugated streptavidin and HRP molecules to minimize competition and background signal. Since Poly-HRP was supplied in a proprietary stabilizer solution of undisclosed composition, chemical conjugation of the detection Ab was discarded. Alternatively, increasing concentrations of MMP-9-bd-PAb were incubated with Poly-HRP for different incubation times and conditions, followed by incubation with biotin to block free biotin-binding sites that could produce conjugate aggregation over storing at 4 °C.

The first step was optimizing the concentration of MMP-9-bd-PAb in the conjugate. For that, a fixed amount of Poly-HRP (10 μg mL^{-1}) was incubated under rotation with MMP-9-bd-PAb concentrations ranging 10–40 μg mL^{-1}. These conjugates were then

used, diluted 1:200, to detect increasing concentrations of MMP-9 or the negative controls without MMP-9 in a one-step magneto-immunoassay (Figure 6.1). This led to final working concentrations of 50–200 ng mL^{-1} for the MMP-9-bd-PAb and to 50 ng mL^{-1} for Poly-HRP (Figure 6.2). While nonspecific binding of unmodified Poly-HRP was irrelevant, all the conjugates detected MMP-9 proportionally to its concentration. Only the conjugate with the lowest concentration of MMP-9-bd-PAb, equivalent to half the concentration used in the 2-step assay, displayed signals considerably lower for most MMP-9 concentrations. The signals registered with the other five conjugates were not statistically different (oneway ANOVA test, $p > 0.05$), as they were the linear ranges, sensitivity, LODs and LOQs. This suggested that a partial loading of the conjugate with MMP-9-bd-PAb was enough for optimal performance. Since any unconjugated MMP-9-bd-PAb remaining in solution could compete with the conjugated bd-PAb and made the assay more expensive, the concentration of MMP-9-bd-PAb selected for subsequent experiments was 100 ng mL^{-1} (equivalent to a 1:2 Poly-HRP: MMP-9-bd-PAb w:w ratio).

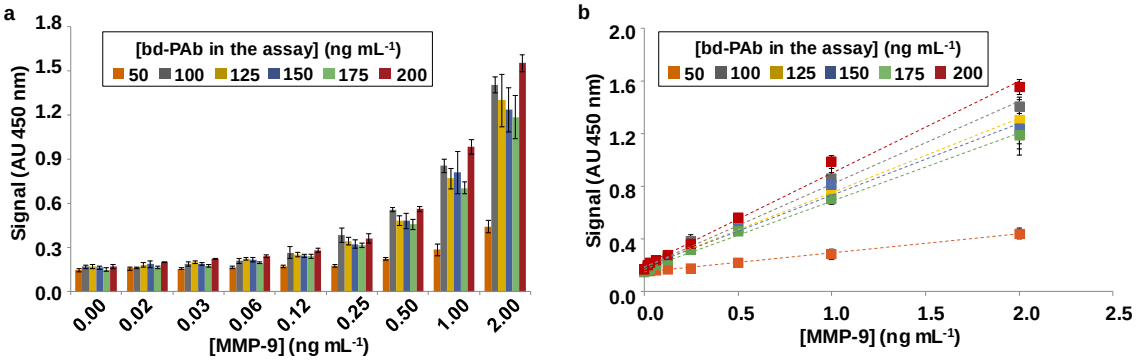

c

	[bd-PAb in the assay] (ng mL^{-1})					
	50	100	125	150	175	200
LOD (ng mL^{-1})	0.24	0.05	0.07	0.05	0.04	0.05
LOQ (ng mL^{-1})	0.53	0.15	0.24	0.16	0.17	0.18
Linear Equation	0.144x + 0.150	0.627x + 0.190	0.564x + 0.187	0.547x + 0.187	0.517x + 0.171	0.700x + 0.198
R^2	0.997	0.993	0.998	0.991	0.997	0.994

Figure 6.2. (a) Signals and LOD/LOQ registered for MMP-9 detection in the one-step magneto-immunoassay using bd-PAb/Poly-HRP conjugates produced with a fixed concentration of Poly-HRP and different bd-PAb loadings. (b) Linear ranges and the corresponding fitting equations of the assays shown in (a). (c) Summary of the LOD, LOQ and linear range for each experimental condition in (a-b).

The incubation time of Poly-HRP with MMMP-9-bd-PAb to produce the immunoconjugate was next optimized by testing times of incubation extending from 20 min to overnight (Figure 6.3).

Figure 6.3a summarizes the signals registered in the one-step magneto-immunoassay when MMP-9 was detected using c-MAb-MB produced with the two-step EDC conjugation protocol and a battery of bd-PAb/Poly-HRP conjugates, which had been prepared by incubating Poly-HRP with bd-PAb for different times. In all cases, the final concentrations of Poly-HRP and bd-PAb were of 50 ng mL^{-1} and 100 ng mL^{-1}, respectively. As it can be observed, the signals registered and the assay sensitivities (slope) were proportional to the time Poly-HRP had been incubated with bd-PAb, except for the 20-min preparation time that displayed values 2-4 times lower than the rest. This conjugate resulted consistently in lower assay sensitivity and worse LOD/LOQ. This was attributed to a higher amount of bd-PAb remaining free in solution after short incubation times, which competed later with the conjugate for MMP-9 binding.

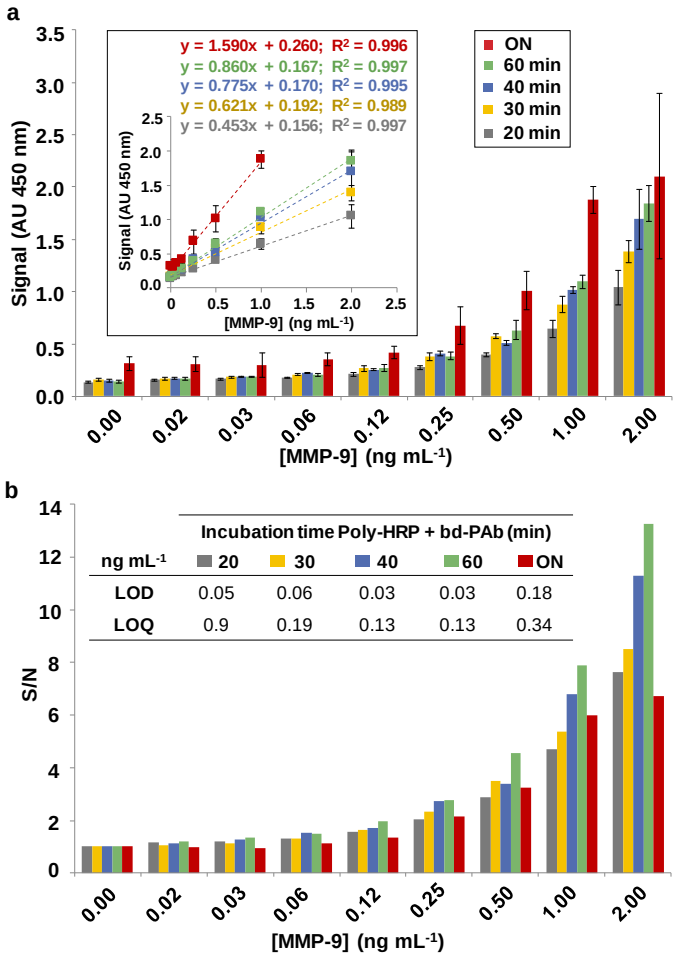

Figure 6.3. (a) Comparative performance of the one-step magneto-immunoassay when the conjugate was produced by incubating Poly-HRP with bd-PAb for different times. The insert shows the linear ranges and the corresponding fitting equations of the assays. (b) S/N ratios for the assays performed with the experimental conditions of (a). The insert summarizes the LOD and LOQ.

On the other hand, the overnight incubation displayed also the highest slope, but the narrowest linear range and the highest variability (inter assay %CV of 15-20%) (Figure 6.3a, Insert). This could be produced by a certain degree of conjugate aggregation/crossbinding over longer preparation times, resulting in attachment of bigger HRP complexes per binding event on the MB (both specific and non-specific). In addition, the high background noise generated by this preparation resulted in lower S/N ratios than the rest of conjugates tested (Figure 6.3b).

As it can be observed, the differences between the results obtained for 30–90 min preparation times were not statistically significant (one-way ANOVA test, $p > 0.05$). It was thus concluded that 30-min incubation was enough for conjugate preparation, which was consistent with fast streptavidin-biotin binding.

The best-performing conjugates were tested also using MMP-9-c-MAb-MB that had been produced with the one-step EDC conjugation protocol, see Section 3.4.3 (Figure 6.4a). In this case, the signals, LOD and LOQ registered for the conjugates obtained after incubation of Poly-HRP with bd-PAb for 30, 60 and 90 min were not statistically different in a one-way ANOVA test ($p > 0.05$). Using one-step EDC conjugation, MMP-9-c-MAb-MB resulted in LOD/LOQ that were half those obtained for MMP-9-c-MAb-MB produced through the two-step EDC conjugation, as well as twice as steep slopes (Figure 6.4b). Noteworthy, under these experimental conditions, the whole assay linear range shifted towards lower concentrations of MMP-9 without shrinking compared to the assays using the two-step EDC conjugated MMP-9-c-MAb-MB (Figure 6.4a, insert). These results confirmed that, for working under these experimental conditions, a 30-min incubation was enough for the preparation of the conjugate.

a

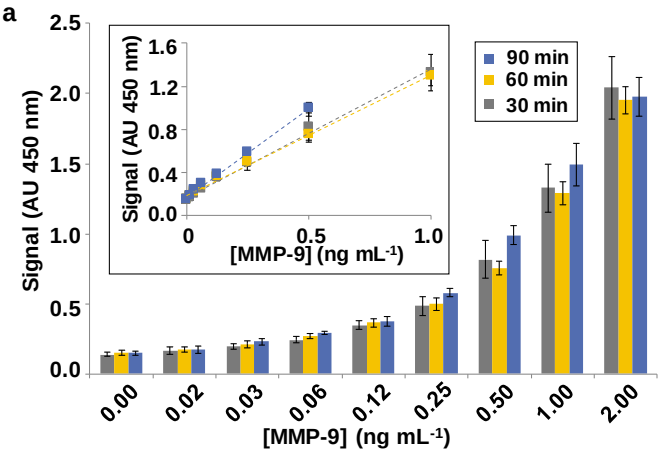

b

	Incubation Poly-HRP + db-Pab (min)		
	30	60	90
LOD (ng mL^{-1})	0.025	0.023	0.018
LOQ (ng mL^{-1})	0.103	0.110	0.079
Linear Equation	1.191x + 0.168	1.121x + 0.186	1.654x + 0.166
R^2	0.994	0.995	0.997

Figure 6.4. (a) Comparative performance of the one-step magneto-immunoassay when the conjugate was produced by incubating Poly-HRP with bd-PAb for different times and using the one-step MB conjugation protocol. (Insert) Linear range for these experimental conditions. (b) Summary of the LOD, LOQ and linear range for each experimental condition in (a).

Consistently with the results obtained previously, the c-MAb-MB produced through the improved one-step conjugation displayed signals 24% higher, LOD/LOQ 50% lower, and higher sensitivity (slopes of 1.19 and 0.71 UA mL ng^{-1}, respectively) (Figure 6.5a-b). Upon optimization, the one-step assay displayed linear response between 16 and 1000 pg mL^{-1} of MMP-9, sensitivity of 1.19 AU mL^{-1}, LOD of 25 pg mL^{-1}, LOQ of 100 pg mL^{-1}, and signal variability between experiments ranging 8–15%. Performance was still slightly worse than that of the original 2-step magneto-immunoassay (Figure 6.5c–d), with signals 20% lower and higher LOD/LOQ. This could be caused by lower availability and higher steric impediments of the polymer-bound bd-PAb in the one-step assay compared to the bd-PAb free in solution used in the 2-step approach.

On the other hand, the method for producing MMP-9-bd-PAb/Poly-HRP was reproducible, with variabilities in performance below 5% for the stability study of the conjugate. Furthermore, the conjugate was stable at 4 °C in PBS-BSA$_{0.1}$ for up to 4 weeks and the results obtained using a freshly made MMP-9-bd-PAb/Poly-HRP or a 1-month-old conjugate were not statistically different (two-way ANOVA test, $p > 0.05$) (Figure 6.5d, insert).

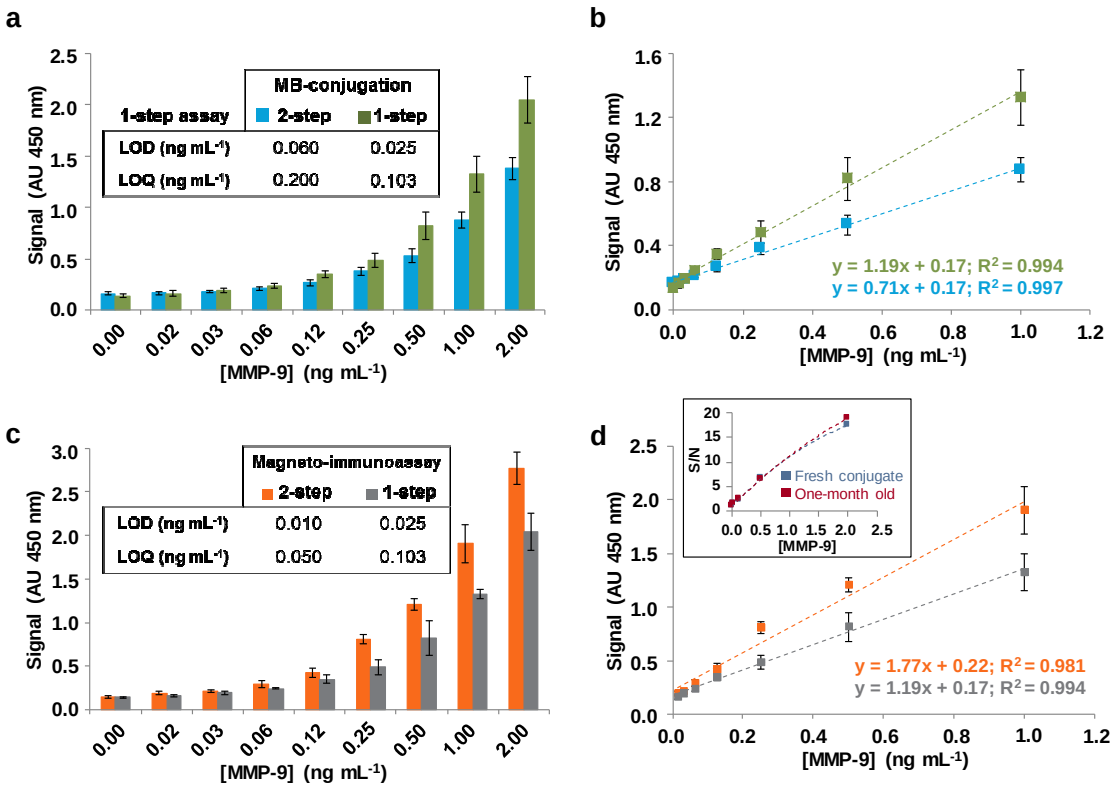

Figure 6.5. (a) Signals registered for increasing MMP-9 concentrations in the one-step magneto-immunoassay when using alternatively c-MAb-MB produced by either a one-step or a two-step conjugation protocol. (b) Linear ranges of the two assays displayed in "a" and the corresponding fitting equations. (c) Comparison of the calibration plots and LOD/LOQ obtained in the initial 2-step performed with the 2-step c-MAb-MB conjugation, and the optimized one-step magneto-immunoassay using the single-step c-MAb-MB conjugation. (d) Linear ranges of the two assays and the corresponding fitting equations. (Insert) Calibration plots obtained using an immunoconjugate either freshly made or after storage at 4 °C for 1 month.

6.1.2. Performance of the one-step magneto-immunoassay for MMP-9 detection in blood plasma

The one-step magneto-immunoassay developed was next tested in spiked samples of increasing complexity. The final objective was to study the potential matrix effect caused by these samples and to determine the comparative performance of the assay under such conditions. This study was carried out in pooled plasma obtained from healthy individuals, which was diluted to different extents, was inoculated with known concentrations of MMP-9, and was assayed using the developed one-step magneto-immunoassay. As it had been done before in Section 5.1.4, three different plasma dilutions were studied here (1:125, 1:250 and 1:500).

The signals registered for all the plasma dilutions studied evidenced an increase of the signals registered for the concentrations of MMP-9 studied and the background noise measured for the unspiked plasma, which were in all cases proportional to the matrix

complexity (Figure 6.6a). As it had been performed in other cases, to reduce this interference and compare the assays between them, the signals registered for the different concentrations of MMP-9 tested were submitted to the subtraction of the background noise obtained for the corresponding blanks (diluted plasma without spiked MMP-9) (Figure 6.6b). As it can be observed, the assay performed well in spiked plasma, producing results comparable to those obtained in saline solution. The MMP-9 recovery for the plasma dilutions tested ranged 99-104% independently of the matrix complexity. This suggested that the one-step magneto-immunoassay was applicable to the study of this type of real samples, in which it provided efficient MMP-9 detection.

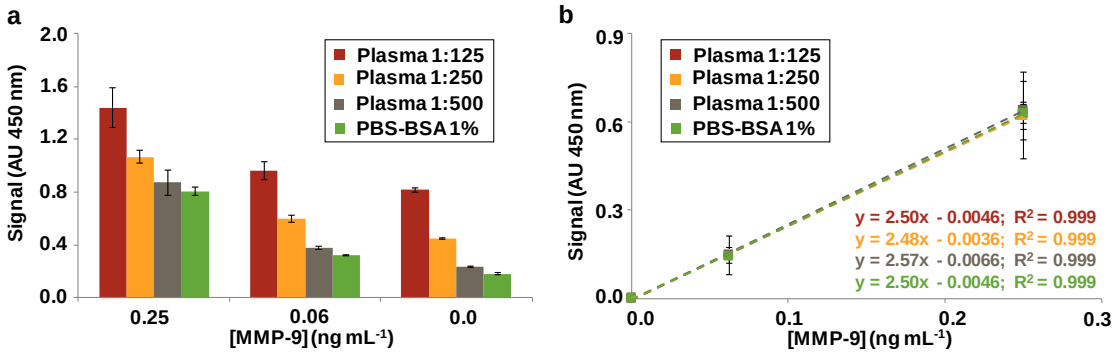

Figure 6.6. (a) Signals registered for increasing concentrations of MMP-9 in the different matrix samples tested. (b) Comparable signals for MMP-9 concentrations after subtracting the corresponding blanks.

The optimized protocol included a single 5-min incubation before the washing and detection steps. Assay handling had thus been simplified considerably. The next target was to shorten the detection step, for which electrochemical detection was implemented.

6.1.3. Electrochemical detection of the one-step MMP-9 magneto-immunoassay

For the electrochemical detection of the one-step magneto-immunoassay, commercial SPCE were placed in a multiplexed customized 8×magnetic holder[415] (see Section 3.8.1). The device contained a base that housed up to 8 SPCE and a sliding component that accommodated 8 neodymium magnets. This sliding bar could reach two different positions, in which the magnets were placed immediately below the SPCE WE or far away from them (Figure 6.7a). This allowed alternate MB confinement and release, facilitating also electrode washing and reutilization.

Although the SPCE WE measured 4 mm in diameter, neodymium magnets 2 mm in diameter were used in the holder. Bigger magnets produced MB confinement beyond the WE perimeter (Figure 6.7b) and stronger MB attachment onto the electrode surface, which made it more difficult to release the MB and re-use the electrode. On the other hand, the sediment produced by MB magnetic confinement was more compact and variable for smaller MB volumes, which produced also lower and more variable signals in the magneto-immunoassay. The best and most reproducible results were obtained for MB volumes of 70 – 100 μL pipetted on the sensors with the magnets in the "on" position, which produced more homogeneous MB sediments as well (Figure 6.7b).

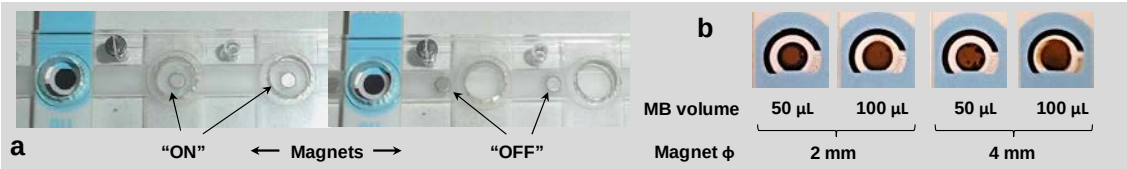

Figure 6.7. MB confinement onto SPCE using a customized magnetic holder for magneto-immunoassay electrochemical detection. (a) Performance of the sliding magnetic bar. (b) Sediments obtained after confinement of a fixed amount of MB in 50 or 100 μL volumes using alternatively magnets 2 or 4 mm in diameter.

Figure 6.8a summarizes the steps needed for the electrochemical detection of the one-step MMP-9 magneto-immunoassay. First, MMP-9 was incubated for 5 min with MMP-9-c-MAb-MB and the MMP-9-bd-PAb/Poly-HRP conjugate, which was followed by two short washing steps. Then, MB were resuspended in 50 μL of PBS and were confined onto the WE of a SPCE, which had been placed in the customized magnetic holder with the magnets in the "on" position to retain the MB. Current was allowed to stabilize in this PBS at −0.05 V vs. Ag pseudo-reference, which allowed confirming that the 8 SPCE were working well. The measurement was then paused, PBS was substituted by ready-to-use TMB substrate solution, and the measurement was resumed for 150 s more. As illustrated in Figure 6.8b, the reduction current registered was proportional to MMP-9 concentration.

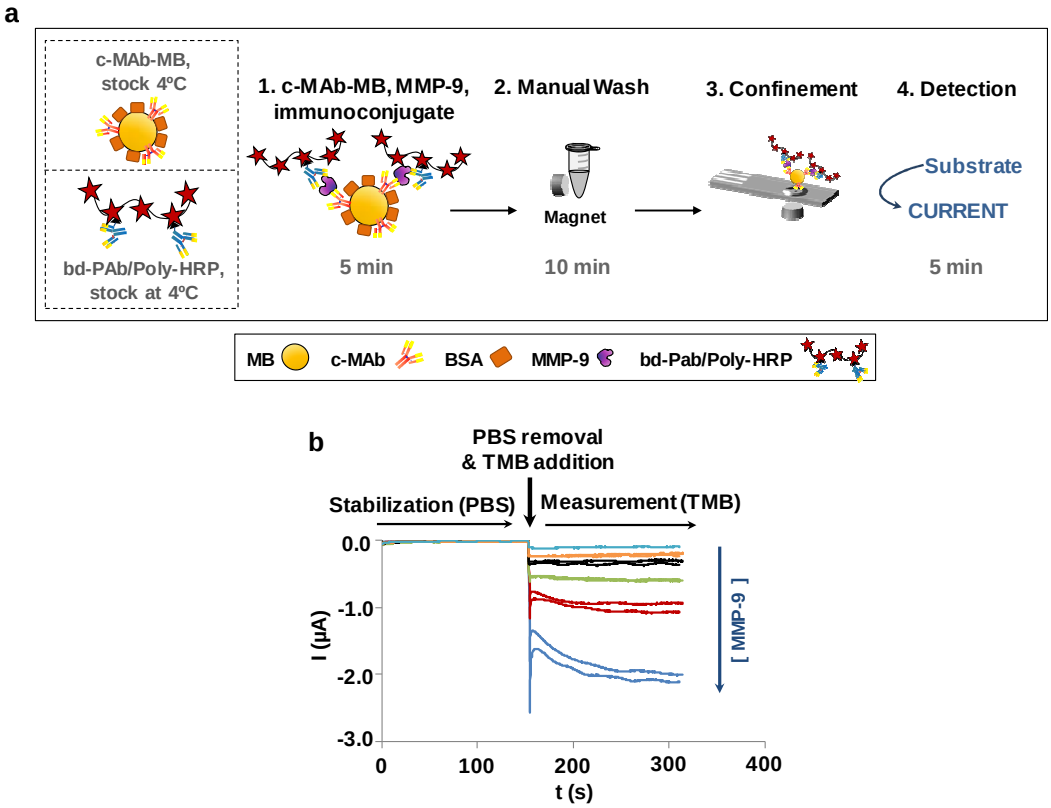

Figure 6.8. (a) Electrochemical one-step magneto-immunosensor for MMP-9 detection. (b) Examples of the chronoamperograms registered for increasing MMP-9 concentrations (from top to bottom, negative control without MMP-9 and MMP-9 0.125, 0.25, 0.5, 1 and 2 ng mL^{-1}; two independent replicates are shown per concentration).

The electrochemical magneto-immunosensor did not show any signal saturation in the concentration range studied and displayed linear response between 30 pg mL^{-1} and 2 ng mL^{-1} of MMP-9 (Figure 6.9a). Although the sensor produced higher currents when measuring at potentials below −0.05 V, background noise and signal variability increased also. The best results were obtained at −0.05 V *vs*. Ag, which provided the best compromise between high S/N and low variability between measurements. Under these experimental conditions, the one-step electrochemical magneto-immunosensor provided slightly better figures of merit than the spectrophotometric detection, with LOD of 13 pg mL^{-1}, LOQ of 70 pg mL^{-1}, and %CV< 6% (compared to LOD of 25 pg mL^{-1}, LOQ of 100 pg mL^{-1}, and %CV ranging 8–15% in the spectrophotometric one-step magneto-immunoassay). Figure 6.9b shows that, although the two assays produced comparable S/N, electrochemical detection granted a wider linear range. Furthermore, electrochemical detection was performed in 5 min, compared to >20 min for TMB colorimetric monitoring, which allowed carrying out the whole assay in about 12–15 min, depending on the skills and training of the user.

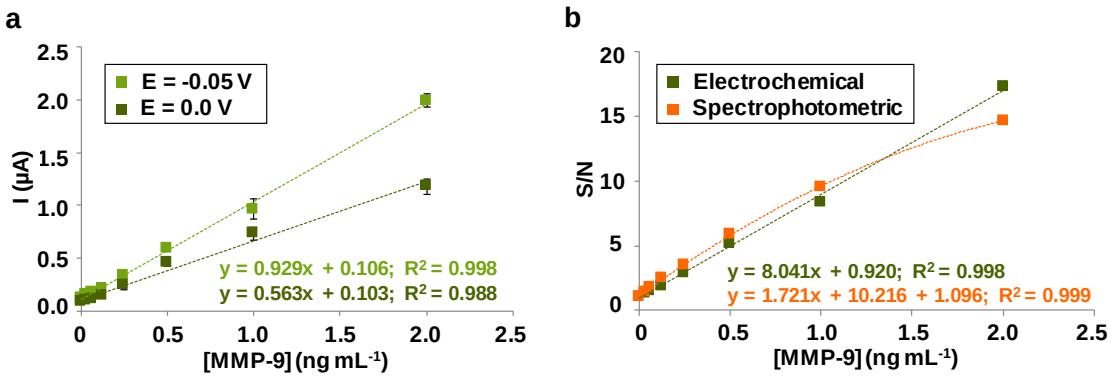

Figure 6.9. (a) Signals registered at SPCE at either 0 or −0.05 V *vs*. Ag for increasing MMP-9 concentrations (diluted in PBS-BSA_1) (b) Compared to spectrophotometric detection, electrochemistry produced S/N ratios of the same order of magnitude, but a wider assay linear range.

6.1.4. Performance of the electrochemical one-step magneto-immunosensor in clinical plasma samples.

Finally, the one-step electrochemical magneto-immunosensor developed was tested in a more realistic diagnostic scenario by studying a battery of clinical samples. According to previous data, plasma samples were diluted 1:250 for the analysis, and MMP-9 was detected in parallel using the one-step electrochemical magneto-immunosensor and the Duoset ELISA. Figure 6.10 plots the concentrations of MMP-9 measured in 10 plasma samples using alternatively the two methods. Both methods detected MMP-9 in all the samples, revealing concentrations ranging 18–388 ng mL^{-1}. These numbers were consistent with those reported previously in the bibliography (60-100 ng mL^{-1} for healthy individuals and concentrations of up to 700 ng mL^{-1} in patients having suffered a stroke)[416]. As it can be observed, the concentrations of MMP-9 estimated by the sensor correlated linearly with those provided by the ELISA, with a positive lineal Pearson correlation coefficient of 0.91 and recoveries ranging 95–120% in most of the cases. Despite the small number of samples analysed, the fact that the plot slope was close to 1.2 suggested that the sensor overestimated MMP-9 concentration by 20% compared to the ELISA, which was consistent with the data obtained before by the two methods in spiked plasma.

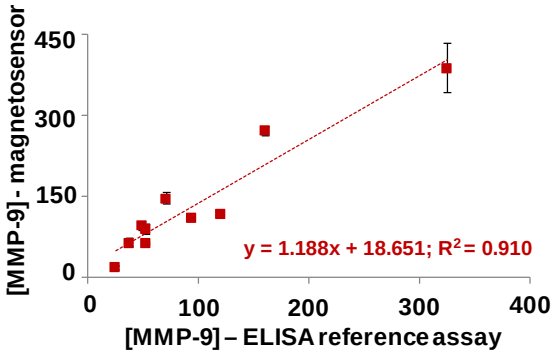

Figure 6.10. Plot of the concentrations of MMP-9 estimated by the electrochemical one-step magneto-immunosensor and the reference ELISA in ten clinical plasma samples.

In conclusion, while ELISA required 5 h to produce results, the electrochemical magneto-immunosensor took < 20 min (< 15 min for the assay plus the time needed for MB washing) and entailed significantly less manipulation by the user. It is true that more samples should be analysed in future. However, these results suggest that the procedure developed in this work is applicable to the study of clinical plasma samples. Furthermore, the simple and fast methodology described would be easier to automate than most currently available multi-step assay paths and easier to operate in POC settings with minimal technical requirements.

6.2. Development of a one-step electrochemical magneto-immunosensor for PfLDH detection in whole blood samples

This section is focused in the development of an electrochemical magneto-immunosensor for the fast, simple and quantitative detection of PfLDH in whole blood samples. The starting point was the 2-step colorimetric magneto-immunoassay developed in Section 5.2.4.

For the development of the one-step electrochemical magneto-immunoassay an immuno-modified Poly-HRP signal amplifier was produced and electrochemical detection was implemented using the multiplexed magnetic holder described before, which allowed to achieve PfLDH quantitative detection in less than 15 min.

6.2.1. Production of a Poly-HRP immunoconjugate and optimization of a one-step magneto-immunoassay for PfLDH detection

A one-step magneto-immunoassay was optimized for PfLDH detection (method in the Section 3.7.3; Figure 6.11).

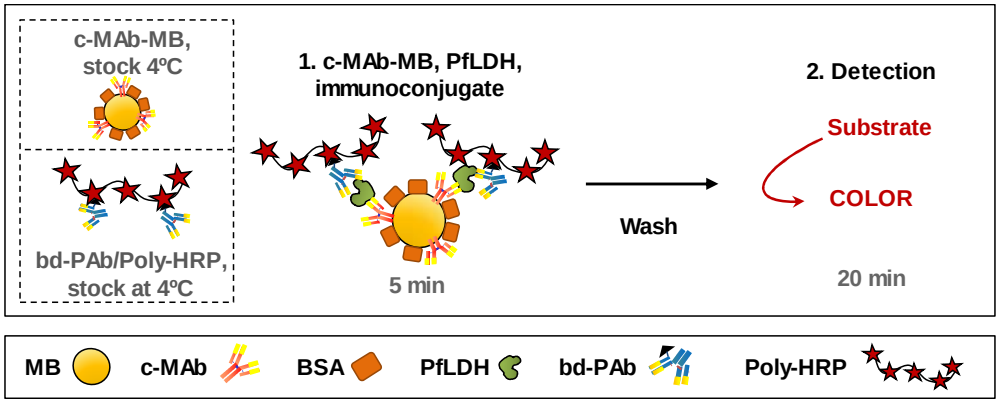

Figure 6.11. Scheme of the one-step magneto-immunoassay for PfLDH detection.

As before, an immuno-modified Poly-HRP signal amplifier was produced by testing increasing concentrations of PLDH-bd-MAb incubated with Poly-HRP and different incubation times and conditions (Figure 6.11). The first step was the optimization of the amount of PLDH-bd-MAb needed for immunoconjugate production. For that, a fixed amount of Poly-HRP (10 µg mL^{-1}) was incubated under rotation with PLDH-bd-MAb concentrations ranging 15–60 µg mL^{-1}. These conjugates were then used, diluted 1:200, to detect increasing concentrations of PfLDH or the negative controls without PfLDH in a one-step magneto-immunoassay (Figure 6.12). This led to final working concentrations of 75–300 ng mL^{-1} for the PfLDH-bd-MAb and 50 ng mL^{-1} for Poly-HRP (Figure 6.12a). The conjugate with the lowest concentration of PfLDH-bd-MAb, equivalent to the concentration used in the 2-step magneto-immunoassay, displayed signals considerably lower for most PfLDH concentrations. As seen in Figure 6.12b, for conjugates produced with PLDH-bd-MAb concentrations higher than 150 ng mL^{-1}, the signals registered were not statistically different (oneway ANOVA test, $p > 0.05$). This suggested that a partial loading of the conjugate with PLDH-bd-MAb was enough for optimal performance. However, the lowest LOD and LOQ were obtained for the highest concentrations of PLDH-bd-MAb, 225 ng mL^{-1} and 300 ng mL^{-1}. Since any unconjugated PLDH-bd-MAb remaining in solution could compete with the conjugated bd-MAb and make the assay more expensive, the concentration of PLDH-bd-MAb selected was 225 ng mL^{-1}. This corresponded to an immunoconjugate produced by

incubating 45 μg mL^{-1} of PfLDH-bd-MAb with 10 μg mL^{-1} of Poly-HRP, which was then diluted 1:200 for its utilization in the one-step magneto-immunoassay.

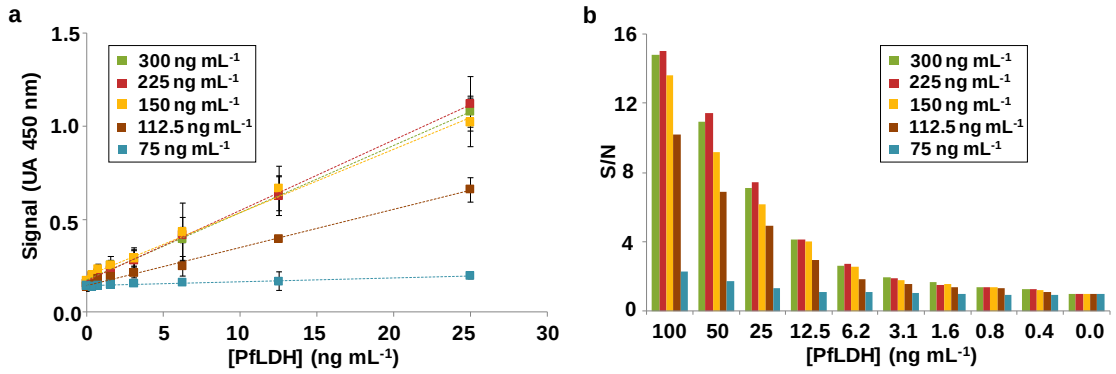

c

	bd-MAb (ng mL^{-1})				
	300	225	150	112.5	75
LOD (ng mL^{-1})	0.14	0.37	0.79	0.54	9.53
LOQ (ng mL^{-1})	2.00	2.44	3.60	3.27	29.02
Linear Equation	0.040 + 0.195	0.042 + 0.186	0.038 + 0.218	0.026 + 0.160	0.002 + 0.160
R^2	0.998	0.998	0.993	0.995	0.970

Figure 6.12. (a) Linear range of the in the one-step magneto-immunoassay when a PfLDH dilution series was detected using bd-MAb/Poly-HRP conjugates produced with a fixed concentration of Poly-HRP and different bd-MAb loadings. (b) S/N ratios and the corresponding LOD and LOQ of the assays shown in (a). The concentrations shown in the figure correspond to concentration of reagent in the final assay (post-dilution). (c) Summary of the LOD, LOQ and linear range for each experimental condition in (a-b).

In order to determine more accurately the most suitable PLDH-bd-MAb/Poly-HRP ratio and establish the conjugate optimal working dilution, three more immunoconjugates were produced by incubating PLDH-bd-MAb at three different concentrations (30, 45 and 60 μg mL^{-1}) with Poly-HRP (10 μg mL^{-1}). This time the conjugates were then submitted to different dilutions (1:150, 1:200 and 1:250) and were tested in the assay. The concentrations of PLDH-bd-MAb and Poly-HRP achieved in each case before and after the corresponding dilution are summarized in Table 6.1. The best performance of the immunoconjugate during the one-step magneto-immunoassay was achieved for PLDH-bd-MAb post-dilution concentrations between 300-150 ng mL^{-1}. For that reason, it was decided that in the assay the immunoconjugates had to be diluted so that the PLDH-bd-MAb working concentrations were within this range (Table 6.1, green boxes).

		Immunoconjugate 1		Immunoconjugate 2		Immunoconjugate 3	
		bd-MAb	Poly-HRP	bd-MAb	Poly-HRP	bd-MAb	Poly-HRP
(μg mL^{-1})	As produced	30	10	45	10	60	10
(ng mL^{-1})	Diluted 1:150	200	67	150	67	400	67
	Diluted 1:200	150	50	225	50	300	50
	Diluted 1:250	120	40	180	40	240	40

Table 6.1. Battery of immunoconjugates produced for PfLDH detection and concentrations of the two components resulting in the working dilutions used for the one-step magneto-immunoassay.

The signals registered for each immunoconjugate and dilutions tested are summarized in the Figure 6.13. As it is shown, the immunoconjugate 1 diluted 1:150 (equivalent to 200 ng mL^{-1} of PLDH-bd-MAb and 66.7 ng mL^{-1} of Poly-HRP in the assay, generated signals ~30-60% higher than the rest of dilutions for all the range of PfLDH concentrations studied, including the negative controls (Figure 6.13a). This was presumably due to the Poly-HRP effect in non-specific signal amplification, inasmuch this immunoconjugate-dilution had the most elevated Poly-HRP concentration tested. The rest of results obtained for the different bd-MAb/Poly-HRP ratios studied were not statistically different from each other (oneway ANOVA test, $p > 0.05$).

The best performance, in terms of highest S/N ratios obtained for the whole range of PfLDH concentrations studied and lowest LOD and LOQ, was achieved for the immunoconjugate 3 diluted 1:200 (300 ng mL^{-1} of PLDH-bd-MAb and 50 ng mL^{-1} of Poly-HRP), the immunoconjugate 2 diluted 1:200 (225 ng mL^{-1} of PLDH-bd-MAb and 50 ng mL^{-1} of Poly-HRP) (Figure 6.13b), and the immunoconjugate 3 diluted 1:250 (240 ng mL^{-1} of PLDH-bd-MAb and 40 ng mL^{-} of Poly-HRP, respectively). In this case, it was determined that the optimum working concentrations were of 225 ng mL^{-1} for PLDH-bd-MAb and 50 ng mL^{-1} for Poly-HRP, which provided the most economical immunoconjugate and results not statistically different from the others (Figure 6.13b, insert).

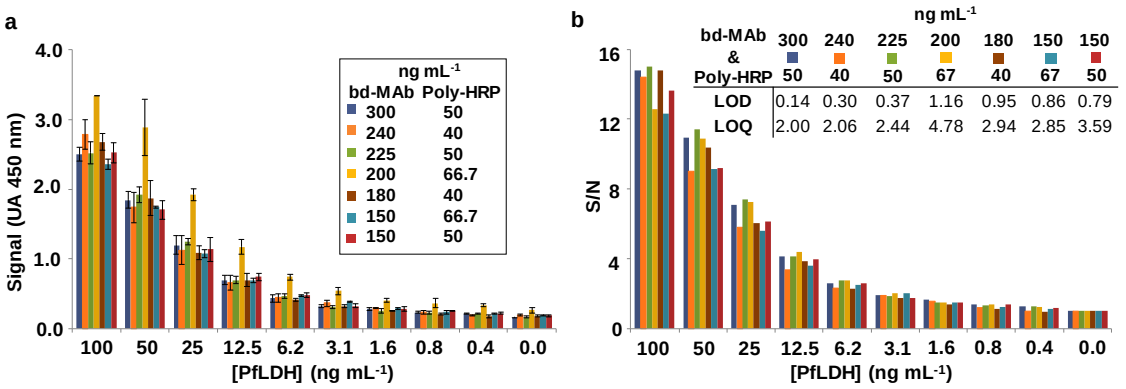

Figure 6.13. (a) Signals registered for PfLDH detection in the one-step magneto-immunoassay using different immunoconjugates and immunoconjugate dilutions. (b) S/N ratios and the corresponding LOD and LOQ of the assays shown in (a).

The incubation time of Poly-HRP with PLDH-bd-MAb was next optimized by comparing times of incubation extending from 30 min to overnight (Figure 6.14). In all cases, the final concentrations of Poly-HRP and bd-MAb were of 50 ng mL^{-1} and 225 ng mL^{-1}, respectively. As it can be observed, the signals registered and the assay sensitivities (slope) were proportionally to the incubation time up to 60 min, to decrease from there on (Figure 6.14a-b). Although the differences between the results obtained for 60-min and 90-min preparation times were not statistically significant (one-way ANOVA test, $p > 0.05$), the LOD and LOQ were better for the 60-min immunoconjugate production time, which produced lower background noise and variability (Figure 6.14a, insert).

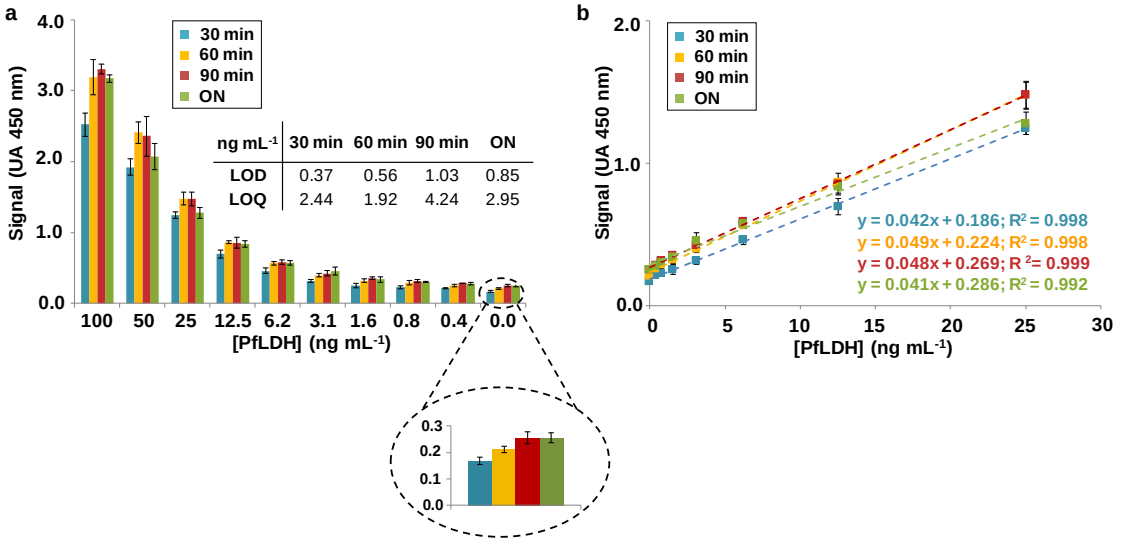

Figure 6.14. (a) Signals registered for PfLDH detection in the one-step magneto-immunoassay using different incubation times for immunoconjugate production. (Insert, top) Corresponding LOD and LOQ of the assays. (Insert, bottom) Amplification of the background noise registered in the blanks. (b) Linear range for each assay of (a)

The last parameter that was optimized was the composition of the buffer used in the 5-min incubation of the one-step magneto-immunoassay. In the case of MMP-9 detection described in the previous section, it was noticed that the addition of 0.05% of Tween to the immunocapture buffer (PBS-BSA_1) contributed to reduce the level of non-target non-specific binding onto the surface of the MB (Figure 6.14a, zoom insert). Here, a similar principle was applied for the decrease in the background noise, in order to improve the sensitivity of PfLDH detection (Figure 6.15). As it is shown, the signals registered for PfLDH concentrations within the assay linear range, 0.4 ng mL^{-1} to 25 ng mL^{-1}, were the same for both incubation buffers (Figure 6.15, insert). However, the background noise decreases considerably when adding Tween, improving the S/N ratio, LOD and LOQ (0.48 ng mL^{-1} and 1.72 ng mL^{-1} in the presence on Tween 0.05%, compared to 0.56 ng mL^{-1} and 1.92 ng mL^{-1} for the incubation in the absence of detergent).

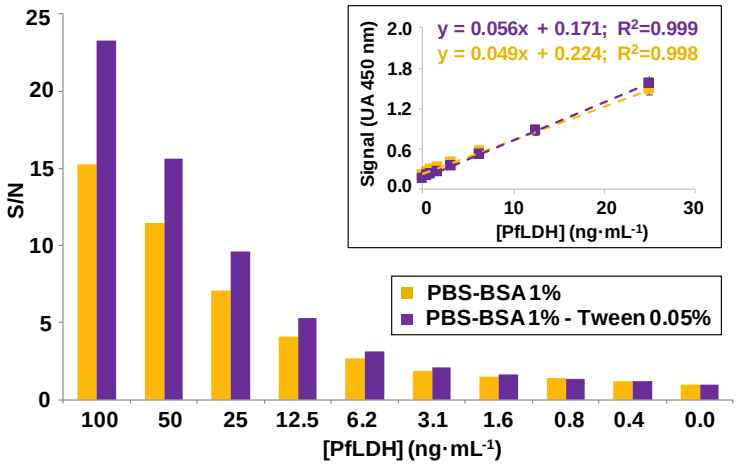

Figure 6.15. S/N ratios registered for the one-step magneto-immunoassay with/without Tween 0.05% in the incubation buffer. The insert displays the linear range for each assay (raw data instead of S/N).

6.2.2. Performance of the one-step magneto-immunoassay for PfLDH detection in whole blood

Finally, the one-step magneto-immunoassay developed for PfLDH detection was applied to the study of real sample matrices. As it has been described in Chapter 2, PLDH is a glycolytic enzyme produced by asexual and sexual stages (gametocytes) of *Plasmodium* parasites, which replicate inside RBC. Consequently, PLDH concentration is higher in whole blood samples than in plasma samples that are depleted of RBC. This is more evident for low PLDH concentrations, such as in submicroscopic parasitemias,

in which the concentration of extracellular PLDH is undetectable by most methods. Here, whole blood samples were lysed to release the intracellular enzyme and improve PLDH detection. The protocol used for this had been optimized by another team member and entailed diluting the sample 1:1 with a lysis buffer that contained triton and imidazole and incubating the mixture for 5 min. Whole blood lysed in this way could be analysed straightforward, without the need to centrifuge or filter, and could be alternatively aliquoted and stored at -80ºC without losing PfLDH over storing time.

The one-step magneto-immunossay was developed with the final objective to analyse fresh capillary blood, obtained *in situ* from the patients. However, whole blood coagulates over time, even after lysis, and cannot be stored. For this reason, assay testing was carried out in venous blood, which could be obtained in larger volumes using blood collection tubes preloaded with an anticoagulant, providing a more stable matrix. Therefore, the effect of the blood treated with different anticoagulants on the magneto-immunoassay was first examined[448]. The Figure 6.16 shows the signals registered in the one-step magneto-immunossay performed in a whole blood sample, spiked or not with PfLDH, which had been obtained from a healthy individual using alternatively three different anticoagulants, ethylenediaminetetraacetic acid (EDTA), acid-citrate-dextrose (ACD), and sodium heparin, or without any anticoagulant at all. As it can be observed, the signals registered in the presence of PfLDH were of the same order in all cases. However, EDTA increased importantly the background noise in the negative controls (without spiked PfLDH), interfering in the assay. Since EDTA had no effect in the 2-step assay, it was concluded that the presence of a chelating agent affected negatively Poly-HRP, but the potential mechanism was not studied additionally. In view of the results, heparin was considered the best option, because it produced the results that better resembled those produced by fresh blood (i.e., low background noise and high S/N ratio).

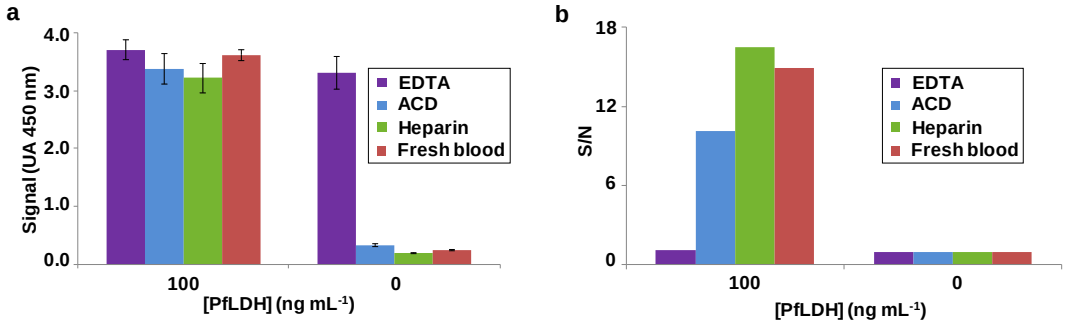

Figure 6.16. Interference of the anticoagulant used during whole blood collection in the one-step magneto-immunoassay for PfLDH detection. (a) The signals registered using the different anticoagulants analysed in samples spiked or not with 100 ng mL^{-1} of PfLDH. (b) The S/N ratio for the same conditions as in (a).

Heparin whole blood was next diluted to different extents (1:10, 1:25 and 1:50), was spiked with increasing concentrations of PfLDH, as was analysed using the one-step magneto-immunoassay to determine the effect of increasingly complex sample matrices in assay performance (Figure 6.17). Plasma diluted 1:10 was studied as well. As it can be observed, the signals registered displayed a slight increase proportional to the complexity and type of matrix, which could be caused by lower washing efficiency after MB incubation in more complex samples. Nonetheless, if signal was normalized by subtracting the corresponding background noise from the blanks (without spiked PfLDH), the signal trends were comparable in all cases. On the other hand, the PfLDH recoveries obtained for the different sample dilutions ranged 85-113 % for the plasma 1:10 and 80-106%, 79-123% and 80-120% for dilutions in blood 1:10, 1:25 and 1:50 respectively.

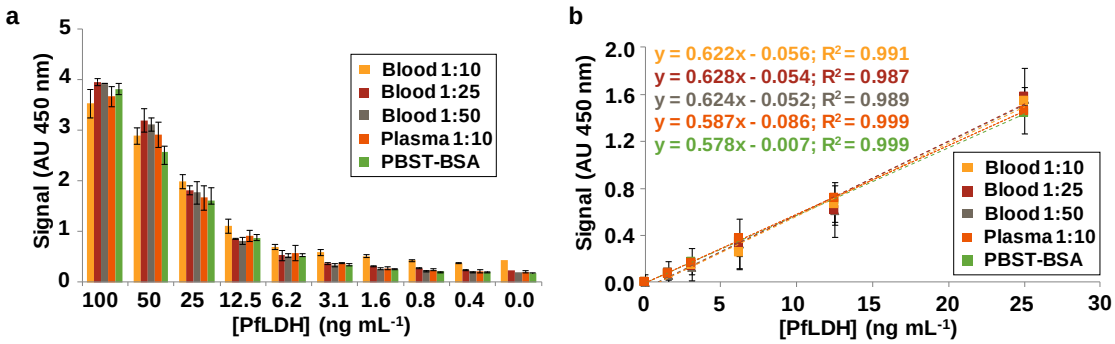

Figure 6.17. (a) Signals registered for increasing concentrations of PfLDH in the different matrix samples tested. (b) Normalized signals after subtracting the corresponding blanks.

In a 1:25 blood dilution, the assay achieved a PfLDH recovery of 98% in average for the whole range of concentrations studied, with a good differentiation between positive and negative (without PfLDH) blood samples (>300 mAU and <200 mAU, respectively). If the LOD and LOQ obtained for these assay conditions were multiplied

per the sample dilution factor (x25), they corresponded to pre-dilution PfLDH concentrations of 30 and 90 ng mL^{-1}, respectively, which were below the LODs of most commercial lateral flow devices (100-200 ng mL^{-1})[384]. It was thus concluded that this was the optimum blood dilution to detect PfLDH in whole blood using the one-step magneto-immunoassay, with a balance between the complexity of the sample and the recovery of protein.

The next target was to shorten the detection step, for which electrochemical detection was implemented.

6.2.2.1 PfLDH detection in cultivated *Plasmodium*-infected RBC

Following, the one-step magneto-immunoassay was employed for the study of cultured RBC infected *in vitro* with controlled parasitemias of *P. falciparum* spanning between 0.0015% and 0.38% (equivalent to 85-24800 parasites μL^{-1}). For standard assays, parasitemia will be adjusted to 3% with 45% hematocrit and the culture was diluted serially with uninfected RBC. Parasitemia was confirmed by flow cytometry counting and PCR.

Previously the samples of the culture plasmodium antigen were lysed for 5 min and according with the study of matrix effect with healthy blood samples, were diluted 1:25 in PBST-BSA 1%. As can be observed in Figure 6.18a the concentrations estimated with the one-step magneto-immunoassay correlated linearly with the detected by the ELISA as reference method (positive lineal Pearson correlation coefficient of 0.98).

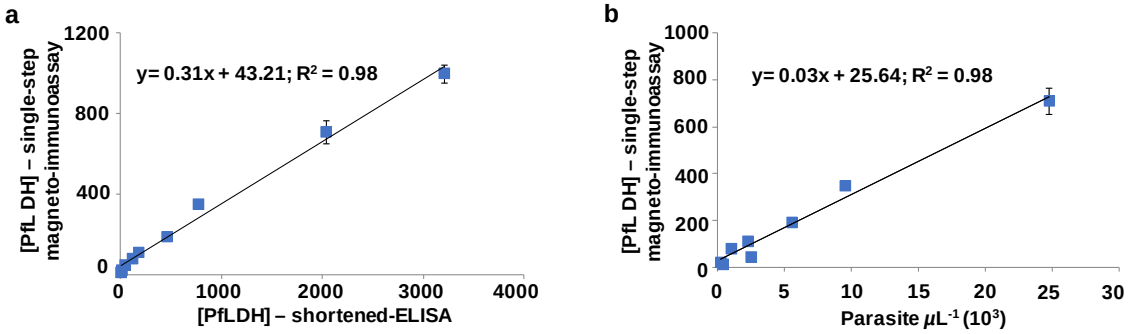

Figure 6.18. (a) Plot of the concentrations of PfLDH estimated by the one-step magneto-immunoassay correlated with the reference ELISA. (b) Correlation between PfLDH concentrations detected with the one-step magneto-immunoassay versus the parasitemia density of the *Plasmodium* cultures.

The one-step magneto-immunoassay detected PfLDH in the whole dilution series and the absorbance measured increased proportionally to the concentration of parasite in the samples, displaying an LOD around 80 parasites·µL^{-1} (Figure 6.19b).

6.2.3. Electrochemical detection of the one-step PfLDH magneto-immunoassay

For the electrochemical detection of the PfLDH one-step magneto-immunoassay, a strategy similar to the one described in previous Section 6.1.3 was followed, including the use of the 8x multiplexed holder with switchable magnets (Figure 6.20). Briefly, the one-step magneto-immunoassay and the washes were carried out in Eppendorf tubes, MB were resuspended in 50 µL of PBS, were transferred to the wells of the holder, and were confined magnetically onto the surface of a SPCE WE. Next, current was allowed to stabilize at 0.00 V *vs*. Ag pseudo-reference, the measurement was then paused, PBS was substituted by ready-to-use TMB substrate solution, and the measurement was resumed for 150 s more.

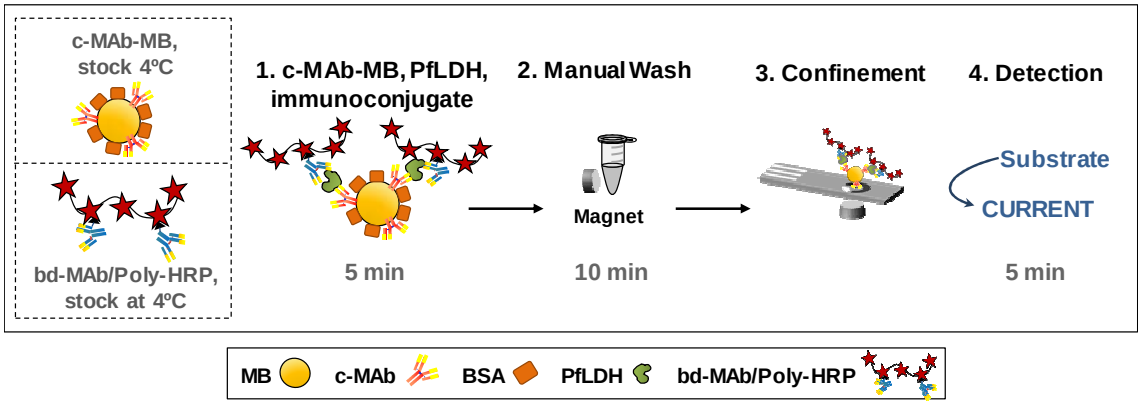

Figure 6.20. Electrochemical one-step magneto-immunosensor for PfLDH detection.

The Figure 6.21a shows that the reduction current registered was proportional to PfLDH concentration. As it had been seen in the previous experiments with MMP-9 (Section 6.1.3), the sensor produced higher currents when measuring at negative potentials, but the background noise increased also and the S/N worsened (Figure 6.21b). The best results were obtained at 0.0 V *vs*. Ag, which provided the best compromise between high S/N and low LOD and LOQ (0.85 ng mL^{-1} and 3.32 ng mL^{-1} respectively).

During the spectrophotometric PfLDH detection, it had been tested and confirmed that Tween$_{0.05}$ addition to the incubation buffer (PBS-BSA$_1$) improved assay performance.

Hence, an incubation buffer supplemented with Tween (PBS-BSA_1-$Tween_{0.05}$) was applied also for the electrochemical sensor. The Figure 6.21c shows the signals registered by the sensor with both incubation buffers. The signals registered when using Tween were higher, contributing to increase by ~10-30% in average the S/N ratio. Furthermore the electrochemical magneto-immunosensor performed with $Tween_{0.05}$ did not show any signal saturation in the concentration range studied and displayed linear response between 3 ng mL^{-1} and 100 ng mL^{-1} of PfLDH (Figure 6.21c, insert). PfLDH detection at low concentrations improved also, and the assay displayed LOD of 0.58 ng mL^{-1} and LOQ of 2.48 ng mL^{-1}, instead of 0.85 ng mL^{-1} and 3.32 ng mL^{-1} with the incubation buffer without $Tween_{0.05}$.

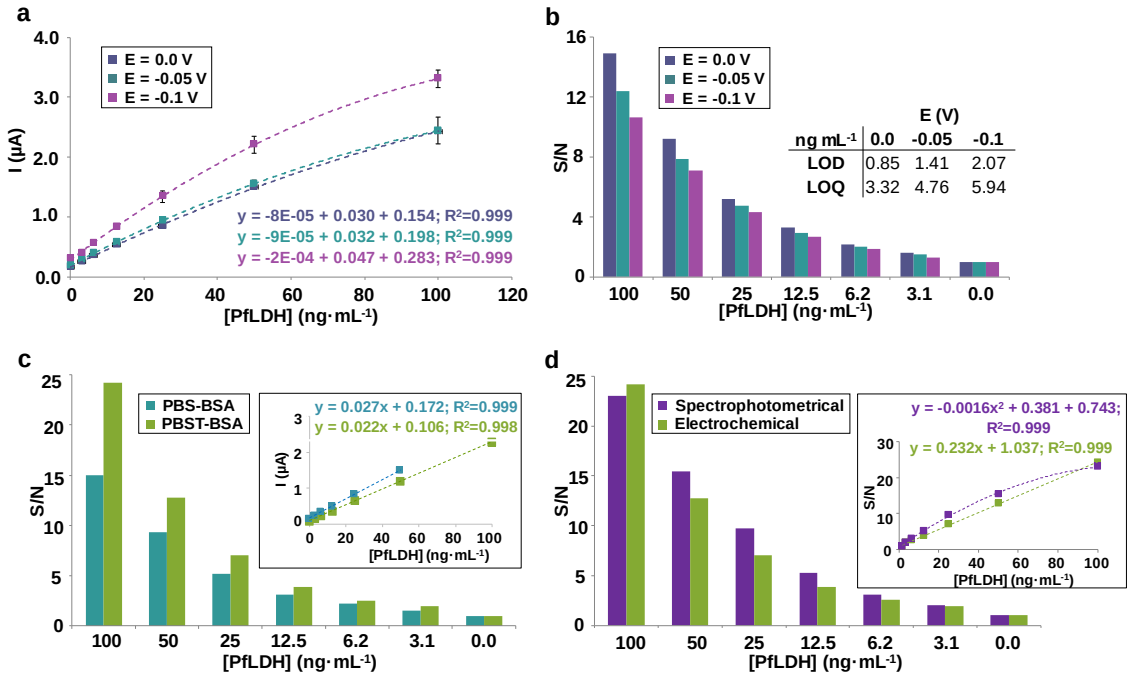

Figure 6.21. (a) Signals registered at SPCE at either 0 V, −0.05 V or -0.1 V *vs*. Ag for increasing PfLDH concentrations (diluted in PBS-BSA_1). (b) S/N ratios, LOD and LOQ for the assays in (a). (c) Comparison of the S/N ratios obtained for the one-step magneto-immunosensor carried out with/without Tween in the incubation buffer. (Insert) Linear range for each assay in (c). (d) Comparison of the S/N ratios displayed by the spectrophotometric and electrochemical detection of the one-step magneto-immunoassay.

Under these experimental conditions, the one-step electrochemical magneto-immunosensor provided similar figures of merit than the spectrophotometric detection, with LOD of 0.58 ng mL^{-1}, LOQ of 2.48 ng mL^{-1}, and %CV< 5.3% (compared to LOD of 0.48 ng mL^{-1}, LOQ of 1.72 ng mL^{-1}, and %CV ranging 6–10% in the spectrophotometric one-step magneto-immunoassay). Figure 6.21d shows that, although the spectrophotometric detection produced around ~20% higher S/N ratios, the electrochemical detection granted a wider linear range. Furthermore, electrochemical

detection was performed in 5 min, compared to >20 min for TMB colorimetric monitoring, which allowed carrying out the whole assay in about 12–15 min.

6.2.4. Performance of the electrochemical one-step magneto-immunosensor in whole blood

Finally, it was studied if the one-step electrochemical magneto-immunosensor was applicable to the study of PfLDH in real sample matrices. In order to do so, lysed whole blood and plasma samples from healthy individuals were diluted to different extents and were spiked with increasing concentrations of PfLDH.

Figure 6.22 plots the signals registered for the different dilutions of real samples with inoculated PfLDH. Compared to PBS-BSA$_1$, the currents registered by the magneto-immunosensor in spiked plasma, diluted 1:10, and spiked blood, diluted 1:50 and 1:25, were higher for all the concentrations of PfLDH tested, including the negative controls without spiked PfLDH. These results were consistent with those obtained previously for the colorimetric detection of the assay. Since the Ab pair used did not show crossbinding to human LDH or other blood components (which was assessed by ELISA), the increase in signal registered in whole blood could be caused by a lower efficiency of MB washing after the incubation in a sample matrix more complex and viscous than PBS-BSA. However, if the currents registered in the corresponding blanks were subtracted from the currents detected in spiked blood, the signal trends registered were comparable in all cases and independently of blood dilution (Figure 6.22, insert).

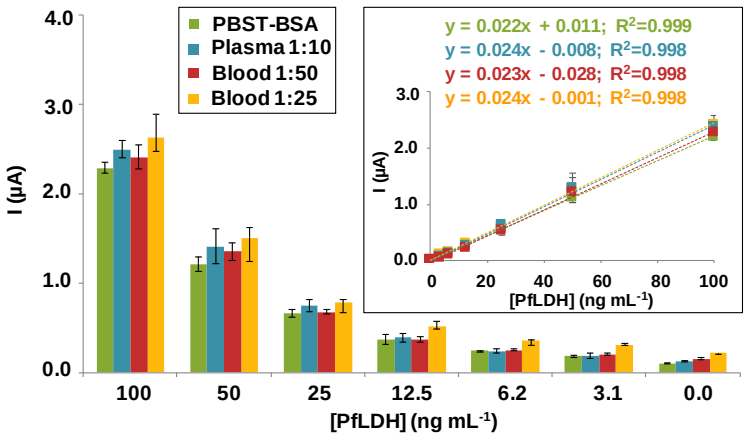

Figure 6.22. Signals register by the electrochemical one-step magneto-immunosensor for PfLDH inoculated in different real sample dilutions. The insert shows the lineal range for the same assay's conditions.

PfLDH recovery for the dilution 1:25 and 1:50 of blood, and the dilution 1:10 of plasma ranged between 94-115%, 60-107% and 70-114%, respectively. As before, the 1:25 dilution was selected as the optimum for the study of whole blood samples using the one-step magneto-immunosensor, because it allowed achieving a higher % of recovery of PfLDH. The LOD and LOQ achieved in this diluted sample multiplied per the dilution factor (x25) were equivalent to pre-dilution PfLDH concentrations ranging 60-160 ng mL^{-1} which, as already observed in the colorimetric assay, were below the LODs displayed by most lateral flow tests commercialized for malaria POC diagnosis.
This suggested that, although the matrix effect due to the complexity of blood samples existed, the one-step magneto-immunosensor for PfLDH detection could be performed in real samples.

6.2.4.1 PfLDH detection in cultivated Plasmodium blood samples

Finally, the one-step electrochemical magneto-immunosensor was applied in cultured RBC infected *in vitro* with controlled parasitemias of *P. falciparum* spanning between 0.0058% and 3% (equivalent to 340-174418 parasites μL^{-1}). For standard assays, parasitemia will be adjusted to 3% with 45% hematocrit and the culture was diluted serially with uninfected RBC. Parasitemia was confirmed by flow cytometry counting and PCR.

Before the study the samples of the culture plasmodium antigen were lysed for 5 min and diluted 1:25 in PBST-BSA 1%, as an optimum dilution. The concentrations estimated with the one-step magneto-immunosensor in the Figure 6.23a, correlated linearly with the detected by the shortened-ELISA as reference method (positive lineal Pearson correlation coefficient of 0.99).

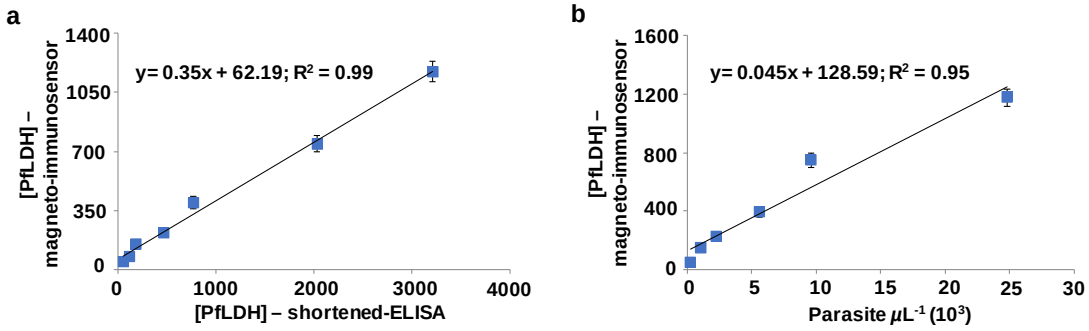

Figure 6.23. (a) Plot of the concentrations of PfLDH estimated by the one-step electrochemical magneto-immunosensor correlated with the reference ELISA. (b) Correlation between PfLDH concentrations detected with the one-step magneto-immunoassay versus the parasitemia density of the *Plasmodium* culture.

The current registered with the one-step magneto-immunosensor for the detection of PfLDH in the whole dilution series increased proportionally to the concentration of parasite in the samples, displaying an LOD around 200 parasites·μL^{-1} (Figure 6.23b).

6.2.4.2 PLDH detection in clinical blood samples

The one-step electrochemical magneto-immunosensor for PLDH detection was tested in a more realistic diagnostic scenario by studying five clinical blood samples.

According to previous data, blood samples were lysed for 5 min and diluted 1:25 in PBST-BSA 1% for the analysis. The one-step magneto-immunosensor was tested in detected PfLDH concentrations between 86 ng mL^{-1} and 1113 ng mL^{-1}, corresponding with parasitaemias ranging 0.03 - 0.6 %.

Figure 6.24 shows the concentrations of PfLDH measured in 5 blood samples obtained from malaria patients, correlated with the valued obtained in parallel using the reference shortened-ELISA method (positive lineal Pearson correlation coefficient of 0.99). As it can be observed, the concentrations of PfLDH estimated by the one-step magneto-immunosensor provided PfLDH recoveries ranging 87–115%.

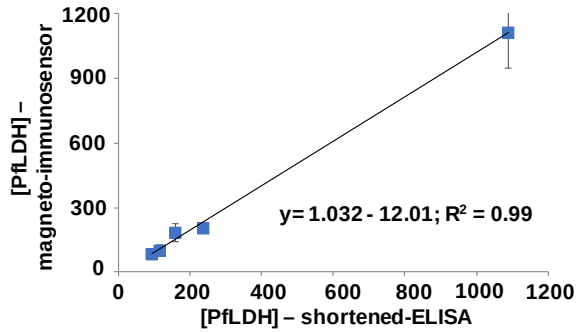

Figure 6.24. Correlation between the concentrations of PfLDH (ng mL^{-1}) estimated by the one-step electrochemical magneto-immunosensor in 5 clinical blood samples and the concentrations of PfLDH according to the reference shortened-ELISA method (n=3).

In conclusion, the one-step PfLDH magneto-immunosensor developed could be used for detection in real samples, with a good recovery of PfLDH and faster result generation than the spectrophotometric detection.

6.3. Conclusions

In this work, two electrochemical magneto-immunosensors have been developed for MMP-9 and PfLDH detection. These magneto-immunosensors were fast, simple and efficient enough for biomarker detection by minimally trained personnel.

In order to achieve this goal, the 2-step magneto-immunoassay format developed in Chapter 5 has been simplified additionally. To do so, a protocol to produce a bd-Ab/Poly-HRP immunoconjugate has been optimized, allowing the development of one-step magneto-immunoassays that included a single 5-min immunocapture of the sample with a reagent cocktail. Next, the detection time of the one-step magneto-immunoassays has been reduced by implementing electrochemical detection, which was accomplished in <5 min instead of >20 min needed for the colorimetric strategy. For that, a customized multiplexed magnetic holder was used, which allowed detecting with 8 SPCE at the same time (Figure 6.25b). The applicability of the whole procedure has been finally tested by detecting MMP-9 and PfLDH in real plasma and blood samples, respectively.

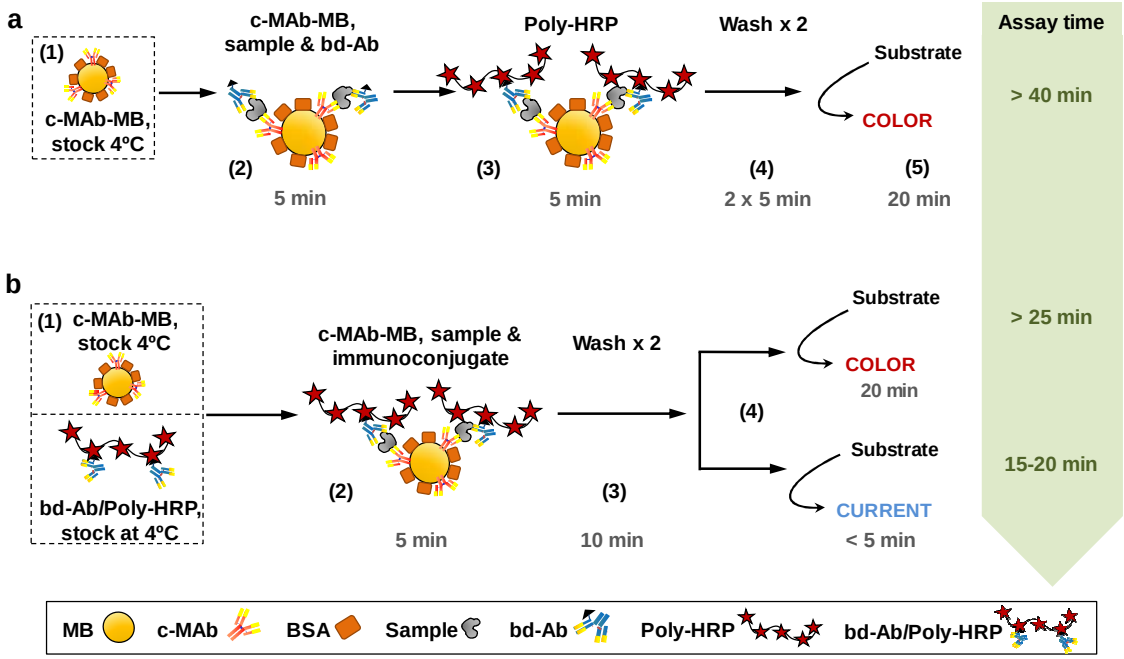

Figure 6.25. (a) Schematic representation of the initial 2-step magneto-immunoassay format developed in Chapter 5. (b) The one-step magneto-immunoassay developed in this work (Chapter 6) using a bd-Ab/Poly-HRP immunoconjugate: (1) c-MAb-MB and bd-Ab/Poly-HRP were produced and stored at 4°C. (2) The magneto-immunoassay consisted of a single 5-min incubation with c-MAb-MB, the sample and bd-Ab/Poly-HRP. (3) MB were washed twice with PBST. (4) For spectrophotometric detection of the assay, substrate solution was added, the enzyme reaction proceeded for 20 min and was stopped with acid before measuring absorbance at 450 nm. Alternatively, electrochemical detection was performed in real time using a customized magnetic holder.

The electrochemical magneto-immunosensor developed for MMP-9 detection provided analyte quantification in less than 20 min, with LOD of 13 pg mL^{-1} and LOQ of 70 pg mL^{-1} (Figure 6.26a). Although the sensitivity was 4 times lower than that of the 2-step magneto-immunoassay, the linear response extended for the whole range of MMP-9 concentrations studied (0.03-2 ng mL^{-1}) and MMP-9 detection was 3 times faster.

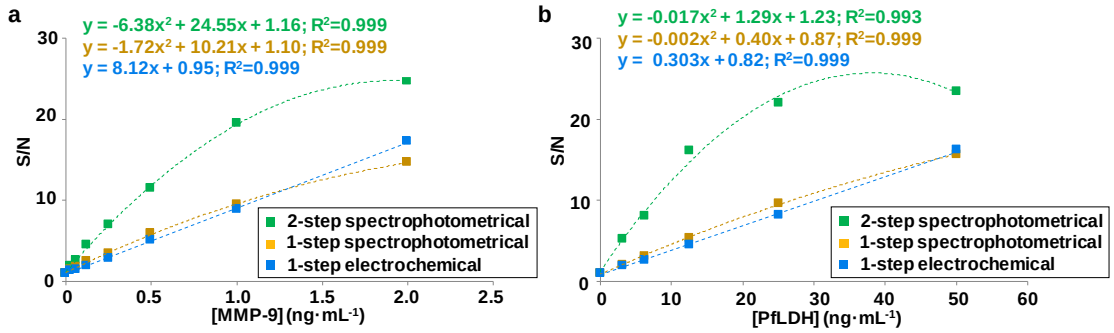

MMP-9	Spectrophotometry		Electrochemical
(ng mL^{-1})	2-step	1-step	1-step
LOD	0.003	0.025	0.013
LOQ	0.02	0.1	0.07

PfLDH	Spectrophotometry		Electrochemical
(ng mL^{-1})	2-step	1-step	1-step
LOD	0.12	0.48	0.58
LOQ	0.58	1.72	2.48

Figure 6.26. (a) Comparison of the initial 2-step and the one-step magneto-immunoassay for MMP-9 detection (by spectrophotometric and electrochemical detection). (Bottom table) LOD and LOQ of the assays in (a). (b) Comparison of the initial 2-step and the one-step magneto-immunoassay for PfLDH detection (by spectrophotometric and electrochemical detection). (Bottom table) LOD and LOQ for the assays in (b).

On the other hand, the electrochemical magneto-immunosensor for PfLDH exhibited characteristics analogous to those displayed by the MMP-9 magneto-immunosensor (Figure 6.26b). The LOD (0.58 ng mL^{-1}) and LOQ (2.48 ng mL^{-1}) were also 4 times worse than the ones obtained for the 2-step PfLDH magneto-immunoassay. However, it achieved the main objective established, the reduction of the detection time to less than 20 min, a wide linear response and handling simplicity, which made it easier to integrate in a low-cost POC device.

Compared to previously reported examples, the protocols developed here entailed very little handling by the user, were not dependent on long and complex production paths, and did not require sophisticated equipment to be performed. The commercial availability of all the reagents needed and the simplicity of the procedures and devices employed made these protocols very easy to reproduce by other teams. Furthermore, the simple and fast methodology described should be easier to automate than most currently available multi-step magneto-immunoassay paths and easier to operate in POC settings with minimal technical requirements. Nevertheless, they still entailed manual processes, such as the washing and detection steps, which should be simplified additionally for

POC testing. The next chapters will summarize how paper microfluidics were exploited to achieve this goal by two different strategies.

Chapter 7

Simplification of electrochemical magneto-immunosensor performance by using SPCE with integrated paper microfluidics

7. Simplification of electrochemical magneto-immunosensor performance by using SPCE with integrated paper microfluidics

As mentioned before, one of the main drawbacks of magneto-sensors is that MB handling is tedious, time consuming, and requires user training. Magneto-immunosensors often entail a magneto-immunoassay performed in tubes, which requires that MB are alternatively agitated with sample and reagent solutions and concentrated in a magnetic rack for supernatant removal and washing. After the last wash, MB are confined magnetically onto an electrode for electrochemical detection. In Chapter 6 it has been shown that using conjugates of Poly-HRP modified with d-Ab allows optimizing extremely fast and simple assays, reducing substantially magneto-immunosensor assay time and level of manual handling[16]. One of the one-step magneto-immunosensors described in Chapter 6 quantitated MMP-9 in about 15 min, with linear response between 0.03 and 2 ng mL^{-1}, and LOD/LOQ of 13 and 70 pg mL^{-1}, respectively[449,450]. Nevertheless, the assay still entailed MB manual washing in tubes, which required user training and would be hard to achieve at a POC setting.

Paper is a flexible, inexpensive, biodegradable and easy to manipulate material. Paper-based microfluidics are popular because of their low cost, ease of fabrication and disposability, which allows producing portable, sensitive and robust detection platforms well-suited for POC diagnostics[38,451]. A few examples have reported the incorporation of paper features to SPE to enhance sensor performance, providing pre-loaded reagents and/or sample pre-treatment. For instance, the incorporation of a paper disk impregnated with reagents onto a SPE provided a microfluidic device for heavy metal quantitation in an example reported by S. N. Tan and co-workers[305]. An origami paper device was used in a similar way to reduce the interference by non-target sample components in a glucose electrochemical enzymatic sensor[306]. In another example, a combination of membranes was exploited as a reagent reservoir and to promote sample and reagents flow above a SPCE electrochemical immunosensor for detection of dengue virus antigen[452].

In this chapter, paper microfluidics have been employed to facilitate the manipulation of SPCE-based electrochemical magneto-immunosensors, and specifically to carry out MB

washing and detection on-chip with minimal handling. To do so, paper devices with different geometric characteristics have been designed and tested, selecting those providing the required flow rate and absorption capacity. In parallel, on-chip MB handling, washing and electrochemical detection have been optimized to provide low background noise and enhanced detection. The paper device produced in this way, has been then employed to detect MMP-9 using the one-step magneto-immunoassay described before, which consisted of a 5-min simultaneous incubation of the sample with immuno-modified MB and a Poly-HRP immuno-conjugate[415] (see Section 5.2.3). After this one-step incubation, the mixture was transferred to a SPCE and all the washing and detection steps were carried out on-chip. For this purpose, a movable paper microfluidic device was placed on the SPCE. The lateral displacement of the paper module turned it on to provide MB washing under flow conditions and waste storage or turned it off to grant electrochemical detection under static conditions. Under these experimental conditions, the sensor detected MMP-9 in patient plasma samples in about 10 min with little intervention of the user, providing quantitative results that correlated linearly to those generated by the reference ELISA that took >5 h. These results demonstrate that paper microfluidics can help simplify electrochemical magneto-immunosensor manipulation, driving this type of assay closer to the POC diagnostic requirements.

7.1. Incorporation of paper microfluidics to commercial SPCE

7.1.1. Design of a switchable paper microfluidic device

The paper fluidic module envisioned here was designed to include a terminal spearhead that could be approached to the SPCE electrochemical cell for solution absorption (for instance, to promote washing under flow conditions), or be removed from the electrodes to work under static conditions when needed (such as for MB magnetic confinement and for electrochemical detection) (Figure 7.1). At the same time, the paper module had to serve as a waste sink and reservoir. Accordingly, the fluidic module had to provide solution absorption at a flow rate that promoted efficient MB washing without attracting the MB and be able to soak and retain the total volume of sample and reagents needed to carry out the whole assay.

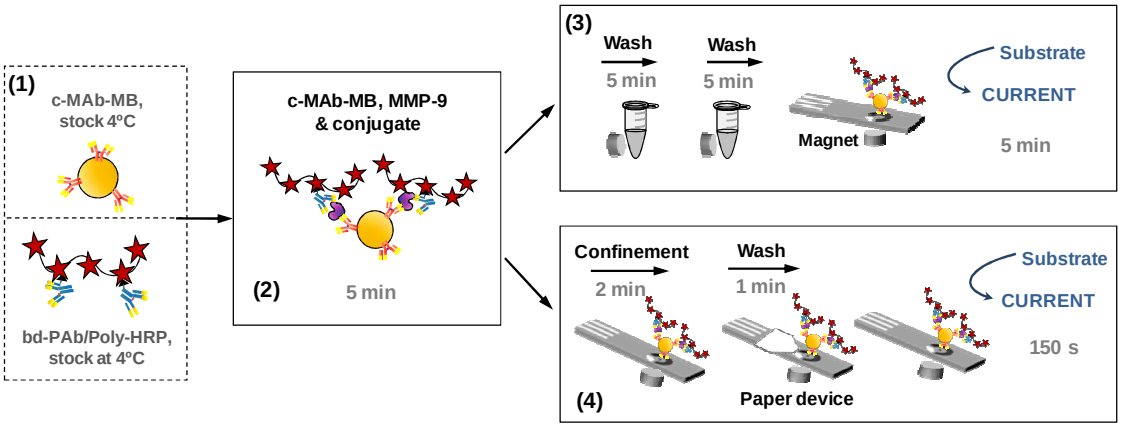

Figure 7.1. Schematic representation of the electrochemical magneto-immunosensor. (1) c-MAb-MB and bd-PAb/Poly-HRP were produced and stored at 4°C. (2) The magneto-immunoassay consisted of a single 5-min incubation with c-MAb-MB, MMP-9 and bd-PAb/Poly-HRP. (3) For classical electrochemical detection, MB were washed twice with 150 µL of PBST in Eppendorf tubes and were confined on the surface of a SPCE using a magnet for detection. (4) Alternatively, MB were confined on the SPCE immediately after the incubation (2) and were washed on-chip using a paper fluidic device.

In order to facilitate multiplexed magneto-immunosensor washing and electrochemical detection using integrated paper microfluidics, an 8x multiplexed paper device was produced that was incorporated to the magnetic device reported previously and described in Chapters 3 and 6 (Section 3.8.1)[438]. As the reader might remember, this was a holder that accommodated eight independent SPCE and a sliding bar with eight magnets, one per electrode (Figure 3.20). This sliding component could be moved to two different positions, which allowed switching on/off the magnetic field that was applied to the electrodes for confining or releasing the MB. Here, a sliding fluidic paper module was incorporated to the previous design (Figure 7.2). This provided switchable and independent absorption of the different solutions deposited over each electrode along magneto-immunosensor performance Section 3.8.2. The objective of this module was that the washing and detection steps of the magneto-immunosensor could be carried out in a simple and economical way, with minimal intervention by the user.

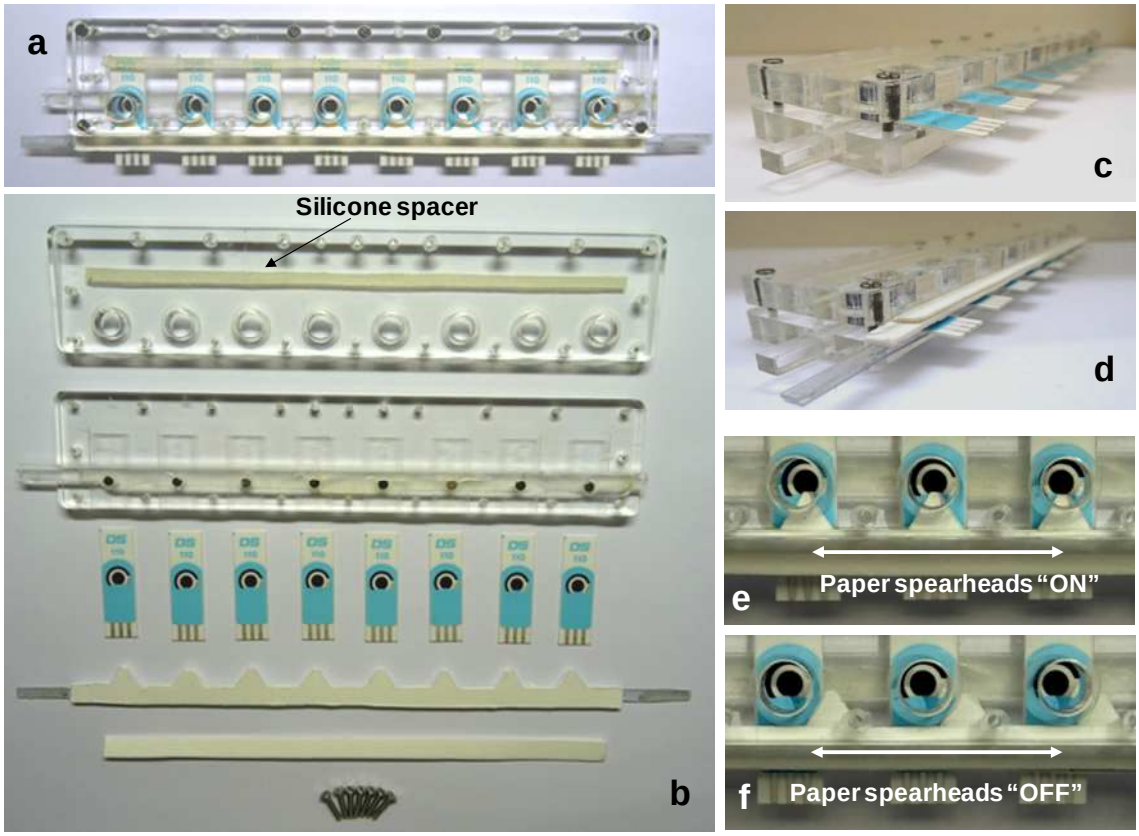

Figure 7.2. (a) Customized magnetic device with integrated paper microfluidics. (b) Image of the 4 components of the upgraded magnetic holder, including base, cover, sliding magnetic bar, a silicone spacer to provide light holder screwing, 8 commercial SPCE, the two components of the paper microfluidic device, and screws. (c) The holder assembled with the SPCE inserted in the corresponding pockets. (d) The inclusion of a silicon spacer impels a 4 mm distance between base and cover and allows the holder to be lightly screwed. This 4 mm space served to introduce the microfluidic paper components. (e-f) Performance of the sliding microfluidic paper device.

7.1.2. Electrochemical SPCE pre-treatment for solution confinement

One of the difficulties for the efficient employment of the fluidic paper module was to control the sequential confinement of the sample/reagents mixture, washing buffer and enzyme substrate onto the SPCE, and their flow rate over magneto-immunosensor processing (Figure 7.2). Also, once the sample/reagents mixture had been pipetted and MB had been magnetically confined on the WE, subsequent solution additions (i.e., washing solution and enzyme substrate) and paper-driven washes should proceed without triggering MB displacement. Finally, while the washing steps were to be carried out under constant paper-driven flow, MB magnetic confinement and electrochemical detection should be more efficient under static conditions. For these reasons, a movable paper module was envisaged that could reach two different positions. While in the "on" position the paper pad would approach the electrodes to promote solution absorption/removal, in the "off" position the paper module would move away allowing solution deposition and incubation onto the electrodes.

The commercial SPCE used here included a hydrophobic insulator (the blue layer in Figure 7.3) that defined the active area of the electrodes, protected the electrical paths and facilitated the confinement of a drop of solution onto the electrodes. However, the properties of this hydrophobic layer changed along the procedure, especially after washing with PBST and removing the fluidic paper module. As a result, the drop of enzymatic substrate spread during electrochemical detection, contributing to increase result variability and eventually moisten the electrical connectors. In order to improve solution confinement, a water-repellent marker was used to print a hydrophobic barrier between the electrodes and the connectors (Figure 7.3). The SPCE modified in this way displayed improved drop confinement along the whole magneto-immunoassay procedure and the presence of the hydrophobic barrier did not alter the electrochemical detection.

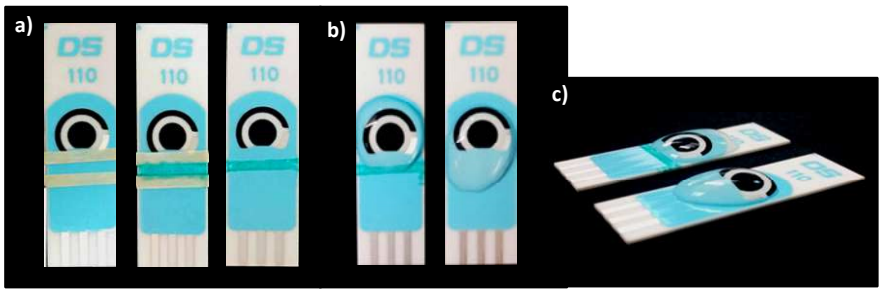

Figure 7.3. (a) Two pieces of tape (white in the left image) served as the template to draw a well-defined hydrophobic barrier (middle image). The tape was then removed (right image). (b-c) The modified devices (left images) displayed better solution confinement above the electrodes than the as-received ones (right images).

7.1.3. Selection of the type of membrane

The fluidic module was conceived to be an economical absorption pad able to draw the sample and washing solution by capillary action and collect and store them until the end of the assay. In this way, the fluid entered the porous material, which acted as both a flow pump and a waste container. Accordingly, the flow rate provided had to be slow enough to prevent turbulences that could disrupt the MB sediment, but fast enough to provide effective MB wash and a rapid assay. Here, two types of absorption material were compared (Figure 7.4a). The first one was Fusion 5, a proprietary hydrophilic material that, according to the manufacturer, could accomplish all the functions of a typical lateral flow test, which usually require a combination of different materials. The second was CF5, a membrane commonly recommended for use as the absorption pad in lateral flow applications.

a

Membrane type	Thickness (µm)	Flow rate (d 4cm^{-1})	Water absorption (mg cm^{-2})	Bed volume (µL cm^{-2})	Material
Fusion 5	370	38	40	1.48	Glass fibre & plastic binder
CF5	954	63.3	99.2	9.46	100% cotton

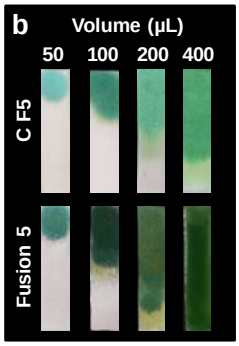

Figure 7.4. (a) Properties of Fusion 5 and CF5 filter paper. (b) CF5 and Fusion 5 strips after pipetting different volumes of a stained solution.

The water absorption capacity of each material was first tested, to select a membrane able to absorb all the volume required to perform the whole magneto-immunoassay. For this, increasing volumes of stained water were pipetted on strips 1 cm x 4 cm of either Fusion 5 or CF5. As it can be seen in Figure 7.4b, only CF5 could absorb volumes large enough, which was consistent with the theoretical maximal water absorption capacity of both materials (160 µL and 396 µL for Fusion 5 and CF5 strips, respectively). In consequence, CF5 was selected to produce the fluidic paper module with minimal material waste.

7.1.4. Optimization of the geometric design of the fluidic paper module

The fluidic module included eight paper spearheads to facilitate individualized volume flow from eight electrodes to the paper sink (Figure 7.2a). Spearhead-shaped paper devices with different profiles and dimensions were tested in order to study the capillary flow rate and absorption efficiency provided by each type of fluidic device, and the corresponding efficiency and reproducibility of the on-chip paper-driven washing steps. The system was used in the one-step magneto-immunosensor developed for MMP-9 detection (see Section 6.1.3). This assay consisted originally of a 5-min incubation of the samples with c-Ab-MB and bd-PAb/Poly-HRP conjugate, followed by a series of washes performed in tubes using a magnetic rack (Figure 3.20). Here, the washes were carried out on-chip, using the 9 types of fluidic paper modules displayed in Figure 7.5b. This study focused in the signals registered in the negative controls (i.e., c-MAb-MB incubated with bd-PAb/Poly-HRP immunoconjugate, without MMP-9), which provided information about the level of reagent non-specific adsorption and washing efficiency.

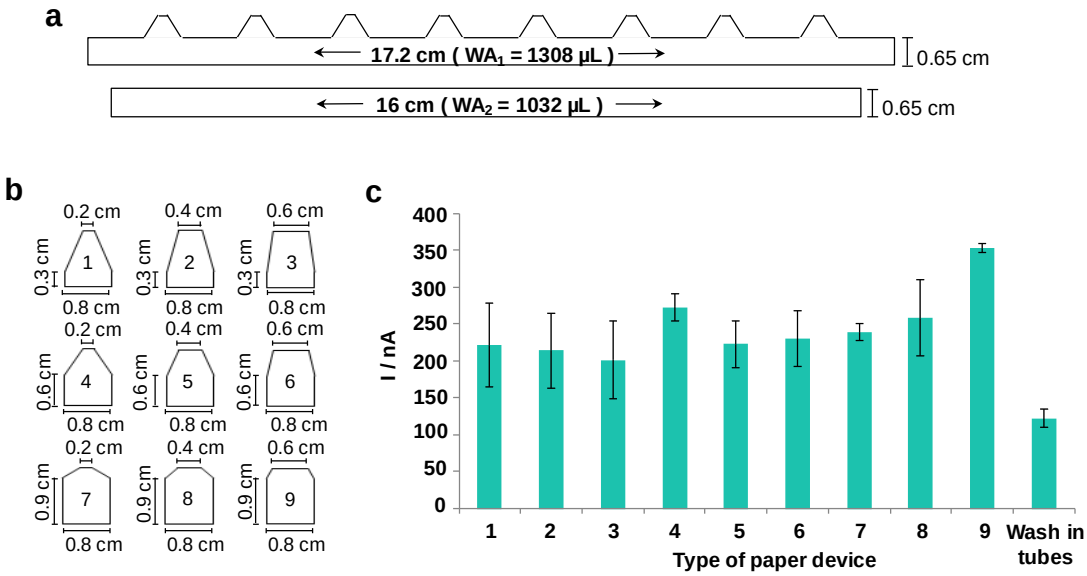

Figure 7.5. (a) Design, dimensions and water absorption capacity for the two components of the paper microfluidic device. (b) Geometry of the spearhead-shaped paper devices tested. (c) Signals registered for the blanks (with all the reagents, without MMP-9) in the one-step magneto-immunoassay after carrying out either off-chip classical washing or on-chip paper-driven washing, in the latter case using alternatively nine different designs of paper spearheads as the movable fluidic module (n=3). *WA* stands for theoretical water absorption capacity.

In general, all the spearhead geometries studied for washing on-chip produced background currents of the order on 200-350 nA (%CV ranging between 2 and 30%), which were 2-4 times higher than the background noise registered when MB were washed in a tube using a classical procedure (Figure 7.5c)[219]. This indicated that the efficiency of the paper-driven washing steps was lower than that of the classical procedure. Nevertheless, most of the unreacted biocomponents in the sample/reagents mixture were washed way using a procedure that was faster and simpler than the typical approach. The highest reproducibility was observed for the spearheads 4, 7 and 9, which displayed %CV of 2-10 %. Among them, the design number 7 provided the lowest background signal (hence, better washing efficiency). However, while the sharp end of number 4 provided complete recession of the fluidic module from the electrode vicinity when turned to the off position, designs 7 and 9 presented blunter extremes that retained contact with the electrode-confined liquid drop in both on/off positions (Figure 7.6a). For this reason, it was concluded that the spearhead design more appropriate for SPCE integrated washing was number 4 (Figure 7.6b).

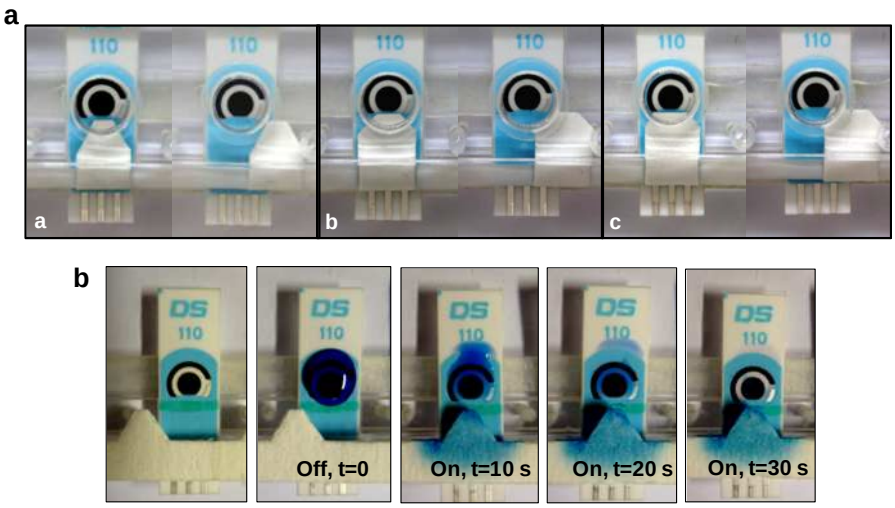

Figure 7.6. (a) Location of the paper spearhead onto the SPCE when placed in the "on" (left) and "off" (right) positions. The pictures illustrate device performance for the designs 4 (a), 7 (b) and 9 (c) of respectively. (b) Spearhead selected (number 4) on a SPCE before ("off" position) and during the absorption procedure ("on" position).

Once the most appropriate spearhead geometry had been selected, it was studied if the resulting paper device would be able to absorb the volume of solutions used along the whole assay. The one-step magneto-immunosensor used here consisted originally of a single incubation of the c-MAb-MB with 100 µL of sample and bd-PAb/Poly-HRP immunoconjugate, and two 150-µL off-chip washes performed in tubes. Accordingly, the expected waste volume raised to 400 µL of solution per electrode, or 3200 µL of volume per 8 electrodes. In contrast, the paper fluidic device designed here could theoretically absorb 1308 µL of water. In order to increase its water absorption capacity without altering flow rate, a second paper piece was incorporated onto the first one, which theoretically absorbed 1032 µL more (Figure 7.5a). This increased the device absorption capacity to 2340 µL of solution, leaving room for up to 192.5 µL of washing solution per electrode (or 1540 µL for 8 electrodes). Nevertheless, washing was limited to 100 µL per electrode to guarantee complete solution removal by the paper device.

7.2. Optimization of the electrochemical MMP-9 magneto-immunosensor with integrated paper-driven washing

7.2.1. Optimization of on-chip paper-driven washing

In order to optimize the paper-driven washing procedure, work started by studying the effect of different washing buffers in the one-step magneto-immunosensor. As before, the 5-min incubation of sample with immuno-modified MB and a Poly-HRP immuno-

conjugate was performed in tubes. The procedure followed to perform the subsequent MB magnetic confinement onto the SPCE and on-chip washing and detection is illustrated in Figure7.7.

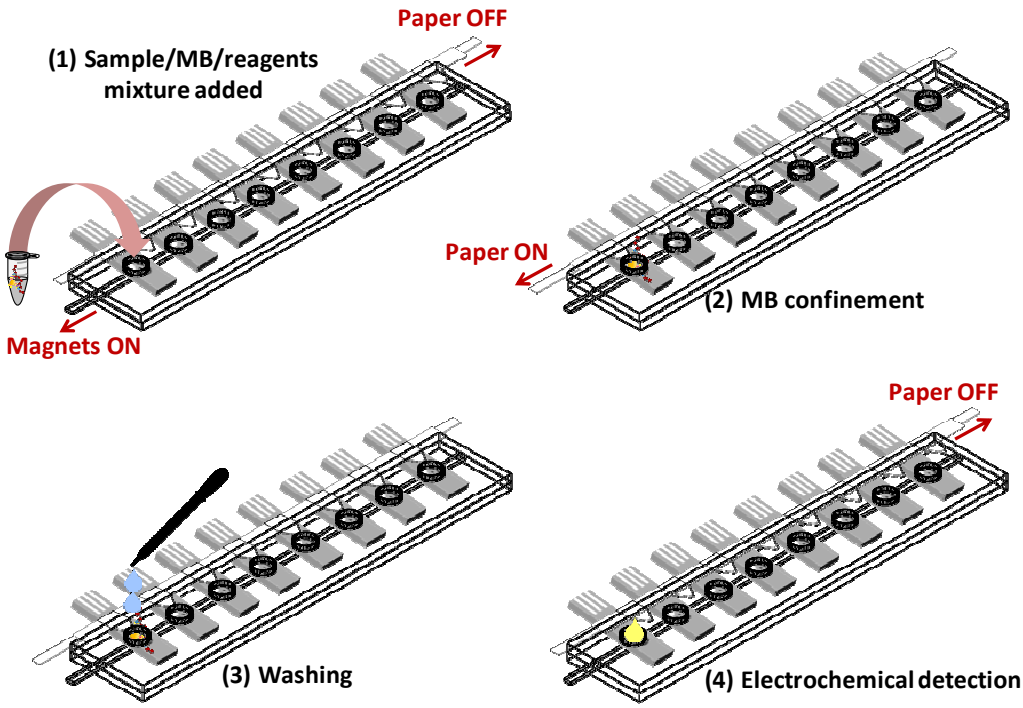

Figure 7.7. Schematic representation of the electrochemical detection of the one-step magneto-immunoassay, when carrying on-chip paper-driven MB washing and detection. (1) After the single 5-min incubation, the mixture of sample/MB/reagents is pipetted onto the SPCE with the magnets placed in "on" position and the paper device in "off" position. (2) The paper device is displaced to the "on" position to absorb the sample and reagents while MB are retained by the magnets on the WE surface. (3) Washing solution is added through the cover windows and MB washing occurs under flow conditions. (4) The paper piece is moved to the "off" position, enzymatic substrate is added and the electrochemical measurement proceeds under static conditions.

Figure 7.8 summarizes the currents registered by amperometry for the magneto-immunosensor carried out on either a positive control (2 ng mL^{-1} of MMP-9) or a negative control (no MMP-9) using different washing buffers (PBS_{1X}; PBS_{1X} with $Tween_{0.025}$; PBS_{1X} with $Tween_{0.1}$; $PBS_{0.1X}$; and $PBS_{0.1X}$ with $Tween_{0.025}$). Compared to washing with only PBS, the addition of Tween contributed to increase slightly result reproducibility (%CV of 13.75% for PBS_{1X}; 14.54% for $PBS_{0.1X}$; 9.97% for PBS_{1X}-$Tween_{0.025}$; 9.67% for PBS_{1X}-$Tween_{0.1}$ and 10.27% for $PBS_{0.1X}$-$Tween_{0.025}$). However, the currents registered for the positive controls decreased as the concentration of Tween increased, without correlating with a clear decrease of the background signals in the negative controls (Figure 7.8b). These results were consistent with previous observations suggesting that Tween promoted Poly-HRP non-specific binding[438 22], but could also indicate that the detergent adsorbed onto the WE affecting electron transfer

later on. The trend changed if the washing buffer was prepared with PBS diluted 1:10. Under these conditions, the addition of Tween had little effect in the positive controls but improved washing and promoted lower background currents (Figure 7.8c). Accordingly, the best S/N ratios were obtained by washing with either PBS_{1X} (without detergent) or $PBS_{0.1X}$ –$Tween_{0.025}$.

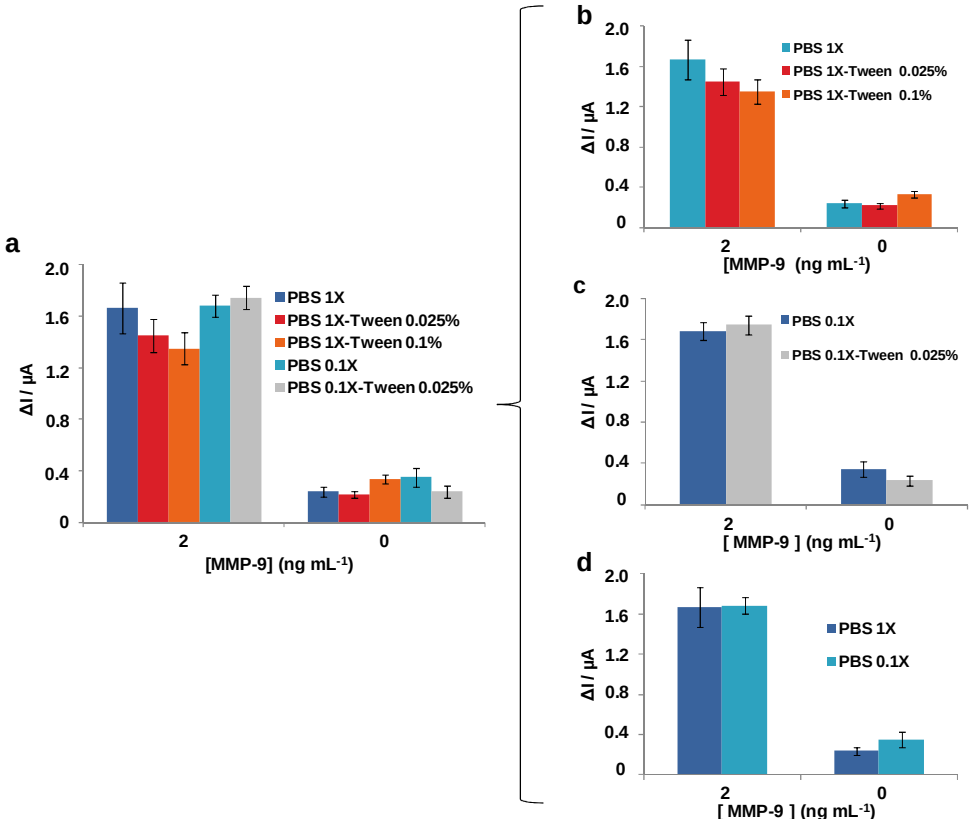

Figure 7.8. (a) Currents registered by amperometry for the singe-step magneto-immunoassay, carried out on either a positive control (2 ng mL^{-1} of MMP-9) or a negative control (no MMP-9), after on-chip paper-driven washing using alternatively different washing buffers (PBS_{1X}; PBS_{1X} with $Tween_{0.025}$; PBS_{1X} with $Tween_{0.1}$; $PBS_{0.1X}$; and $PBS_{0.1X}$ with $Tween_{0.025}$). (b) Compared to washing with only PBS, the addition of tween increased slightly result reproducibility, without decreasing the background signals of the negative controls. (c) When washing was carried with PBS diluted 1:10, the addition of tween improved washing and promoted lower background currents. (d) Substituting PBS by PBS 1:10 had nearly undetectable effect in assay performance.

Figure 7.9a shows the signals registered in the magneto-immunosensor for increasing concentrations of MMP-9 after paper-driven washing using alternatively PBS_{1X} or $PBS_{0.1X}$ –$Tween_{0.025}$. As it can be observed, both washing conditions resulted in signals of the same order of magnitude for all the concentrations of MMP-9 studied and linear ranges extending between 30 pg mL^{-1} and 2 ng mL^{-1}. However, $PBS_{0.1X}$ –$Tween_{0.025}$ produced more reproducible results, lower currents for the blanks, higher S/N (Figure 7.9a, insert), and a tenfold improvement in the LOD and LOQ (LOD/LOQ of 0.01 and 0.15 ng mL^{-1} in front of 0.41 and 1.22 ng mL^{-1}, respectively). On the other hand, washing was more efficient in terms of lower background noise if two serial additions

of 50 µL of washing solution were made, instead of a single addition of 100 µL (Figure 7.9b). As a result, S/N improved. This suggested that the turbulence impelled by solution injection, which caused a slight vibration of the magnetically-confined MB, improved the washing efficiency provided by paper-driven solution flow.

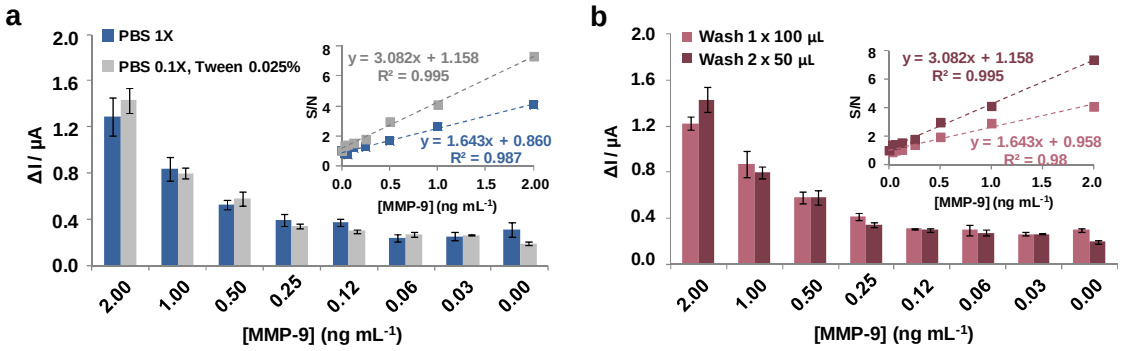

Figure 7.9. (a) Washing carried out alternatively using PBS or $PBS_{0.1X}$ –$Tween_{0.025}$. (b) Washing efficiency after one (x 100 µL) or two additions (x 50 µL each) of $PBS_{0.1X}$ –$Tween_{0.025}$.

7.2.2. Optimization of the electrochemical detection conditions

The optimization of the electrochemical detection conditions started by the study of the measurement potential (-0.1, 0.05 and 0.0 V *vs.* Ag pseudoreference) in the chronoamperometric detection of the magneto-immunosensor (Figure 7.10).

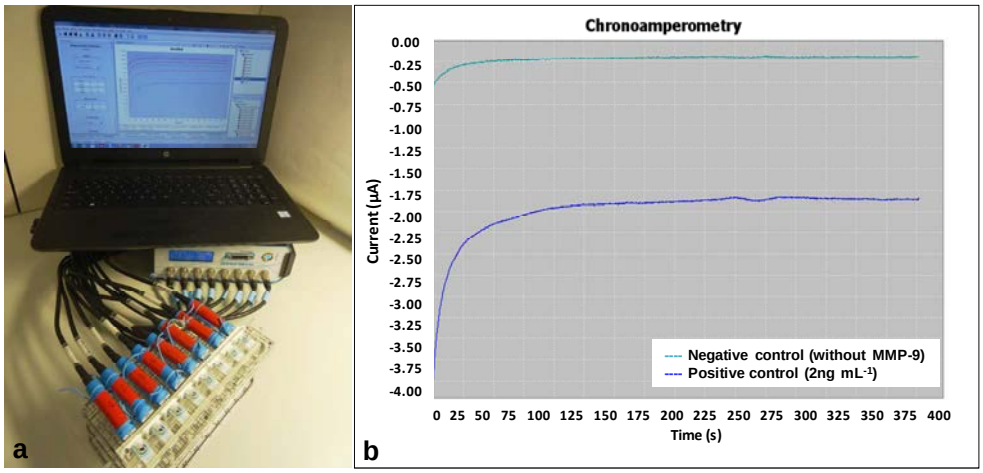

Figure 7.10. Application of the paper fluidic device developed to the electrochemical detection of MMP-9. (a) Magnetic customized device with integrated paper microfluidics plugged to the measurement equipment. (b) Example of the signals registered with the device during the electrochemical detection of negative and positive MMP-9 controls.

As it can be observed in Figure 7.11a, the currents registered increased for all the concentrations of MMP-9 tested as the measurement potential shifted to more negative values, but the negative controls raised as well. Consequently, the highest S/N ratios

were obtained by measuring at 0.0 V *vs.* Ag pseudoreference (Figure 7.11a, insert). This contradicted the results obtained when only detection was performed at SPCE, when the best results were obtained by measuring at -0.05 V *vs.* Ag and suggested that carrying the washes on-chip modified to a certain extent the electrode surface and behaviour.

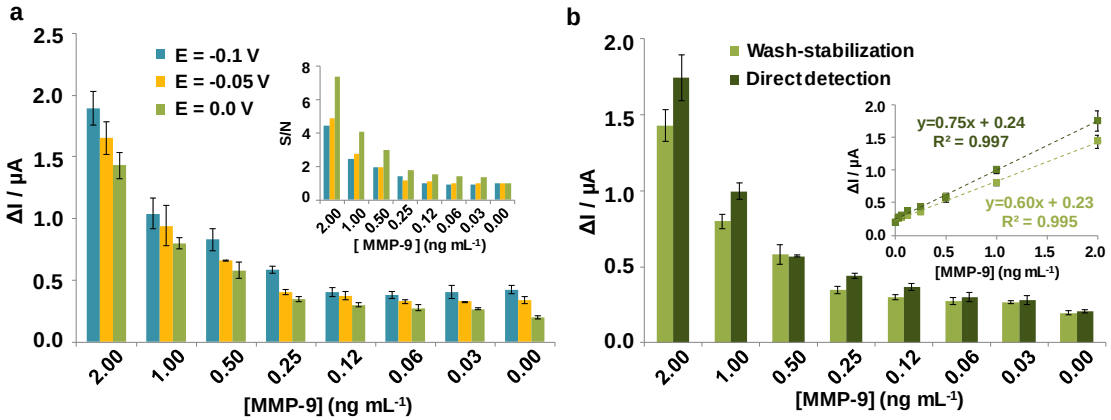

Figure 7.11a. Optimization of the electrochemical detection conditions after carrying MB washing on-chip**. (**a) Amperometric detection at different detection potentials. (b) Measurement at the optimal potential (E=0.0V) after either current stabilization during washing or direct detection upon substrate addition. In all cases, the insert shows the S/N ratios with the linear ranges and equations of the corresponding plots (n=3).

To this point, the magneto-immunoassay performed with the new paper fluidic device detected MMP-9 in about 12 min, which included 5 min of incubation of the sample with c-MAb-MB and bd-PAb/Poly-HRP, 2 min of MB magnetic confinement on the WE surface, paper-driven wash performed over 2.5 min simultaneously to the chronoamperometric detection for current stabilization, and finally 2.5 min for the electrochemical detection of the Poly-HRP enzymatic reaction. Nevertheless, the washing step took *per se* just 1 min. In order to minimize the total assay time, direct electrochemical detection, without current stabilization during the washing step, was tested also. To do this, paper washing was allowed to proceed for 1 min, the TMB enzyme substrate was added and, only then, detection was turned on to register TMB reduction over 150 seconds. As it can be seen in Figure 7.11b, this procedure resulted in a slight improvement in the signals registered for all the concentrations of MMP-9 tested and the assay sensitivity in terms of slope (0.75 μA mL ng^{-1} vs. 0.60 μA mL ng^{-1}), with LOD and LOQ of 0.01 ng mL^{-1} and 0.09 ng mL^{-1}, respectively (Table 7.1). Again, this suggested that employing the SPCE over longer measurement times affected negatively measurement efficiency.

	On-chip washing and detection				Off-chip washing "reference assay"
	Wash stabilization and detection			Direct detection	
E *vs.* Ag (V)	**-0.1**	**-0.05**	**0.00**	**0.00**	**-0.05**
LOD (ng mL^{-1})	0.19	0.20	0.01	0.01	0.013
LOQ (ng mL^{-1})	0.51	0.54	0.15	0.09	0.07

Table 7.1. Summary of the LODs and LOQs displayed by the magneto-immunosensor for the different electrochemical detection strategies tested. *Off-chip washing* refers to the classical electrochemical magneto-immunosensor, in which MB washing was performed in tubes and MB were magnetically confined onto a SPE only for detection. For *on-chip washing and detection*, after the 5-min incubation of samples with c-MAb-MB and bd-PAb/Poly-HRP, the mixture was placed on the SPE for paper-driven washing and electrochemical detection. In the latter case, the electrochemical measurement started either during the washing step, which provided signal stabilization before TMB addition (*Wash stabilization and detection*), or after TMB addition (*Direct detection*).

Interestingly, the whole protocol could be carried out in just 10 min, which would be acceptable for a POC diagnostic device. In this respect, it is worth noting that although the different device components were operated manually, which would not be trivial at a POC setting, automating the whole procedure should be easier than automating a classical multi-step magneto-immunoassay.

7.2.3. Detection of MMP-9 in plasma samples

Finally, it was studied if the magneto-immunosensor developed would be applicable to the study of clinical samples. Blood derivatives are complex matrices that contain a large number of components, such as proteins and electrolytes, which could affect detection. In the specific case of ischemic stroke, blood circulation occlusion by a thrombus produces brain injury, massive upregulation of the inflammatory response, and overexpression of numerous hormones, neurotransmitters, receptors, enzymes and structural proteins[453,454].

The specificity and performance of the magneto-immunosensor was studied by spiking pooled plasma from healthy individuals, diluted 1:250 and 1:500, with increasing concentrations of MMP-9. Compared to PBS-BSA$_1$, the currents registered by the magneto-immunosensor in spiked plasma were higher for all the concentrations of MMP-9 tested, including the negative controls without spiked MMP-9 (Figure 7.12a). However, Figure 7.12b shows that if the currents registered in the blanks were subtracted, the signal trends registered were comparable in all cases, except for a slight

decrease in sensitivity (slopes of 0.75, 0.73 and 0.67 µA mL ng^{-1} for PBS-BSA$_1$, plasma 1:500 and plasma 1:250, respectively). This suggested that, for the dilutions tested, the sample matrix had little effect in sensor performance. Accordingly, the currents registered in unspiked plasma were attributed to endogenous MMP-9.

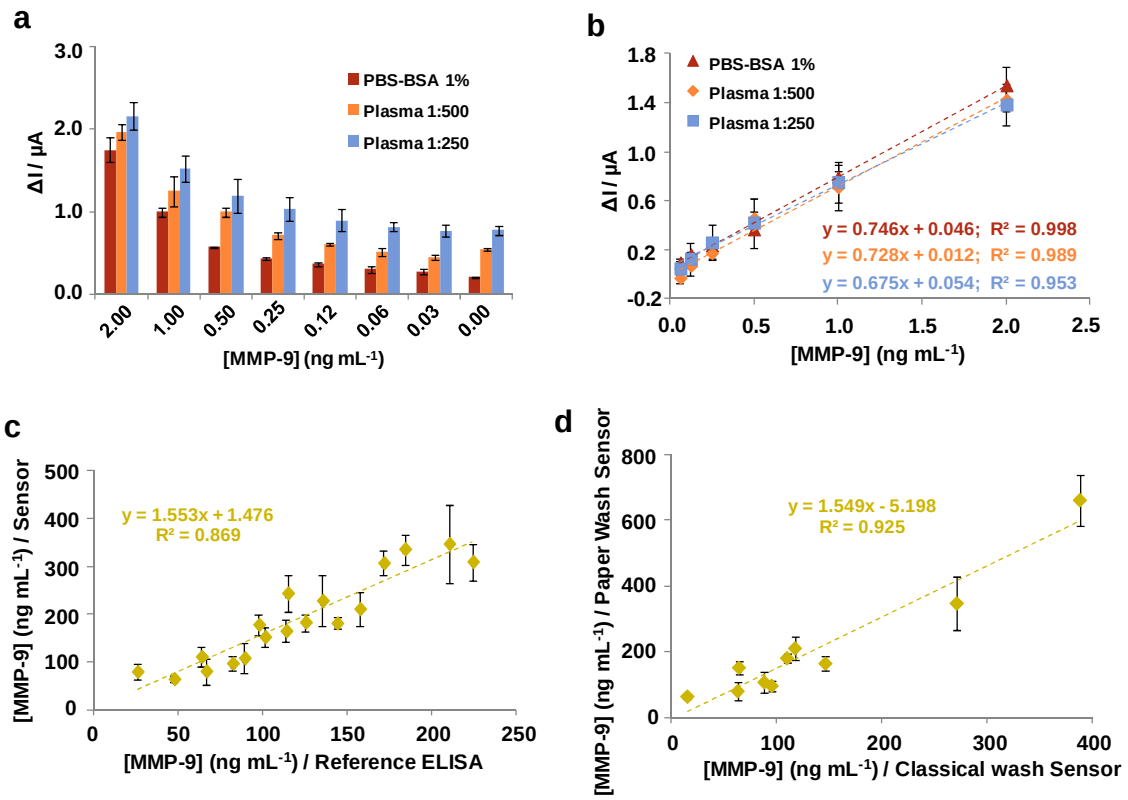

Figure 7.12. (a) Electrochemical detection of increasing concentrations of MMP-9 spiked in either PBS-BSA$_1$ or plasma (diluted 1:500 or 1:250 with PBS-BSA$_1$). (b) Linear correlation of the currents registered in (a) after subtracting the signals obtained for the negative controls (with no MMP-9). (c) Plot of the concentrations of MMP-9 in 18 plasma samples from patients estimated using the optimized electrochemical magneto-immunosensor versus those revealed by a classical reference ELISA. (d) Correlation of the concentrations of MMP-9 estimated with the magneto-immunosensor using the paper washing system versus the classical wash.

The electrochemical magneto-immunosensor with integrated paper-driven washes was finally employed to detect MMP-9 in 18 plasma samples from stroke patients, diluted 1:250 for their study. The currents registered for each sample were then interpolated in the calibration plot and multiplied per the dilution factor to estimate the concentration of MMP-9 in prediluted samples. As it can be observed in Figure 7.12c, the sensor quantified MMP-9 in the 18 samples, revealing concentrations ranging 75-350 ng mL^{-1} and displaying %CV of the order of 8-30% and below 15 % for most of the samples. Nine of the samples were assayed also using the magneto-immunosensor and classical off-chip washes performed in tubes. As shown in Figure 7.12d, the concentrations of

MMP-9 estimated by both methods correlated linearly, which indicated that the paper-driven washes were efficient even in these complex samples.

The concentrations of MMP-9 estimated using the sensor were in average 50% higher than those provided in parallel by the reference classical ELISA, with MMP-9 recoveries ranging 120-180%. This was initially attributed to three different factors: the matrix effect produced by the presence of potential interferents in the real samples, compared to the PBS-BSA_1 and spiked plasma used for the calibration experiments; the possibility that the bd-Ab/Poly-HRP immunoconjugate could be acting as an affinity binding promoter, enhancing the capture of the MMP-9 present in the samples; and/or a slightly less efficient washing. It was anticipated that any of these issues would affect more importantly the simplified magneto-assay than ELISA, which included several series of washes carried out between every two steps. However, the results obtained later during the optimization of the one-step magneto-immunoassay for PfLDH detection showed that blood samples treated with EDTA interfered in the one-step magneto-immunoassay. This suggested that MMP-9 concentration overestimation in the one-step magneto-immunosensor carried in spiked and clinical plasma samples could be also caused by EDTA, because all samples had been obtained in EDTA tubes. The fact that EDTA interfered less in MMP-9 that in PfLDH detection would be then related to the higher sample dilution needed in this case (1:250-500 for MMP-9, while 1:25-50 for PfLDH). This issue could not be studied additionally, because MMP-9 detection was validated employing a collection of retrospective samples but will have to be taken into account for the acquisition of additional samples in future. Nevertheless, the results obtained by both methods, the electrochemical magneto-immunosensor and the reference ELISA, when detecting MMP-9 correlated linearly, which was noticeable taking into account that while the ELISA took >5 h, the sensor produced results in about 10 min with minimal intervention by the user.

These results show that the method developed could be applied to the study of complex clinical samples and demonstrate for the first time that paper microfluidics can be exploited as a low-cost strategy for SPCE magneto-immunosensor handling simplification.

7.3. Conclusions

Although MB have been used extensively for the development of relatively fast and simple magneto-immunoassays and sensors, MB concentration and washing using magnets is a tedious and demanding procedure that would be difficult to accomplish in a POC setting and/or by poorly trained personnel. In this work, MB classical washes that are usually carried out manually have been substituted by a paper-driven procedure performed on-chip that entailed less intervention of the user. To achieve this goal, the paper microfluidic device was carefully optimized, designing and testing different geometric features to select those providing the required flow rate and absorption capacity. Paper assembly and SPCE pre-treatment were also adjusted to grant minimum solution spreading and improve reproducibility. Finally, MB handling, washing and electrochemical detection conditions were tuned to reduce background noise and enhance detection. Upon optimization, the electrochemical magneto-immunosensor detected MMP-9 in about 10 min, with lineal response between 30 pg mL^{-1} and 2 ng mL^{-1}, assay sensitivity of 0.75 µA mL ng^{-1}, and LOD/LOQ of 0.01 and 0.09 ng mL^{-1}, respectively. The subsequent quantitation of MMP-9 in 18 plasma samples from patients provided values that correlated linearly with those obtained by the reference ELISA. Furthermore, user intervention was limited to the initial preparation of reagents for analyte magnetic separation, and the serial addition of washing and substrate solutions on-chip. In view of the results presented, the procedure developed would be easier to carry out by non-specially trained users than the classical set-up and should be easier to automate for the future development of POC electrochemical magneto-immunosensors.

Chapter 8

Microfluidic paper SPCE (MP-SPCE) for on-chip washing and electrochemical detection of one-step magneto-immunoassays

8. Microfluidic paper SPCE (MP-SPCE) for on-chip washing and electrochemical detection of one-step magneto-immunoassays

As has been explained in the previous Chapters 5 and 6, magneto-immunoassays involve numerous incubations and washing steps, as well as the alternating application of a magnetic field. This drawback was solved in the context of this PhD thesis by employing a paper microfluidic device to facilitate the manipulation of SPCE-based electrochemical magneto-immunosensors, carrying out MB washing and electrochemical detection on-chip. The development of POC analytical devices has recently benefited from the increasing interest raised by printing SPE in paper as a substrate[24,455,456]. Paper offers benefits, such as acting as a microfluidic pump to flow volumes through capillary forces, which is highly useful to perform the assay washing steps by dragging the non-bound biocomponents to a reservoir pad. Some groups presented their own paper-based devices with electrodes printed on lateral flow membranes[457–460], or combining screen-printing of the electrodes and conducting parts, and wax printing[302] to define fluidic structures and electrode passivation areas, which results in a batch manufacturing process. However, works describing fully (screen) printed devices are scarce[461].

This chapter presents an accessible and affordable way to print electrodes directly on lateral flow membranes using screen-printing alone, which allows producing highly customized devices without the need for advanced resources and at an affordable cost. The devices produced here were a lateral flow strip incorporating a three-electrode electrochemical cell. Such microfluidic paper SPCEs (MP-SPCEs) have been used to integrate the washing and detection steps of magneto-immunoassays, contributing to simplify MB manipulation greatly.

8.1. Microfluidic paper single-sided SPCE (MP-ssSPCE) for the detection of the MPO magneto-immunoassay

The first MP-SPCE were produced by screen-printing a three-electrode cell on one of the sides of a strip made of Fusion 5 membrane (see the methodological details in section 3.3.2). While the electrodes and connection pads were located at the two opposite extremes of the strip, the middle section acted as a flow pump and waste reservoir (Figure 8.1). As a proof of concept, the devices produced in this way were employed to carry on-chip the washing and detection steps of the MPO one-step magneto-immunoassay developed in Chapter 4. As it will be shown, the detection of MPO was accomplished at clinically relevant concentrations in diluted human serum, in less than 15 minutes, and with minimal handling by the user.

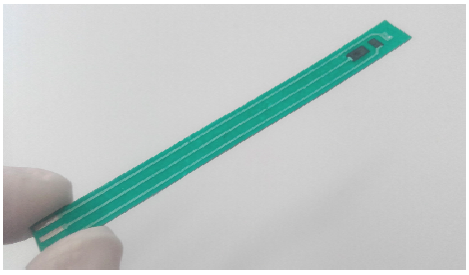

Figure 8.1. MP-ssSPCE for the MPO magneto-immunoassay

These results suggest that screen printed lateral flow electrochemical devices could provide a simple and economical platform to produce electrochemical magneto-immunoassay POC devices.

8.1.1. Design, production and characterization of the MP-ssSPCE

Fusion 5 paper was chosen as the printing substrate over smoother lateral-flow materials, such as chromatography membrane, because its high hydrophilicity made membrane blocking steps unnecessary for this specific application. In addition, using Fusion 5 simplified device construction as, according to its manufacturer, this membrane can accomplish all the functions of a typical lateral flow test, which usually requires a combination of different materials.

Screen-printing of electrodes on Fusion 5 membrane required printing a thin layer of dielectric material first, to effectively isolate the conducting tracks and pads from the

flowing solution (Figure 8.2a). However, this coating had to be homogeneous and its penetration into the membrane needed to be controlled to keep its capillary properties. In this case, the high viscosity of screen-printing pastes prevented the free flow of the paste into the membrane, allowing the former to remain mostly on the membrane surface (Figure 8.2b-c).

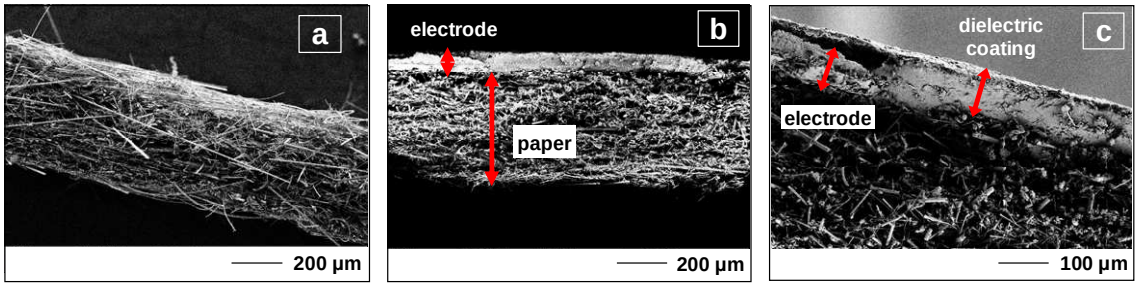

Figure 8.2. SEM images of different magnifications, showing the fibres of the Fusion 5 membrane and the full thickness of the paper (a), the electrode area covered by the conductive carbon ink (b), and a section coated with conductive ink and dielectric (c).

The rest of the screen-printing process consisted of printing the carbon working (1 mm x 2 mm) and auxiliary (3 mm x 2 mm) electrodes and then cure at 90ºC for 20 min. The silver pseudo-reference electrode (1 mm x 2 mm), tracks and contact pads were printed next through a 77-mesh screen, and were cured at 120ºC for 15 min. The tracks were then protected with a new dielectric coating, this time printed through a 90–48 mesh screen. Last, to prevent the solution from creeping up to the connector, a 1 cm-wide band was printed on the back of the contacts through a 43–90 mesh screen. After printing, the Fusion 5 substrates were laser-cut into individual strips and ready to use with a standard 2.54 mm pitch connector.

Once produced, each device, with the dimensions of 6 x 80 mm, included a three-electrode cell consisting of an Ag pseudo-RE, and graphite WE and CE, directly screen-printed on Fusion 5 strips.

The amount of paste dispensed in screen-printing depends largely on the quality of the screen used, and crucially on mesh count, two parameters that were carefully optimized at IMB-CNM (CSIC) by Dr. Javier del Campo team[314]. In brief, devices were screen-printed with the same dielectric using alternatives screens meshed at 90, 120 and 140 threads per cm in the Fusion 5 strips. Then, the dry and soaked weighs of the resulting strips were compared. The results evidenced an inverse correlation between mesh count

and free volume left in the strips: using mesh counts of 90, 120, and 140 the free volumes were of 157 ± 2 µL, 160 ± 2µL and 172 ± 2 µL, respectively.

In order to evaluate the effect of the printed mesh and free volume on the strip, increasing MPO concentrations (0.004 ng mL^{-1}, 0.12 ng mL^{-1} and 2 ng mL^{-1}) were detected with the magneto-immunoassay developed in Chapter 4. For that, it was performed a 5-min-incubation of all the assay reagents (c-MAb-MB, MPO and bd-MAb-HRP), which was followed by two manual washes and a-20 min incubation with TMB. For the chronoamperometric detection, first 50 µL of PBS were added to the MP-ssSPCE while current was allowed to stabilize for 10 s at 0.0 V *vs*. the Ag RE. Then, two consecutive 5-µL injections of each concentration of MPO studied were carried out over time (increasing concentration addition) (Figure 8.3).

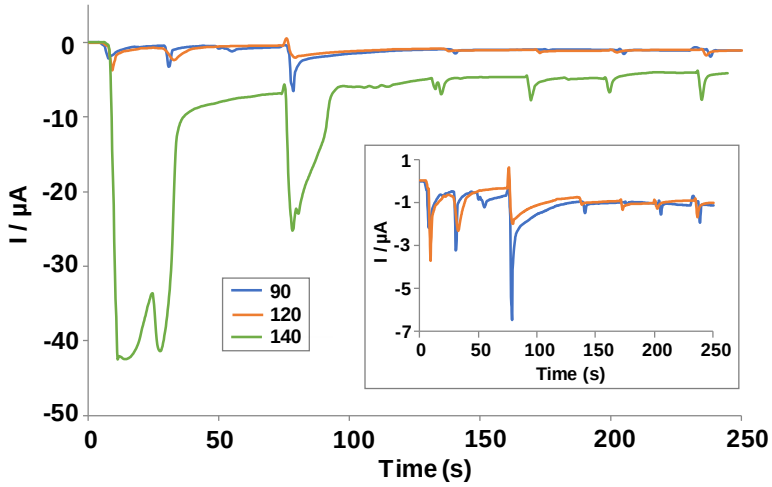

Figure 8.3. Response of MP-ssSPCEs, produced with the three different dielectric densities studied, after serial injections of TMB preincubated for 20 min with increasing MPO concentrations (0.004 ng mL^{-1}, 0.12 ng mL^{-1} and 2 ng mL^{-1}). Insert, zoom of the signals registered for dielectrics printed through meshes displaying 90 and 120 threads per cm.

It was noticed that the MP-ssSPCE strip with dielectric printed using 140 threads per cm exhibited the fastest water absorption and the highest signals generated, which was attributed to the large free volume available. On the other hand, when using 90 and 120 threads per cm, the strips presented currents very similar, although the 120 level of screen-printed dielectric showed more stable and reproducible signals (Figure 8.3, insert).

On the other hand, flow rate was significantly affected by the presence of the dielectric coating on one of the membrane sides. The flow rate along the paper strips was evaluated using a coloured eosine solution in a wet out regime[462,463]. For this, strips

were immersed in an aqueous eosine solution and the progress of the front was recorded over time. A flow rate of 83 µL min^{-1} was obtained in the case of an unmodified membrane, while a flow rate of 42 µL min^{-1} was calculated for the coated membranes. This difference was partly attributed to the volume taken from the lateral flow membrane by the dielectric coating, but also to mechanical changes induced in the strip during the screen-printing process.

Then, the IMB-CNM (CSIC) team printed three different designs of the MP-ssSPCE, varying the positions of the electrodes on the strip (Figure 8.4a).

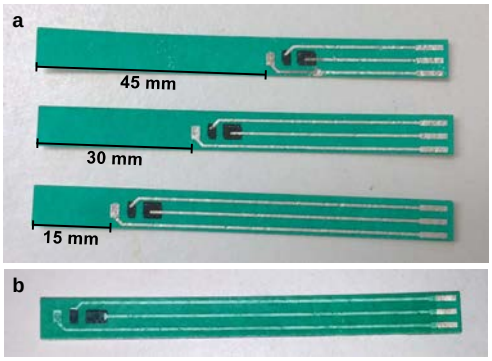

Figure 8.4. (a) Designs of the three different positions of the electrodes in the MP-ssSPCE. (b) Optimal design of the MP-ssSPCE.

The three strip designs were evaluated by adding 150 µL of methylene blue 0.1% (Ref. J60823, Alfa Aesar, Germany) to determine volume displacement through the strip. In all cases, the volume was injected over the electrodes zone, and it run in a bidirectional way. However, to integrate successfully the washes of the magneto-immunoassay in the MP-ssSPCE, it was needed that the solution flowed in a unidirectional way in order to drag the non-binding components far from the electrodes. For that reason, it was decided that the most suitable MP-ssSPCE strip should display the electrodes as close as possible to the strip terminal edge (Figure 8.4b).

Once selected the optimal MP-ssSPCE design and printing process, this device was electrochemically characterized by CV in a 25 mM ferrocyanide solution prepared in 0.1 M sulphuric acid using different scan rates (Figure 8.5a). A sharp current drop after the oxidation peak was observed in all the CVs registered. This sudden drop differed from that observed at flat inlaid electrodes in the absence of convection, and which was expected to decay proportionally to $t^{-1/2}$ [464]. This pointed at the presence of thin-layer effects, an issue that is common to porous electrodes[465]. The fibrous nature of the lateral

flow membrane on which the electrodes were printed, leaded to a rough electrode surface, which presumably summed to the typical porosity of most SPCE. In addition to this, at scan rates below 100 mVs^{-1}, a steady state current appeared after the current peak. Although these CV were recorded with the strip immersed in a solution to avoid this, some convection still happened, which was presumably caused by the evaporation of the solution from the strip above the solution level.

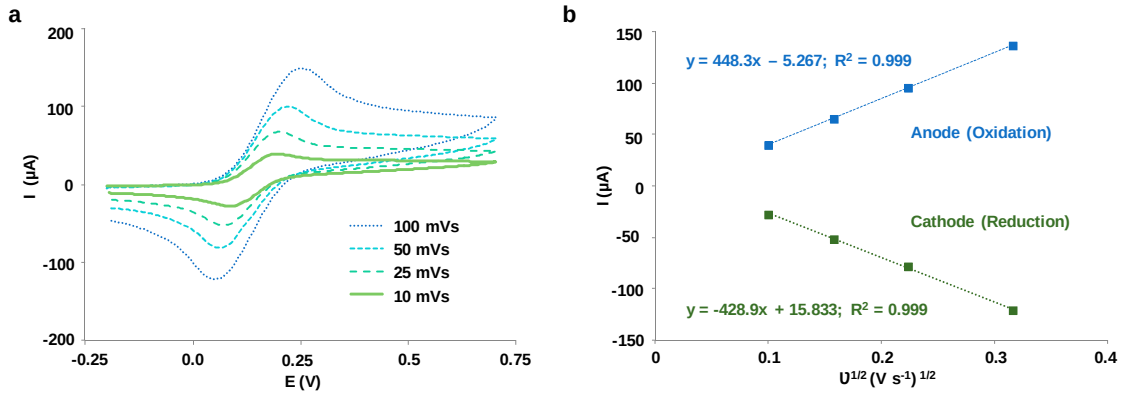

Figure 8.5 (a) CV obtained at MP-ssSPCE for a 25 mM solution of ferrocyanide in sulphuric acid 0.1 M. (b) Plot for the anodic and cathodic peak currents as a function of the square root of the scan rate for 25 mM of ferrocyanide.

The linear relationship between the anodic and cathodic peak currents and the square root of the scan rates tested (Figure 8.5b) confirmed the diffusion-limited behaviour of the ferrocyanide solution during the oxidation and reduction reaction, which involved also a reversible electron transfer[108].

The Randles–Sevcik equation and the plot of the peak current *vs*. the square root of the scan rate ($\upsilon^{1/2}$), could be used to calculate the diffusion coefficient for ferrocyanide.
The Randles–Sevcik equation is described as:

$$ip = 0.4463nFAC^0\left(\frac{nFvD}{RT}\right)^{1/2} = \left[0.4463nFAC^0\left(\frac{nFD}{RT}\right)^{1/2}\right]v^{1/2}$$

where ip is the peak current (A), n the number of electrons (to reduce/oxidize one molecule of analyte), F the Faraday constant (96485 C mol^{-1}), A the area of the (planar) electrode in cm^2, C^0 the initial concentration of the reducible analyte (mol cm^{-3}), v the scan rate (V s^{-1}), D the diffusion coefficient for the species (cm^2 s^{-1}), R the gas constant (8.314472 J K^{-1} mol^{-1}) and T the temperature (K).

Extracting D from the Randles-Sevick equation and using the slope of the linear equation of the current versus the scan rate,

$$D = \left(\frac{slope}{0.4463nFAC^0}\right)^2 \frac{RT}{nF}$$

the diffusion coefficient for the oxidized and reduced ferrocyanide at 25 mM using the MP-ssSPCE was of $5.57 \cdot 10^{-6}$ cm^2 s^{-1} and $5.09 \cdot 10^{-6}$ cm^2 s^{-1}, respectively. These values were close to the numbers reported in the literature ($6.5 \cdot 10^{-6}$ cm^2 s^{-1}) [466,467].

8.1.2. Electrochemical magneto-immunodetection of MPO using the MP-ssSPCE

The shortened MPO magneto-immunoassay consisted of a single 5-min immunocapture but included also a series of washing steps that had to be manually performed tube by tube and took longer than immunomagnetic binding itself (>7 min per sample and up to 15–20 min for a series of 8–12 tubes). MB had to be then manually transferred to the electrode surface to be magnetically confined onto the WE and perform the electrochemical detection. For this reason, this part of the work explored the possibility to carry out the washing and electrochemical detection steps of the magneto-immunoassay directly in the MP-ssSPCE (Figure 8.6).

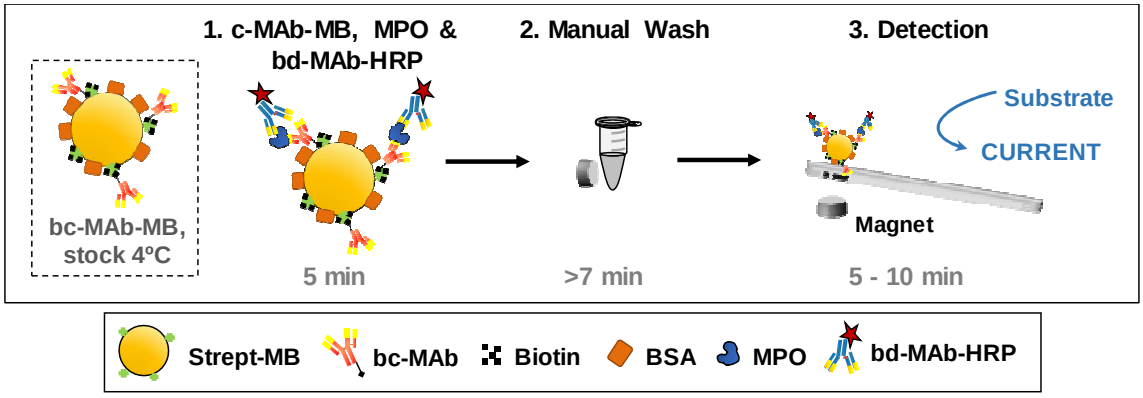

Figure 8.6. Schematic representation of the electrochemical magneto-immunoassay with the integration of the detection step in the MP-ssSPCE

To start with, MPO immunocapture and MB washing were performed in tubes as usual. After the washes, the MB we re-suspended in 25, 50 or 100 µL of PBS_{1X} and were pipetted onto the paper device. A magnet had been placed under the WE to confine the MB over it (Figure 8.7a). Figure 8.7a (zoomed insert) shows that MB were retained by the magnet. However, they ended up scattered across the whole membrane and did not just cluster on the electrode surface.

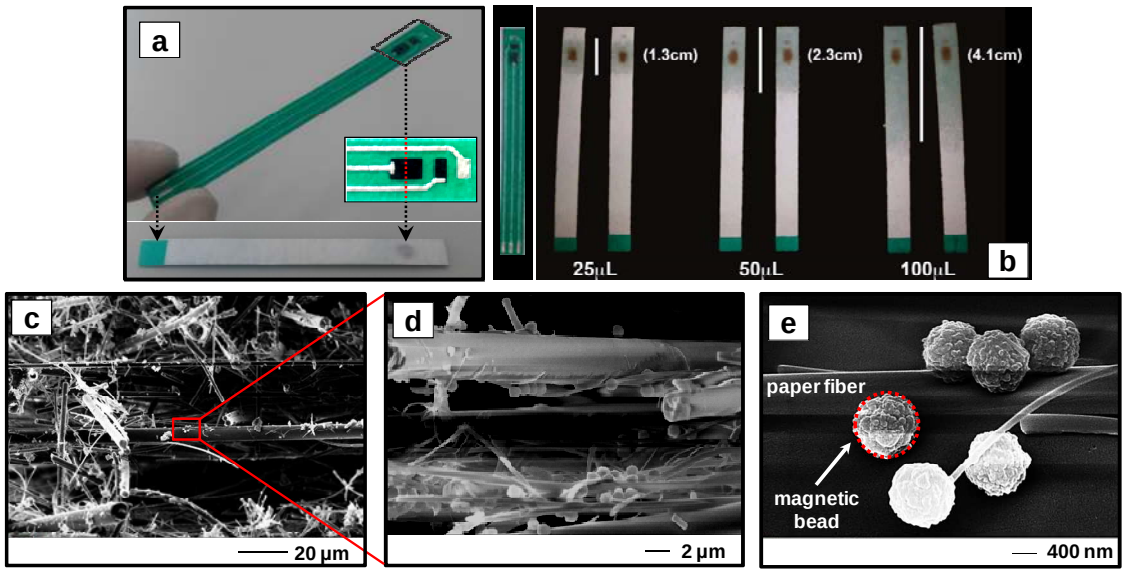

Figure 8.7. (a) Photograph of both sides of the strip, indicating the cross-sectional area of the MB deposition; (b) Modification of the paper strip with MB re-suspended in different volumes (25, 50, and 100 µL). (c–e) SEM images of different magnifications, showing the dispersion of the MBs through the full thickness of the paper, reaching the electrode area.

For the measurement, current was stabilized at 0 V *vs*. Ag for 150 s while PBS flowed along the paper matrix. TMB was next pipetted (25–50 µL) and was allowed to flow while current was registered for 600 additional seconds. As it can be observed, when pipetting the MB in 50–100 µL, PBS flowed simultaneously around the injection site, dispersing the solution over a wide paper area (Figure 8.7b). This was important, because if real samples were to be pipetted on the chip for subsequent washing, sample/reagent flow upstream from the electrodes in the paper strip would produce incomplete washing later. Pipetting 100 µL of solution wetted half of the paper device leaving little space for the reagents of the subsequent washing and detection steps. In addition, higher solution volumes correlated with wider dispersion of the MB, with part of the MB running too far from the electrode area to be detected. In agreement with this, the best MB confinement was obtained for a 25-µL volume (Figures 8.7b). Accordingly, it was decided to work in 25-µL immunocapture volumes, which had produced in previous experiments lower assay sensitivity, but LOD/LOQ of the same order and wider linear range than when working with 50 and 100-µL sample volumes (see results in Chapter 4).

On the other hand, using a bigger magnet to retain the MB made them cluster and interfered with the subsequent electrochemical detection. This indicated that successful

integration of the washing and detection assay steps required a careful balance between magnetic retention strength and flow drag.

The level of MB confinement also affected the electrochemical detection. For instance, detection after confinement of the MB in 50 µL displayed maximal signals after approximately 600 s of measurement with TMB. For 25 µL volumes, signal stabilization was faster, with maximal signals after 300 s and signal saturation afterwards (Figure 8.8a). Hence, when better confined, more MB acted on enzyme substrate close to the electrode, favouring detection. However, MB clustering could also result in steric hindrance and local substrate exhaustion, which could explain the earlier signal saturation registered under such conditions.

Electrochemical detection of this assay was carried in parallel using commercial SPCE (Figure 8.8b). In this case, following incubation and washing, MB were confined using a magnet onto the SPCE WE, current was allowed to stabilize in 50 µL of PBS, the measurement was paused, PBS was substituted by TMB and the measurement was resumed for 150s. As it can be observed, when only detection was carried at the two types of electrodes, the MP-ssSPCE registered slightly lower currents for all the concentrations on MPO tested (included the negative controls without MPO), but general signal trends were obtained in both cases.

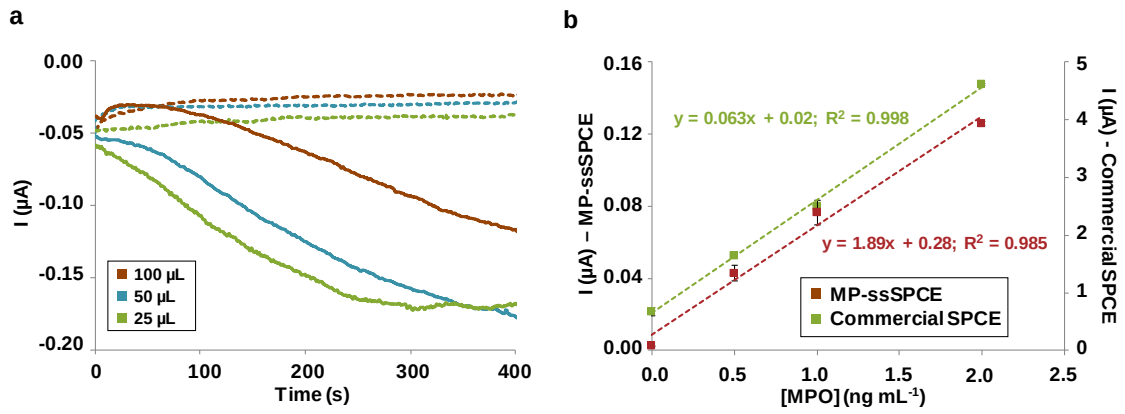

Figure 8.8. MPO sandwich magneto-immunoasay performed in tubes and detected electrochemically at either commercial SPCE or the MP-ssSPCE. (a) Amperometric response registered at MP-ssSPCE for negative controls with no MPO (dashed lines) and positive controls with MPO 2 ng mL^{-1} (straight lines) if the MBs were resuspended after washing in 100 µL, 50 µL or 25µL of PBS before being pipetted on the chip. (b) Comparison of the signal response for increasing MPO concentrations detected with the commercial SPCE and the MP-ssSPCE.

8.1.2.1 MB washing on-chip using the MP-ssSPCE

The next step was to integrate on-chip the MB washes before detection. In a first approach, after the 5-min incubation in tube, the supernatant was removed, MB were re-suspended in 25 µL of PBS and they were incorporated on the paper (**Figure 8.9**). Then, different volumes of PBST were added to wash the MB while current was measured for 150 s. Finally, TMB was incorporated and detection proceeded for 450 more seconds. This implied that the washes were carried out on-chip, but the incubation solution (hence the excess of reagents) had been previously removed and was not pipetted on the paper device.

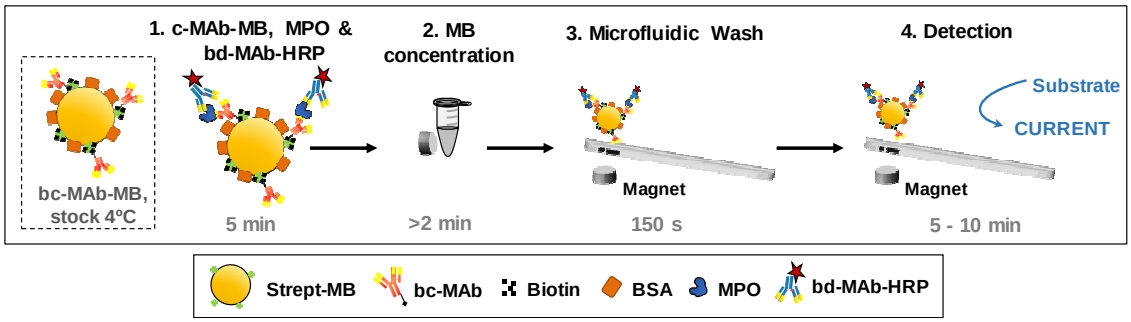

Figure 8.9. Schematic representation of the electrochemical magneto-immunoassay when performing the washes and the detection integrated in the MP-ssSPCE.

Figure 8.10a shows that, while the current registered was of about 20–30 nA in the negative controls (i. e.: without MPO) after a single wash with 50 µL of PBST, it was negligible if two consecutive 50 µL washes were implemented. Since the signals in the presence of MPO were comparable in both cases, the S/N ratio was significantly higher after two washes. In contrast, the addition of supplementary washes or the implementation of higher volume of washing solution did not improve the results further and contributed to dragging higher amounts of MB downstream from the detection area. Again, optimal performance required careful adjustment of washing solution volume to guarantee MB retention by the magnet. On the other hand, washing with PBS instead of PBST produced higher background signals, presumably caused by a lower washing efficiency.

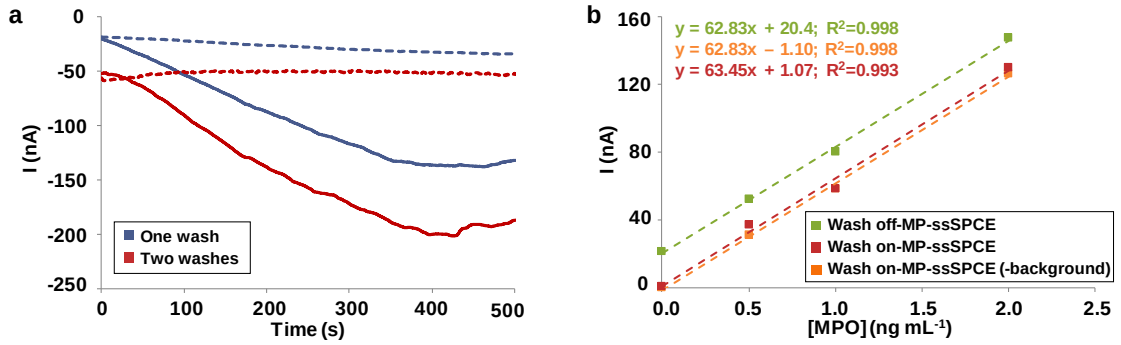

Figure 8.10. (a) Amperometric response for negative controls (dashed lines) and positive controls (straight lines) using one or two washing steps integrated on-chip. (b) Plot of current intensity against MPO concentration using off-chip and on-chip washing. Orange marks represent the off-strip washing signal with the background subtracted.

Figure 8.10b compares the results of the experiments performed with off-chip and on-chip washing, where the signals registered in both experiments were comparable after background subtraction. This could indicate either that washing of unbound reagents was faintly better or that more MB were lost downstream when the washes were integrated. Independently of this, most MB remained in place after the integrated washing steps and could be detected electrochemically.

In view of these results, the whole washing procedure was finally implemented on-chip (Figure 8.11).

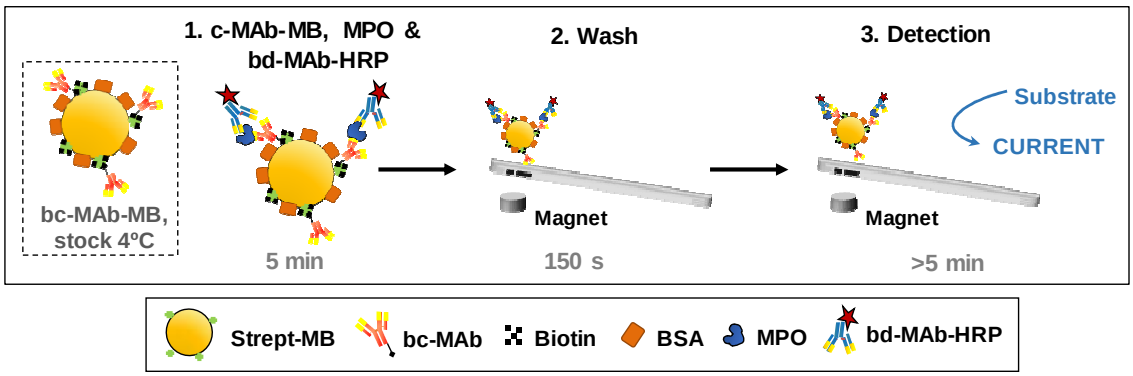

Figure 8.11. Representation of the electrochemical magneto-immunoassay optimized with integrated on-chip washing and detection steps.

For this, the 5-min magneto-immunocapture was performed in 25-µL sample volumes and the whole mixture was immediately transferred to the MP-ssSPCE surface, the washing buffer was added to flow during 150 s, the enzymatic substrate was injected and the chronoamperometric detection was carried for 5 min.

Figure 8.12 shows the signals registered for the magneto-immunoassay on the MP-ssSPCE after either previous concentration of the MB in PBS, or direct sample injection

after immunocapture. The decrease of signal observed after the direct injection of the sample plus reagents mixture was justified by the higher concentration of nonbinding components present, which were presumably trapped within the membrane fibres. This resulted in a systematic increment of the negative control (without MPO) by non-specific binding, and the requirement of more efficient washes, which ultimately caused a drop of the signal registered. The assay sensitivity was also compromised, with an LOD of 0.11 ng mL^{-1} and LOQ of 0.26 ng mL^{-1} in the first case, and LOD of 0.63 ng mL^{-1} and LOQ of 1.04 ng mL^{-1} when the sample-reagents mixture was directly treated on-chip.

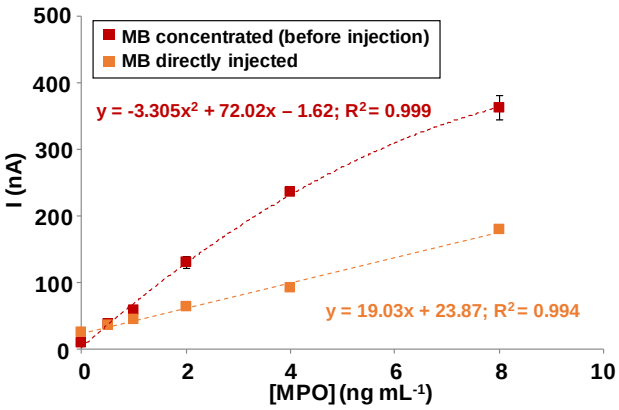

Figure 8.12. Comparison for the signals registered for increasing MPO concentrations when performing two washes and the electrochemical detection on-chip using the MP-ssSPCE. (Red) Concentration of the MB in 25 µL after immunocapture, followed by injection on the MP-ssSPCE; (Orange) After the immunocapture, direct injection of the sample-reagents mixture on the MP-ssSCPE.

Although the assay linear range was wider if the sample-reagents mixture was directly injected on the MP-ssSPCE, the signals registered were far from the expected, with a loss of 40% in average.

8.1.3. Detection of MPO in human serum with the MP-ssSPCE

Finally, the applicability of the magneto-immunoassay developed here was studied using commercial pooled human serum. With this purpose, serum was diluted 1:100 with PBS-$BSA_{0.1}$ and was spiked with increasing concentrations of MPO. It followed incubation of 25-µL volumes for 5 min with MPO-bc-MAb-MB and bd-MAb-HRP, the whole mixture was pipetted onto a lateral flow device and washing, and detection were performed on-chip as indicated before.

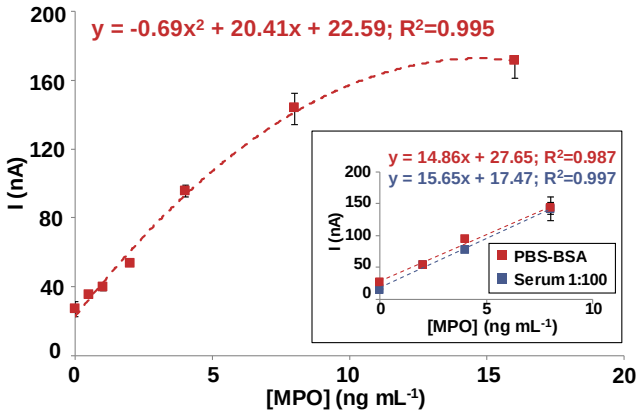

Figure 8.13. Plot of current intensity against MPO concentration when using the MP-ssSPCE with the integrated magneto-immunoassay. Insert, comparison of the linear range obtained for MPO detection using the MP-ssSPCE in PBS-BSA and serum diluted 1:100. Error bars represent the standard deviation of n=4 measurements.

Figure 8.13 shows the results obtained for the electrochemical detection of MPO using the MP-ssSPCE in diluted spiked human serum. As it can be observed, the signals registered were not significantly different from those registered in PBS-$BSA_{0.1}$, with MPO recovery efficiencies ranging 95%–108%. Under these conditions, the assay displayed linear response up to 8 ng mL^{-1} of MPO, LOD of 0.18 ng mL^{-1}, LOQ of 0.62 ng mL^{-1}, and sensitivity (slope) of 15.17 nA mL ng^{-1} (Table 8.1).

Although these LOD/LOQ were 18–20 times higher than the numbers obtained for the magneto-immunoassay detected spectrophotometrically and detection at commercial SPCE, assay time was nearly 5 times shorter and handling was significantly easier.

Assay type	**Spectrophotometric**	**Electrochemical**		
Washing	In tubes	In tubes / MP-ssSPCE	On-chip / MP-ssSPCE	
Immunobinding	PBS-$BSA_{0.1}$	PBS-$BSA_{0.1}$	PBS-$BSA_{0.1}$	Serum 1:100
LOD (ng mL^{-1})	0.01	0.13	0.63	0.18
LOQ (ng mL^{-1})	0.03	0.36	1.04	0.62
Linear range (ng mL^{-1})	0.004 - 4	0.25 - 2	0.25 - 8	0.25 - 8
Sensitivity (slope)[a]	0.85	62.86	14.92	15.17
%CV[b]	<10	<10	<8	<12
Assay time	~ 60 min	~ 20 min	< 13 min	< 13 min

Table 8.1. Comparison of the analytical performance of the three methods used for the quantification of MPO. [a] Slope in UA·mL·ng^{-1} (spectrophotometric) or in nA·mL·ng^{-1} (electrochemical). [b] %CV stands for variation coefficient [%CV=(SD/mean) X 100].

Figure 8.14 shows that the signals registered were proportional to the concentration of MPO for all the magneto-immunoassay methods of detection performed. As illustrated in Figure 8.14d, under these experimental conditions the figures of merit of the

colorimetric and electrochemical assays were comparable (LODs of 1–10 ng mL^{-1}, LOQs of 18–30 ng mL^{-1}, %CV<10%). However, detection using the MP-ssSPCE provided currents that were in average ~20-30 times lower than the currents registered at a commercial SPCE for similar MPO concentrations. This was attributed to two issues. First, the fact that while the MB clustered immediately over the WE at SPCE, they scattered across the whole thickness of the paper membrane in the MP-ssSPCE (Figure 8.14b and c). Second, the evidence that part of the enzyme product (TMB_{ox}) produced by the HRP label flowed downstream from the electrode before being detected. This suggested that better electrode design and selection of a different membrane material could improve performance.

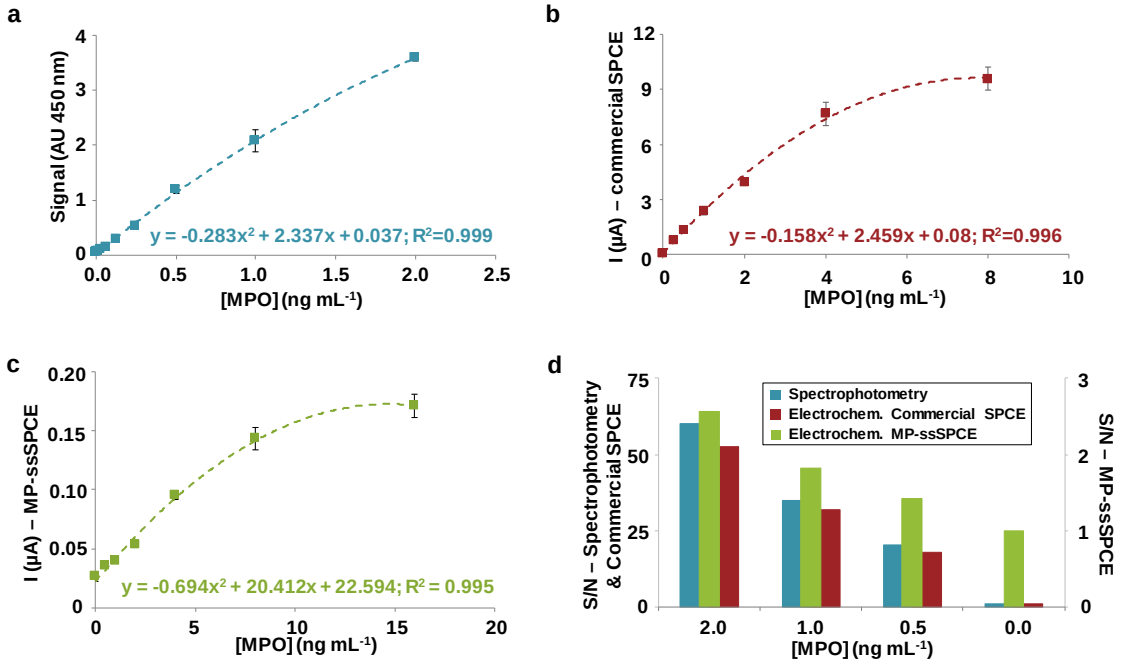

Figure 8.14. Plots of signal *vs*. MPO concentration obtained when the sandwich magneto-immunoassay was detected alternatively using spectrophotometric detection (a), electrochemical detection at a commercial SPCE (b), or electrochemical detection using the MP-ssSPCE (c). Error bars (represent the standard deviation of n=3 measurements. (d) S/N ratio for the plots in (a), (b) and (c). The bars for spectrophotometric and electrochemical detection at SPCE are show at a different scale (left axis) than those displayed for MP-ssSPCE (right axis).

These results confirmed that washing and detection could be integrated in the paper device, even when magneto immunocapture was performed in a complex matrix such as diluted serum. Nevertheless, the fact that the currents registered at the lateral flow electrode were in average 30 times lower than those obtained at SPCE suggested as well that detection could be improved by re-designing the flow device.

8.2. Microfluidic paper double-side SPCE (MP-dsSPCE) for PLDH magneto-immunoassay electrochemical detection

In Section 8.1, a MP-ssSPCE was used to perform on-chip the washes and detection of a one-step magneto-immunosensor with minimal intervention by the user, although the sensibility achieved was still far from the numbers obtained with a commercial SPCE[445]. The next step was to enhance the sensitivity of the paper electrode, which was achieved in collaboration with Dr.'s Javier del Campo team (IMB-CNM, CSIC) by developing an improved version of the single-use printed electrode in which WE electrodes were printed on both sides of the device. The objective was to increase both the WE active area and the collection efficiency of the flowing TMB. This MP-dsSPCE was assembled in a customized cartridge that included also an integrated microfluidic washing system for malaria diagnosis in whole blood samples, employing the one-step magneto-immunoassay described in Section 5.2. As it will be shown, the system facilitated the simple execution of the test, with rapid, sensitive and quantitative PLDH detection.

8.2.1. Design and electrochemical characterization of the MP-dsSPCE

MP-dsSPCE was designed to be used in a horizontal position while solution drops were pipetted onto the top. Each device measured 9 x 19.5 mm and contained a 3-electrode electrochemical cell in the bottom side and additional WE and CE on the top, which were cross-circuited with the corresponding bottom counterparts (Figures 8.14). This provided not only larger WE active area, but also more efficient detection of electroactive species flowing along the device and across the whole paper matrix thickness. The entire device surface was protected by a water-proof dielectric layer, except for the chip laser-cut edges and the centre of the top WE, which displayed ring-shaped geometry. This circular opening allowed the entry of MB and solutions into the paper matrix, for their transportation along the chip by capillary flow. The frontal edge, on the other hand, was exploited to connect an adsorbent pad, which provided solution draining and waste storage. In this way, MP-dsSPCE could be used alternatively to carry electrochemical measurements under static and flow conditions.

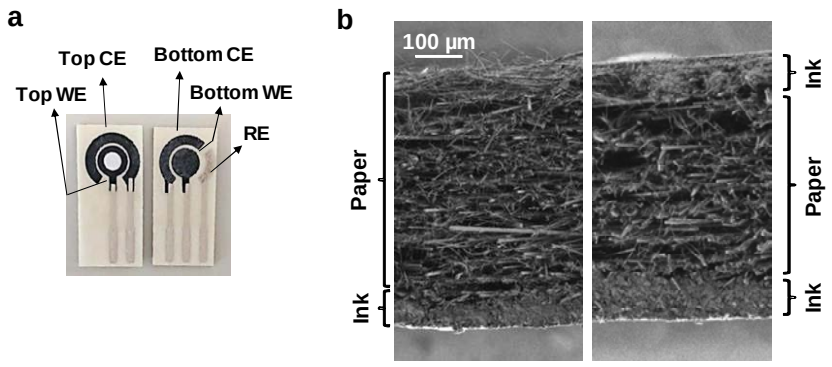

Figure 8.14. Design and production of the MP-dsSPCE. (a) Photograph of both sides of the MP-dsSPCE. (b) Scanning electron microscopy (SEM) images of a transversal cut of the MP-dsSPCE carried at either the center of the ring-shaped WE (left, showing a layer of conductive ink on the bottom side of the chip) or outside it (right, showing ink layers both on the top and bottom sides of the chip).

For their utilization, MP-dsSPCE were connected to the potentiostat using a standard 2.54 mm pitch connector. However, solutions could also flow upstream from the electrodes and the unprotected back edge of the chip allowed fluid passage into the connectors and eventual electrical short circuit. For this reason, a transparent impermeabilizing solution (Rubson SX9000, Henkel, Germany) was used to protect the paper fibres in the connectors' zone, creating a hydrophobic barrier. This economical product, which was sold for the impermeabilization of building materials, was acquired at a local retailer.

The volume of water repellent necessary to penetrate only the area of interest, without affecting the electrochemical cell, was first determined. For this, several MP-dsSPCE were inserted in the wells of a 96-well microtiter plate, containing increasing volumes of impermeabilizing solution. When the solution had been adsorbed, the MP-dsSPCE were dried for 3 h in an incubator at 36°C. The two sides of the chips were then striped from each other. As it can be observed in Figure 8.15, 15 µL of solution were needed to protect completely the connector paths without reaching the electrodes. Higher volumes, on the other hand, provided irregular paper protection, often affecting the areas that displayed the electrodes.

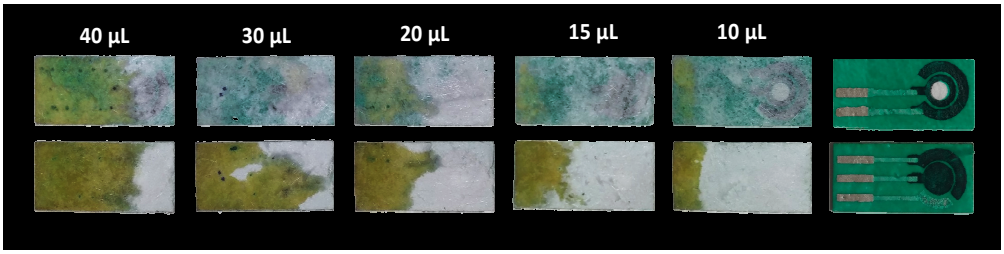

Figure 8.15. Impermeabilization of the MP-dsSPCE connectors with increasing volumes of a water-repelent solution.

The behaviour of the MP-dsSPCE was studied electrochemically by performing CV using alternatively the top, bottom and top-bottom cross-circuited WE/CE, employing in all cases the bottom RE. To do that, CVs were registered in a 25 mM ferrocyanide solution prepared in 0.1 M sulfuric acid at a scan rate of 50 $mV \cdot s^{-1}$ (Figure 8.16). CV were obtained alternatively under flow and static conditions (in the first case by letting the drop flow along the paper electrode to which an absorbent pad had been attached).

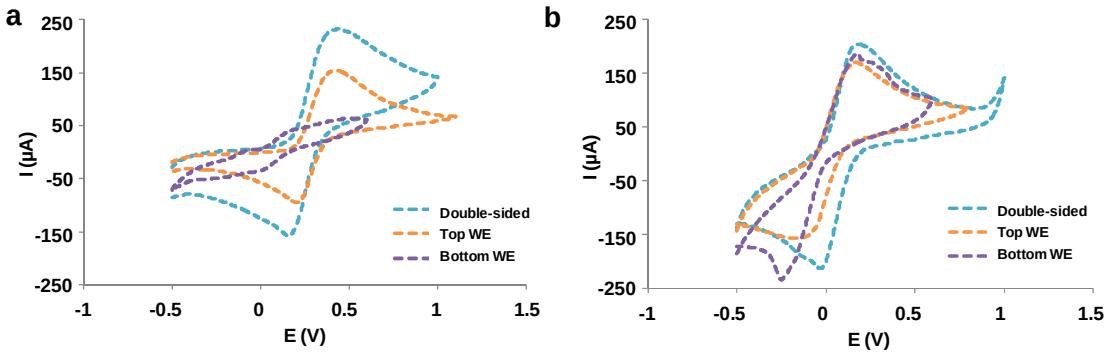

Figure 8.16. Characterization of the MP-dsSPCE. CVs obtained at MP-dsSPCE, for a 25 mM solution of ferrocyanide in sulfuric acid 0.1 M (50 $mV \cdot s^{-1}$), using alternatively the top, bottom and top-bottom cross circuited WE/CE under flow (a) or static (b) conditions.

As it can be observed, while under static conditions top and bottom WE displayed similar performance, under flow conditions the bottom electrodes registered significantly lower currents, larger peak-to-peak separation (ΔEp) and more negative potentials. This confirmed that solution flow compromised detection using electrodes at the bottom of the chip, which was the configuration displayed by the original MP-ssSPCE. In spite of this, using double side connection provided in all cases higher currents that using only the top or bottom WE, suggesting that this was the best electrode arrangement for these MP-dsSPCE.

MP-dsSPCE used in the double-sided WE configuration were additionally evaluated by registering CVs at increasing scan rates (10, 25 and 50 mV s^{-1}), both under static and flow conditions (Figure 8.17).

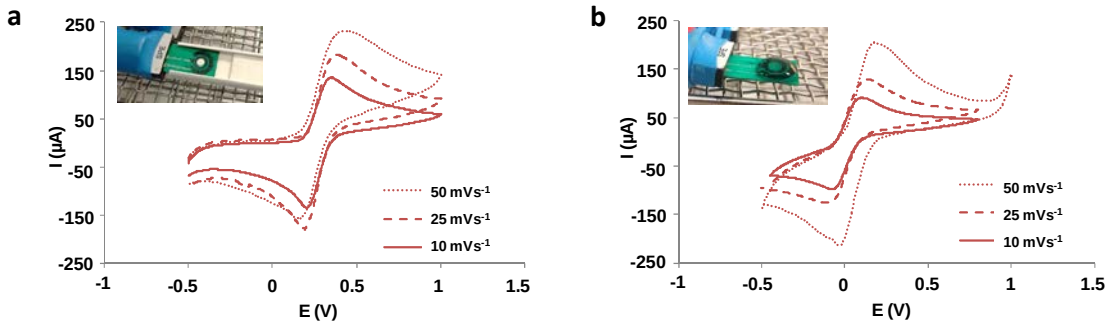

Figure 8.17. CVs obtained at the double-sided WE at different scan rates under flow (a) or static (b) conditions. Insert. Photographs of the MP-dsSPCE connected to a standard 2.54 mm pitch connector and employed to carry out a measurement under either flow or static conditions. In the flow case, a pile of adsorbent paths was located in contact with the frontal edge of the chip to provide solution drainage, and the whole assembly was placed inside a segment of electrical cable trunking, used here as a physical holder. In the static case, a drop of solution was placed onto the electrochemical cell.

The experimental ΔEp obtained from these CV were used to estimate the electron transfer coefficient (k0) of ferrocyanide under the different measurement conditions tested. This was done using the method proposed by Irma Lavagenini[412] combining the Nicholson's treatment and the Klingler and Kochi method[413] using the following equation:

$$\Psi = k0[\pi DnvF/(RT)]^{-1/2}$$

where Ψ is a kinetic parameter (which is tabulated for ΔEp, at a set temperature (298 K), for a one-electron process whatever the scan rate employed), D is the diffusion coefficient ($cm^2\ s^{-1}$), n is the number of electrons involved in the process, v is the scan rate ($V\ s^{-1}$), F is the Faraday constant (96485 $C\ mol^{-1}$), R the gas constant ($J\ mol^{-1}\ K^{-1}$), and T the temperature (K).

The function of Ψ (ΔEp), which fits Nicholson's data, for practical usage is given by:

$$\Psi = (-0.6288 + 0.0021X)/(1 - 0.017)$$

where X = ΔEp is used to determine Ψ as a function of ΔEp of the recorded voltammetry. Following these premises, k0 corresponds to the slope of the plot of Ψ versus $[\pi DnF/(RT)]^{-1/2}v^{-1/2}$ in Figure 8.18.

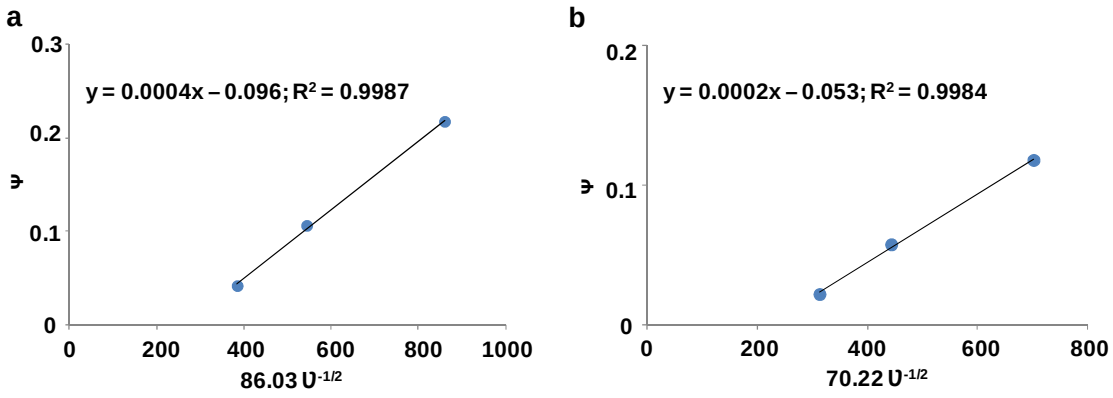

Figure 8.18. Electrochemical characterization of the MP-dsSPCE. Plot of Ψ versus $[\pi DnF/(RT)]^{-1/2}\nu^{-1/2}$ for the measurements carried out under flow (a) and static conditions (b).

The k0 values obtained in this way were of 4 x 10^{-4} cm s^{-1} and 2 x 10^{-4} cm s^{-1} for the measurements carried out under flow and static conditions, respectively, which were of the same order of magnitude.

Diffusion coefficients were calculated chronoamperometrically employing the Cottrel equation:

$$i = (nFAC_o\sqrt{D})/\sqrt{\pi t},$$

where i is current (A), n the number of electrons (to reduce/oxidize one molecule of analyte), F the Faraday constant (96485 C mol^{-1}), A the area of the (planar) electrode in cm^2, Co the initial concentration of the reducible analyte (mol cm^{-3}), D the diffusion coefficient for the species (cm^2 s^{-1}) and t the time (s).

The values of D calculated for potassium ferricyanide under flow and static conditions using this approach were of 1.10 x 10^{-6} cm^2 $s\text{-}^{1}$ and 1.66 x 10^{-6} cm^2 $s\text{-}^{1}$, respectively, which again were of the same order of magnitude.

Finally, the CVs registered under flow conditions with the MP-dsSPCE developed here were compared to those provided by the single-sided version described in Section 8.1[314] and the commercial SPCE. As it can be observed in Figure 8.19, the upgraded double-sided device registered currents that were 20 times higher than the ones detected by the previous version and closer to those observed for commercial SPCE.

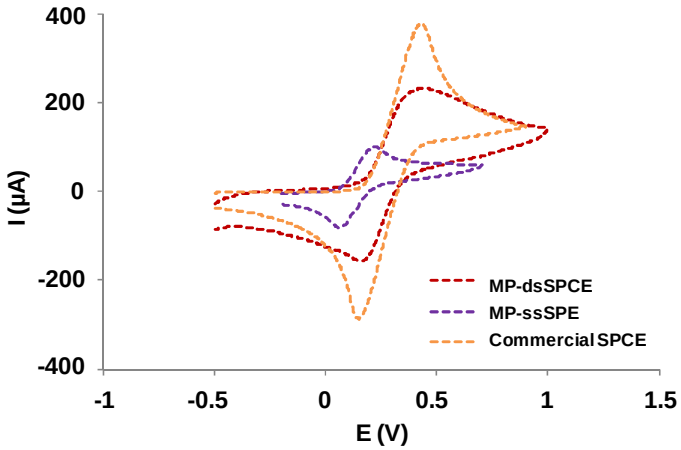

Figure 8.19. Comparison of the CVs registered with the MP-dsSPCE and MP-ssSPCE developed and a commercial SPCE.

8.2.2. Assembly of the MP-dsSPCE in a low-cost fluidic cartridge

8.2.2.1 Design and assembly of the fluidic cartridge

In order to perform most of the steps of a magneto-immunoassay on-chip, an extremely simple and economical cartridge was produced that could provide serial MB magnetic confinement, washing and electrochemical detection (Figure 8.20).

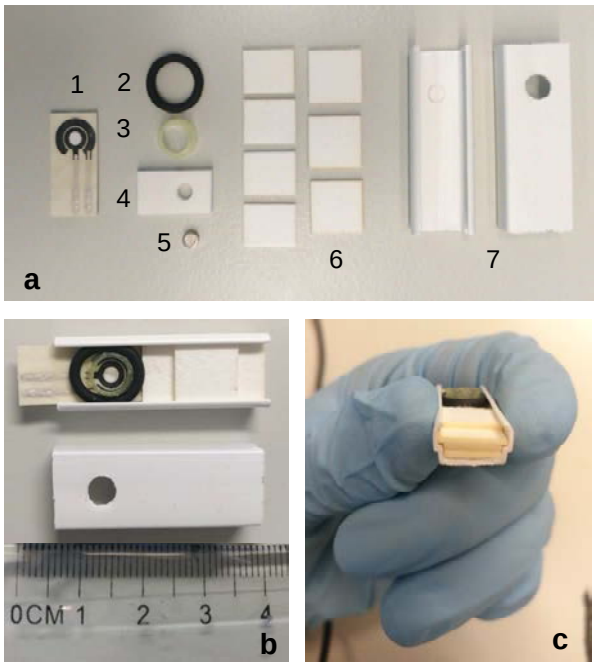

Figure 8.20. Production of the MP-dsSPCE-containing fluidic cartridge. a) Components of the cartridge. (1) MP-dsSPCE, (2) o-ring, (3) segment of a pipette tip, (4) silicon sheet with a perforation for the insertion of a magnet (5), (6) adsorbent pads, and (7) segment of electrical cable trunking. b-c) Assembled device and detail of the pile of absorbent pads.

For this, the MP-dsSPCE was inserted in a 4.5-cm segment of PVC electrical cable trunking (45x12x0.7 mm; SevenOn elec, Hidalgo's Group, Spain), which served as the platform holder. The device detection system was composed of the MP-dsSPCE, which was placed so that the electrical connectors protruded from the holder. A piece of silicone elastomer (15x8x2 mm; Ref. SI303200; GoodFellow, England) with a perforation allowed embedding a neodymium magnet. The magnet (3 mm Ø x 1.5 mm thickness; IMA, Spain), was added to retain the MB within the paper matrix between the bottom and top WE. A plastic ring, cut from the bottom of a polypropylene pipette tip (4 mm high, 5 mm Ø; Ref. 162001, Nirco, Spain), was placed above the top electrochemical cell to prevent solution spreading. Finally, a Viton o-ring (6.1 mm internal Ø, 9.5 mm external Ø, 1.78 mm wall thickness; Ref. Z542490, Sigma Aldrich) kept all the system components in place inside the PVC holder, which displayed a window that granted access to the electrodes for solution transfer. In this way, when a suspension of MB was pipetted in the system, the solution flowed across the orifice in the top WE and into the paper matrix, while MB were retained by the magnet, and an absorbent pad provided absorption of sample and reagents, wash under flow conditions, and waste storage as well.

8.2.2.2 Assembly of the paper absorption system

The MP-dsSPCE could absorb approximately 85 µL of aqueous solution, but the whole magneto-immunoassay took about 500-600 µL of sample and reagents. For this reason, it was necessary to incorporate an external absorbent pad to the system. A selection of membranes was evaluated for this purpose. Numerous membranes are commercially available with several physical and chemical attributes that affect the capillary flow properties. Here, nine types of pads were evaluated for their application in the lateral flow test (Table 8.2)[411].

Membrane	Material	Properties	Lateral flow application	Thickness (µm)	Capillary flow rate (s/4cm)	Water absorption (mg/cm^2)
LF1	Bound glass fibre	Works well with whole blood or serum samples and can act as a blood separator as well	Blood separation	247	35,6	25.3
MF1			Blood separation	367	29,7	39.4
VF2			Blood separation	785	23,8	86.2
Standard 17		Faster flow than cotton, with lower sample retention	Conjugate release	370	34,5	44.9
GF/DVA		Works well with saliva samples and can act as a blood separator also	Blood separation	785	28,2	93
CF5	100% cotton linter	Medium weight	Absorption pad	954	63,3	99.2
CF4			Sample application & absorption pad	482	67,3	49.9
Fusion 5	Glass fibre with a plastic binder	Can be used as a lateral flow blood separator	Blood separation & conjugate release	370	38	40
Prima 40	Nitrocellulose	-	Backed reservoir pad	192	44	-

Table 8.2. Characteristic of the nine commercial membranes studied as absorption pad in the MP-dsSPCE.

In order to corroborate the water absorption capacity facilitated by the manufacturer for each membrane, a test was performed by adding 100 µL of methylene blue 0.1% (Ref. J60823, Alfa Aesar, Germany) to a 40 x 10 mm strip of each type of membrane and the distance run by the solution was measured (Figure 8.21). It was expected that the distance run by a fixed volume of solution would be inversely proportional to the water absorption capacity of the material. As it can be observed, C5, GF/DVA and VF2 provided the highest absorption capacity, which was consistent with the data facilitated by the provider (99.2, 93 and 86.2 mg cm^{-2}, respectively). However, C5 provided the

most homogeneous flow and was selected for the production of the MP-dsSPCE absorption pad.

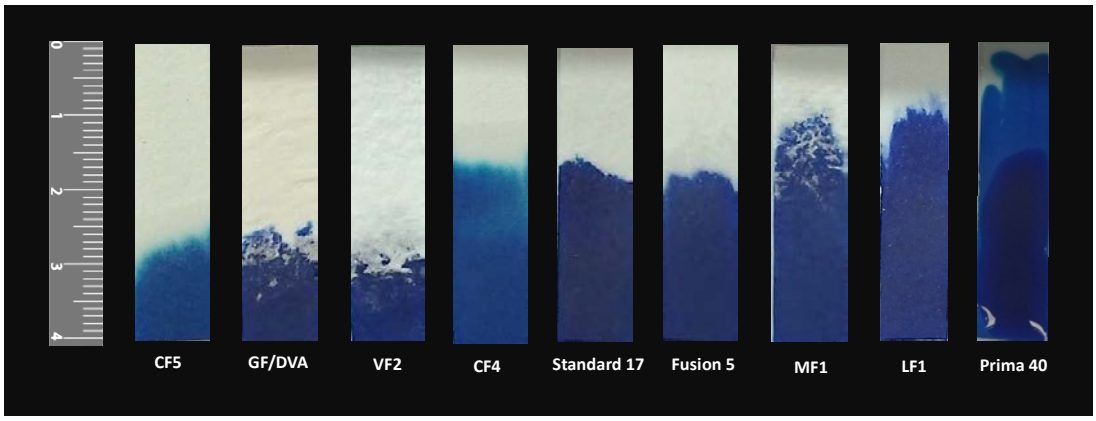

Figure 8.21. Study of the absorption capacity of different commercial membranes.

Considering the water absorption capacity of the selected membrane, the minimal indispensable area of CF5 membrane needed to retain the ~600µL of total waste volume generated during the magneto-immunoassay was of 6.05 cm^2 of CF5. Because the plastic holder displayed an irregular section, the external absorbent pad was formed by assembling seven CF5 pieces of different dimensions in 4 piled layers (Figure 8.20c). The first one was situated on the base of the cable trunking and was composed by two 10 mm x 7 mm CF5 pieces connected to each other and to the edge of the MP-dsSPCE. A second layer was placed on the top of the first and was formed by two more 10 mm x 7 mm pieces in contact with the MP-sdSPCE; the third and fourth layers had a single 10 mm x 10 mm piece each.

8.2.3. Electrochemical magneto-immunodetection of PLDH using the MP-dsSPCE

8.2.3.1 Optimization of the electrochemical detection on the MP-dsSPCE

The paper microfluidic system developed was next used to carry out the one-step magneto-immunoassay for PLDH detection optimized in Section 6.2. Work started by performing only the electrochemical detection on the MP-dsSPCE and the rest of the assay was performed in tubes in the absence or in the presence of PfLDH (12.5 and 100 ng mL^{-1}). To do so, the 5-min incubation of the mixture of sample and reagents was followed by two manually washes of 150 µL PBST in tubes. After the last wash, MB were resuspended in 100 µL of TMB substrate solution and were pipetted on the MP-

dsSPCE for detection (Figure 8.22). Several parameters had to be optimized, including the measurement potential, the volume of enzymatic substrate, the amount of MB per sample, and the magnet location.

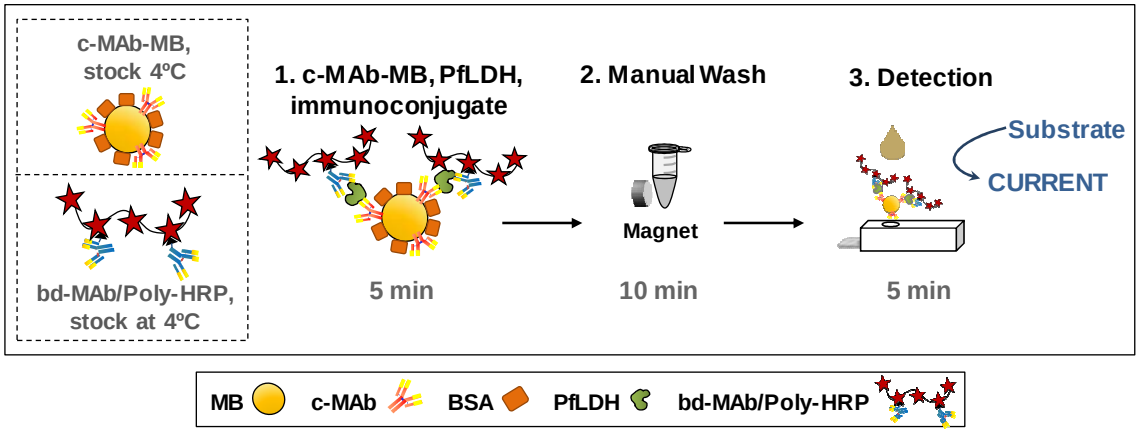

Figure 8.22. Scheme of the one-step PLDH magneto-immunoassay performed in tubes with the electrochemical detection carried out using the MP-dsSPCE.

Measurement potential

The amperometric measurement was carried out on-chip at three different measurement potentials (0.0 V, -0.05 V, -0.1 V *vs*. the Ag pseudo-reference), either under static or under flow conditions (Figure 8.23). In general, the currents registered under flow conditions were 40% lower than those detected in a static drop, and the S/N ratios were 20% worse as well. This was attributed to the partial loss of MB and enzymatic substrate, which flowed along the MP-dsSPCE during the measurement and before being detected. The best measurement potential was considered -0.05V in both cases, which provided the highest S/N.

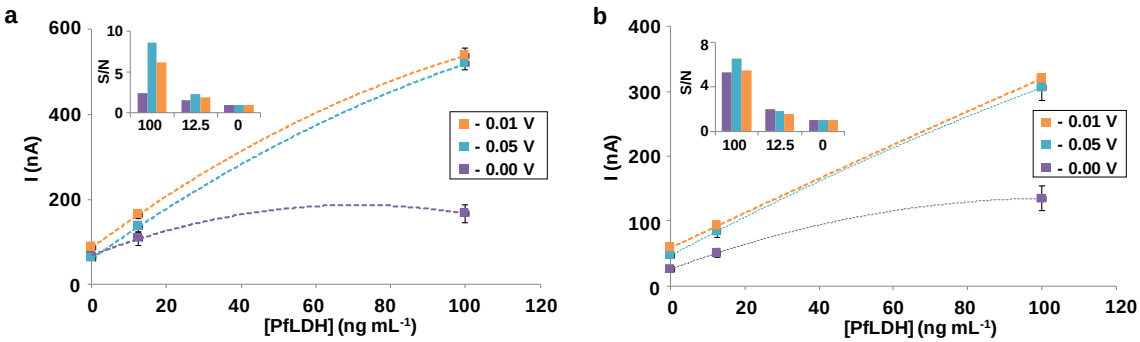

Figure 8.23. Optimization of assay measurement potential in static (a) and flow (b) conditions using MP-dsSPCE.

MB concentration

The optimal concentration of MB in the magneto-immunoassay detected colorimetrically was of 0.2 mg mL^{-1}. Higher amounts of MB did not improve the assay and produced higher background noise, while lower MB quantities provided lower signals and larger result variability.

In the case of detection at the MP-dsSPCE, electrochemical detection under static conditions produced comparable currents and S/N if the assay was performed with 10, 15 or 20 µg of MB per sample, but result reproducibility improved with MB load (%CV of 19.27%, 12.68% and 5.63%, respectively, in average) (Figure 8.24). This was presumably caused by more efficient magnetic retention of higher MB loads during the incubation and washing steps, which had been performed in tubes and was consistent with previously reported results[156]. The effect of the MB concentration was clearer under flow measurement conditions, where both current and S/N increase with the amount of MB (%CV of 17.69%, 13.55% and 8.17% for 10, 15 or 20 MB µg, respectively, in average).

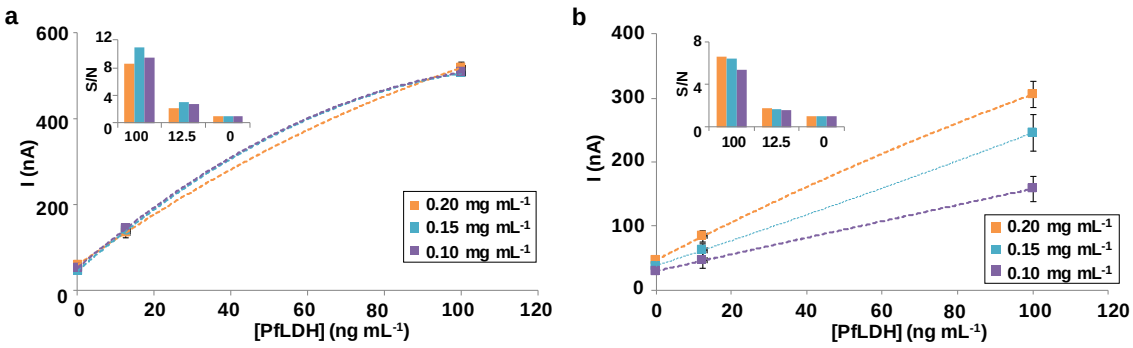

Figure 8.24. Optimization of MB concentration in the one-step magneto-immunoassay detected electrochemically using MP-sdSPCE, under static (a) and flow (b) conditions.

Magnet location

The way MB were magnetically confined in the electrode had also a profound effect in both detection methods. It was observed that placing a magnet immediately below the MP-dsSPCE produced MB surface confinement faster than solution flow. For this reason, MB accumulated on the chip surface instead of entering the paper matrix, lowering solution flow rate as well. Accordingly, if the magnet was placed 1 mm apart

from the electrode, both current and S/N improved (Figure 8.25). Unexpectedly, the highest currents were obtained if the mixture of MB and TMB substrate solution were pipetted without magnet, because MB entered slower in the device matrix, driven only by solution flow capillary.

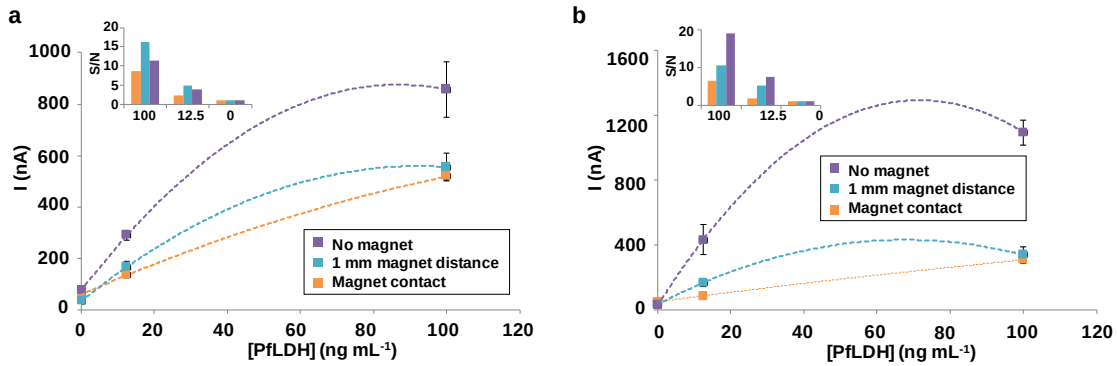

Figure 8.25. Magnet location during the MB confinement in the MP-dsSPCE under static (a) and flow (b) conditions.

Volume of enzymatic substrate

The last factor studied was the volume of enzymatic substrate used for the detection. Since the currents registered for PfLDH in a static drop were independent of the volume of TMB, the best S/N rations were obtained for detections carried out in 25 µL of substrate solution, the lowest volume tested. In contrast, flow detection benefited of using higher TMB volumes, which permitted extending the measurement for longer times, generating higher currents, although not better S/N ratios (Figure 8.26).

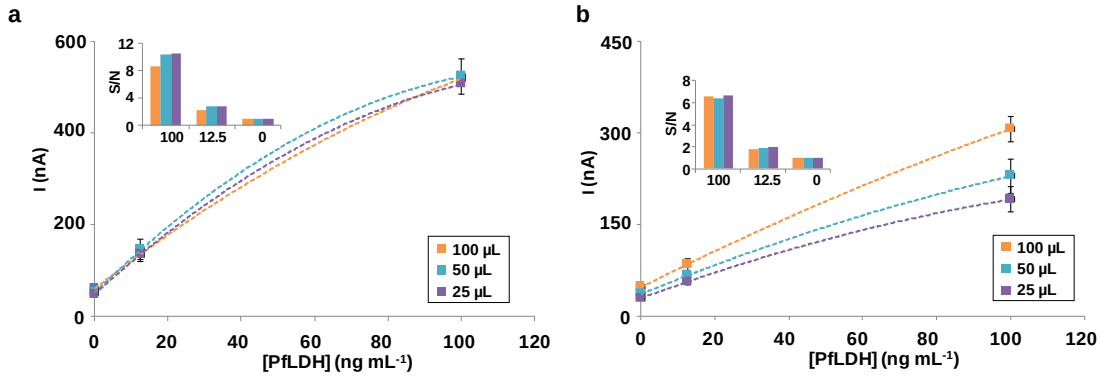

Figure 8.26. Optimization of the enzymatic substrate volume using the MP-dsSPCE under either static (a) or flow (e) conditions.

8.2.3.2 Optimization of magneto-immunoassay on-chip washing and detection using the MP-dsSPCE

The next step was to integrate the MB washing and detection on the MP-dsSPCE. In a first approach, after the 5-min incubation in tube, the mixture of sample, MB and reagents was transferred to the MP-dsSPCE through the cartridge window. Then, two consecutive injections of 100µL of PBST were added to wash the MB, while current was allowed to stabilize for 300 s at different potentials (0.0 V, -0.05 V, -0.1 V, -0.15 V, and -0.2 V vs. the Ag RE). Finally, 100 µL of TMB substrate solution was added and current was monitored for 150 s more (Figure 8.27).

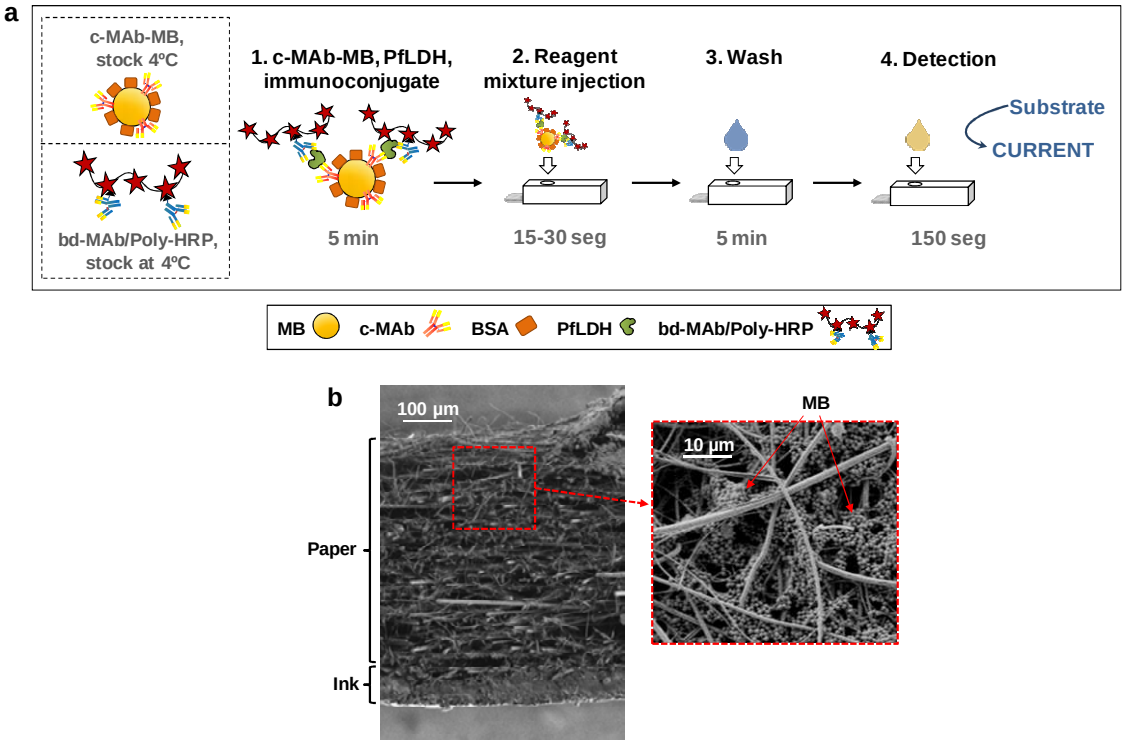

Figure 8.27. (a) Scheme of the PLDH one-step magneto-immunoassay with the washing and detection steps integrated on-chip using the MP-dsSPCE. (b) MB confinement in the MP-dsSPCE fibres by the effect of the magnet. As it can be observed, MB remained in place even after extensive washing under flow conditions.

For magneto-immunoassay wash and detection integration on the MP-dsSPCE, part of the parameters that had been previously optimized were studied again, which were the measurement potential, the magnet location, and the way the mixture of sample and reagents was injected on the chip.

During the optimization of the measurement potential, and as it had been observed before, the currents registered increased as the measurement potential shifted to more

negative values, but the background noise raised as well (Figure 8.28a). As before, the best S/N ratios were attained at -0.05 V, which provided also the lowest LOD/LOQ.

On the other hand, and in contrast with the results obtained when only the detection was performed using the MP-dsSPCE, for integrated MB washing on-chip it was necessary to use a magnet closely attached to the chip surface in order to retain the MB near the WEs. Placing the magnet 1 mm apart produced lower currents and S/N, and MB were washed away if a magnet was not used at all (Figure 8.28b).

Finally, when solutions were pipetted directly on top of the MP-dsSPCE, they flowed relatively fast, which contributed to the low currents registered under flow measurement conditions. For this reason, a conical canal was incorporated between the electrochemical cell and the holder window. When the holder was closed, this canal facilitated solution positioning onto the electrodes, prevented liquid spreading, and ultimately resulted in the acquisition of higher currents and lower LOD/LOQ (Figure 8.28c).

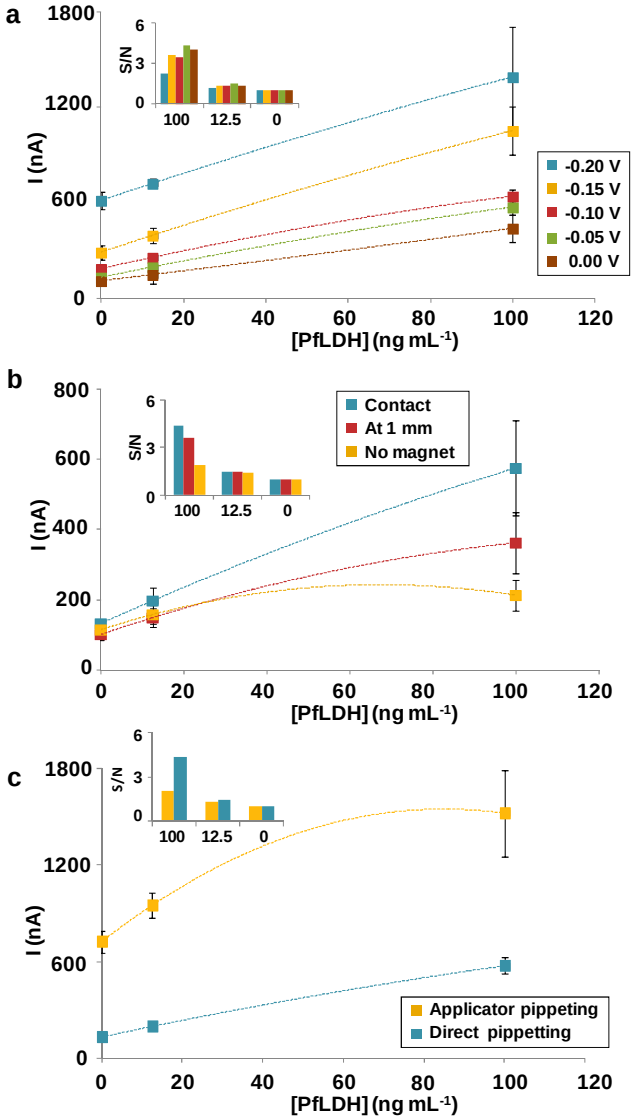

E (V)	(ng·mL^{-1}) LOD	LOQ
-0.20	19.74	69.55
-0.15	15.88	55.38
-0.10	15.52	57.17
-0.05	15.16	54.18
0.00	18.85	65.02

Magnet	(ng·mL^{-1}) LOD	LOQ
Contact	15.16	54.18
At 1 mm	15.83	64.32
No mag.	30.31	55.50

Magnet	(ng·mL^{-1}) LOD	LOQ
Direct pippeting	15.16	54.18
Aplicator pippeting	11.12	48.53

Figure 8.28. Optimization of conditions for MB on-chip integrated wash. a) Measurement potential. b) Magnet position. c) Sample injection.

Nevertheless, the new flow conditions produced also significantly higher background noise, which was attributed to worse MB washing efficiency. This issue was compensated by including a detergent in the one-step incubation buffer. As it can be observed in Figure 8.29a, carrying the assay in 1xRD supplemented with Tween 0.05% provided currents 3.5 times lower for the blanks than when preparing the samples in just 1xRD. In contrast, the currents registered in the samples containing PfLDH were comparable in both cases. As a result, the background noise was reduced, which contributed to improve the S/N, the LOD and LOQ, and the assay sensibility (slope).

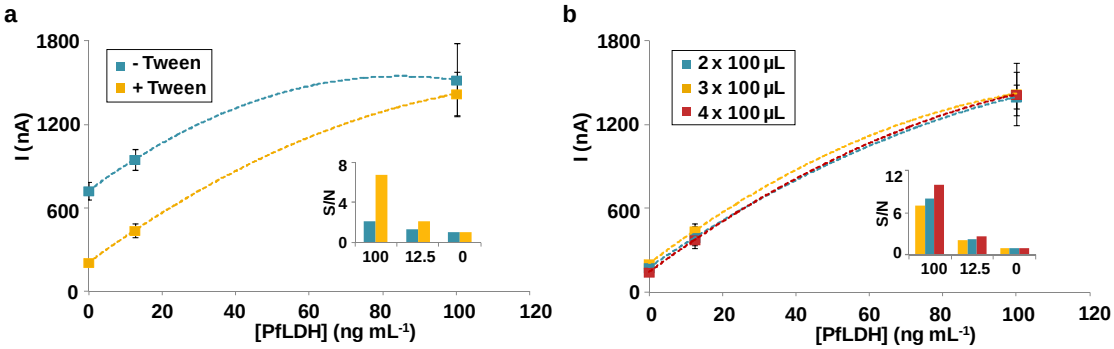

Assay incubation	(ng mL^{-1}) LOD	LOQ
- Tween	11.12	48.53
+ Tween	3.41	11.74

Washes	(ng mL^{-1}) LOD	LOQ
2x100 µL	3.41	11.74
3x100 µL	2.84	9.68
4x100 µL	2.51	8.55

Figure 8.29. Optimization of the assay conditions for PfLDH detection using the sample applicator on the MP-dsSPCE. a) Incubation buffer b) Number of washes performed.

Finally, the on-chip washing step was optimized by increasing the number of washing steps, and thus total volume of washing buffer used per sample (200 µL, 300 µL and 400 µL), always taking into account that the applicator maximal sample capacity was of 100 µL per wash (Figure 8.29b). Although the results obtained did not change drastically, four consecutive additions of washing buffer were the best condition to improve the S/N and achieve an LOD of 2.51 ng·mL^{-1} and LOQ of 8.55 ng·mL^{-1}, without a complex manipulation by the final user. It is worth noting that although the best performing commercial RDTs claim detection of down to 25 ng mL^{-1} of PfLDH, most available RDTs do not reach these numbers[385].

8.2.4. Detection of PfLDH in whole blood

The applicability of the magneto-immunosensor developed was assessed by studying its performance in whole blood. Whole blood samples were obtained in collection tubes containing anticoagulant in order to facilitate blood handling and storage. However, because blood thinners may interfere in assay performance[448], the potential effect of different anticoagulants on the one-step magneto-immunoassay was first examined. With this purpose, whole blood was obtained from a healthy individual using alternatively 3 different blood thinners (ethylenediaminetetraacetic acid (EDTA), acid-citrate-dextrose (ACD), and sodium heparin), or no anticoagulant at all. Each blood sample was then assayed using the one-step magneto-immunoassay, before and after spiking 100 ng mL^{-1} of PfLDH. As it can be observed, EDTA interfered in assay

performance and produced unacceptably high background noise. On the other hand, heparin-treated blood produced the lowest level of interference in the immunoassay, providing the signals and S/N ratios that better resembled those obtained in fresh blood without anticoagulant (Figure 8.30).

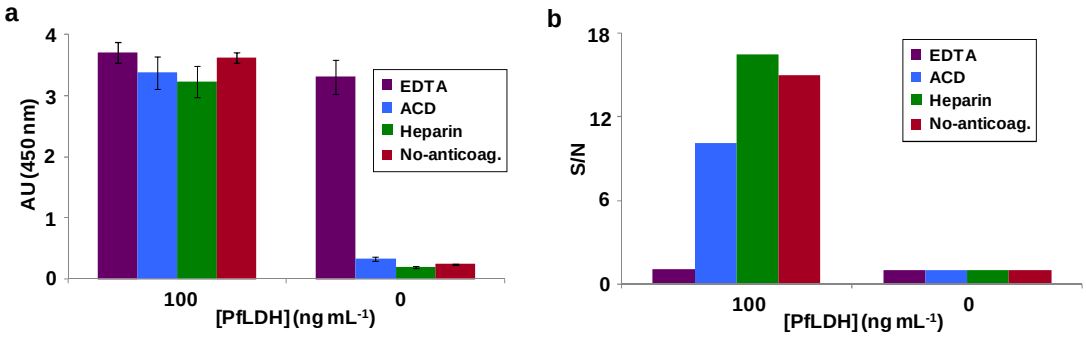

Figure 8.30. Effect of the anticoagulant in PfLDH detection using the one-step the magneto-immunoassay (a) signal acquired by spectrophotometry. (b) S/N ratio of (a).

8.2.4.1 Study of the matrix effect in control blood samples with inoculated PfLDH

In order to study the matrix effect with a highly complex sample during the magneto-immunoassay, MP-dsSPCE performance was determined in spiked human whole blood, obtained in BCT Heparin tubes. Immediately before the analysis, blood was lysed. RBC lysis released intracellular parasites, increasing the concentration of free PfLDH, but supplemented the sample with detergent and intracellular components and produced cell debris as well. When lysed blood was directly pipetted on the MP-dsSPCE, sample constituents were retained within the chip paper matrix that were not removed efficiently by on-chip washing, contributing to raise background noise and worsening the sensor LOD/LOQ. This drawback was solved by incorporating a filtration unit (Figure 8.31).

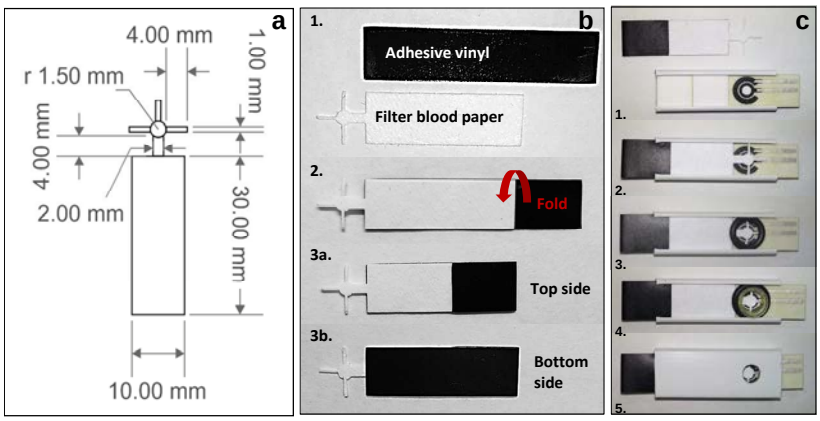

Figure 8.31. Design and performance of the blood filtration unit incorporated to the washing system. (a) Geometry and dimensions of the paper device. (b) Steps for the fabrication of the blood filtration device, including attachment of an adhesive vinyl to avoid solution cross-flow with the MP-dsSPCE and absorbent pad. (c) Steps for the assembly of the filter device with the MP-dsSPCE in the fluidic cartridge.

The device developed was a Fusion 5 strip (30 x10 mm), with a protruding star-like fringe. The latter included in the centre a circular section of similar diameter than the top WE. When placed onto the MP-dsSPCE, this section behaved as a MB retention zone and prevented sample entry through the orifice in the top WE into the MP-dsSPCE by directing the flow towards the main body of the filtration unit, which acted as both flow pump and waste container.

The applicability of the developed MP-dsSPCE was first tested in spiked lysed whole blood. For these experiments, pooled human blood was lysed for 5 min, was diluted 1:50 and 1:25 in PBST-BSA$_{1\%}$ and was spiked with increasing concentrations of PfLDH. Matrix interference in the electrochemical detection was prevented through two alternative strategies (Figure 8.32a).

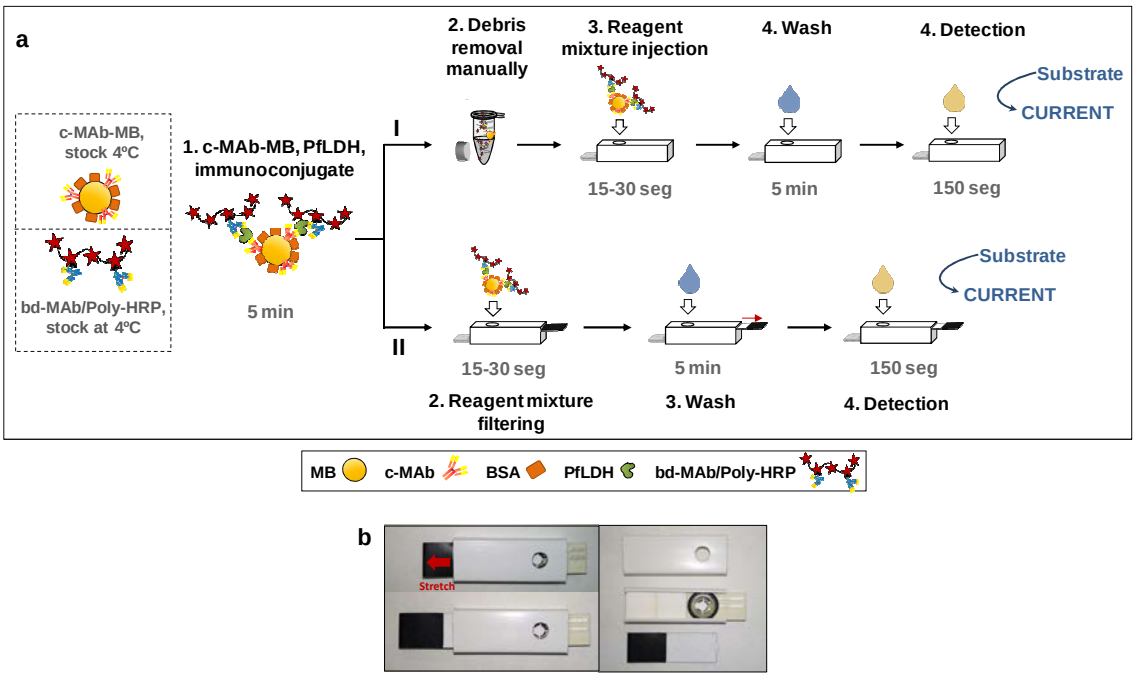

Figure 8.32. (a) Scheme of the alternatives tested for the on-chip washing and electrochemical detection of the PfLDH magneto-immunoassay performed in whole blood samples. (I) Manual debris removal before MB injection in the chip. (II) On-chip sample filtering by incorporating a paper filtration unit. (b) Performance of the filtration unit developed to filter the blood debris during the magneto-immunoassay with the MP-dsSPCE detection.

In the first case, after the 5-min incubation of sample, MB and reagents, the tubes were placed in the magnetic rack for MB confinement and the supernatant containing cell debris was removed. MB were then resuspended in 100 µL of PBS and were injected in

the MP-dsSPCE to perform the washes and the electrochemical detection on-chip. Alternatively, the mixture of sample, MB and reagents was directly pipetted on a MP-dsSPCE displaying a filtration unit. Once all the solution had been adsorbed, the filtration unit was pulled out, breaking the joint between the MB retention zone and the paper container, and on-chip washing and detection proceeded as before (Figure 8.32b).The currents registered for the different conditions evaluated were comparable for the range of PfLDH concentrations studied (Figure 8.33). However, the background noise increased proportionally to the matrix complexity. Accordingly, the assay S/N, LOD and sensitivity worsened (Figure 8.33b).

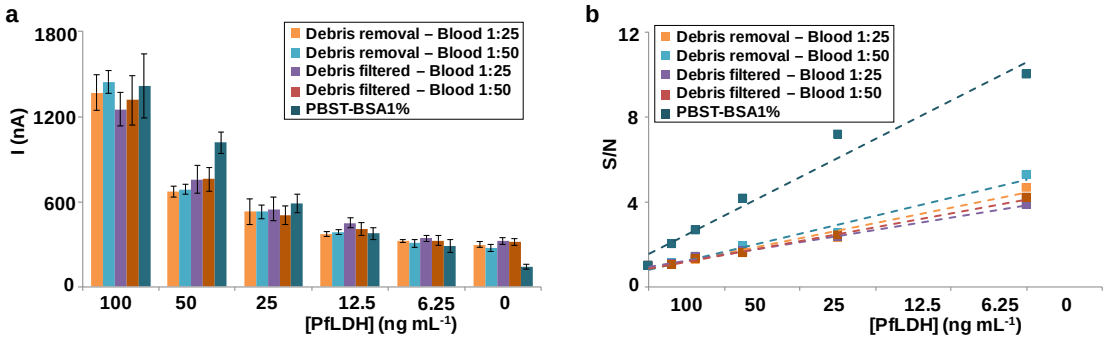

c

	Debris removal		Debris filtered		PBST-BSA1%
Blood dilution	**1:25**	**1:50**	**1:25**	**1:50**	
LOD (ng mL^{-1})	8.50	8.31	9.41	11.59	2.04
LOQ (ng mL^{-1})	25.74	26.40	29.23	31.49	8.38
Linear equation	0.036x + 0.834	0.042x + 0.836	0.027x + 0.939	0.032x + 0.864	0.098x + 1.000
R^2	0.977	0.979	0.997	0.995	0.949

Figure 8.33. (a) Signals registered by the sensor for increasing concentrations of PfLDH spiked in lysed whole blood (diluted 1:50 or 1:25). The excess of sample and reagents was removed alternatively using a magnetic rack previous to MB injection in the MP-dsSPCE, or by on-chip filtration using the filtration unit developed. (b) S/N ratio of (a). (c) Summary of S/N, fitting equations and LODs/LOQs of the assays in (a).

The sensor linear response spanned between 6.25 to 100 ng mL^{-1} in all cases, showing that the MP-dsSPCE could be used for the analysis of whole blood samples and that the filtration unit developed provided efficient sample pre-treatment with less handling than the classical approach. The sensor displayed an LOD of 9.41 ng mL^{-1} in lysed whole blood diluted 1:25, equivalent to a predilution PfLDH concentration of around 200 ng mL^{-1}, and quantitative detection in the whole detection range, which was comparable or better than the performance claimed for most RDTs detecting PfLDH.

8.2.4.2 PfLDH detection in cultured *Plasmodium*-infected RBC

The sensor was next employed for the study or cultured RBC, infected *in vitro* with controlled parasitemias of *P. falciparum* spanning between 0.0058% and 1.5% (equivalent to 340-87209 parasites μL^{-1}). For these assays, parasitemia was initially adjusted to 3% with 45% haematocrit and the culture was diluted serially with uninfected RBC. Parasitemia was confirmed by flow cytometry counting and by PCR. Previous to their analysis, these samples were lysed for 5 min and were diluted 1:25 in PBST-BSA 1%. The concentrations of PfLDH estimated by the MP-dsSPCE-based protocol correlated linearly with those provided by the ELISA and the magneto-immunosensor detected using classical washes in tubes and detection at commercial SPCE (positive lineal Pearson correlation coefficient of 0.97 and 0.99 respectively) (Figure 8.34a-b). As it can be observed, the MP-dsSPCE-based sensor detected PfLDH in the whole dilution series and the current registered increased proportionally to the concentration of parasite in the samples, displaying an LOD around 300 parasites·μL^{-1} (Figure 8.34c).

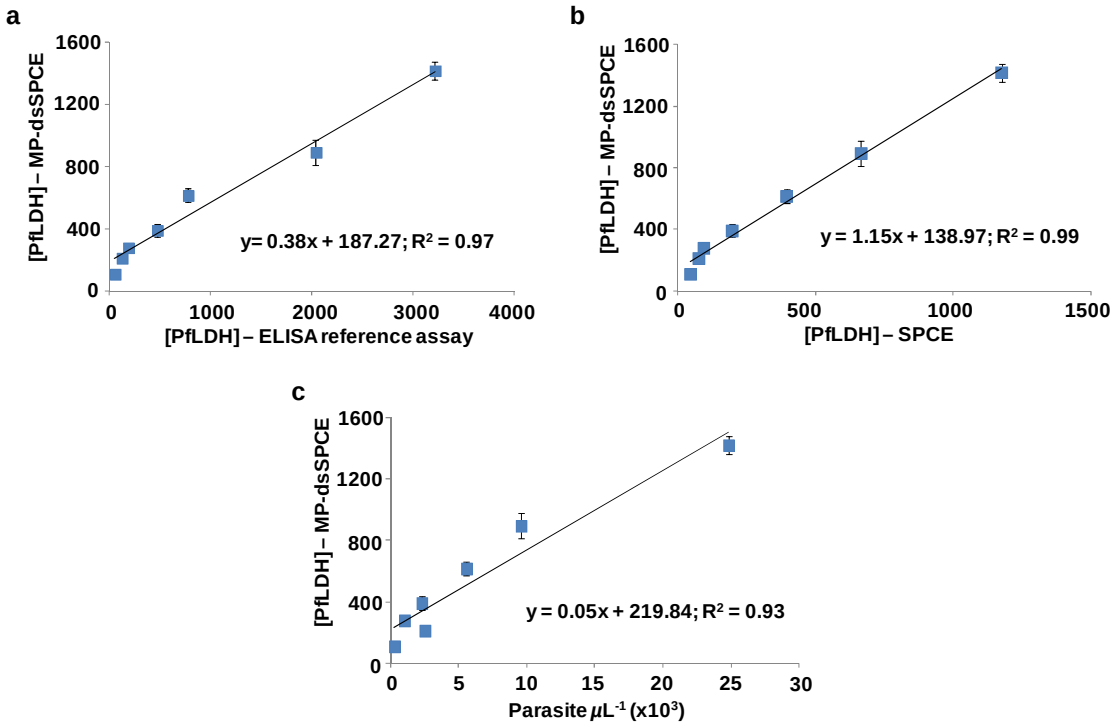

Figure 8.34. Plot of the concentrations of PfLDH estimated by the MP-dsSPCE correlated with those provided by the reference ELISA (a) and the magneto-immunosensor with washes in tube and detection at commercial SPCE (b). (c) Correlation between PfLDH concentrations detected with the MP-dsSPCE-based protocol versus the theoretical parasitemia density in the *Plasmodium* culture.

8.2.4.3 PfLDH detection in clinical blood samples

The sensor was finally employed to study 6 real blood samples, three obtained from patients infected with malaria and other 3 obtained from healthy volunteers. All samples were lysed for 5 min and diluted 1:25 before the analysis. As it can be observed in Figure 8.35, the currents registered for the two types of samples were below and above the LOD calculated for the sensor in spiked lysed whole blood, respectively. Although a higher number of samples will have to be tested in future, these results suggest that the assay and device developed here could provide PfLDH-based diagnosis of mid-to-high malaria parasitemias, with little handling by the used, LOD comparable or better that those exhibited by most RDTs, and quantitative detection over the whole assay range.

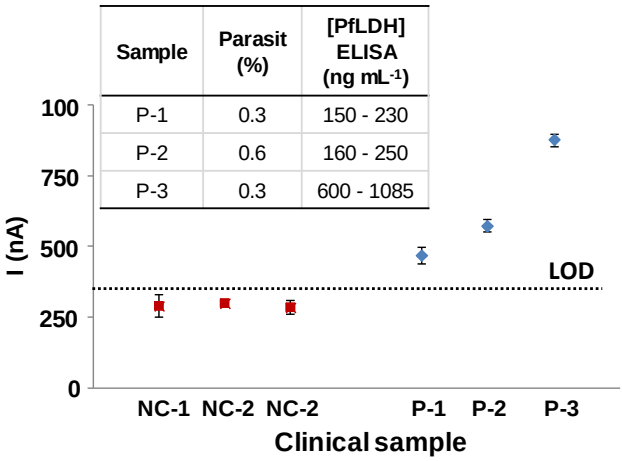

Figure 8.35. Detection of 3 clinical samples obtained from patients suffering malaria or from 3 healthy volunteers.

8.3. Conclusions

In this chapter, we accomplished two principal objectives. First, it has been demonstrated that electrochemical lateral flow devices can be produced entirely using screen-printing. The procedure reported here is based on a highly affordable manual process, showing that it is possible to manufacture highly customized devices without the need for costly infrastructure and resources. The use of screen-printing alone is also interesting, as the process can be easily adapted to a continuous manufacturing environment, and so the devices presented here can be mass-produced.

Second, it was shown that lateral flow electrode devices produced in this way can be exploited to simplify handling of immunomagnetic assays. Except for immunomagnetic binding, which entailed a 5-min incubation off-chip in a tube, washing and electrochemical detection could be performed on-chip. This involved significantly less intervention by the user than in conventional immunomagnetic assays, in which the tubes with MB are alternatively submitted to several cycles of MB magnetic concentration, supernatant removal and MB re-suspension before detection. These results suggest that the integration of new components in lateral flow electrode devices could be useful for the production of simple and economical electrochemical magneto-immunosensor POC devices, as reported here.

Chapter 9

Conclusions and future work

9. Conclusions and future work

This chapter presents the conclusions drawn from the work carried out and the results obtained along this PhD Thesis. The chapter finishes discussing the work in progress and some proposals of future work that would give continuity and strength to this research work.

9.1. General conclusions

The main aim of this PhD Thesis was to explore strategies that would allow exploiting MB for the development of POC diagnostic immunoassays. This ambition originated from the previous results obtained by the research group, which although having produced extremely efficient electrochemical magneto-immunosensors, had to accept that the protocols developed entailed too much handling to be carried out by poorly trained users. These observations were consistent with the state of the art, because the significant number of scientific articles having reported magneto-immunoassays and magneto-immunosensors did not seem to translate into the development of MB-based tools compatible with low-cost POCT. We hypothesised that this could be related to the fact that most of the magneto-immunoassays reported included in fact numerous serial MB washing and incubation steps. This entailed approaching and removing magnets along the whole protocol and concentrating and resuspending the MB several times, which was tedious, time consuming and an important source of result variability.

For this reason, the tasks planned originally for this PhD Thesis pursued accomplishing two types of objectives. The first one was the development of extremely fast and simple magneto-immunoassays and electrochemical magneto-immunosensors that could be performed by users minimally trained. The second one was designing an extremely simple and inexpensive single-use device that served to automate most of the steps of the magneto-immunoassay produced, providing magneto-immunoassay efficient operation with minimal user intervention.

In this context, and as a result of the tasks carried out along the Thesis in order to achieve the objectives raised in Chapter 1, some conclusions can be extracted that will be summarized next:

1. **MB are a useful tool to produce enhanced bioassays, often more sensitive and/or shorter than classical ELISA.** Here, a direct ELISA was optimized for MPO detection that took 3 h and generated an LOD of 4.87 ng mL^{-1}, which was successfully formatted into a 15-min magneto-immunoassay that had an LOD of 1.65 ng mL^{-1} (12 times faster and 3 times more sensitive). Sandwich multi-step magneto-immunoassays were also produced for MMP-9 and PLDH detection, which were 1.5 and 2.75 times faster and 3.75 and 3.7 times more sensitive than the corresponding ELISAs.

2. **Optimization of clue magneto-immunoassay parameters, and specifically MB agitation conditions, is crucial in order to achieve a more efficient and sensitive assay.** The results obtained confirmed the importance of the optimization of some well-known parameters for optimal assay performance, such as the amount of c-Ab, d-Ab and MB per sample, the different incubation times, or the number and conditions of the washing steps. Besides, the results revealed that the agitation conditions impelled to the mixture of sample and MB during the immunocapture had a profound effect on binding efficiency, and that an accurate balance between agitation strategy and sample volume had to be reached to achieve maximal target detection. For instance, fast vortexing provided extremely high analyte binding efficiency in small sample volumes (100 μL), but also high sample dispersion in the tubes and high result variability. In contrast, some rotation conditions seemed more reproducible, but needed larger sample volumes (>500 μL) to produce comparable capture levels. Focusing in the eventual integration of MB mixing strategies in a low-cost POCT device, these results suggested that a combination of vortexing-like fast agitation and mild rotation would be desirable.

3. **The signal enhancement produced by signal amplifiers can be exploited to optimize, not only ultrasensitive assays, but also fast and simple magneto-immunoassays, which can provide in 40 min results comparable to classical 5-h multi-step ELISAs.** The results confirmed that the careful selection of a highly specific and sensitive pair of Ab permitted immunoassay simplification by performing a single immunocapture with c-Ab, sample and d-Ab. As it has been shown, such simplified assay paths were as efficient as the original multi-step formats, but included less incubation and washing steps. However, one of

the main contributions of this PhD has been the observation that substituting the classical streptavidin-HRP labels by a Poly-HRP signal amplifier facilitated reducing the incubation times significantly without decreasing assay performance. These two issues combined allowed optimizing simplified 2-step magneto-immunoassays that were faster and easier to perform than the original 3-step alternatives and, although they displayed narrower linear ranges, provided LODs/LOQs of the same order than the reference ELISA assays.

Two examples were produce to corroborate this fact. A multi-step ELISA for MMP-9 detection that took >5 h was replaced by a 2-step magneto-immunoassay (5-min per incubation) that was performed in 40 min (including 20 min of incubation with the chromogenic TMB substrate solution). This assay achieved MMP-9 detection, a biomarker for ischemic stroke complications, with LOD of 3 pg mL^{-1}, LOQ of 20 pg mL^{-1}, and linear range spanning 15-1000 ng mL^{-1} (compared to the LOD of 5-15 pg mL^{-1}, LOQ of 13-40 pg mL^{-1}, and linear range between 30 and 500 displayed by the 5-h ELISA). In another case, a 2-step magneto-immunoassay (also 5-min incubation per immunocapture step) was developed for PfLDH detection in lysed whole blood samples, which exhibited a linear range of 0.4-12.5 ng mL^{-1}, LOD of 0.12 ng mL^{-1} and LOQ of 0.58 ng mL^{-1}, in less than 40 min (compared to the 5-h ELISA that was characterized by a linear range spanning 3.13-50 ng mL^{-1}, LODs between 0.116-0.138 ng mL^{-1} and LOQs between 0.369-0.679 ng mL^{-1}).

4. **The incorporation of immunomodified Poly-HRP and electrochemical detection to the simplified magneto-immunoassay path developed makes it possible the optimization of one-step electrochemical magneto-immunosensors that, although less sensitive, generate results in <15 min.** The production of Poly-HRP immunocojugates allowed reducing the magneto-immunoassay incubation steps to a single 5-min immunocapture of the sample with all the assay reagents (i.e., c-Ab-MB, bd-Ab/Poly-HRP and sample diluent). Two electrochemical one-step magneto-immunosensors have been developed for MMP-9 and PfLDH detection. In both cases, the implementation of electrochemical detection using a multiplexed magnetic holder granted real time detection in 8 SPCE at the same time, in less than 15 min. The MMP-9 magneto-immunosensor had an LOD of 13 pg mL^{-1}, LOQ of 70 pg mL^{-1} and

linear range of 0.2-2 ng mL^{-1}, and performed successfully in clinical plasma samples (diluted 1:250). In the case of the PfLDH magneto-immunosensor, it displayed LOD of 0.58 ng mL^{-1}, LOQ of 2.48 ng mL^{-1}, and linear range of 1.6 – 100 ng mL^{-1}, and was it was evaluated in lysed whole blood (final dilution 1:25).

5. **Paper microfluidics can be employed to replace the manual MB washes performed in tubes by on-chip capillary flow washes that entail less manipulation for the user.** MB concentration and washing using magnets is a tedious and demanding procedure that would be difficult to accomplish in a POC setting and/or by poorly trained personnel. Here, MB classical washes have been substituted by a paper-driven procedure performed on-chip that entailed less intervention of the user. In order to achieve this goal, a mobile multiplexed paper absorption pad was developed that was assembled in a multiplexed magnetic device to work in combination with commercial SPCE. The resulting electrochemical magneto-immunosensor with paper-driven washes detected MMP-9 in plasma samples in ~10 min, with linear response spanning 30 pg mL^{-1} - 2 ng mL^{-1}, assay sensitivity of 0.75 µA mL ng^{-1}, and LOD/LOQ of 0.01 and 0.09 ng mL^{-1}, respectively. It is worth noting that although in this example the magnetic and paper devices had to be manually repositioned along the protocol, the procedure was potentially automated, which would guarantee minimal user intervention.

6. **A novel type of microfluidic paper screen-printed carbon electrode (MP-SPCE) has been developed that has been exploited to simplify handling of magneto-immunoassays.** Two prototypes were fabricated by screen-printing using a highly affordable manual process that could be easily customized without the need for costly infrastructure and resources, but was also compatible with future mass production. The first one, used to detect MPO in serum in <13 min, with LOD of 0.18 ng mL^{-1}, LOQ of 0.62 ng mL^{-1} and linear range 25 – 8 ng mL^{-1}, served to demonstrate that MB wash and detection could be performed on-chip using a single-piece paper electrode device. The second upgraded prototype was produced by double-sided screen-printing in order to increase the WE active area and improve detection sensitivity. Furthermore, this MP-dsSPCE was integrated in a low-cost customized cartridge that contained as well all the components needed to perform on-chip most of the steps of the magneto-

immunoassay. This device was used to detect PfLDH with LOD of 9.41 ng mL^{-1}, LOQ of 29.23 ng mL^{-1} and linear range from 6.25 to 100 ng mL^{-1}, in less than 13 min, and was successfully tested in lysed whole blood samples.

7. **The protocols and devices developed have been tested in real diagnostic scenarios, showing that they are applicable to the study of liquid biological samples.** Although a larger number of clinical samples should be analysed, the results obtained suggested that the simplified magneto-immunoassays/sensor formats developed were applicable to the study of liquid clinical samples. In this respect, the most promising results were obtained with the PfLDH electrochemical magneto-immunosensor, which could detect malaria parasitemias above 0.01% in lysed whole blood diluted 1:25.

9.2. Work in progress and future perspectives

In spite of the results obtained along this PhD Thesis, the protocols and devices developed have displayed limitations as well. Specially, assay simplification and shortening has systematically derived in worsening of the assays LOD/LOQ, which limits protocol implementation. Besides, all the protocols relied on the detection of enzyme labels, which requires addition of an appropriate enzyme substrate, and the employment of bench-top measurement equipment, which are poorly compatible with POCT. With this aims in mind, four different future perspectives may be proposed in order to improve some aspects of the work carried out, and will briefly discussed next. Besides, future research lines could involve the development of miniaturized POC systems with automated sample acquisition and pre-treatment and MB mixing, washing and detection.

1. **Improvement of the sensitivity of the one-step magneto-immunosensors**

   The one-step magneto-immunosensors developed in this work reduced the total assay time by 4 times compared with the corresponding 2-step spectrophotometric magneto-immunoassays. However, it is true that the sensitivity achieved for the biomarkers detected (MMP-9 and PfLDH) was sacrificed. In both cases, the sensor LOD was 4 times below that obtained for the colorimetric 2-step counterpart.

A solution could be improving the immuno-functionalization of the MB, a strategy that is being currently explored. This part of the work is being focused in the improvemnet of cAb orientation and load on the MB surface during conjugation, and may contemplate in future the study of the comparative performance of additional types of MB from different providers.

2. **Improvement of the microfluidic-paper electrode device**

   The second version of MP-SPCE produced in this project registered currents 20 times higher than those obtained with the previous version. However, they were still lower than expected, which indicates that device design can be improved additionally to obtain results similar to those obtained when using a commercial SPCE. For this reason, the methodology of impression will be changed in future to inject-printing, which will facilitate a more versatile electrode re-design and production. In this way, paper devices with different electrode geometries and component distribution will be produced and evaluated, in order to achieve higher responses, better solution flow and integrated sample pre-treatment.

3. **Implementation of enzyme-less detection strategies**

   Until this moment, all the magneto-immunosensors produced in the context of this PhD Thesis used HRP/Poly-HRP enzymatic labels for detection. Nonetheless, it is well known that enzymatic detection has some drawbacks. On the one hand, detection requires incubating with an appropriate substrate so that the enzymatic reaction occurs. This extends the total assay time and implies adding a light- and temperature-sensitive reagent to the detection protocol. On the other hand, the detection of HRP/Poly-HRP in real samples could produce cross-reaction with peroxidases present in the blood and is negatively affected by the presence of some anticoagulants. Accordingly, two different alternative strategies are being explored and will be tested in future.

   One of the team membershas optimized a protocol for the electrochemical detection of AuNP. Contrary to most works reported previously, this protocol does not need acidic electrodissolution of the AuNPs and should be more convenient for POCT. The preliminary results displayed limited assay LOD/LOQ and performance in complex sample matrices compared to the use of Poly-HRP. This work is being currently extended in order to determine if

AuNPs could be employed in future as non-enzymatic labels in the simplified magneto-immunoassays reported here.

In a different approach, the group is collaborating with the Instrumentation and Communications Systems Research Group (Electronic and Biomedical Engineering Department, University of Barcelona, UB), who are developing a portable fluorescence measurement equipment for fast and sensitive POCT. One of the first prototypes has been validated in our laboratory by detecting a simplified PfLDH ELISA using in parallel the POC device and two commercial desktop fluorescence ELISA readers. The results obtained confirmed that the fluorescent detection contributed to improve the assay sensitivity, extending the linear range and reducing the detection time to 5 min. This detection strategy will be implemented in future in the magneto-immunoassays developed, in order to achieve better PfLDH detection than with the colorimetric and electrochemical detection paths. Non-enzymatic fluorescent labels, such as QD, may be assayed as well.

4. Implementation of hand-held measurement equipment

During this PhD Thesis, a collaboration was established with the Nanobioneginering and Bioelectronics Research Group (Electronic and Biomedical Engineering Department, UB), who have developed a low-cost, portable and miniaturized USB-based potentiostat for electrochemical POCT. This portable device was validated as part of this PhD work using commercial SPCE to detect different concentrations on HRP in a substrate solution. The results obtained were compared with those acquired with three different high-cost commercial potentiostats (μStat 8000 multipotentiostat, μStat 400 potentiostat and the CH Instruments 1030C multipotentiostat). The results obtained with this device were comparable to those obtained using the three commercial electrochemical systems (**Figure 9.1**; manuscript in preparation).

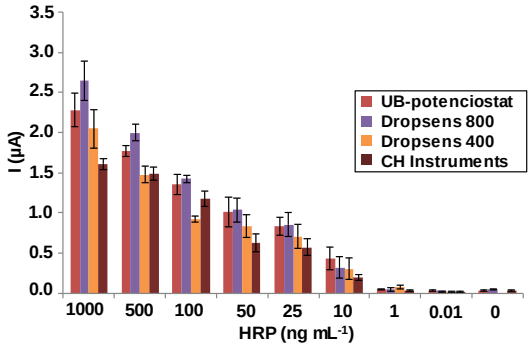

Figure 9.1. Comparison of the currents recorded for increasing concentrations of HRP spiked in a TMB-H_2O_2 commercial substrate solution with the different commercial potentiostats and the mini-potentiostat produced at the UB.

This platform will be the basis for the future development of a more compact detections system, with more functionalities, such as a more complex software, a Bluetooth or NFC communication module, and a rechargeable battery, in order to create a more flexible and portable device.

When the new prototype is developed, it will be tested with the improved magneto-immunosensor for PfLDH detection.

Bibliography

(1) da Silva, E. T. S. G.; Souto, D. E. P.; Barragan, J. T. C.; de F. Giarola, J.; de Moraes, A. C. M.; Kubota, L. T. Electrochemical Biosensors in Point-of-Care Devices: Recent Advances and Future Trends. *ChemElectroChem* **2017**, *4*, 778–794.

(2) Ríos, Á.; Zougagh, M.; Avila, M. Miniaturization through Lab-on-a-Chip: Utopia or Reality for Routine Laboratories? A Review. *Anal. Chim. Acta* **2012**, *740*, 1–11.

(3) Wen, W.; Yan, X.; Zhu, C.; Du, D.; Lin, Y. Recent Advances in Electrochemical Immunosensors. *Anal. Chem.* **2017**, *89*, 138–156.

(4) Justino, C. I. L.; Duarte, A. C.; Rocha-Santos, T. A. P. Critical Overview on the Application of Sensors and Biosensors for Clinical Analysis. *TrAC - Trends Anal. Chem.* **2016**, *85*, 36–60.

(5) Labib, M.; Sargent, E. H.; Kelley, S. O. Electrochemical Methods for the Analysis of Clinically Relevant Biomolecules. *Chem. Rev.* **2016**, *116*, 9001–9090.

(6) Wan, Y.; Su, Y.; Zhu, X.; Liu, G.; Fan, C. Development of Electrochemical Immunosensors towards Point of Care Diagnostics. *Biosens. Bioelectron.* **2013**, *47*, 1–11.

(7) Baldrich, E.; del Campo, F. J.; Muñoz, F. X. Biosensing at Disk Microelectrode Arrays. Inter-Electrode Functionalisation Allows Formatting into Miniaturised Sensing Platforms of Enhanced Sensitivity. *Biosens. Bioelectron.* **2009**, *25*, 920–926.

(8) Xu, Y.; Wang, E. Electrochemical Biosensors Based on Magnetic Micro/Nano Particles. *Electrochim. Acta* **2012**, *84*, 62–73.

(9) Goode, J. A.; Rushworth, J. V. H.; Millner, P. A. Biosensor Regeneration: A Review of Common Techniques and Outcomes. *Langmuir* **2015**, *31*, 6267–6276.

(10) Metters, J. P.; Kadara, R. O.; Banks, C. E. New Directions in Screen Printed Electroanalytical Sensors: An Overview of Recent Developments. *Analyst* **2011**, *136*, 1067–1076.

(11) Couto, R. A. S.; Lima, J. L. F. C.; Quinaz, M. B. Recent Developments, Characteristics and Potential Applications of Screen-Printed Electrodes in Pharmaceutical and Biological Analysis. *Talanta* **2016**, *146*, 801–814.

(12) Kuramitz, H. Magnetic Microbead-Based Electrochemical Immunoassays. *Anal. Bioanal. Chem.* **2009**, *394*, 61–69.

(13) Rocha-Santos, T. A. P. Sensors and Biosensors Based on Magnetic Nanoparticles. *TrAC - Trends Anal. Chem.* **2014**, *62*, 28–36.

(14) Xianyu, Y.; Wang, Q.; Chen, Y. Magnetic Particles-Enabled Biosensors for Point-of-Care Testing. *TrAC - Trends Anal. Chem.* **2018**, *106*, 213–224.

(15) Tangchaikeeree, T.; Polpanich, D.; Elaissari, A.; Jangpatarapongsa, K. Magnetic Particles for in Vitro Molecular Diagnosis: From Sample Preparation to Integration into Microsystems. *Colloids Surf. B* **2017**, *158*, 1–8.

(16) Herrasti, Z.; De La Serna, E.; Ruiz-Vega, G.; Baldrich, E. Developing Enhanced Magnetoimmunosensors Based on Low-Cost Screen-Printed Electrode Devices. *Rev. Anal. Chem.* **2016**, *35*, 53–58.

(17) Moral-Vico, J.; Barallat, J.; Abad, L.; Olivé-Monllau, R.; Muñoz-Pascual, F. X.; Galán Ortega, A.; del Campo, F. J.; Baldrich, E. Dual Chronoamperometric Detection of Enzymatic Biomarkers Using Magnetic Beads and a Low-Cost Flow Cell. *Biosens. Bioelectron.* **2015**, *69*, 328–336.

(18) Van Reenen, A.; De Jong, A. M.; Den Toonder, J. M. J.; Prins, M. W. J. Integrated Lab-on-Chip Biosensing Systems Based on Magnetic Particle Actuation-a Comprehensive Review. *Lab Chip* **2014**, *14*, 1966–1986.

(19) Laczka, O.; Maesa, J. M.; Godino, N.; del Campo, J.; Fougt-Hansen, M.; Kutter, J. P.; Snakenborg, D.; Muñoz-Pascual, F. X.; Baldrich, E. Improved Bacteria Detection by Coupling Magneto-Immunocapture and Amperometry at Flow-Channel Microband Electrodes. *Biosens. Bioelectron.* **2011**, *26*, 3633–3640.

(20) Cortina, M. E.; Melli, L. J.; Roberti, M.; Mass, M.; Longinotti, G.; Tropea, S.; Lloret, P.; Serantes, D. A. R.; Salomón, F.; Lloret, M.; et al. Electrochemical Magnetic Microbeads-Based Biosensor for Point-of-Care Serodiagnosis of Infectious Diseases. *Biosens. Bioelectron.* **2016**, *80*, 24–33.

(21) Regiart, M.; Fernández-Baldo, M. A.; Spotorno, V. G.; Bertolino, F. A.; Raba, J. Ultra Sensitive Microfluidic Immunosensor for Determination of Clenbuterol in Bovine Hair Samples Using Electrodeposited Gold Nanoparticles and Magnetic Micro Particles as Bio-Affinity Platform. *Biosens. Bioelectron.* **2013**, *41*, 211–217.

(22) Jamshaid, T.; Neto, E. T. T.; Eissa, M. M.; Zine, N.; Kunita, M. H.; El-Salhi, A. E.; Elaissari, A. Magnetic Particles: From Preparation to Lab-on-a-Chip, Biosensors, Microsystems and Microfluidics Applications. *TrAC - Trends Anal. Chem.* **2016**, *79*, 344–362.

(23) Maxwell, E. J.; Mazzeo, A. D.; Whitesides, G. M. Paper-Based Electroanalytical Devices for Accessible Diagnostic Testing. *MRS Bull.* **2013**, *38*, 309–314.

(24) Yetisen, A. K.; Akram, M. S.; Lowe, C. R. Paper-Based Microfluidic Point-of-Care Diagnostic Devices. *Lab Chip* **2013**, *13*, 2210–2251.

(25) Byrnes, S.; Thiessen, G.; Fu, E. Progress in the Development of Paper-Based Diagnostics for Low-Resource Point-of-Care Settings. *Bioanalysis* **2013**, *5*, 2821–2836.

(26) Economou, A.; Kokkinos, C.; Prodromidis, M. Flexible Plastic, Paper and Textile Lab-on-a Chip Platforms for Electrochemical Biosensing. *Lab Chip* **2018**, *18*, 1812–1830.

(27) Syedmoradi, L.; Daneshpour, M.; Alvandipour, M.; Gomez, F. A.; Hajghassem, H.; Omidfar, K. Point of Care Testing: The Impact of Nanotechnology. *Biosens.*

Bioelectron. **2017**, *87*, 373–387.

(28) Consden, R.; Gordon, A. H.; Martin, A. J. C.-1258072 E. T.-1944/01/01. Qualitative Analysis of Proteins: A Partition Chromatographic Method Using Paper. *Biochem J* **1944**, *38*, 224–232.

(29) Luntz, G. A Simple Quick Test for Glucose in Urine Report on Use of Clinistix. *Br. Med. J.* **1957**, *1*, 499–500.

(30) Teles, F. S. R. R.; De Tavora Tavira, L. A. P.; Da Fonseca, L. J. P. Biosensors as Rapid Diagnostic Tests for Tropical Diseases. *Crit. Rev. Clin. Lab. Sci.* **2010**, *47*, 139–169.

(31) Wong, R.; Tse, H. *Lateral Flow Immunoassay*, 1st ed.; Humana Press, Ed.; Springer Science + Business Media: New York, NY 10013, 2009.

(32) de Puig, H.; Bosch, I.; Gehrke, L.; Hamad-Schifferli, K. Challenges of the Nano–Bio Interface in Lateral Flow and Dipstick Immunoassays. *Trends Biotechnol.* **2017**, *35*, 1169–1180.

(33) Morbioli, G. G.; Mazzu-Nascimento, T.; Stockton, A. M.; Carrilho, E. Technical Aspects and Challenges of Colorimetric Detection with Microfluidic Paper-Based Analytical Devices (MPADs) - A Review. *Anal. Chim. Acta* **2017**, *970*, 1–22.

(34) Kosack, C. S.; Page, A. L.; Klatser, P. R. A Guide to Aid the Selection of Diagnostic Tests. *Bull. World Health Organ.* **2017**, *95*, 639–645.

(35) Mak, W. C.; Beni, V.; Turner, A. P. F. Lateral-Flow Technology: From Visual to Instrumental. *TrAC - Trends Anal. Chem.* **2016**, *79*, 297–305.

(36) Connolly, R.; O' Kennedy, R. Magnetic Lateral Flow Immunoassay Test Strip Development – Considerations for Proof of Concept Evaluation. *Methods* **2017**, *116*, 132–140.

(37) Zhan, L.; Guo, S. Z.; Song, F.; Gong, Y.; Xu, F.; Boulware, D. R.; McAlpine, M. C.; Chan, W. C. W.; Bischof, J. C. The Role of Nanoparticle Design in Determining Analytical Performance of Lateral Flow Immunoassays. *Nano Lett.* **2017**, *17*, 7207–7212.

(38) Ahmed, S.; Bui, M. P. N.; Abbas, A. Paper-Based Chemical and Biological Sensors: Engineering Aspects. *Biosens. Bioelectron.* **2016**, *77*, 249–263.

(39) Akyazi, T.; Basabe-Desmonts, L.; Benito-Lopez, F. Review on Microfluidic Paper-Based Analytical Devices towards Commercialisation. *Anal. Chim. Acta* **2018**, *1001*, 1–17.

(40) Yager, P.; Domingo, G. J.; Gerdes, J. Point-of-Care Diagnostics for Global Health. *Annu. Rev. Biomed. Eng.* **2008**, *10*, 107–144.

(41) Mabey, D.; Peeling, R. W.; Ustianowski, A.; Perkins, M. D. Diagnostics for the Developing World. *Nat. Rev. Microbiol.* **2004**, *2*, 231–240.

(42) Wang, S.; Lifson, M. A.; Inci, F.; Liang, L. G.; Sheng, Y. F.; Demirci, U.

Advances in Addressing Technical Challenges of Point-of-Care Diagnostics in Resource-Limited Settings. *Expert Rev. Mol. Diagn.* **2016**, *16*, 449–459.

(43) Drain, P. K.; Hyle, E. P.; Noubary, F.; Freedberg, K. A.; Wilson, D.; Bishai, W. R.; Rodriguez, W.; Bassett, I. V. Diagnostic Point-of-Care Tests in Resource-Limited Settings. *Lancet Infect. Dis.* **2014**, *14*, 239–249.

(44) Zarei, M. Advances in Point-of-Care Technologies for Molecular Diagnostics. *Biosens. Bioelectron.* **2017**, *98*, 494–506.

(45) Wang, P.; Kricka, L. J. Current and Emerging Trends in Point-of-Care Technology and Strategies for Clinical Validation and Implementation. *Clin. Chem.* **2018**, *64*, 1439–1452.

(46) Zarei, M. Portable Biosensing Devices for Point-of-Care Diagnostics: Recent Developments and Applications. *TrAC, Trends Anal. Chem* **2017**, *91*, 26–41.

(47) Vashist, S. K. Point-of-Care Diagnostics: Recent Advances and Trends. *Biosensors* **2017**, *7*, 62.

(48) Gous, N.; Boeras, D. I.; Cheng, B.; Takle, J.; Cunningham, B.; Peeling, R. W. The Impact of Digital Technologies on Point-of-Care Diagnostics in Resource-Limited Settings. *Expert Rev. Mol. Diagn* **2018**, *18*, 385–397.

(49) Gubala, V.; Harris, L. F.; Ricco, A. J.; Tan, M. X.; Williams, D. E. Point of Care Diagnostics: Status and Future. *Anal. Chem.* **2012**, *84*, 487–515.

(50) Luppa, P. B.; Müller, C.; Schlichtiger, A.; Schlebusch, H. Point-of-Care Testing (POCT): Current Techniques and Future Perspectives. *TrAC, Trends Anal. Chem* **2011**, *30*, 887–898.

(51) Kost, G. J.; Tran, N. K.; Louie, R. F. Point-of-Care Testing: Principles, Practice, and Critical-Emergency-Disaster Medicine. In *Encyclopedia of Analytical Chemistry*; John Wiley & Sons, 2008.

(52) Koumantakis, G.; Watkinson, L. Contribution of Industry to PoCT Implementation. *Clin. Biochem. Rev.* **2010**, *31*, 89–91.

(53) Chen, H.; Liu, K.; Li, Z.; Wang, P. Point of Care Testing for Infectious Diseases. *Clin. Chim. Acta* **2019**, *493*, 138–147.

(54) Shandilya, R.; Bhargava, A.; Bunkar, N.; Tiwari, R.; Goryacheva, I. Y.; Mishra, P. K. Nanobiosensors: Point-of-Care Approaches for Cancer Diagnostics. *Biosens. Bioelectron.* **2019**, *130*, 14–165.

(55) Christodouleas, D. C.; Kaur, B.; Chorti, P. From Point-of-Care Testing to EHealth Diagnostic Devices (EDiagnostics). *ACS Cent. Sci.* **2018**, *4*, 1600–1616.

(56) Infoholic Research. *POINT-OF-CARE DIAGNOSTICS MARKET*; 2018.

(57) Global Intellegence Alliance. *Healthcare/Medical Simulation Market– Trends & Global Forecasts To 2017*; Northbrook, IL, 2013.

(58) Land, K. J.; Boeras, D. I.; Chen, X. S.; Ramsay, A. R.; Peeling, R. W. REASSURED Diagnostics to Inform Disease Control Strategies, Strengthen

Health Systems and Improve Patient Outcomes. *Nat. Microbiol.* **2019**, *4*, 46–54.

(59) Wu, G.; Zaman, M. H. Low-Cost Tools for Diagnosing and Monitoring HIV Infection in Low-Resource Settings. *Bull. World Health Organ.* **2015**, *90*, 914–920.

(60) Nayak, S.; Blumenfeld, N. R.; Laksanasopin, T.; Sia, S. K. Point-of-Care Diagnostics: Recent Developments in a Connected Age. *Anal. Chem.* **2017**, *89*, 102–123.

(61) Kanchi, S.; Sabela, M. I.; Mdluli, P. S.; Inamuddin; Bisetty, K. Smartphone Based Bioanalytical and Diagnosis Applications: A Review. *Biosens. Bioelectron.* **2018**, *102*, 136–149.

(62) Gagnon, M. P.; Ngangue, P.; Payne-Gagnon, J.; Desmartis, M. M-Health Adoption by Healthcare Professionals: A Systematic Review. *J. Am. Med. Informatics Assoc.* **2016**, *23*, 212–220.

(63) Geng, Z.; Zhang, X.; Fan, Z.; Lv, X.; Su, Y.; Chen, H. Recent Progress in Optical Biosensors Based on Smartphone Platforms. *Sensors* **2017**, *17*, 2449.

(64) Meng, X.; Huang, H.; Yan, K.; Tian, X.; Yu, W.; Cui, H.; Kong, Y.; Xue, L.; Liu, C.; Wang, S. Smartphone Based Hand-Held Quantitative Phase Microscope Using the Transport of Intensity Equation Method. *Lab Chip* **2017**, *17*, 104–109.

(65) Kim, S. C.; Jalal, U. M.; Im, S. B.; Ko, S.; Shim, J. S. A Smartphone-Based Optical Platform for Colorimetric Analysis of Microfluidic Device. *Sensors Actuators, B Chem.* **2017**, *239*, 52–59.

(66) Wang, X.; Chang, T. W.; Lin, G.; Gartia, M. R.; Liu, G. L. Self-Referenced Smartphone-Based Nanoplasmonic Imaging Platform for Colorimetric Biochemical Sensing. *Anal. Chem.* **2017**, *89*, 611–615.

(67) Choi, S. Powering Point-of-Care Diagnostic Devices. *Biotechnol. Adv.* **2016**, *34*, 321–330.

(68) Wen, W.; Yan, X.; Zhu, C.; Du, D.; Lin, Y. Recent Advances in Electrochemical Immunosensors. *Anal. Chem.* **2017**, *89*, 138–156.

(69) Guo, J. Smartphone-Powered Electrochemical Dongle for Point-of-Care Monitoring of Blood β-Ketone. *Anal. Chem.* **2017**, *89*, 8609–8613.

(70) Smith, S.; Korvink, J. G.; Mager, D.; Land, K. The Potential of Paper-Based Diagnostics to Meet the ASSURED Criteria. *RSC Adv.* **2018**, *8*, 34012–34034.

(71) Mak, W. C.; Beni, V.; Turner, A. P. F. Lateral-Flow Technology: From Visual to Instrumental. *TrAC - Trends Anal. Chem.* **2016**, *79*, 297–305.

(72) Koczula, K. M.; Gallotta, A. Lateral Flow Assays. *Essays Biochem.* **2016**, *60*, 111–120.

(73) Yamada, K.; Shibata, H.; Suzuki, K.; Citterio, D. Toward Practical Application of Paper-Based Microfluidics for Medical Diagnostics: State-of-the-Art and Challenges. *Lab Chip* **2017**, *17*, 1206–1249.

(74) Wang, K.; Qin, W.; Hou, Y.; Xiao, K.; Yan, W. The Application of Lateral Flow Immunoassay in Point of Care Testing: A Review. *Nano Biomed. Eng.* **2016**, *8*, 172–183.

(75) Morbioli, G. G.; Mazzu-Nascimento, T.; Stockton, A. M.; Carrilho, E. Technical Aspects and Challenges of Colorimetric Detection with Microfluidic Paper-Based Analytical Devices (MPADs) - A Review. *Anal. Chim. Acta* **2017**, *970*, 1–22.

(76) McPartlin, D. A.; O'Kennedy, R. J. Point-of-Care Diagnostics, a Major Opportunity for Change in Traditional Diagnostic Approaches: Potential and Limitations. *Expert Rev. Mol. Diagn.* **2014**, *14*, 979–998.

(77) Sher, M.; Zhuang, R.; Demirci, U.; Asghar, W. Paper-Based Analytical Devices for Clinical Diagnosis: Recent Advances in the Fabrication Techniques and Sensing Mechanisms. *Expert Rev. Mol. Diagn.* **2017**, *17*, 351–366.

(78) Hu, J.; Wang, S. Q.; Wang, L.; Li, F.; Pingguan-Murphy, B.; Lu, T. J.; Xu, F. Advances in Paper-Based Point-of-Care Diagnostics. *Biosens. Bioelectron.* **2014**, *54*, 585–597.

(79) Dekker, S.; Buesink, W.; Blom, M.; Alessio, M.; Verplanck, N.; Hihoud, M.; Dehan, C.; César, W.; Le Nel, A.; van den Berg, A.; et al. Standardized and Modular Microfluidic Platform for Fast Lab on Chip System Development. *Sensors Actuators, B Chem.* **2018**, *272*, 468–478.

(80) Becker, H.; Gärtner, C. Microfluidics-Enabled Diagnostic Systems: Markets, Challenges, and Examples. In *Microchip Diagnostics. Methods in Molecular Biology*; Taly V., Viovy JL., D. S., Ed.; Humana Press: New York, NY, 2017; pp 3–21.

(81) Sonker, M.; Sahore, V.; Woolley, A. T. Recent Advances in Microfluidic Sample Preparation and Separation Techniques for Molecular Biomarker Analysis: A Critical Review. *Anal. Chim. Acta* **2017**, *986*, 1–11.

(82) Pandey, C. M.; Augustine, S.; Kumar, S.; Kumar, S.; Nara, S.; Srivastava, S.; Malhotra, B. D. Microfluidics Based Point-of-Care Diagnostics. *Biotechnol. J.* **2018**, *13*, 1700047.

(83) Chiu, D. T.; DeMello, A. J.; Di Carlo, D.; Doyle, P. S.; Hansen, C.; Maceiczyk, R. M.; Wootton, R. C. R. Small but Perfectly Formed? Successes, Challenges, and Opportunities for Microfluidics in the Chemical and Biological Sciences. *Chem* **2017**, *2*, 201–223.

(84) Chin, C. D.; Laksanasopin, T.; Cheung, Y. K.; Steinmiller, D.; Linder, V.; Parsa, H.; Wang, J.; Moore, H.; Rouse, R.; Umviligihozo, G.; et al. Microfluidics-Based Diagnostics of Infectious Diseases in the Developing World. *Nat. Med.* **2011**, *17*, 1015–1019.

(85) Laksanasopin, T.; Guo, T. W.; Nayak, S.; Sridhara, A. A.; Xie, S.; Olowookere, O. O.; Cadinu, P.; Meng, F.; Chee, N. H.; Kim, J.; et al. A Smartphone Dongle for Diagnosis of Infectious Diseases at the Point of Care. *Sci. Transl. Med.* **2015**, *7*, 273re1.

(86) Martin, C. L. I-STAT – Combining Chemistry and Haematology in PoCT. *Clin. Biochem Rev.* **2010**, *31*, 81–84.

(87) Liu, Y.; Jiang, X. Why Microfluidics? Merits and Trends in Chemical Synthesis. *Lab Chip* **2017**, *17*, 3960–3978.

(88) Caicedo, H. H.; Brady, S. T. Microfluidics: The Challenge Is to Bridge the Gap Instead of Looking for a "Killer App." *Trends Biotechnol.* **2016**, *34*, 1–3.

(89) Pashchenko, O.; Shelby, T.; Banerjee, T.; Santra, S. A Comparison of Optical, Electrochemical, Magnetic, and Colorimetric Point-of-Care Biosensors for Infectious Disease Diagnosis. *ACS Infect. Dis.* **2018**, *4*, 1162–1178.

(90) Vasan, A. S. S. Point-of-Care Biosensor System. *Front. Biosci.* **2012**, *1*, 39–71.

(91) Kokkinos, C.; Economou, A.; Prodromidis, M. I. Electrochemical Immunosensors: Critical Survey of Different Architectures and Transduction Strategies. *TrAC - Trends Anal. Chem.* **2016**, *79*, 88–105.

(92) Bettazzi, F.; Marrazza, G.; Minunni, M.; Palchetti, I.; Scarano, S. Biosensors and Related Bioanalytical Tools. In *Comprehensive Analytical Chemistry*; 2017; pp 1–33.

(93) Kirsch, J.; Siltanen, C.; Zhou, Q.; Revzin, A.; Simonian, A. Biosensor Technology: Recent Advances in Threat Agent Detection and Medicine. *Chem. Soc. Rev.* **2013**, *42*, 8733–8768.

(94) Kaushik, A.; Mujawar, M. A. Point of Care Sensing Devices: Better Care for Everyone. *Sensors* **2018**, *18*, 4303.

(95) Chen, S.; Shamsi, M. H. Biosensors-on-Chip: A Topical Review. *J. Micromech. Microeng.* **2017**, *27*, 083001.

(96) Anik, U. Electrochemical Medical Biosensors for POC Applications. In *Medical Biosensors for Point of Care (POC) Applications*; Elsevier Ltd, 2016; pp 275–292.

(97) Hammond, J. L.; Formisano, N.; Estrela, P.; Carrara, S.; Tkac, J. Electrochemical Biosensors and Nanobiosensors. *Essays Biochem.* **2016**, *60*, 69–80.

(98) Lakshmipriya, T.; Gopinath, S. C. B. 1 - An Introduction to Biosensors and Biomolecules. In *Nanobiosensors for Biomolecular Targeting*; Gopinath, S. C. B., Lakshmipriya, T., Eds.; Micro and Nano Technologies; Elsevier, 2019; pp 1–21.

(99) Ding, E. Y. J. and S.-N. Recent Advances on Electrochemical Enzyme Biosensors. *Curr. Anal. Chem.* **2016**, *12*, 5–21.

(100) Zhang, L.; Gu, C.; Ma, H.; Zhu, L.; Wen, J.; Xu, H.; Liu, H.; Li, L. Portable Glucose Meter: Trends in Techniques and Its Potential Application in Analysis. *Anal. Bioanal. Chem.* **2019**, *411*, 21–36.

(101) Veloso, A. J.; Cheng, X. R.; Kerman, K. 1 - Electrochemical Biosensors for Medical Applications. In *Biosensors for Medical Applications*; Higson, S., Ed.;

Woodhead Publishing Series in Biomaterials; Woodhead Publishing, 2012; pp 3–40.

(102) Bahadir, E. B.; Sezgintürk, M. K. Electrochemical Biosensors for Hormone Analyses. *Biosens. Bioelectron.* **2015**, *68*, 62–71.

(103) Ronkainen, N. J.; Halsall, H. B.; Heineman, W. R. Electrochemical Biosensors. *Chem. Soc. Rev.* **2010**, *39*, 1747.

(104) Bakker, E.; Pretsch, E. Potentiometric Sensors for Trace-Level Analysis. *TrAC - Trends Anal. Chem.* **2005**, *24*, 199–207.

(105) Brett, C. M. A.; Oliveira-Brett, A. M. Electrochemical Sensing in Solution-Origins, Applications and Future Perspectives. *J. Solid State Electrochem.* **2011**, *15*, 1487–1494.

(106) Cecchetto, J.; Carvalho, F. C.; Santos, A.; Fernandes, F. C. B.; Bueno, P. R. An Impedimetric Biosensor to Test Neat Serum for Dengue Diagnosis. *Sensors Actuators, B Chem.* **2015**, *213*, 150–154.

(107) Bahadir, E. B.; Sezgintürk, M. K. A Review on Impedimetric Biosensors. *Artif. Cells, Nanomedicine Biotechnol.* **2016**, *44*, 248–262.

(108) Elgrishi, N.; Rountree, K. J.; McCarthy, B. D.; Rountree, E. S.; Eisenhart, T. T.; Dempsey, J. L. A Practical Beginner's Guide to Cyclic Voltammetry. *J. Chem. Educ.* **2018**, *95*, 197–206.

(109) Inzelt, G. Pseudo-Reference Electrodes. In *Handbook of Reference Electrodes*; 2013; pp 331–332.

(110) Grieshaber, D.; MacKenzie, R.; Vörös, J.; Reimhult, E. Electrochemical Biosensors - Sensor Principles and Architectures. *Sensors* **2008**, *8*, 1400–1458.

(111) Yamanaka, K.; Vestergaard, M. C.; Tamiya, E. Printable Electrochemical Biosensors: A Focus on Screen-Printed Electrodes and Their Application. *Sensors* **2016**, *16*, 1761.

(112) Abdulbari, H.; Basheer, E. Electrochemical Biosensors: Electrode Development, Materials, Design, and Fabrication. *ChemBioEng Rev.* **2017**, *4*, 92–105.

(113) Serafín, V.; Martínez-García, G.; Aznar-Poveda, J.; Lopez-Pastor, J. A.; Garcia-Sanchez, A. J.; Garcia-Haro, J.; Campuzano, S.; Yáñez-Sedeño, P.; Pingarrón, J. M. Determination of Progesterone in Saliva Using an Electrochemical Immunosensor and a COTS-Based Portable Potentiostat. *Anal. Chim. Acta* **2019**, *1049*, 65–73.

(114) Cinti, S.; Arduini, F. Graphene-Based Screen-Printed Electrochemical (Bio)Sensors and Their Applications: Efforts and Criticisms. *Biosens. Bioelectron.* **2017**, *89*, 107–122.

(115) Taleat, Z.; Khoshroo, A.; Mazloum-Ardakani, M. Screen-Printed Electrodes for Biosensing: A Review (2008-2013). In *Microchimica Acta*; 2014; pp 865–891.

(116) Cate, D. M.; Adkins, J. A.; Mettakoonpitak, J.; Henry, C. S. Recent

Developments in Paper-Based Microfluidic Devices. *Anal. Chem.* **2015**, *87*, 19–41.

(117) Chu, Z.; Peng, J.; Jin, W. Advanced Nanomaterial Inks for Screen-Printed Chemical Sensors. *Sensors Actuators, B Chem.* **2017**, *243*, 919–926.

(118) Khan, F. *The Elements Of Immunology*; Pearson Education: Delhi; Upper Saddle River, N.J, 2009.

(119) Konstantinou, G. N. Enzyme-Linked Immunosorbent Assay (ELISA). In *Methods in Molecular Biology*; 2017; pp 79–94.

(120) Omidfar, K.; Khorsand, F.; Darziani Azizi, M. New Analytical Applications of Gold Nanoparticles as Label in Antibody Based Sensors. *Biosens. Bioelectron.* **2013**, *43*, 336–347.

(121) Key, M. *Immunohistochemistry Staining Methods*, Sixth edit.; Dako Denmark A/S, An Agilent Technologies Company: Denmark, 2006.

(122) Nistor, C.; Emnéus, J. Chapter 9 Immunoassay: Potentials and Limitations. In *Biosensors and Modern Biospecific Analytical Techniques*; Comprehensive Analytical Chemistry; Elsevier, 2005; Vol. 44, pp 375–427.

(123) Gubala, V.; Klein, R.; Templeton, D. M.; Schwenk, M. Immunodiagnostics and Immunosensor Design. *Pure Appl. Chem.* **2014**, *86*, 1539–1571.

(124) Grange, R. D.; Thompson, J. P.; Lambert, D. G.; Mahajan, R. P. Radioimmunoassay, Enzyme and Non-Enzyme-Based Immunoassays. *Br. J. Anaesth.* **2014**, *112*, 213–216.

(125) Wild, D.; Kodak, E. *The Immunoassay Handbook*; Wild, D., Ed.; Elsevier Science, 2013.

(126) Gan, S. D.; Patel, K. R. Enzyme Immunoassay and Enzyme-Linked Immunosorbent Assay. *J. Invest. Dermatol.* **2013**, *133*, 1–3.

(127) A Arugula, M.; Simonian, A. Novel Trends in Affinity Biosensors: Current Challenges and Perspectives. *Meas. Sci. Technol.* **2014**, *25*, 32001.

(128) Pingarrón, J.; Campuzano, S.; González-Cortés, A.; Yáñez-Sedeño, P. Electrochemical Immunosensors for Clinical Diagnostics. In *Reference Module in Chemistry, Molecular Sciences and Chemical Engineering*; 2017; pp 359–414.

(129) Wang, J. Electrochemical Biosensors: Towards Point-of-Care Cancer Diagnostics. *Biosens. Bioelectron.* **2006**, *21*, 1887–1892.

(130) Felix, F. S.; Angnes, L. Electrochemical Immunosensors – A Powerful Tool for Analytical Applications. *Biosens. Bioelectron.* **2018**, *102*, 470–478.

(131) Karunakaran, C.; Pandiaraj, M.; Santharaman, P. Immunosensors. In *Biosensors and Bioelectronics*; 2015; pp 206–243.

(132) Gopinath, S. C. B.; Tang, T. H.; Citartan, M.; Chen, Y.; Lakshmipriya, T. Current Aspects in Immunosensors. *Biosens. Bioelectron.* **2014**, *57*, 292–302.

(133) Ricci, F.; Adornetto, G.; Palleschi, G. A Review of Experimental Aspects of Electrochemical Immunosensors. *Electrochim. Acta* **2012**, *84*, 74–83.

(134) Moina, C.; Ybarr, G. Fundamentals and Applications of Immunosensors. In *Advances in Immunoassay Technology*; 2012; pp 65–80.

(135) Mahato, K.; Kumar, S.; Srivastava, A.; Maurya, P. K.; Singh, R.; Chandra, P. Electrochemical Immunosensors: Fundamentals and Applications in Clinical Diagnostics. In *Handbook of Immunoassay Technologies*; Vashist, S. K., Luong, J. H. T., Eds.; Academic Press, 2018; pp 359–414.

(136) Ghindilis, A. L.; Atanasov, P.; Wilkins, M.; Wilkins, E. Immunosensors: Electrochemical Sensing and Other Engineering Approaches. *Biosens. Bioelectron.* **1998**, *13*, 113–131.

(137) Mohammed, L.; Gomaa, H. G.; Ragab, D.; Zhu, J. Magnetic Nanoparticles for Environmental and Biomedical Applications: A Review. *Particuology.* **2017**, *30*, 1–14.

(138) Bakhtiary, Z.; Saei, A. A.; Hajipour, M. J.; Raoufi, M.; Vermesh, O.; Mahmoudi, M. Targeted Superparamagnetic Iron Oxide Nanoparticles for Early Detection of Cancer: Possibilities and Challenges. *Nanomedicine Nanotechnology, Biol. Med.* **2016**, *12*, 287–307.

(139) Mahmoudi, M.; Sant, S.; Wang, B.; Laurent, S.; Sen, T. Superparamagnetic Iron Oxide Nanoparticles (SPIONs): Development, Surface Modification and Applications in Chemotherapy. *Adv. Drug Deliv. Rev.* **2011**, *63*, 24–46.

(140) Richardson, J.; Hawkins, P.; Luxton, R. The Use of Coated Paramagnetic Particles as a Physical Label in a Magneto-Immunoassay. *Biosens. Bioelectron.* **2001**, *16*, 989–993.

(141) Jamshaid, T.; Neto, E. T. T.; Eissa, M. M.; Zine, N.; Kunita, M. H.; El-Salhi, A. E.; Elaissari, A. Magnetic Particles: From Preparation to Lab-on-a-Chip, Biosensors, Microsystems and Microfluidics Applications. *TrAC - Trends Anal. Chem.* **2016**, *79*, 344–362.

(142) Sandhu, A.; Handa, H.; Abe, M. Synthesis and Applications of Magnetic Nanoparticles for Biorecognition and Point of Care Medical Diagnostics. *Nanotechnology* **2010**, *21*, 442001.

(143) Bárcena, C.; Sra, A. K.; Gao, J. Applications of Magnetic Nanoparticles in Biomedicine. *Nanoscale Magn. Mater. Appl.* **2009**, *36*, 591–626.

(144) Iranmanesh, M.; Hulliger, J. Magnetic Separation: Its Application in Mining, Waste Purification, Medicine, Biochemistry and Chemistry. *Chem. Soc. Rev.* **2017**, *46*, 5925–5934.

(145) Aguilar-Arteaga, K.; Rodriguez, J. A.; Barrado, E. Magnetic Solids in Analytical Chemistry: A Review. *Anal. Chim. Acta* **2010**, *674*, 157–165.

(146) Bohara, R. A.; Thorat, N. D.; Pawar, S. H. Role of Functionalization: Strategies to Explore Potential Nano-Bio Applications of Magnetic Nanoparticles. *RSC Adv.* **2016**, *6*, 43989–44012.

(147) Lu, A. H.; Salabas, E. L.; Schüth, F. Magnetic Nanoparticles: Synthesis, Protection, Functionalization, and Application. *Angew. Chemie - Int. Ed.* **2007**, *46*, 1222–1244.

(148) Herrasti, Z.; De La Serna, E.; Ruiz-Vega, G.; Baldrich, E. Developing Enhanced Magnetoimmunosensors Based on Low-Cost Screen-Printed Electrode Devices. *Rev. Anal. Chem.* **2016**, *35*, 53–58.

(149) Gupta, A. K.; Gupta, M. Synthesis and Surface Engineering of Iron Oxide Nanoparticles for Biomedical Applications. *Biomaterials* **2005**, *26*, 3995–4021.

(150) Chastellain, M.; Petri, A.; Hofmann, H. Particle Size Investigations of a Multistep Synthesis of PVA Coated Superparamagnetic Nanoparticles. *J. Colloid Interface Sci.* **2004**, *278*, 353–360.

(151) Moreno-Guzmán, M.; Eguílaz, M.; Campuzano, S.; González-Cortés, A.; Yáñez-Sedeño, P.; Pingarrón, J. M. Disposable Immunosensor for Cortisol Using Functionalized Magnetic Particles. *Analyst* **2010**, *135*, 1926–1933.

(152) Jodra, A.; López, M. Á.; Escarpa, A. Disposable and Reliable Electrochemical Magnetoimmunosensor for Fumonisins Simplified Determination in Maize-Based Foodstuffs. *Biosens. Bioelectron.* **2015**, *64*, 633–638.

(153) Sapsford, K. E.; Algar, W. R.; Berti, L.; Gemmill, K. B.; Casey, B. J.; Oh, E.; Stewart, M. H.; Medintz, I. L. Functionalizing Nanoparticles with Biological Molecules: Developing Chemistries That Facilitate Nanotechnology. *Chem. Rev.* **2013**, *113*, 1904–2074.

(154) Gijs, M. A.; Lacharme, F.; Lehmann, U. Microfluidic Applications of Magnetic Particles for Biological Analysis and Catalysis. *Chem Rev* **2010**, *110*, 1518–1563.

(155) Horák, D.; Babič, M.; Macková, H.; Beneš, M. J. Preparation and Properties of Magnetic Nano- and Microsized Particles for Biological and Environmental Separations. *J. Sep. Sci.* **2007**, *30*, 1751–1772.

(156) Ruiz-Vega, G.; Baldrich, E. Effect of Agitation in Magneto-Assay Performance. *Sensors Actuators, B Chem.* **2017**, *247*, 718–726.

(157) He, S.; He, L.; Liu, B.; Yu, S.; Liu, L.; Tian, Y.; Wang, J.; Ding, L.; Wang, Y.; Qu, L.; et al. Development of a Rapid and Sensitivity Magnetic Chemiluminescence Immunoassay for DNA Methyltransferase 1 in Human Serum. *Chinese Chem. Lett.* **2019**, *30*, 1031–1034.

(158) Jia, Y.; Zhang, B.; Chang, H.; Yu, F.; Zhao, Z. TiO 2 /SnO x -Au Nanocomposite Catalyzed Photochromic Reaction for Colorimetric Immunoassay of Tumor Marker. *J. Pharm. Biomed. Anal.* **2019**, *169*, 75–81.

(159) Peng, J.; Guan, J.; Yao, H.; Jin, X. Magnetic Colorimetric Immunoassay for Human Interleukin-6 Based on the Oxidase Activity of Ceria Spheres. *Anal. Biochem.* **2016**, *492*, 63–68.

(160) Xi, Z.; Huang, R.; Li, Z.; He, N.; Wang, T.; Su, E.; Deng, Y. Selection of HBsAg-Specific DNA Aptamers Based on Carboxylated Magnetic Nanoparticles and Their Application in the Rapid and Simple Detection of Hepatitis b Virus

Infection. *ACS Appl. Mater. Interfaces* **2015**, *7*, 11215–11223.

(161) Ma, L.; Sun, Y.; Kang, X.; Wan, Y. Development of Nanobody-Based Flow Injection Chemiluminescence Immunoassay for Sensitive Detection of Human Prealbumin. *Biosens. Bioelectron.* **2014**, *61*, 165–171.

(162) Wang, H.; Zhai, X.; Liu, T.; Liang, J.; Bian, L.; Lin, L.; Chen, Z.; Li, P.; Dong, Z.; Li, Z.; et al. Development of a Novel Immunoassay for the Simple and Fast Quantitation of Neutrophil Gelatinase-Associated Lipocalin Using Europium(III)Chelate Microparticles and Magnetic Beads. *J. Immunol. Methods* **2019**, *470*, 15–19.

(163) Hou, J. Y.; Liu, T. C.; Lin, G. F.; Li, Z. X.; Zou, L. P.; Li, M.; Wu, Y. S. Development of an Immunomagnetic Bead-Based Time-Resolved Fluorescence Immunoassay for Rapid Determination of Levels of Carcinoembryonic Antigen in Human Serum. *Anal. Chim. Acta* **2012**, *734*, 93–98.

(164) Qu, F.; Li, T.; Yang, M. Colorimetric Platform for Visual Detection of Cancer Biomarker Based on Intrinsic Peroxidase Activity of Graphene Oxide. *Biosens. Bioelectron.* **2011**, *26*, 3927–3931.

(165) Liu, M.; Jia, C.; Huang, Y.; Lou, X.; Yao, S.; Jin, Q.; Zhao, J.; Xiang, J. Highly Sensitive Protein Detection Using Enzyme-Labeled Gold Nanoparticle Probes. *Analyst* **2010**, *135*, 327–331.

(166) Fu, X.; Liu, Y.; Qiu, R.; Foda, M. F.; Zhang, Y.; Wang, T.; Li, J. The Fabrication of Magnetic Particle-Based Chemiluminescence Immunoassay for Human Epididymis Protein-4 Detection in Ovarian Cancer. *Biochem. Biophys. Reports* **2018**, *13*, 73–77.

(167) Yoon, J.; Choi, N.; Ko, J.; Kim, K.; Lee, S.; Choo, J. Highly Sensitive Detection of Thrombin Using SERS-Based Magnetic Aptasensors. *Biosens. Bioelectron.* **2013**, *47*, 62–67.

(168) Hong, W.; Sun, G.; Zhang, Y.; Xing, Z.; Huang, B.; Zhang, S.; Zhang, X. Simultaneous Detection of Three Gynecological Tumor Biomarkers in Clinical Serum Samples Using an ICP-MS-Based Magnetic Immunoassay. *Anal. Methods* **2017**, *9*, 2546–2552.

(169) Wang, Y. R.; Yang, Y. H.; Lu, C. Y.; Chen, S. H. Utilization of Magnetic Nanobeads for Analyzing Haptoglobin in Human Plasma as a Marker of Alzheimer's Disease by Capillary Electrophoretic Immunoassay with Laser-Induced Fluorescence Detection. *Anal. Chim. Acta* **2015**, *865*, 76–82.

(170) Lai, W.; Tang, D.; Zhuang, J.; Chen, G.; Yang, H. Magnetic Bead-Based Enzyme-Chromogenic Substrate System for Ultrasensitive Colorimetric Immunoassay Accompanying Cascade Reaction for Enzymatic Formation of Squaric Acid-Iron(III) Chelate. *Anal. Chem.* **2014**, *86*, 5061–5068.

(171) Gao, Z.; Xu, M.; Hou, L.; Chen, G.; Tang, D. Magnetic Bead-Based Reverse Colorimetric Immunoassay Strategy for Sensing Biomolecules. *Anal. Chem.* **2013**, *85*, 6945–6952.

(172) Cao, Y.; Mo, G.; Feng, J.; He, X.; Tang, L.; Yu, C.; Deng, B. Based on ZnSe

Quantum Dots Labeling and Single Particle Mode ICP-MS Coupled with Sandwich Magnetic Immunoassay for the Detection of Carcinoembryonic Antigen in Human Serum. *Anal. Chim. Acta* **2018**, *1028*, 22–31.

(173) De Souza Castilho, M.; Laube, T.; Yamanaka, H.; Alegret, S.; Pividori, M. I. Magneto Immunoassays for Plasmodium Falciparum Histidine-Rich Protein 2 Related to Malaria Based on Magnetic Nanoparticles. *Anal. Chem.* **2011**, *83*, 5570–5577.

(174) Yang, Y.; Xu, J.; Zhang, Q. Detection of Urinary Survivin Using a Magnetic Particles-Based Chemiluminescence Immunoassay for the Preliminary Diagnosis of Bladder Cancer and Renal Cell Carcinoma Combined with LAPTM4B. *Oncol. Lett.* **2018**, *15*, 7923–7933.

(175) Zhang, X.; Chen, B.; He, M.; Zhang, Y.; Xiao, G.; Hu, B. Magnetic Immunoassay Coupled with Inductively Coupled Plasma Mass Spectrometry for Simultaneous Quantification of Alpha-Fetoprotein and Carcinoembryonic Antigen in Human Serum. *Spectrochim. Acta - Part B At. Spectrosc.* **2015**, *106*, 20–27.

(176) Li, Z. Y.; Zhang, Q. Y.; Zhao, L. X.; Li, Z. J.; Hu, G. M.; Lin, J. M.; Wang, S. Micro-Plate Magnetic Chemiluminescence Immunoassay and Its Applications in Carcinoembryonic Antigen Analysis. *Sci. China Chem.* **2010**, *53*, 812–819.

(177) Pires, F.; Arcos-Martinez, M. J.; Dias-Cabral, A. C.; Vidal, J. C.; Castillo, J. R. A Rapid Magnetic Particle-Based Enzyme Immunoassay for Human Cytomegalovirus Glycoprotein B Quantification. *J. Pharm. Biomed. Anal.* **2018**, *156*, 372–378.

(178) Pei, H.; Zhu, S.; Yang, M.; Kong, R.; Zheng, Y.; Qu, F. Graphene Oxide Quantum Dots@silver Core-Shell Nanocrystals as Turn-on Fluorescent Nanoprobe for Ultrasensitive Detection of Prostate Specific Antigen. *Biosens. Bioelectron.* **2015**, *74*, 909–914.

(179) Vidal, J. C.; Bertolín, J. R.; Bonel, L.; Asturias, L.; Arcos-Martínez, M. J.; Castillo, J. R. Rapid Determination of Recent Cocaine Use with Magnetic Particles-Based Enzyme Immunoassays in Serum, Saliva, and Urine Fluids. *J. Pharm. Biomed. Anal.* **2016**, *125*, 54–61.

(180) Qin, G.; Zhao, S.; Huang, Y.; Jiang, J.; Ye, F. Magnetic Bead-Sensing-Platform-Based Chemiluminescence Resonance Energy Transfer and Its Immunoassay Application. *Anal. Chem.* **2012**, *84*, 2708–2712.

(181) Carinelli, S.; Xufré, C.; Alegret, S.; Martí, M.; Pividori, M. I. CD4 Quantification Based on Magneto ELISA for AIDS Diagnosis in Low Resource Settings. *Talanta* **2016**, *160*, 36–45.

(182) Ali, Z.; Wang, J.; Tang, Y.; Liu, B.; He, N.; Li, Z. Simultaneous Detection of Multiple Viruses Based on Chemiluminescence and Magnetic Separation. *Biomater. Sci.* **2017**, *5*, 57–66.

(183) Chen, Y. T.; Kolhatkar, A. G.; Zenasni, O.; Xu, S.; Lee, T. R. Biosensing Using Magnetic Particle Detection Techniques. *Sensors* **2017**, *17*, 2300.

(184) Hsing, I. M.; Xu, Y.; Zhao, W. Micro- and Nano- Magnetic Particles for Applications in Biosensing. *Electroanalysis* **2007**, *19*, 755–768.

(185) Yáñez-Sedeño, P.; Campuzano, S.; Pingarrón, J. M. Magnetic Particles Coupled to Disposable Screen Printed Transducers for Electrochemical Biosensing. *Sensors* **2016**, *16*, 1585.

(186) Aseri, A.; Garg, S. K.; Nayak, A.; Trivedi, S. K.; Ahsan, M. Magnetic Nanoparticles: Magnetic Nano-Technology Using Biomedical Applications and Future Prospects. *Int. J. Pharm. Sci. Rev. Res.* **2015**, *31*, 119–131.

(187) Lin, H. Y.; Huang, C. H.; Park, J.; Pathania, D.; Castro, C. M.; Fasano, A.; Weissleder, R.; Lee, H. Integrated Magneto-Chemical Sensor for On-Site Food Allergen Detection. *ACS Nano* **2017**, *11*, 10062–10069.

(188) Pastucha, M.; Farka, Z.; Lacina, K.; Mikušová, Z.; Skládal, P. Magnetic Nanoparticles for Smart Electrochemical Immunoassays: A Review on Recent Developments. *Microchim. Acta* **2019**, *186*, 312.

(189) Reverté, L.; Prieto-Simón, B.; Campàs, M. New Advances in Electrochemical Biosensors for the Detection of Toxins: Nanomaterials, Magnetic Beads and Microfluidics Systems. A Review. *Anal. Chim. Acta* **2016**, *908*, 8–21.

(190) Pohanka, M. Magnetic Particles in Electrochemical Analyses. *Int. J. Electrochem. Sci.* **2018**, *13*, 12000–12009.

(191) Moral-Vico, J.; Barallat, J.; Abad, L.; Olivé-Monllau, R.; Muñoz-Pascual, F. X.; Galán Ortega, A.; del Campo, F. J.; Baldrich, E. Dual Chronoamperometric Detection of Enzymatic Biomarkers Using Magnetic Beads and a Low-Cost Flow Cell. *Biosens. Bioelectron.* **2015**, *69*, 328–336.

(192) Gädke, J.; Thies, J. W.; Kleinfeldt, L.; Schulze, T.; Biedendieck, R.; Rustenbeck, I.; Garnweitner, G.; Krull, R.; Dietzel, A. Selective Manipulation of Superparamagnetic Nanoparticles for Product Purification and Microfluidic Diagnostics. *Eur. J. Pharm. Biopharm.* **2018**, *126*, 67–74.

(193) Zorione Herrasti, Fernando Martínez, E. B. Carbon Nanotube Wiring for Signal Amplification of Electrochemical Magneto Immunosensors: Application to Myeloperoxidase Detection. *Anal. Bioanal. Chem.* **2014**, *406*, 5487–5493.

(194) Valverde, A.; Povedano, E.; Montiel, V. R. V.; Yáñez-Sedeño, P.; Garranzo-Asensio, M.; Barderas, R.; Campuzano, S.; Pingarrón, J. M. Electrochemical Immunosensor for IL-13 Receptor A2 Determination and Discrimination of Metastatic Colon Cancer Cells. *Biosens. Bioelectron.* **2018**, *117*, 766–772.

(195) De Oliveira, R. A. G.; Materon, E. M.; Melendez, M. E.; Carvalho, A. L.; Faria, R. C. Disposable Microfluidic Immunoarray Device for Sensitive Breast Cancer Biomarker Detection. *ACS Appl. Mater. Interfaces* **2017**, *9*, 27433–27440.

(196) Sánchez-Tirado, E.; Martínez-García, G.; González-Cortés, A.; Yáñez-Sedeño, P.; Pingarrón, J. M. Electrochemical Immunosensor for Sensitive Determination of Transforming Growth Factor (TGF) - B1 in Urine. *Biosens. Bioelectron.* **2017**, *88*, 9–14.

(197) Eletxigerra, U.; Martinez-Perdiguero, J.; Merino, S.; Barderas, R.; Ruiz-Valdepeñas Montiel, V.; Villalonga, R.; Pingarrón, J. M.; Campuzano, S. Electrochemical Magnetoimmunosensor for Progesterone Receptor Determination. Application to the Simultaneous Detection of Estrogen and Progesterone Breast-Cancer Related Receptors in Raw Cell Lysates. *Electroanalysis* **2016**, *28*, 1787–1794.

(198) Torrente-Rodríguez, R. M.; Campuzano, S.; Ruiz-Valdepeñas-Montiel, V.; Pedrero, M.; Fernández-Aceñero, M. J.; Barderas, R.; Pingarrón, J. M. Rapid Endoglin Determination in Serum Samples Using an Amperometric Magneto-Actuated Disposable Immunosensing Platform. *J. Pharm. Biomed. Anal.* **2016**, *129*, 288–293.

(199) Ruiz-Valdepeñas Montiel, V.; Campuzano, S.; Conzuelo, F.; Torrente-Rodríguez, R. M.; Gamella, M.; Reviejo, A. J.; Pingarrón, J. M. Electrochemical Magnetoimmunosensing Platform for Determination of the Milk Allergen β-Lactoglobulin. *Talanta* **2015**, *131*, 156–162.

(200) Ojeda, I.; Moreno-Guzmán, M.; González-Cortés, A.; Yáñez-Sedeño, P.; Pingarrón, J. M. Electrochemical Magnetoimmunosensor for the Ultrasensitive Determination of Interleukin-6 in Saliva and Urine Using Poly-HRP Streptavidin Conjugates as Labels for Signal Amplification. *Anal. Bioanal. Chem.* **2014**, *406*, 6363–6371.

(201) Eletxigerra, U.; Martinez-Perdiguero, J.; Merino, S.; Villalonga, R.; Pingarrón, J. M.; Campuzano, S. Amperometric Magnetoimmunoassay for the Direct Detection of Tumor Necrosis Factor Alpha Biomarker in Human Serum. *Anal. Chim. Acta* **2014**, *838*, 37–44.

(202) de la Escosura-Muñiz, A.; Maltez-da Costa, M.; Sánchez-Espinel, C.; Díaz-Freitas, B.; Fernández-Suarez, J.; González-Fernández, Á.; Merkoçi, A. Gold Nanoparticle-Based Electrochemical Magnetoimmunosensor for Rapid Detection of Anti-Hepatitis B Virus Antibodies in Human Serum. *Biosens. Bioelectron.* **2010**, *26*, 1710–1714.

(203) Campuzano, S.; Salema, V.; Moreno-Guzmán, M.; Gamella, M.; Yáñez-Sedeño, P.; Fernández, L. A.; Pingarrón, J. M. Disposable Amperometric Magnetoimmunosensors Using Nanobodies as Biorecognition Element. Determination of Fibrinogen in Plasma. *Biosens. Bioelectron.* **2014**, *52*, 255–260.

(204) Conzuelo, F.; Gamella, M.; Campuzano, S.; Reviejo, A. J.; Pingarrón, J. M. Disposable Amperometric Magneto-Immunosensor for Direct Detection of Tetracyclines Antibiotics Residues in Milk. *Anal. Chim. Acta* **2012**, *737*, 29–36.

(205) Eguílaz, M.; Moreno-Guzmán, M.; Campuzano, S.; González-Cortés, A.; Yáñez-Sedeño, P.; Pingarrón, J. M. An Electrochemical Immunosensor for Testosterone Using Functionalized Magnetic Beads and Screen-Printed Carbon Electrodes. *Biosens. Bioelectron.* **2010**, *26*, 517–522.

(206) Du, D.; Wang, J.; Wang, L.; Lu, D.; Smith, J. N.; Timchalk, C.; Lin, Y. Magnetic Electrochemical Sensing Platform for Biomonitoring of Exposure to Organophosphorus Pesticides and Nerve Agents Based on Simultaneous Measurement of Total Enzyme Amount and Enzyme Activity. *Anal. Chem.* **2011**,

83, 3770–3777.

(207) Medina-Sánchez, M.; Miserere, S.; Morales-Narváez, E.; Merkoçi, A. On-Chip Magneto-Immunoassay for Alzheimer's Biomarker Electrochemical Detection by Using Quantum Dots as Labels. *Biosens. Bioelectron.* **2014**, *54*, 279–284.

(208) Al-Khafaji, Q. A. M.; Harris, M.; Tombelli, S.; Laschi, S.; Turner, A. P. F.; Mascini, M.; Marrazza, G. An Electrochemical Immunoassay for HER2 Detection. *Electroanalysis* **2012**, *24*, 735–742.

(209) Hsu, S. M.; Raine, L.; Fanger, H. Use of Avidin-Biotin-Peroxidase Complex (ABC) in Immunoperoxidase Techniques: A Comparison between ABC and Unlabeled Antibody (PAP) Procedures. *J. Histochem. Cytochem.* **1981**, *29*, 577–580.

(210) Ding, L.; Bond, A. M.; Zhai, J.; Zhang, J. Utilization of Nanoparticle Labels for Signal Amplification in Ultrasensitive Electrochemical Affinity Biosensors: A Review. *Anal. Chim. Acta* **2013**, *797*, 1–12.

(211) Huang, H.; Zhu, J.-J. The Electrochemical Applications of Quantum Dots. *Analyst* **2013**, *138*, 5855–5865.

(212) Wu, J.; Wang, X.; Wang, Q.; Lou, Z.; Li, S.; Zhu, Y.; Qin, L.; Wei, H. Nanomaterials with Enzyme-like Characteristics (Nanozymes): Next-Generation Artificial Enzymes (II). *Chem. Soc. Rev.* **2019**, *48*, 1004–1076.

(213) Pei, X.; Zhang, B.; Tang, J.; Liu, B.; Lai, W.; Tang, D. Sandwich-Type Immunosensors and Immunoassays Exploiting Nanostructure Labels: A Review. *Anal. Chim. Acta* **2013**, *758*, 1–18.

(214) Tang, D.; Hou, L.; Niessner, R.; Xu, M.; Gao, Z.; Knopp, D. Multiplexed Electrochemical Immunoassay of Biomarkers Using Metal Sulfide Quantum Dot Nanolabels and Trifunctionalized Magnetic Beads. *Biosens. Bioelectron.* **2013**, *46*, 37–43.

(215) López-Marzo, A. M.; Hoyos-De-La-Torre, R.; Baldrich, E. NaNO3/NaCl Oxidant and Polyethylene Glycol (PEG) Capped Gold Nanoparticles (AuNPs) as a Novel Green Route for AuNPs Detection in Electrochemical Biosensors. *Anal. Chem.* **2018**, *90*, 4010–4018.

(216) Marin, S.; Merkoçi, A. Direct Electrochemical Stripping Detection of Cystic-Fibrosis-Related DNA Linked through Cadmium Sulfide Quantum Dots. *Nanotechnology* **2009**, *20*, 055101.

(217) Kim, C.; Searson, P. C. Magnetic Bead-Quantum Dot Assay for Detection of a Biomarker for Traumatic Brain Injury. *Nanoscale* **2015**, *7*, 17820–17826.

(218) Kim, C.; Hoffmann, G.; Searson, P. C. Integrated Magnetic Bead-Quantum Dot Immunoassay for Malaria Detection. *ACS Sensors* **2017**, *2*, 766–772.

(219) Ruiz-Vega, G.; García-Robaina, A.; Ben Ismail, M.; Pasamar, H.; García-Berrocoso, T.; Montaner, J.; Zourob, M.; Othmane, A.; del Campo, F. J.; Baldrich, E. Detection of Plasma MMP-9 within Minutes. Unveiling Some of the Clues to Develop Fast and Simple Electrochemical Magneto-Immunosensors.

Biosens. Bioelectron. **2018**, *115*, 45–52.

(220) Tang, Z.; Ma, Z. Multiple Functional Strategies for Amplifying Sensitivity of Amperometric Immunoassay for Tumor Markers: A Review. *Biosens. Bioelectron.* **2017**, *98*, 100–112.

(221) Vranish, J. N.; Ancona, M. G.; Walper, S. A.; Medintz, I. L. Pursuing the Promise of Enzymatic Enhancement with Nanoparticle Assemblies. *Langmuir* **2018**, *34*, 2901–2925.

(222) Fang, C.; Cao, L.; Chen, Z. Disposable Electrochemical Immunosensor Based on Dual-Labeled Gold Nanoprobe (Ab-Au-HRP) for Detection of Alpha-Fetoprotein. *J. Nanosci. Nanotechnol.* **2017**, *17*, 5109–5114.

(223) Lai, W.; Zeng, Q.; Tang, J.; Zhang, M.; Tang, D. A Conventional Chemical Reaction for Use in an Unconventional Assay: A Colorimetric Immunoassay for Aflatoxin B 1 by Using Enzyme-Responsive Just-in-Time Generation of a MnO 2 Based Nanocatalyst. *Microchim. Acta* **2018**, *185*, 92.

(224) Vasilov, R. G.; Tsitsikov, E. N. An Ultrasensitive Immunoassay for Human IgE Measurement in Cell-Culture Supernatant. *Immunol. Lett.* **1990**, *26*, 283–284.

(225) D. Yu. Plaksin, M. B. R. and E. T. G. The Method of Stereospecific Assay and the Method of the Conjugate for Stereospecifis Assay . 20899212, 1997.

(226) Vasilov, R. G.; Tsitsikov, E. N. An Ultrasensitive Immunoassay for Human IgE Measurement in Cell-Culture Supernatant. *Immunol. Lett.* **1990**, *26*, 283–284.

(227) Diagnostics Intelligence. European Diagnostics Companies Taking Note of Russian Biotech Startup. **1991**, No. 3, 5–6.

(228) Kiseleva, V. I.; Kolesnik, T. B.; Turchinsky, M. F.; Wagner, L. L.; Kovalenko, V. A.; Plaksin, D. J.; Koukalová, B.; Kuhrová, V.; Brábec, V.; Poverenny, A. M. Trans-Diamminedichlorplatinum (II)-Modified Probes for Detection of Picogram Quantities of DNA. *Anal. Biochem.* **1992**, *206*, 43–49.

(229) Plaksin D. Yu and Gromakovska E. G. Poly-HRP Conjugates: Novel Reagents for Ultrasensitive Detection in Immunoassays, Nucleic Acid Hybridization and Ligand-Receptor Assay Systems. *J. NIH Res.* **1994**, 6–98.

(230) Sukhacheva, E.; Novikov, V.; Plaksin, D.; Pavlova, I.; Ambrosova, S. Highly Sensitive Immunoassays for Detection of Barley Stripe Mosaic Virus and Beet Necrotic Yellow Vein Virus. *J. Virol. Methods* **1996**, *56*, 199–207.

(231) Scientific, T. F. Polymerized Conjugates for Biological Applications. WO 2009/055387, 2009.

(232) Marquette, C. A.; Hezard, P.; Degiuli, A.; Blum, L. J. Macro-Molecular Chemiluminescent Complex for Enhanced Immuno-Detection onto Microtiter Plate and Protein Biochip. *Sensors Actuators, B Chem.* **2006**, *113*, 664–670.

(233) Damen, C. W. N.; de Groot, E. R.; Heij, M.; Boss, D. S.; Schellens, J. H. M.; Rosing, H.; Beijnen, J. H.; Aarden, L. a. Development and Validation of an Enzyme-Linked Immunosorbent Assay for the Quantification of Trastuzumab in

Human Serum and Plasma. *Anal. Biochem.* **2009**, *391*, 114–120.

(234) Munge, B. S.; Fisher, J.; Millord, L. N.; Krause, C. E.; Dowd, R. S.; Rusling, J. F. Sensitive Electrochemical Immunosensor for Matrix Metalloproteinase-3 Based on Single-Wall Carbon Nanotubes. *Analyst* **2010**, *135*, 1345–1350.

(235) Sánchez-Tirado, E.; Salvo, C.; González-Cortés, A.; Yáñez-Sedeño, P.; Langa, F.; Pingarrón, J. M. Electrochemical Immunosensor for Simultaneous Determination of Interleukin-1 Beta and Tumor Necrosis Factor Alpha in Serum and Saliva Using Dual Screen Printed Electrodes Modified with Functionalized Double–walled Carbon Nanotubes. *Anal. Chim. Acta* **2017**, *959*, 66–73.

(236) Gan, N.; Du, X.; Cao, Y.; Hu, F.; Li, T.; Jiang, Q. An Ultrasensitive Electrochemical Immunosensor for HIV P24 Based on Fe3O4@SiO2 Nanomagnetic Probes and Nanogold Colloid-Labeled Enzyme-Antibody Copolymer as Signal Tag. *Mater.* **2013**, *6*, 1255–1269.

(237) Xiong, P.; Gan, N.; Cao, Y.; Hu, F.; Li, T.; Zheng, L. An Ultrasensitive Electrochemical Immunosensor for Alpha-Fetoprotein Using an Envision Complex-Antibody Copolymer as a Sensitive Label. *Materials (Basel).* **2012**, *5*, 2757–2772.

(238) Sánchez-Tirado, E.; Martínez-García, G.; González-Cortés, A.; Yáñez-Sedeño, P.; Pingarrón, J. M. Electrochemical Immunosensor for Sensitive Determination of Transforming Growth Factor (TGF) - B1 in Urine. *Biosens. Bioelectron.* **2017**, *88*, 9–14.

(239) Li, D.; Ying, Y.; Wu, J.; Niessner, R.; Knopp, D. Comparison of Monomeric and Polymeric Horseradish Peroxidase as Labels in Competitive ELISA for Small Molecule Detection. *Microchim. Acta* **2013**, *180*, 711–717.

(240) Sánchez-Tirado, E.; González-Cortés, A.; Yáñez-Sedeño, P.; Pingarrón, J. M. Carbon Nanotubes Functionalized by Click Chemistry as Scaffolds for the Preparation of Electrochemical Immunosensors. Application to the Determination of TGF-Beta 1 Cytokine. *Analyst* **2016**.

(241) Wen, Y.; Wang, L.; Xu, L.; Li, L.; Ren, S.; Cao, C.; Jia, N.; Aldalbahi, A.; Song, S.; Shi, J.; et al. Electrochemical Detection of PCR Amplicons of: Escherichia Coli Genome Based on DNA Nanostructural Probes and PolyHRP Enzyme. *Analyst* **2016**, *141*, 5304–5310.

(242) Carvajal, S.; Fera, S. N.; Jones, A. L.; Baldo, T. A.; Mosa, I. M.; Rusling, J. F.; Krause, C. E. Disposable Inkjet-Printed Electrochemical Platform for Detection of Clinically Relevant HER-2 Breast Cancer Biomarker. *Biosens. Bioelectron.* **2018**, *104*, 158–162.

(243) Martínez-Periñán, E.; Sánchez-Tirado, E.; González-Cortés, A.; Barderas, R.; Sánchez-Puelles, J. M.; Martínez-Santamaría, L.; Campuzano, S.; Yáñez-Sedeño, P.; Pingarrón, J. M. Amperometric Determination of Endoglin in Human Serum Using Disposable Immunosensors Constructed with Poly(Pyrrolepropionic) Acid-Modified Electrodes. *Electrochim. Acta* **2018**, *292*, 887–894.

(244) Mani, V.; Paleja, B.; Larbi, K.; Kumar, P.; Tay, J. A.; Siew, J. Y.; Inci, F.; Wang,

S. Q.; Chee, C.; Wang, Y. T.; et al. Microchip-Based Ultrafast Serodiagnostic Assay for Tuberculosis. *Sci. Rep.* **2016**, *6*, 35845.

(245) Mahato, K.; Srivastava, A.; Chandra, P. Paper Based Diagnostics for Personalized Health Care: Emerging Technologies and Commercial Aspects. *Biosens. Bioelectron.* **2017**, *96*, 246–259.

(246) Ching, K. H. Lateral Flow Immunoassay. In *ELISA. Methods in Molecular Biology*; Humana Press: New York, NY, 2015; pp 127–137.

(247) Credou, J.; Berthelot, T. Cellulose: From Biocompatible to Bioactive Material. *J. Mater. Chem. B* **2014**, *2*, 4767–4788.

(248) Yang, Y.; Noviana, E.; Nguyen, M. P.; Geiss, B. J.; Dandy, D. S.; Henry, C. S. Paper-Based Microfluidic Devices: Emerging Themes and Applications. *Anal. Chem.* **2017**, *89*, 71–91.

(249) Gao, B.; Chi, J.; Liu, H.; Gu, Z. Vertical Paper Analytical Devices Fabricated Using the Principles of Quilling and Kirigami. *Sci. Rep.* **2017**, *7*, 7255.

(250) Xia, Y.; Si, J.; Li, Z. Fabrication Techniques for Microfluidic Paper-Based Analytical Devices and Their Applications for Biological Testing: A Review. *Biosens. Bioelectron.* **2016**, *77*, 774–789.

(251) Zhu, G.; Yin, X.; Jin, D.; Zhang, B.; Gu, Y.; An, Y. Paper-Based Immunosensors: Current Trends in the Types and Applied Detection Techniques. *TrAC Trends Anal. Chem.* **2019**, *111*, 100–117.

(252) Zhong, Z.; Wang, Z.; X. D. Huang, G. Investigation of Wax and Paper Materials for the Fabrication of Paper-Based Microfluidic Devices. In *Microsystem Technologies*; 2012; Vol. 18, pp 649–659.

(253) Millipore. Rapid Lateral Flow Test Strips: Considerations for Product Development. *EMD Millipore Corp. Billerica, MA., Ger.* **2008**, 1–42.

(254) Pelton, R. Bioactive Paper Provides a Low-Cost Platform for Diagnostics. *TrAC Trends Anal. Chem.* **2009**, *28*, 925–942.

(255) O'Sullivan, A. C. Cellulose: The Structure Slowly Unravels. *Cellulose* **1997**, *4*, 173–207.

(256) Hristov, D.; Rodriguez-Quijada, C.; Zacapa Gomez-Marquez, J.; Hamad-Schifferli, K. Designing Paper-Based Immunoassays for Biomedical Applications. *Sensors* **2019**, *19*, 554.

(257) Desmet, C.; Marquette, C. A.; Blum, L. J.; Doumèche, B. Paper Electrodes for Bioelectrochemistry: Biosensors and Biofuel Cells. *Biosens. Bioelectron.* **2016**, *76*, 145–163.

(258) He, Y.; Wu, Y.; Fu, J.-Z.; Wu, W.-B. Fabrication of Paper-Based Microfluidic Analysis Devices: A Review. *RSC Adv.* **2015**, *5*, 78109–78127.

(259) Gong, M.; Sinton, D. Turning the Page: Advancing Paper-Based Microfluidics for Broad Diagnostic Application. *Chem. Rev.* **2017**, *117*, 8447–8480.

(260) Bracher, P. J.; Gupta, M.; Whitesides, G. M. Patterning Precipitates of Reactions in Paper. *J. Mater. Chem.* **2010**, *20*, 5117–5122.

(261) Campbell, J. M.; Balhoff, J. B.; Landwehr, G. M.; Rahman, S. M.; Vaithiyanathan, M.; Melvin, A. T. Microfluidic and Paper-Based Devices for Disease Detection and Diagnostic Research. *Int. J. Mol. Sci.* **2018**, *19*, 2731.

(262) Fu, L.-M.; Wang, Y.-N. Detection Methods and Applications of Microfluidic Paper-Based Analytical Devices. *TrAC Trends Anal. Chem.* **2018**, *107*, 196–211.

(263) Tian, T.; Bi, Y.; Xu, X.; Zhu, Z.; Yang, C. Integrated Paper-Based Microfluidic Devices for Point-of-Care Testing. *Anal. Methods* **2018**, *10*, 3567–3581.

(264) Singh, T. A.; Lantigua, D.; Meka, A.; Taing, S.; Pandher, M.; Camci-Unal, G. Paper-Based Sensors: Emerging Themes and Applications. *Sensors* **2018**, *18*, 2838.

(265) Alfred H. Free, Ernest C. Adams, Mary Lou Kercher, Helen M. Free, M. H. C. Simple Specific Test for Urine Glucose. *Clin. Chem.* **1957**, *3*, 163–168.

(266) Zhao, W.; Van Den Berg, A. Lab on Paper. *Lab Chip* **2008**, *8*, 1988–1991.

(267) Kumar, A.; Hens, A.; Arun, R. K.; Chatterjee, M.; Mahato, K.; Layek, K.; Chanda, N. A Paper Based Microfluidic Device for Easy Detection of Uric Acid Using Positively Charged Gold Nanoparticles. *Analyst* **2015**, *140*, 1817–1821.

(268) Posthuma-Trumpie, G. A.; Korf, J.; Van Amerongen, A. Lateral Flow (Immuno)Assay: Its Strengths, Weaknesses, Opportunities and Threats. A Literature Survey. *Anal. Bioanal. Chem.* **2009**, *393*, 569–582.

(269) López-Marzo, A. M.; Merkoçi, A. Paper-Based Sensors and Assays: A Success of the Engineering Design and the Convergence of Knowledge Areas. *Lab Chip* **2016**, *16*, 3150–3176.

(270) Liana, D. D.; Raguse, B.; Justin Gooding, J.; Chow, E. Recent Advances in Paper-Based Sensors. *Sensors (Switzerland)* **2012**, *12*, 11505–11526.

(271) Martinez, A. W.; Phillips, S. T.; Butte, M. J.; Whitesides, G. M. Patterned Paper as a Platform for Inexpensive, Low-Volume, Portable Bioassays. *Angew. Chemie - Int. Ed.* **2007**, *46*, 1318–1320.

(272) Martinez AW1, Phillips ST, Whitesides GM, C. E. Diagnostics for the Developing World: Microfluidic Paper-Based Analytical Devices. *Anal. Chem.* **2010**, *82*, 3–10.

(273) Martinez, A. W.; Phillips, S. T.; Whitesides, G. M. Three-Dimensional Microfluidic Devices Fabricated in Layered Paper and Tape. *Proc. Natl. Acad. Sci.* **2008**, *105*, 19606–19611.

(274) Nie, Z.; Nijhuis, C. A.; Gong, J.; Chen, X.; Kumachev, A.; Martinez, A. W.; Narovlyansky, M.; Whitesides, G. M. Electrochemical Sensing in Paper-Based Microfluidic Devices. *Lab Chip* **2010**, *10*, 477–483.

(275) Xu, Y.; Liu, M.; Kong, N.; Liu, J. Lab-on-Paper Micro- and Nano-Analytical

Devices: Fabrication, Modification, Detection and Emerging Applications. *Microchim. Acta* **2016**, *183*, 1521–1542.

(276) Lim, W. Y.; Goh, B. T.; Khor, S. M. Microfluidic Paper-Based Analytical Devices for Potential Use in Quantitative and Direct Detection of Disease Biomarkers in Clinical Analysis. *J. Chromatogr. B Anal. Technol. Biomed. Life Sci.* **2017**, *1060*, 424–442.

(277) Liu, L.; Yang, D.; Liu, G. Signal Amplification Strategies for Paper-Based Analytical Devices. *Biosens. Bioelectron.* **2019**, *136*, 60–75.

(278) Abdollahi-Aghdam, A.; Majidi, M. R.; Omidi, Y. Microfluidic Paper-Based Analytical Devices (MPADs) for Fast and Ultrasensitive Sensing of Biomarkers and Monitoring of Diseases. *Bioimpacts* **2018**, *8*, 237–240.

(279) Almeida, M. I. G. S.; Jayawardane, B. M.; Kolev, S. D.; McKelvie, I. D. Developments of Microfluidic Paper-Based Analytical Devices (MPADs) for Water Analysis: A Review. *Talanta* **2018**, *177*, 176–190.

(280) Tian, T.; Liu, H.; Li, L.; Yu, J.; Ge, S.; Song, X.; Yan, M. Paper-Based Biosensor for Noninvasive Detection of Epidermal Growth Factor Receptor Mutations in Non-Small Cell Lung Cancer Patients. *Sensors Actuators B Chem.* **2017**, *251*, 440–445.

(281) Kaneta, T.; Alahmad, W.; Varanusupakul, P. Microfluidic Paper-Based Analytical Devices with Instrument-Free Detection and Miniaturized Portable Detectors. *Appl. Spectrosc. Rev.* **2018**, *54*, 1–25.

(282) Mazzu, T.; Gianini Morbiol, G.; Milan, L.; Silva, D.; Cristina Donofrio, F.; Mestriner, C.; Carrilho, E. Improved Assessment of Accuracy and Performance Indicators in Paper-Based ELISA. *Anal. methods* **2017**, *9*, 2644–2653.

(283) Mazzu-Nascimento, T.; Morbioli, G. G.; Milan, L. A.; Donofrio, F. C.; Mestriner, C. A.; Carrilho, E. Development and Statistical Assessment of a Paper-Based Immunoassay for Detection of Tumor Markers. *Anal. Chim. Acta* **2016**, *950*, 156–161.

(284) LEE, V. B. C.; MOHD-NAIM, N. F.; TAMIYA, E.; AHMED, M. U. Trends in Paper-Based Electrochemical Biosensors: From Design to Application. *Anal. Sci.* **2018**, *34*, 7–18.

(285) Ashebr, T.; Asfaw, T.; Gebremicael, S.; Linert, W.; Nayathuparambil, M.; Berhanu, T. Recent Advances in and Potential Utilities of Paper-Based Electrochemical Sensors: Beyond Qualitative Analysis. *Analyst* **2019**, *144*, 2467–2479.

(286) Dungchai, W.; Chailapakul, O.; Henry, C. S. Electrochemical Detection for Paper-Based Microfluidics. *Anal. Chem.* **2009**, *81*, 5821–5826.

(287) Mettakoonpitak, J.; Boehle, K.; Nantaphol, S.; Teengam, P.; Adkins, J.; Srisa-Art, M.; Henry, C. Electrochemistry on Paper-Based Analytical Devices: A Review. *Electroanalysis* **2016**, *28*, 1420–1436.

(288) Ding, J.; He, N.; Lisak, G.; Qin, W.; Bobacka, J. Paper-Based Microfluidic

Sampling and Separation of Analytes for Potentiometric Ion Sensing. *Sensors Actuators, B Chem.* **2017**, *243*, 346–352.

(289) Zhao, C.; Mwangi Thuo, M.; Liu, X. A Microfluidic Paper-Based Electrochemical Biosensor Array for Multiplexed Detection of Metabolic Biomarkers. *Sci. Technol. Adv. Mater.* **2013**, *14*, 4402.

(290) Tortorich, R.; Shamkhalichenar, H.; Choi, J.-W. Inkjet-Printed and Paper-Based Electrochemical Sensors. *Appl. Sci.* **2018**, *8*, 288.

(291) Silveira, C. M.; Monteiro, T.; Almeida, M. G. Biosensing with Paper-Based Miniaturized Printed Electrodes-A Modern Trend. *Biosensors* **2016**, *6*, 51.

(292) Fu, X.; Xia, B.; Ji, B.; Lei, S.; Zhou, Y. Flow Controllable Three-Dimensional Paper-Based Microfluidic Analytical Devices Fabricated by 3D Printing Technology. *Anal. Chim. Acta* **2019**, *1065*, 64–70.

(293) Wu, Y.; Ren, Y.; Han, L.; Yan, Y.; Jiang, H. Three-Dimensional Paper Based Platform for Automatically Running Multiple Assays in a Single Step. *Talanta* **2019**, *200*, 177–185.

(294) Hasanzadeh, M.; Shadjou, N. Electrochemical and Photoelectrochemical Nano-Immunesensing Using Origami Paper Based Method. *Mater. Sci. Eng. C* **2015**, *61*, 979–1001.

(295) Zang, D.; Ge, L.; Yan, M.; Song, X.; Yu, J. Electrochemical Immunoassay on a 3D Microfluidic Paper-Based Device. *Chem. Commun.* **2012**, *48*, 4683.

(296) Nie, Z.; Deiss, F.; Liu, X.; Akbulut, O.; Whitesides, G. M. Integration of Paper-Based Microfluidic Devices with Commercial Electrochemical Readers. *Lab Chip* **2010**, *10*, 3163–3169.

(297) Lim, S. A.; Ahmed, M. U. Electrochemical Immunosensors and Their Recent Nanomaterial-Based Signal Amplification Strategies: A Review. *RSC Adv.* **2016**, *6*, 24995–25014.

(298) Sriram, G.; Bhat, M. P.; Patil, P.; Uthappa, U. T.; Jung, H.-Y.; Altalhi, T.; Kumeria, T.; Aminabhavi, T. M.; Pai, R. K.; Madhuprasad; et al. Paper-Based Microfluidic Analytical Devices for Colorimetric Detection of Toxic Ions: A Review. *TrAC Trends Anal. Chem.* **2017**, *93*, 212–227.

(299) Hughes, G.; Westmacott, K.; Honeychurch, K.; Crew, A.; Pemberton, R.; Hart, J. Recent Advances in the Fabrication and Application of Screen-Printed Electrochemical (Bio)Sensors Based on Carbon Materials for Biomedical, Agri-Food and Environmental Analyses. *Biosensors* **2016**, *6*, 50.

(300) García-González, R.; Fernández-Abedul, M. T.; Pernía, A.; Costa-García, A. Electrochemical Characterization of Different Screen-Printed Gold Electrodes. *Electrochim. Acta - Electrochim ACTA* **2008**, *53*, 3242–3249.

(301) Dungchai, W.; Chailapakul, O.; Henry, C. A Low-Cost, Simple, and Rapid Fabrication Method for Paper-Based Microfluidics Using Wax Screen-Printing. *Analyst* **2011**, *136*, 77–82.

(302) Carrilho, E.; Martinez, A. W.; Whitesides, G. M. Understanding Wax Printing: A Simple Micropatterning Process for Paper-Based Microfluidics. *Anal. Chem.* **2009**, *81*, 7091–7095.

(303) Shamkhalichenar, H.; Choi, J.-W. An Inkjet-Printed Non-Enzymatic Hydrogen Peroxide Sensor on Paper. *J. Electrochem. Soc.* **2017**, *164*, B3101–B3106.

(304) Kong, F.-Y.; Gu, S.-X.; Li, W.-W.; Chen, T.-T.; Xu, Q.; Wang, W. A Paper Disk Equipped with Graphene/Polyaniline/Au Nanoparticles/Glucose Oxidase Biocomposite Modified Screen-Printed Electrode: Toward Whole Blood Glucose Determination. *Biosens. Bioelectron.* **2014**, *56*, 77–82.

(305) Tan, S. N.; Ge, L.; Wang, W. Paper Disk on Screen Printed Electrode for One-Step Sensing with an Internal Standard. *Anal. Chem.* **2010**, *82*, 8844–8847.

(306) Liang, B.; Zhu, Q.; Fang, L.; Cao, Q.; Liang, X.; Ye, X. An Origami Paper Device for Complete Elimination of Interferents in Enzymatic Electrochemical Biosensors. *Electrochem. commun.* **2017**, *82*, 43–46.

(307) Sinawang, P. D.; Fajs, L.; Elouarzaki, K.; Nugraha, J.; Marks, R. S. TEMPO-Based Immuno-Lateral Flow Quantitative Detection of Dengue NS1 Protein. *Sensors Actuators, B Chem.* **2018**, *259*, 354–363.

(308) Ge, X.; Zhang, W.; Lin, Y.; Du, D. Magnetic Fe 3 O 4 @TiO 2 Nanoparticles-Based Test Strip Immunosensing Device for Rapid Detection of Phosphorylated Butyrylcholinesterase. *Biosens. Bioelectron.* **2013**, *50*, 486–491.

(309) Ge, S.; Liu, W.; Ge, L.; Yan, M.; Yan, J.; Huang, J.; Yu, J. In Situ Assembly of Porous Au-Paper Electrode and Functionalization of Magnetic Silica Nanoparticles with HRP via Click Chemistry for Microcystin-LR Immunoassay. *Biosens. Bioelectron.* **2013**, *49*, 111–117.

(310) Li, X.; Scida, K.; Crooks, R. M. Detection of Hepatitis B Virus DNA with a Paper Electrochemical Sensor. *Anal. Chem.* **2015**, *87*, 9009–9015.

(311) Cunningham, J. C.; Scida, K.; Kogan, M. R.; Wang, B.; Ellington, A. D.; Crooks, R. M. Paper Diagnostic Device for Quantitative Electrochemical Detection of Ricin at Picomolar Levels. *Lab Chip* **2015**, *15*, 3707–3715.

(312) Chan, K. Y.; Ye, W. W.; Zhang, Y.; Xiao, L. D.; Leung, P. H. M.; Li, Y.; Yang, M. Ultrasensitive Detection of E. Coli O157:H7 with Biofunctional Magnetic Bead Concentration via Nanoporous Membrane Based Electrochemical Immunosensor. *Biosens. Bioelectron.* **2013**, *41*, 532–537.

(313) Ye, W.; Xu, Y.; Zheng, L.; Zhang, Y.; Yang, M.; Sun, P. A Nanoporous Alumina Membrane Based Electrochemical Biosensor for Histamine Determination with Biofunctionalized Magnetic Nanoparticles Concentration and Signal Amplification. *Sensors* **2016**, *16*, 1767.

(314) Ruiz-vega, G.; Kitsara, M.; Pellitero, M. A.; Baldrich, E. Electrochemical Lateral Flow Devices : Towards Rapid. *ChemElectroChem* **2017**, *4*, 880–889.

(315) WHO (World Health Organization). Biomarkers in risk assessment: validity and validation.

(316) Wholley, D. The Biomarkers Consortium. *Nat. Rev. Drug Discov.* **2014**.

(317) Strimbu, K.; Tavel, J. A. What Are Biomarkers? *Current Opinion in HIV and AIDS*. 2010.

(318) Atkinson, A. J.; Colburn, W. A.; DeGruttola, V. G.; DeMets, D. L.; Downing, G. J.; Hoth, D. F.; Oates, J. A.; Peck, C. C.; Schooley, R. T.; Spilker, B. A.; et al. Biomarkers and Surrogate Endpoints: Preferred Definitions and Conceptual Framework. *Clinical Pharmacology and Therapeutics*. 2001.

(319) Dhawan, D. Biotechnology for Biomarkers: Towards Prediction, Screening, Diagnosis, Prognosis, and Therapy. In *Omics Technologies and Bio-engineering: Towards Improving Quality of Life*; 2017.

(320) World Health Statistics 2018: Monitoring Health for the SDGs, Sustainable Development Goals. **2018**, Geneva: World Health Organization. Licence: CC BY-.

(321) World Health Organization (WHO). Prevention and Control of Noncommunicable Diseases in the European Region: A Progress Report. **2014**, World Health Organization Regional Officer for Eur.

(322) Ndrepepa, G. Myeloperoxidase – A Bridge Linking Inflammation and Oxidative Stress with Cardiovascular Disease. *Clin. Chim. Acta* **2019**, *493*, 36–51.

(323) Aratani, Y. Myeloperoxidase: Its Role for Host Defense, Inflammation, and Neutrophil Function. *Arch. Biochem. Biophys.* **2018**, *640*, 47–52.

(324) Taylor, A. M. The Resurrection of Myeloperoxidase as a Therapeutic Target. *JACC Basic to Transl. Sci.* **2016**, *1*, 644–646.

(325) Nauseef, W. M. Biosynthesis of Human Myeloperoxidase. *Arch. Biochem. Biophys.* **2018**, *642*, 1–9.

(326) Vanhamme, L.; Zouaoui Boudjeltia, K.; Van Antwerpen, P.; Delporte, C. The Other Myeloperoxidase: Emerging Functions. *Arch. Biochem. Biophys.* **2018**, *649*, 1–14.

(327) Strzepa, A.; Pritchard, K. A.; Dittel, B. N. Myeloperoxidase: A New Player in Autoimmunity. *Cell. Immunol.* **2017**, *317*, 1–8.

(328) Ray, R. S.; Katyal, A. Myeloperoxidase: Bridging the Gap in Neurodegeneration. *Neurosci. Biobehav. Rev.* **2016**, *68*, 611–620.

(329) Kataoka, Y.; Shao, M.; Wolski, K.; Uno, K.; Puri, R.; Murat Tuzcu, E.; Hazen, S. L.; Nissen, S. E.; Nicholls, S. J. Myeloperoxidase Levels Predict Accelerated Progression of Coronary Atherosclerosis in Diabetic Patients: Insights from Intravascular Ultrasound. *Atherosclerosis* **2014**, *232*, 377–383.

(330) Ferrante, G.; Nakano, M.; Prati, F.; Niccoli, G.; Mallus, M. T.; Ramazzotti, V.; Montone, R. A.; Kolodgie, F. D.; Virmani, R.; Crea, F. High Levels of Systemic Myeloperoxidase Are Associated with Coronary Plaque Erosion in Patients with Acute Coronary Syndromes: A Clinicopathological Study. *Circulation* **2010**, *122*, 2505–2513.

(331) Yun, S.; Ryu, H.; Lee, E. K. Immunomagnetic Separation of Human Myeloperoxidase Using an Antibody-Mimicking Peptide Identified by Phage Display. *J. Biotechnol.* **2017**, *257*, 118–121.

(332) Barallat, J.; Olivé-Monllau, R.; Gonzalo-Ruiz, J.; Ramírez-Satorras, R.; Muñoz-Pascual, F. X.; Ortega, A. G.; Baldrich, E. Chronoamperometric Magneto Immunosensor for Myeloperoxidase Detection in Human Plasma Based on a Magnetic Switch Produced by 3d Laser Sintering. *Anal. Chem.* **2013**, *85*, 9049–9056.

(333) Herrasti, Z.; Martínez, F.; Baldrich, E. Carbon Nanotube Wiring for Signal Amplification of Electrochemical Magneto Immunosensors: Application to Myeloperoxidase Detection. *Anal. Bioanal. Chem.* **2014**, *406*, 5487–5493.

(334) Hajnsek, M.; Schiffer, D.; Harrich, D.; Koller, D.; Verient, V.; Palen, J. V.D.; Heinzle, A.; Binder, B.; Sigl, E.; Sinner, F.; et al. An Electrochemical Sensor for Fast Detection of Wound Infection Based on Myeloperoxidase Activity. *Sensors Actuators, B Chem.* **2015**, *209*, 265–274.

(335) Lu, L.; Liu, B.; Li, S.; Zhang, W.; Xie, G. Improved Electrochemical Immunosensor for Myeloperoxidase in Human Serum Based on Nanogold/Cerium Dioxide-BMIMPF6/L-Cysteine Composite Film. *Colloids Surfaces B Biointerfaces* **2011**, *86*, 339–344.

(336) McDonnell, B.; Hearty, S.; Finlay, W. J. J.; O'Kennedy, R. A High-Affinity Recombinant Antibody Permits Rapid and Sensitive Direct Detection of Myeloperoxidase. *Anal. Biochem.* **2011**, *410*, 1–6.

(337) Windmiller, J. R.; Chinnapareddy, S.; Santhosh, P.; Halámek, J.; Chuang, M. C.; Bocharova, V.; Tseng, T. F.; Chou, T. Y.; Katz, E.; Wang, J. Strip-Based Amperometric Detection of Myeloperoxidase. *Biosens. Bioelectron.* **2010**, *26*, 886–889.

(338) Lin, K. C.; Kunduru, V.; Bothara, M.; Rege, K.; Prasad, S.; Ramakrishna, B. L. Biogenic Nanoporous Silica-Based Sensor for Enhanced Electrochemical Detection of Cardiovascular Biomarkers Proteins. *Biosens. Bioelectron.* **2010**, *25*, 2336–2342.

(339) Venkatraman, V. L.; Reddy, R. K.; Zhang, F.; Evans, D.; Ulrich, B.; Prasad, S. Iridium Oxide Nanomonitors: Clinical Diagnostic Devices for Health Monitoring Systems. *Biosens. Bioelectron.* **2009**, *24*, 3078–3083.

(340) Towfighi, A.; Saver, J. L. Stroke Declines from Third to Fourth Leading Cause of Death in the United States: Historical Perspective and Challenges Ahead. *Stroke* **2011**, *42*, 2351–2355.

(341) Beevers, D. G. The Atlas of Heart Disease and Stroke. *J. Hum. Hypertens.* **2005**, *19*, 505.

(342) Lo, E. H.; Dalkara, T.; Moskowitz, M. A. Mechanisms, Challenges and Opportunities in Stroke. *Nat. Rev. Neurosci.* **2003**, *4*, 399–415.

(343) Kulbe, J. R.; Geddes, J. W. Current Status of Fluid Biomarkers in Mild Traumatic Brain Injury. *Exp. Neurol.* **2016**, *275*, 334–352.

(344) Robin, X.; Turck, N.; Hainard, A.; Lisacek, F.; Sanchez, J. C.; Müller, M. Bioinformatics for Protein Biomarker Panel Classification: What Is Needed to Bring Biomarker Panels into in Vitro Diagnostics? *Expert Rev. Proteomics* **2009**, *6*, 675–689.

(345) Chaturvedi, M.; Kaczmarek, L. MMP-9 Inhibition: A Therapeutic Strategy in Ischemic Stroke. *Mol. Neurobiol.* **2014**, *49*, 563–573.

(346) Vandooren, J.; Van Den Steen, P. E.; Opdenakker, G. Biochemistry and Molecular Biology of Gelatinase B or Matrix Metalloproteinase-9 (MMP-9): The next Decade. *Crit. Rev. Biochem. Mol. Biol.* **2013**, *48*, 222–272.

(347) Huntley, G. W. Synaptic Circuit Remodelling by Matrix Metalloproteinases in Health and Disease. *Nat. Rev. Neurosci.* **2012**, *13*, 743–757.

(348) Zielinska-Turek, J.; Dorobek, M.; Turek, G.; Barcikowska-Kotowicz, M. MMP-9 and/or TIMP as Predictors of Ischaemic Stroke in Patients with Symptomatic and Asymptomatic Atherosclerotic Stenosis of Carotid Artery Treated by Stenting or Endarterectomy – A Review. *Neurol. Neurochir. Pol.* **2018**, *52*, 555–561.

(349) Nagase, H.; Visse, R.; Murphy, G. Structure and Function of Matrix Metalloproteinases and TIMPs. *Cardiovasc. Res.* **2006**, *69*, 562–573.

(350) Kurzepa, J.; M, A.; Czechowska, G.; Kurzepa, J.; Celiński, K.; Kazmierak, W.; Slstrokomka, M. Role of MMP-2 and MMP-9 and Their Natural Inhibitors in Liver Fibrosis, Chronic Pancreatitis and Non-Specific Inflammatory Bowel Diseases. *Hepatobiliary Pancreat. Dis. Int.* **2014**, *13*, 570–579.

(351) J., V.; P.E., V. D. S.; G., O. Biochemistry and Molecular Biology of Gelatinase B or Matrix Metalloproteinase-9 (MMP-9): The next Decade. *Crit. Rev. Biochem. Mol. Biol.* **2013**, *48*, 222–272.

(352) Gaubatz, J. W.; Ballantyne, C. M.; Wasserman, B. A.; He, M.; Chambless, L. E.; Boerwinkle, E.; Hoogeveen, R. C. Association of Circulating Matrix Metalloproteinases with Carotid Artery Characteristics: The Atherosclerosis Risk in Communities Carotid Mri Study. *Arterioscler. Thromb. Vasc. Biol.* **2010**, *30*, 1034–1042.

(353) Balami, J. S.; Chen, R.-L.; Grunwald, I. Q.; Buchan, A. M. Neurological Complications of Acute Ischaemic Stroke. *Lancet Neurol.* **2011**, *10*, 357–371.

(354) Morancho, A.; Rosell, A.; García-Bonilla, L.; Montaner, J. Metalloproteinase and Stroke Infarct Size: Role for Anti-Inflammatory Treatment? *Ann. N. Y. Acad. Sci.* **2010**, *1207*, 123–133.

(355) Montaner, J.; Molina, C. A.; Monasterio, J.; Abilleira, S.; Arenillas, J. F.; Ribó, M.; Quintana, M.; Alvarez-Sabín, J. Matrix Metalloproteinase-9 Pretreatment Level Predicts Intracranial Hemorrhagic Complications after Thrombolysis in Human Stroke. *Circulation* **2003**, *107*, 598–603.

(356) Hacke, W. Intravenous Thrombolysis With Recombinant Tissue Plasminogen Activator for Acute Hemispheric Stroke. *JAMA* **2011**, *274*, 1017–1025.

(357) Tsuji, K.; Aoki, T.; Tejima, E.; Arai, K.; Lee, S. R.; Atochin, D. N.; Huang, P. L.;

Wang, X.; Montaner, J.; Lo, E. H. Tissue Plasminogen Activator Promotes Matrix Metalloproteinase-9 Upregulation after Focal Cerebral Ischemia. *Stroke* **2005**, *36*, 1954–1959.

(358) Lo, E. H.; Wang, X.; Louise Cuzner, M. Extracellular Proteolysis in Brain Injury and Inflammation: Role for Plasminogen Activators and Matrix Metalloproteinases. *J. Neurosci. Res.* **2002**, *69*, 1–9.

(359) Pierot, L.; Soize, S.; Benaissa, A.; Wakhloo, A. K. Techniques for Endovascular Treatment of Acute Ischemic Stroke: From Intra-Arterial Fibrinolytics to Stent-Retrievers. *Stroke* **2015**, *46*, 909–914.

(360) Hacke, W.; Kaste, M.; Bluhmki, E.; Brozman, M.; Dávalos, A.; Guidetti, D.; Larrue, V.; Lees, K. R.; Medeghri, Z.; Machnig, T.; et al. Thrombolysis with Alteplase 3 to 4.5 Hours after Acute Ischemic Stroke. *N. Engl. J. Med.* **2008**, *359*, 1317–1329.

(361) Biela, A.; Watkinson, M.; Meier, U. C.; Baker, D.; Giovannoni, G.; Becer, C. R.; Krause, S. Disposable MMP-9 Sensor Based on the Degradation of Peptide Cross-Linked Hydrogel Films Using Electrochemical Impedance Spectroscopy. *Biosens. Bioelectron.* **2015**, *68*, 660–667.

(362) Mohseni, S.; Moghadam, T. T.; Dabirmanesh, B.; Jabbari, S.; Khajeh, K. Development of a Label-Free SPR Sensor for Detection of Matrixmetalloproteinase-9 by Antibody Immobilization on Carboxymethyldextran Chip. *Biosens. Bioelectron.* **2016**, *81*, 510–516.

(363) Maliszewska, M.; Mäder, M.; Schöll, U.; Azeh, I.; Hardeland, R.; Felgenhauer, K.; Beuche, W.; Weber, F. Development of an Ultrasensitive Enzyme Immunoassay for the Determination of Matrix Metalloproteinase-9 (MMP-9) Levels in Normal Human Cerebrospinal Fluid. *J. Neuroimmunol.* **2001**, *116*, 233–237.

(364) Ocaña, M. F.; Neubert, H. An Immunoaffinity Liquid Chromatography-Tandem Mass Spectrometry Assay for the Quantitation of Matrix Metalloproteinase 9 in Mouse Serum. *Anal. Biochem.* **2010**, *399*, 202–210.

(365) Jing, S.; Yu, B.; Qiao, H.; Huang, Y.; Liao, X. Development of Electrochemical Sensor for Coronary Heart Disease Biomarker MMP-9 Analysis. *Int. J. Electrochem. Sci.* **2017**, *12*, 5233–5242.

(366) Ciani, I.; Schulze, H.; Corrigan, D. K.; Henihan, G.; Giraud, G.; Terry, J. G.; Walton, A. J.; Pethig, R.; Ghazal, P.; Crain, J.; et al. Development of Immunosensors for Direct Detection of Three Wound Infection Biomarkers at Point of Care Using Electrochemical Impedance Spectroscopy. *Biosens. Bioelectron.* **2012**, *31*, 413–418.

(367) Jiang, F.; Zhang, J.-J.; Zhang, J.-R.; Zhu, J.-J. Ultrasensitive Immunoassay Based on Dual Signal Amplification of the Electrically Heated Carbon Electrode and Quantum Dots Functionalized Labels for the Detection of Matrix Metalloproteinase-9. *Analyst* **2013**, *138*, 1962–1965.

(368) Shi, J. J.; He, T. T.; Jiang, F.; Abdel-Halim, E. S.; Zhu, J. J. Ultrasensitive Multi-

Analyte Electrochemical Immunoassay Based on GNR-Modified Heated Screen-Printed Carbon Electrodes and PS@PDA-Metal Labels for Rapid Detection of MMP-9 and IL-6. *Biosens. Bioelectron.* **2014**, *55*, 51–56.

(369) Lee, J. W.; Yun, J. Y.; Lee, W. C.; Choi, S.; Lim, J. H.; Jeong, H.; Shin, D. S.; Park, Y. J. A Reference Electrode-Free Electrochemical Biosensor for Detecting MMP-9 Using a Concentric Electrode Device. *Sensors Actuators, B Chem.* **2017**, *240*, 735–741.

(370) Yee, E. H.; Lathwal, S.; Shah, P. P.; Sikes, H. D. Detection of Biomarkers of Periodontal Disease in Human Saliva Using Stabilized, Vertical Flow Immunoassays. *ACS Sensors* **2017**, *2*, 1589–1593.

(371) Nguyen, P. D.; Cong, V. T.; Baek, C.; Min, J. Fabrication of Peptide Stabilized Fluorescent Gold Nanocluster/Graphene Oxide Nanocomplex and Its Application in Turn-on Detection of Metalloproteinase-9. *Biosens. Bioelectron.* **2017**, *89*, 666–672.

(372) Shoji, A.; Kabeya, M.; Sugawara, M. Real-Time Monitoring of Matrix Metalloproteinase-9 Collagenolytic Activity with a Surface Plasmon Resonance Biosensor. *Anal. Biochem.* **2011**, *419*, 53–60.

(373) Zhao, P.; Li, H. xia; Li, D. wei; Hou, Y. jun; Mao, L.; Yang, M.; Wang, Y. A SERS Nano-Tag-Based Magnetic-Separation Strategy for Highly Sensitive Immunoassay in Unprocessed Whole Blood. *Talanta* **2019**, *198*, 527–533.

(374) Scarano, S.; Dausse, E.; Crispo, F.; Toulmé, J. J.; Minunni, M. Design of a Dual Aptamer-Based Recognition Strategy for Human Matrix Metalloproteinase 9 Protein by Piezoelectric Biosensors. *Anal. Chim. Acta* **2015**, *897*, 1–9.

(375) World Malaria Report 2018. Geneva: World Health Organization; 2018. Licence: CC BY-NC-SA 3.0 IGO.

(376) Mori, T.; Hirai, M.; Mita, T. See-through Observation of Malaria Parasite Behaviors in the Mosquito Vector. *Sci. Rep.* **2019**, *9*, 1768.

(377) World Health Organization; World Health Organization. Global Malaria Programme. *Global Technical Strategy for Malaria, 2016-2030*; 2015.

(378) Ashley, E. A.; Pyae Phyo, A.; Woodrow, C. J. Malaria. *Lancet* **2018**, *391*, 1608–1621.

(379) Michalakis, Y.; Renaud, F. Malaria: Evolution in Vector Control. *Nature* **2009**, *462*, 298–300.

(380) Plewes, K.; Leopold, S. J.; Kingston, H. W. F.; Dondorp, A. M. Malaria: What's New in the Management of Malaria? *Infect. Dis. Clin. North Am.* **2019**, *33*, 39–60.

(381) Pham, N. M.; Karlen, W.; Beck, H. P.; Delamarche, E. Malaria and the "last" Parasite: How Can Technology Help? *Malar. J.* **2018**, *17*, 260.

(382) World Health Organization. (2015). Guidelines for the Treatment of Malaria, 3rd Ed. World Health Organization.

Https://Apps.Who.Int/Iris/Handle/10665/162441.

(383) Mukkala, A. N.; Kwan, J.; Lau, R.; Harris, D.; Kain, D.; Boggild, A. K. An Update on Malaria Rapid Diagnostic Tests. *Curr. Infect. Dis. Rep.* **2018**, *20*, 49.

(384) World Health Organization; Foundation for Innovative New Diagnostics; Centers for Disease Control & Prevention. *Malaria Rapid Diagnostic Test Performance. Results of WHO Product Testing of Malaria RDTs: Round 6 (2014-2015)*; 2015.

(385) Kolluri, N.; Klapperich, C. M.; Cabodi, M. Towards Lab-on-a-Chip Diagnostics for Malaria Elimination. *Lab Chip* **2017**, *18*, 75–94.

(386) Ragavan, K. V.; Kumar, S.; Swaraj, S.; Neethirajan, S. Advances in Biosensors and Optical Assays for Diagnosis and Detection of Malaria. *Biosens. Bioelectron.* **2018**, *105*, 188–210.

(387) Paul, B.; Panigrahi, A. K.; Singh, V.; Singh, S. G. A Multi-Walled Carbon Nanotube-Zinc Oxide Nanofiber Based Flexible Chemiresistive Biosensor for Malaria Biomarker Detection. *Analyst* **2017**, *142*, 2128–2135.

(388) Cardoso, A. R.; Cabral-Miranda, G.; Reyes-Sandoval, A.; Bachmann, M. F.; Sales, M. G. F. Detecting Circulating Antibodies by Controlled Surface Modification with Specific Target Proteins: Application to Malaria. *Biosens. Bioelectron.* **2017**, *91*, 833–841.

(389) Santos, G. P. dos; Corrêa, C. C.; Kubota, L. T. A Simple, Sensitive and Reduced Cost Paper-Based Device with Low Quantity of Chemicals for the Early Diagnosis of Plasmodium Falciparum Malaria Using an Enzyme-Based Colorimetric Assay. *Sensors Actuators, B Chem.* **2018**, *255*, 2113–2120.

(390) Hemben, A.; Ashley, J.; Tothill, I. E. An Immunosensor for Parasite Lactate Dehydrogenase Detection as a Malaria Biomarker – Comparison with Commercial Test Kit. *Talanta* **2018**, *187*, 321–329.

(391) Pham, N. M.; Rusch, S.; Temiz, Y.; Beck, H. P.; Karlen, W.; Delamarche, E. Immuno-Gold Silver Staining Assays on Capillary-Driven Microfluidics for the Detection of Malaria Antigens. *Biomed. Microdevices* **2019**, *21*, 24.

(392) Guirgis, B. S. S.; Sá E Cunha, C.; Gomes, I.; Cavadas, M.; Silva, I.; Doria, G.; Blatch, G. L.; Baptista, P. V.; Pereira, E.; Azzazy, H. M. E.; et al. Gold Nanoparticle-Based Fluorescence Immunoassay for Malaria Antigen Detection. *Anal. Bioanal. Chem.* **2012**, *402*, 1019–1027.

(393) Juul, S.; Nielsen, C. J. F.; Labouriau, R.; Roy, A.; Tesauro, C.; Jensen, P. W.; Harmsen, C.; Kristoffersen, E. L.; Chiu, Y. L.; Frohlich, R.; et al. Droplet Microfluidics Platform for Highly Sensitive and Quantitative Detection of Malaria-Causing Plasmodium Parasites Based on Enzyme Activity Measurement. *ACS Nano* **2012**, *6*, 10676–10683.

(394) Lillehoj, P. B.; Huang, M. C.; Truong, N.; Ho, C. M. Rapid Electrochemical Detection on a Mobile Phone. *Lab Chip* **2013**, *13*, 2950–2955.

(395) Pereira, D. Y.; Chiu, R. Y. T.; Zhang, S. C. L.; Wu, B. M.; Kamei, D. T. Single-Step, Paper-Based Concentration and Detection of a Malaria Biomarker. *Anal.*

Chim. Acta **2015**, *882*, 83–89.

(396) Grant, B. D.; Smith, C. A.; Karvonen, K.; Richards-Kortum, R. Highly Sensitive Two-Dimensional Paper Network Incorporating Biotin-Streptavidin for the Detection of Malaria. *Anal. Chem.* **2016**, *88*, 2553–2557.

(397) Deraney, R. N.; Mace, C. R.; Rolland, J. P.; Schonhorn, J. E. Multiplexed, Patterned-Paper Immunoassay for Detection of Malaria and Dengue Fever. *Anal. Chem.* **2016**, *88*, 6161–6165.

(398) Brince Paul, K.; Kumar, S.; Tripathy, S.; Vanjari, S. R. K.; Singh, V.; Singh, S. G. A Highly Sensitive Self Assembled Monolayer Modified Copper Doped Zinc Oxide Nanofiber Interface for Detection of Plasmodium Falciparum Histidine-Rich Protein-2: Targeted towards Rapid, Early Diagnosis of Malaria. *Biosens. Bioelectron.* **2016**, *80*, 39–46.

(399) Castro-Sesquen, Y. E.; Kim, C.; Gilman, R. H.; Sullivan, D. J.; Searson, P. C. Nanoparticle-Based Histidine-Rich Protein-2 Assay for the Detection of the Malaria Parasite Plasmodium Falciparum. *Am. J. Trop. Med. Hyg.* **2016**, *95*, 354–357.

(400) Mathison, B. A.; Pritt, B. S. Update on Malaria Diagnostics and Test Utilization. *J. Clin. Microbiol.* **2017**, *20*, 49.

(401) Boggild, A.; Brophy, J.; Charlebois, P.; Crockett, M.; Geduld, J.; Ghesquiere, W.; McDonald, P.; Plourde, P.; Teitelbaum, P.; Tepper, M.; et al. Summary of Recommendations for the Prevention of Malaria by the Committee to Advise on Tropical Medicine and Travel (CATMAT). *Canada Commun. Dis. Rep.* **2014**, *40*, 133–143.

(402) Mathema, V. B.; Na-Bangchang, K. A Brief Review on Biomarkers and Proteomic Approach for Malaria Research. *Asian Pac. J. Trop. Med.* **2015**, *8*, 253–262.

(403) Jain, P.; Chakma, B.; Patra, S.; Goswami, P. Potential Biomarkers and Their Applications for Rapid and Reliable Detection of Malaria. *Biomed Res. Int.* **2014**, *2014*, 852645.

(404) Mouatcho, J. C.; Goldring, J. P. Malaria Rapid Diagnostic Tests: Challenges and Prospects. *J Med Microbiol* **2013**, *62*, 1491–1505.

(405) Barber, B. E.; William, T.; Grigg, M. J.; Piera, K.; Yeo, T. W.; Anstey, N. M. Evaluation of the Sensitivity of a PLDH-Based and an Aldolase-Based Rapid Diagnostic Test for Diagnosis of Uncomplicated and Severe Malaria Caused by PCR-Confirmed Plasmodium Knowlesi, Plasmodium Falciparum, and Plasmodium Vivax. *J. Clin. Microbiol.* **2013**, *51*, 1118–1123.

(406) Atchade, P. S.; Doderer-Lang, C.; Chabi, N.; Perrotey, S.; Abdelrahman, T.; Akpovi, C. D.; Anani, L.; Bigot, A.; Sanni, A.; Candolfi, E. Is a Plasmodium Lactate Dehydrogenase (PLDH) Enzyme-Linked Immunosorbent (ELISA)-Based Assay a Valid Tool for Detecting Risky Malaria Blood Donations in Africa? *Malar. J.* **2013**, *12*, 279.

(407) Houzé, S.; Hubert, V.; Le Pessec, G.; Le Bras, J.; Clain, J. Combined Deletions

of Pfhrp2 and Pfhrp3 Genes Result in Plasmodium Falciparum Malaria False-Negative Rapid Diagnostic Test. *J. Clin. Microbiol.* **2011**, *49*, 2694–2696.

(408) Gerstl, S.; Dunkley, S.; Mukhtar, A.; De Smet, M.; Baker, S.; Maikere, J. Assessment of Two Malaria Rapid Diagnostic Tests in Children under Five Years of Age, with Follow-up of False-Positive PLDH Test Results, in a Hyperendemic Falciparum Malaria Area, Sierra Leone. *Malar. J.* **2010**, *9*, 28.

(409) Shoemark, D. K.; Cliff, M. J.; Sessions, R. B.; Clarke, A. R. Enzymatic Properties of the Lactate Dehydrogenase Enzyme from Plasmodium Falciparum. *FEBS J.* **2007**, *274*, 2738–2748.

(410) Olivé-Monllau, R.; Muñoz-Pascual, F. X.; Baldrich, E. Characterization and Optimization of Carbon Nanotube Electrodes Produced by Magnetic Entrapment: Application to Paracetamol Detection. *Sensors Actuators, B Chem.* **2013**.

(411) Healthcare, G. E.; Sciences, L. Helping You Build a Smarter Diagnostic Assay Helping You Build a Smarter Diagnostic Assay.

(412) Lavagnini, I.; Antiochia, R.; Magno, F. An Extended Method for the Practical Evaluation of the Standard Rate Constant from Cyclic Voltammetric Data. *Electroanalysis* **2004**, *16*, 505–506.

(413) Nicholson, R. S. Theory and Application of Cyclic Voltammetry for Measurement of Electrode Reaction Kinetics. *Anal. Chem.* **1965**, *37*, 1351–1355.

(414) Jamshaid, T.; Neto, E. T. T.; Eissa, M. M.; Zine, N.; Kunita, M. H.; El-Salhi, A. E.; Elaissari, A. Magnetic Particles: From Preparation to Lab-on-a-Chip, Biosensors, Microsystems and Microfluidics Applications. *TrAC - Trends Anal. Chem.* **2016**, *79*, 344–362.

(415) Ruiz-Vega, G.; García-Robaina, A.; Ben Ismail, M.; Pasamar, H.; García-Berrocoso, T.; Montaner, J.; Zourob, M.; Othmane, A.; del Campo, F. J.; Baldrich, E. Detection of Plasma MMP-9 within Minutes. Unveiling Some of the Clues to Develop Fast and Simple Electrochemical Magneto-Immunosensors. *Biosens. Bioelectron.* **2018**, *115*, 45–52.

(416) de la Serna, E.; Martínez-García, E.; García-Berrocoso, T.; Penalba, A.; Gil-Moreno, A.; Colas, E.; Montaner, J.; Baldrich, E. Using PolyHRP to Produce Simplified Immunoassays and Electrochemical Immunosensors. Application to MMP-9 Detection in Plasma and Uterine Aspirates. *Sensors Actuators, B Chem.* **2018**, *269*, 377–384.

(417) Lambros, C.; Vanderberg, J. P. Synchronization of Plasmodium Falciparum Erythrocytic Stages in Culture. *J. Parasitol.* **1979**, *65*, 418–420.

(418) Laczka, O.; Maesa, J. M.; Godino, N.; del Campo, J.; Fougt-Hansen, M.; Kutter, J. P.; Snakenborg, D.; Muñoz-Pascual, F. X.; Baldrich, E. Improved Bacteria Detection by Coupling Magneto-Immunocapture and Amperometry at Flow-Channel Microband Electrodes. *Biosens. Bioelectron.* **2011**, *26*, 3633–3640.

(419) Vidal, J. C.; Bonel, L.; Ezquerra, A.; Duato, P.; Castillo, J. R. An Electrochemical Immunosensor for Ochratoxin A Determination in Wines Based on a Monoclonal Antibody and Paramagnetic Microbeads. *Anal. Bioanal. Chem.*

2012, *403*, 1585–1593.

(420) Centi, S.; Silva, E.; Laschi, S.; Palchetti, I.; Mascini, M. Polychlorinated Biphenyls (PCBs) Detection in Milk Samples by an Electrochemical Magneto-Immunosensor (EMI) Coupled to Solid-Phase Extraction (SPE) and Disposable Low-Density Arrays. *Anal. Chim. Acta* **2007**, *594*, 9–16.

(421) Engvall, E.; Perlmann, P. Enzyme-Linked Immunosorbent Assay (ELISA) Quantitative Assay of Immunoglobulin G. *Immunochemistry* **1971**, *8*, 871–874.

(422) Lequin, R. M. Enzyme Immunoassay (EIA)/Enzyme-Linked Immunosorbent Assay (ELISA). *Clin. Chem.* **2005**.

(423) Moreno-Guzmán, M.; González-Cortés, A.; Yáñez-Sedeño, P.; Pingarrón, J. M. A Disposable Electrochemical Immunosensor for Prolactin Involving Affinity Reaction on Streptavidin-Functionalized Magnetic Particles. *Anal. Chim. Acta* **2011**, *692*, 125–130.

(424) Ojeda, I.; Moreno-Guzmán, M.; González-Cortés, A.; Yáñez-Sedeño, P.; Pingarrón, J. M. A Disposable Electrochemical Immunosensor for the Determination of Leptin in Serum and Breast Milk. *Analyst* **2013**, *138*, 4284–4291.

(425) Wang, Y.; Zhe, J.; Chung, B. T. F.; Dutta, P. A Rapid Magnetic Particle Driven Micromixer. *Microfluid. Nanofluidics* **2008**, *4*, 375–389.

(426) Moral-Vico, J.; Barallat, J.; Abad, L.; Olivé-Monllau, R.; Muñoz-Pascual, F. X.; Galán Ortega, A.; del Campo, F. J.; Baldrich, E. Dual Chronoamperometric Detection of Enzymatic Biomarkers Using Magnetic Beads and a Low-Cost Flow Cell. *Biosens. Bioelectron.* **2015**.

(427) Horng, H. E.; Yang, S. Y.; Hong, C. Y.; Yang, H. C.; Liao, S. H.; Liu, C. M.; Wu, C. C. Magnetic Nano-Particles and Their Applications in Immunoassays. *J. Korean Phys. Soc.* **2006**, *48*, 999–1003.

(428) Borlido, L.; Azevedo, A. M.; Roque, A. C. A.; Aires-Barros, M. R. Magnetic Separations in Biotechnology. *Biotechnology Advances*. 2013, pp 1374–1385.

(429) Hu, C.; Yue, W.; Yang, M. Nanoparticle-Based Signal Generation and Amplification in Microfluidic Devices for Bioanalysis. *Analyst*. 2013, pp 6709–6720.

(430) Shen, J.; Li, Y.; Gu, H.; Xia, F.; Zuo, X. Recent Development of Sandwich Assay Based on the Nanobiotechnologies for Proteins, Nucleic Acids, Small Molecules, and Ions. *Chem. Rev.* **2014**, *114*, 7631–7677.

(431) Viswambari Devi, R.; Doble, M.; Verma, R. S. Nanomaterials for Early Detection of Cancer Biomarker with Special Emphasis on Gold Nanoparticles in Immunoassays/Sensors. *Biosensors and Bioelectronics*. 2015, pp 688–698.

(432) Vasilov, R. G.; Tsitsikov, E. N. An Ultrasensitive Immunoassay for Human IgE Measurement in Cell-Culture Supernatant. *Immunol. Lett.* **1990**, *26*, 283–284.

(433) Charbgoo, F.; Mirshahi, M.; Sarikhani, S.; Saifi Abolhassan, M. Synthesis of a

Unique High-Performance Poly-Horseradish Peroxidase Complex to Enhance Sensitivity of Immunodetection Systems. *Biotechnol. Appl. Biochem.* **2012**, *59*, 45–49.

(434) Li, D.; Ying, Y.; Wu, J.; Niessner, R.; Knopp, D. Comparison of Monomeric and Polymeric Horseradish Peroxidase as Labels in Competitive ELISA for Small Molecule Detection. *Microchim. Acta* **2013**, *180*, 711–717.

(435) Miao, Y.; Gan, N.; Li, T.; Zhang, H.; Cao, Y.; Jiang, Q. A Colorimetric Aptasensor for Chloramphenicol in Fish Based on Double-Stranded DNA Antibody Labeled Enzyme-Linked Polymer Nanotracers for Signal Amplification. *Sensors Actuators, B Chem.* **2015**, *220*, 679–687.

(436) Sánchez-Tirado, E.; Martínez-García, G.; González-Cortés, A.; Yáñez-Sedeño, P.; Pingarrón, J. M. Electrochemical Immunosensor for Sensitive Determination of Transforming Growth Factor (TGF) - B1 in Urine. *Biosens. Bioelectron.* **2016**, *88*, 9–14.

(437) Xiong, P.; Gan, N.; Cao, Y.; Hu, F.; Li, T.; Zheng, L. An Ultrasensitive Electrochemical Immunosensor for Alpha-Fetoprotein Using an Envision Complex-Antibody Copolymer as a Sensitive Label. *Mater.* **2012**, *5*, 2757–2772.

(438) Ben Ismail, M.; de la Serna, E.; Ruiz-Vega, G.; García-Berrocoso, T.; Montaner, J.; Zourob, M.; Othmane, A.; Baldrich, E. Using Magnetic Beads and Signal Amplifiers to Produce Short and Simple Immunoassays: Application to MMP-9 Detection in Plasma Samples. *Anal. Chim. Acta* **2018**, *999*, 144–154.

(439) Gervais, L.; De Rooij, N.; Delamarche, E. Microfluidic Chips for Point-of-Care Immunodiagnostics. *Adv. Mater.* **2011**, *23*.

(440) Giouroudi, I.; Kokkinis, G. Recent Advances in Magnetic Microfluidic Biosensors. *Nanomater.* **2017**, *7*, 171.

(441) Tekin, H. C.; Gijs, M. a M. Ultrasensitive Protein Detection: A Case for Microfluidic Magnetic Bead-Based Assays. *Lab Chip* **2013**, *13*, 4711–4739.

(442) van Reenen, A.; de Jong, A. M.; den Toonder, J. M. J.; Prins, M. W. J. Integrated Lab-on-Chip Biosensing Systems Based on Magnetic Particle Actuation – a Comprehensive Review. *Lab Chip* **2014**, *14*, 1966.

(443) Gómez-de Pedro, S.; Berenguel-Alonso, M.; Couceiro, P.; Alonso-Chamarro, J.; Puyol, M. Automatic Microfluidic System to Perform Multi-Step Magneto-Biochemical Assays. *Sens. Actuators, B Chem.* **2017**, *245*, 477–483.

(444) Moral-Vico, J.; Barallat, J.; Abad, L.; Olivé-Monllau, R.; Muñoz-Pascual, F. X.; Galán Ortega, A.; del Campo, F. J.; Baldrich, E. Dual Chronoamperometric Detection of Enzymatic Biomarkers Using Magnetic Beads and a Low-Cost Flow Cell. *Biosens. Bioelectron.* **2015**, *69*, 328–336.

(445) Ruiz-Vega, G.; Kitsara, M.; Pellitero, M. A.; Baldrich, E.; del Campo, F. J. Electrochemical Lateral Flow Devices: Towards Rapid Immunomagnetic Assays. *ChemElectroChem* **2017**, *4*, 880–889.

(446) Zirath, H.; Peham, J. R.; Schnetz, G.; Coll, A.; Brandhoff, L.; Spittler, A.;

Vellekoop, M. J.; Redl, H. A Compact and Integrated Immunoassay with On-Chip Dispensing and Magnetic Particle Handling. *Biomed. Microdevices* **2016**, *18*, 16.

(447) Giri, B.; Pandey, B.; Neupane, B.; Ligler, F. S. Signal Amplification Strategies for Microfluidic Immunoassays. *TrAC - Trends Anal. Chem.* **2016**, *79*, 326–334.

(448) Bowen, R. A. R.; Remaley, A. T. Interferences from Blood Collection Tube Components on Clinical Chemistry Assays. *Biochemia Medica*. 2014, pp 31–44.

(449) Chaturvedi, M.; Kaczmarek, L. MMP-9 Inhibition: A Therapeutic Strategy in Ischemic Stroke. *Mol. Neurobiol.* **2014**, *49*, 563–573.

(450) Vandooren, J.; Van Den Steen, P. E.; Opdenakker, G. Biochemistry and Molecular Biology of Gelatinase B or Matrix Metalloproteinase-9 (MMP-9): The next Decade. *Critical Reviews in Biochemistry and Molecular Biology*. 2013.

(451) Akyazi, T.; Basabe-Desmonts, L.; Benito-Lopez, F. Review on Microfluidic Paper-Based Analytical Devices towards Commercialisation. *Anal. Chim. Acta* **2018**.

(452) Sinawang, P. D.; Fajs, L.; Elouarzaki, K.; Nugraha, J.; Marks, R. S. TEMPO-Based Immuno-Lateral Flow Quantitative Detection of Dengue NS1 Protein. *Sensors Actuators, B Chem.* **2018**, *259*, 354–363.

(453) World Health Organization. *Global Status Report on Noncommunicable Diseases*; WHO Library Cataloguing: Switzerland, 2014.

(454) Bonaventura, A.; Liberale, L.; Vecchié, A.; Casula, M.; Carbone, F.; Dallegri, F.; Montecucco, F. Update on Inflammatory Biomarkers and Treatments in Ischemic Stroke. *Int. J. Mol. Sci.* **2016**, *17*, 1967.

(455) Jane Maxwell, E.; Mazzeo, A. D.; Whitesides, G. M. Paper-Based Electroanalytical Devices for Accessible Diagnostic Testing. *MRS Bull.* **2013**.

(456) Byrnes, S.; Thiessen, G.; Fu, E. Progress in the Development of Paper-Based Diagnostics for Low-Resource Point-of-Care Settings. *Bioanalysis*. 2013.

(457) Du, D.; Wang, J.; Wang, L.; Lu, D.; Lin, Y. Integrated Lateral Flow Test Strip with Electrochemical Sensor for Quantification of Phosphorylated Cholinesterase: Biomarker of Exposure to Organophosphorus Agents. *Anal. Chem.* **2012**, *84*, 1380–1385.

(458) Godino, N.; Gorkin, R.; Bourke, K.; Ducrée, J. Fabricating Electrodes for Amperometric Detection in Hybrid Paper/Polymer Lab-on-a-Chip Devices. *Lab Chip* **2012**, *12*, 3281.

(459) Liu, H.; Xiang, Y.; Lu, Y.; Crooks, R. M. Aptamer-Based Origami Paper Analytical Device for Electrochemical Detection of Adenosine. *Angew. Chemie - Int. Ed.* **2012**, *51*, 6925–6928.

(460) Wang, P.; Ge, L.; Yan, M.; Song, X.; Ge, S.; Yu, J. Paper-Based Three-Dimensional Electrochemical Immunodevice Based on Multi-Walled Carbon Nanotubes Functionalized Paper for Sensitive Point-of-Care Testing. *Biosens.*

Bioelectron. **2012**, *32*, 238–243.

(461) Lamas-Ardisana, P. J. Disposable Electrochemical Paper-Based Devices Fully Fabricated by Screen-Printing Technique_Answers Reviewers.

(462) Fu, E.; Ramsey, S. A.; Kauffman, P.; Lutz, B.; Yager, P. Transport in Two-Dimensional Paper Networks. *Microfluid. Nanofluidics* **2011**.

(463) Masoodi, R.; Pillai, K. M. Darcy's Law-Based Model for Wicking in Paper-like Swelling Porous Media. *AIChE J.* **2010**.

(464) Compton, R. G.; Banks, C. E. *Understanding Voltammetry*; 2017.

(465) Henstridge, M. C.; Dickinson, E. J. F.; Compton, R. G. Mass Transport to and within Porous Electrodes. Linear Sweep Voltammetry and the Effects of Pore Size: The Prediction of Double Peaks for a Single Electrode Process. *Russ. J. Electrochem.* **2012**, *48*, 629–635.

(466) Sid Kalal, H.; R. Nabi Bidhendi, G.; Hoveidi, H. *Principles of Electrochemistry*; 2008.

(467) Aikens, D. A. Electrochemical Methods, Fundamentals and Applications. *J. Chem. Educ.* **2009**.

ANNEX A1

Publications produced as a result of this PhD Thesis

A. ANNEX

A.1. Publications

A. 1.1. Journal Articles

(1) **Ruiz-Vega, G.**; Baldrich, E. Effect of Agitation in Magneto-Assay Performance. Sensors Actuators, B Chem. 2017, 247, 718–726.

Sensors and Actuators B 247 (2017) 718–726

Contents lists available at ScienceDirect

Sensors and Actuators B: Chemical

journal homepage: www.elsevier.com/locate/snb

Effect of agitation in magneto-assay performance

G. Ruiz-Vega[a], E. Baldrich[a,b,*]

[a] Diagnostic Nanotools Group. Molecular Biology and Biochemistry Research Center for Nanomedicine (Cibbim-Nanomedicine), Vall d'Hebron Hospital Research Institute (VHIR), Universitat Autònoma de Barcelona, Passeig Vall d'Hebron 119-129, Barcelona 08035, Spain
[b] CIBER de Bioingeniería, Biomateriales y Nanomedicina (CIBER-BBN), Spain

Complete manuscript available from: http://dx.doi.org/10.1016/j.snb.2017.03.076

(2) **Ruiz-Vega, G.**; Kitsara, M.; Pellitero, M. A.; Baldrich, E.; del Campo, F. J. Electrochemical Lateral Flow Devices: Towards Rapid Immunomagnetic Assays. ChemElectroChem 2017, 4, 880-889.

ChemPubSoc Europe

DOI: 10.1002/celc.201600902

CHEMELECTROCHEM Articles

Special Issue

Electrochemical Lateral Flow Devices: Towards Rapid Immunomagnetic Assays

Gisela Ruiz-Vega,[a] Maria Kitsara,[c] Miguel Aller Pellitero,[c] Eva Baldrich,*[a, b] and F. Javier del Campo*[c]

ChemElectroChem 2017, 4, 880 – 889 Wiley Online Library 880

Complete manuscript available from: http://dx.doi.org/10.1002/celc.201600902

(3) Ben Ismail, M.; de la Serna, E.; **Ruiz-Vega, G.;** García-Berrocoso, T.; Montaner, J.; Zourob, M.; Othmane, A.; Baldrich, E. Using Magnetic Beads and Signal Amplifiers to Produce Short and Simple Immunoassays: Application to MMP-9 Detection in Plasma Samples. Anal. Chim. Acta 2018, 999, 144-154.

Analytica Chimica Acta 999 (2018) 144–154

Contents lists available at ScienceDirect

Analytica Chimica Acta

journal homepage: www.elsevier.com/locate/aca

Using magnetic beads and signal amplifiers to produce short and simple immunoassays: Application to MMP-9 detection in plasma samples

Manel Ben Ismail [a, b], Erica de la Serna [b], Gisela Ruiz-Vega [b], Teresa García-Berrocoso [c], Joan Montaner [c], Mohammed Zourob [d], Ali Othmane [a], Eva Baldrich [b, e, *]

[a] Laboratory of Biophysics, Faculty of Medicine of Monastir, University of Monastir, Tunisia
[b] Diagnostic Nanotools Group, Cibbim-Nanomedicine, Vall Hebron Research Institute (VHIR), Universitat Autònoma de Barcelona, Barcelona, Spain
[c] Neurovascular Research Laboratory, Vall d'Hebron Institute of Research (VHIR), Universitat Autònoma de Barcelona, Barcelona, Spain
[d] Department of Chemistry, Alfaisal University, Riyadh, Saudi Arabia
[e] CIBER de Bioingeniería, Biomateriales y Nanomedicina (CIBER-BBN), Spain

Complete manuscript available from: https://doi.org/10.1016/j.aca.2017.11.013

(4) **Ruiz-Vega, G.**; García-Robaina, A.; Ben Ismail, M.; Pasamar, H.; García-Berrocoso, T.; Montaner, J.; Zourob, M.; Othmane, A.; del Campo, F. J.; Baldrich, E. Detection of Plasma MMP-9 within Minutes. Unveiling Some of the Clues to Develop Fast and Simple Electrochemical Magneto-Immunosensors. Biosens. Bioelectron. 2018, 115, 45–52.

Biosensors and Bioelectronics 115 (2018) 45–52

Contents lists available at ScienceDirect

Biosensors and Bioelectronics

journal homepage: www.elsevier.com/locate/bios

Detection of plasma MMP-9 within minutes. Unveiling some of the clues to develop fast and simple electrochemical magneto-immunosensors

Gisela Ruiz-Vega[a], Alicia García-Robaina[a], Manel Ben Ismail[a,b], Helena Pasamar[a], Teresa García-Berrocoso[c], Joan Montaner[c], Mohammed Zourob[d], Ali Othmane[b], F. Javier del Campo[e], Eva Baldrich[a,f,*]

[a] Diagnostic Nanotools Group, Cibbim-Nanomedicine, Vall Hebron Research Institute (VHIR), Universitat Autònoma de Barcelona, Barcelona, Spain
[b] Laboratory of Biophysics, Faculty of Medicine of Monastir, University of Monastir, Tunisia
[c] Neurovascular Research Laboratory, Vall d'Hebron Institute of Research (VHIR), Universitat Autònoma de Barcelona, Barcelona, Spain
[d] Department of Chemistry, Alfaisal University, Riyadh, Saudi Arabia
[e] Instituto de Microelectrónica de Barcelona, IMB-CNM (CSIC), Esfera UAB. Campus Universitat Autònoma de Barcelona, Bellaterra, Barcelona, Spain
[f] CIBER de Bioingeniería, Biomateriales y Nanomedicina (CIBER-BBN), Spain

Complete manuscript available from: https://doi.org/10.1016/j.bios.2018.05.020

Review

Herrasti, Z.; De La Serna, E.; **Ruiz-Vega, G.**; Baldrich, E. Developing Enhanced Magnetoimmunosensors Based on Low-Cost Screen-Printed Electrode Devices. Rev. Anal. Chem. 2016, 35, 53–58.

A. 1.2. In process

Ruiz-Vega, G; Garcia-Berrocoso, Teresa; Montaner, Joan; Baldrich, Eva. Screen-printed electrodes with integrated paper microfluidics for electrochemical magneto-immunosensor performance with minimal user intervention. Analytical Chemistry. (*Submitted, under review)*

Ruiz-Vega, G.; de-la-Serna, E.; Arias Alpízar, K.; Borgheti-Cardoso, L.; Sulleiro Igual, E.; Molina Romero, I.; Fernandez Busquets, X.; del Campo, F. J.; Sánchez Montalvá, A.; Baldrich, E. Microfluidic paper Point-of-Care (MP-POC) device with magnetic beads for the fast and quantitative detection of *Plasmodium* antigen. (*In preparation*)

Montes-Cebrián, Y.; Álvarez-Carulla, A.; **Ruiz-Vega, G.**; Colomer-Farrarons, J.; Puig-Vidal, M.; Baldrich, E.; Miribel- Català, P.L. A high-performance low-cost portable potentiostat for POC applications: a comparative case of HRP detection. (*In preparation*)

Chapter

Ruiz-Vega, G.; Lopez-Marzo, A.; de-la-Serna, Erica; Sanchez-Cano, Ana; Baldrich, E. Electrochemical magneto-immunosensors as fast and efficient tools for point-of-care diagnostics. Immunosensors. Royal Society of Chemistry. (*In press)*

ANNEX A2

Presentations in congresses, seminars and other scientific events

A.2. Presentations in congresses, seminars and other scientific events

Ruiz-Vega, G.; Baldrich E. Effect of mixing on magnetic particle based biosensing. Poster (022) Biosensors 2016. 25-27 May 2016, Gothenburg, Sweden.

Baldrich E.; **Ruiz-Vega, G**.; Development of a simple and ultrafast magneto-immunoassay using a polymeric signal amplifier and a paper detection device. Oral presentation. CIBBIM-Nanomedicine conference. 3 November 2016. Vall d'Hebron Research Institute, Barcelona, Spain.

Ruiz-Vega, G.; Baldrich, E. Effect of mixing on magnetic particle based biosensing. Poster. 10th conference of Vall d'Hebron Research Institute. 13-16 December 2016. Vall d'Hebron Research Institute, Barcelona, Spain

Ruiz-Vega, G.; Kitsara, M.; Aller Pellitero, M.; Baldrich, E.; del Campo, F. J. Electrochemical lateral flow devices for the simplification of rapid immunomagnetic-assays. Poster (166). 5th International conference on bio-sensing technology 2017. 7-10 May 2017. Riva del Garda, Italy.

Ruiz-Vega, G.; Kitsara, M.; Aller Pellitero, M.; Baldrich, E.; del Campo, F. J. Electrochemical lateral flow devices for the simplification of rapid immunomagnetic-assays. Poster (19). 3rd Scientific Meeting of Bcn-b Students. 8-9 November 2017. Autonomous University of Barcelona (ICMAB-CSIC), Barcelona, Spain.

Ruiz-Vega, G; Baldrich, E. Electrochemical Biosensors for fast and simple point of care diagnostics. Oral presentation. CIBBIM-Nanomedicine conference. 9 November 2017. Vall d'Hebron Research Institute, Barcelona, Spain.

Ruiz-Vega, G.; Kitsara, M.; Aller Pellitero, M.; Baldrich, E.; del Campo, F. J. Electrochemical lateral flow devices for the simplification of rapid immunomagnetic-assays. Poster. 11th conference of Vall d'Hebron Research Institute. 13-15 December 2017. Vall d'Hebron Research Institute, Barcelona, Spain.

Ruiz-Vega, G.: Baldrich, E. Using magnetic beads for the fast and quantitative detection of *Plasmodium* antigen: towards malaria point-of-care diagnosis. Oral presentation. CIBBIM-Nanomedicine conference. 6 November 2018. Vall d'Hebron Research Institute, Barcelona, Spain.

Ruiz Vega, G.; de-la-Serna, E.; Sánchez Montalvá, A.; Sulleiro Igual, E.; Molina Romero, I.; del Campo, F. J.; Baldrich, E. Point of care (POC) device with magnetic beads for the fast and quantitative electrochemical detection of *Plasmodium* antigen. Poster. 12th conference of Vall d'Hebron Research Institute. 12-14 December 2018. Vall d'Hebron Research Institute, Barcelona, Spain.

Ruiz-Vega, G.; Sánchez Montalvá, A.; Sulleiro Igual, E.; Molina Romero, I.; del Campo, F. J.; Baldrich, E. Point of care (POC) device with magnetic beads and microfluidic paper electrodes for the fast and quantitative electrochemical detection of

Plasmodium antigen. Poster (0276). 6th International Conference on Bio-Sensing Technology 2019. 16-19 June 2019, Kuala Lumpur, Malaysia

Alonso, O.; Franch, N.; Canals, J.; de-la-Serna, E.; **Ruiz-Vega, G.**; Baldrich, E.; Diéguez, A. Development of an IoT-based point-of-care: an application to malaria testing. Oral Presentation (0258). 6th International Conference on Bio-Sensing Technology 2019. 16-19 June 2019, Kuala Lumpur, Malaysia

Ruiz Vega, G.; Arias Alpízar, K.; de-la-Serna, E.; Neves Borgheti-Cardoso, L.; Sulleiro Igual, E.; Molina Romero, I.; Fernandez-Busquets, X.; del Campo, F. J.; Sánchez Montalvá, A.; Baldrich, E. Electrochemical quantitation of malaria infection from whole blood in <20 min by using magnetic beads, poly-HRP and microfluidic paper electrode. Oral presentation. 20th Euroanalysis conference. 1-5 September 2019. Istanbul, Turkey.